

Copyright  
by  
Ashish Rastogi  
2009

**The Dissertation Committee for Ashish Rastogi Certifies that this is the approved  
version of the following dissertation:**

**Design, Development, and Evaluation  
of a Scalable Micro Perforated Drug Delivery Device  
Capable of Long-term Zero Order Release**

**Committee:**

---

Salomon A. Stavchansky, Supervisor

---

Phillip D. Bowman

---

Paul S. Ho

---

James W. McGinity

---

Robert O. Williams III

**Design, Development, and Evaluation  
of a Scalable Micro Perforated Drug Delivery Device  
Capable of Long-term Zero Order Release**

**by**

**Ashish Rastogi, B.Pharm**

**Dissertation**

Presented to the Faculty of the Graduate School of  
The University of Texas at Austin  
in Partial Fulfillment  
of the Requirements  
for the Degree of

**Doctor of Philosophy**

**The University of Texas at Austin**

**December 2009**

## **Dedication**

I dedicate this dissertation to my family  
for their love, support and for being a source of all my strength.

Thank you for believing in me.

## **Acknowledgements**

I would like to sincerely thank my research advisor and mentor Dr. Salomon Stavchansky for taking me under his wing and sharing with me his immense knowledge and experience. I am grateful to him for his continued guidance, patience and encouragement as my teacher, guide, and mentor. I am also thankful to Dr. Phillip D. Bowman and express my most sincere gratitude for his constant support and advice. I am also deeply thankful to Dr. Paul S. Ho, and his students Zhiquan Luo, and Zhuozie Wu for their assistance in coating of tubes, FEM analysis, and photolithography process. I would also like to thank my other committee members, Dr. James W. McGinity and Dr. Robert O. Williams III, for their valuable advice and review of this dissertation. I would also like to take this opportunity to thank Dr. Sean Kerwin for his guidance and Dr. Michael Schmerling for his training with SEM. I am also thankful to Ms. Mickie Sheppard for all her efforts to help me secure TA positions and for her continued direction and assistance. I would also like to thank my other friends and colleagues for their support during my graduate career. Finally, I would like to thank my family and friends from the bottom of my heart. I would especially like to thank my wife, Tanvi, my parents, Sudhir and Veena Rastogi, my parents in law, Ravindra and Ira Rastogi, my brother and sister in law Manish and Shuchi Rastogi, and my brother in law Tanuj Rastogi for their endless love.

**Design, Development, and Evaluation  
of a Scalable Micro Perforated Drug Delivery Device  
Capable of Long-term Zero Order Release**

Publication No. \_\_\_\_\_

Ashish Rastogi, PhD.

The University of Texas at Austin, 2009

Supervisor: Salomon Stavchansky

Chronic diseases can often be managed by constantly delivering therapeutic amounts of drug for prolonged periods. A controlled release for extended duration would replace the need for multiple and frequent dosing. Local drug release would provide added benefit as a lower dose of drug at the target site will be needed as opposed to higher doses required by whole body administration. This would provide maximum efficacy with minimum side effects.

Nonetheless, a problem with the known implantable drug delivery devices is that the delivery rate cannot be controlled, which leads to drug being released in an unpredictable pattern resulting in poor therapeutic management of patients. This dissertation is the result of development of an implantable drug delivery system that is capable of long-term zero order local release of drugs. The device can be optimized to

deliver any pharmaceutical agent for any time period up to several years maintaining a controlled and desired rate.

Initially significant efforts were dedicated to the characterization, biocompatibility, and loading capacity of nanoporous metal surfaces for controlled release of drugs. The physical characterization of the nanoporous wafers using Scanning electron microscopy (SEM) and atomic force microscopy techniques (AFM) yielded  $3.55 \times 10^4 \text{ nm}^3$  of pore volume /  $\mu\text{m}^2$  of wafer surface. *In vitro* drug release study using 2 - octyl cyanoacrylate and methyl orange as the polymer-drug matrix was conducted and after 7 days,  $88.1 \pm 5.0 \%$  drug was released. However, the initial goal to achieve zero order drug release rates for long periods of time was not achieved.

The search for a better delivery system led to the design of a perforated microtube. The delivery system was designed and appropriate dimensions for the device size and hole size were estimated. Polyimide microtubes in different sizes (125-1000  $\mu\text{m}$ ) were used. Micro holes with dimensions ranging from 20-600  $\mu\text{m}$  were fabricated on these tubes using photolithography, laser drilling, or manual drilling procedures.

Small molecules such as crystal violet, prednisolone, and ethinyl estradiol were successfully loaded inside the tubes in powder or solution using manual filling or capillary filling methods. A drug loading of 0.05 – 5.40 mg was achieved depending on the tube size and the drug filling method used.

The delivery system in different dimensions was characterized by performing *in vitro* release studies in phosphate buffered saline (pH 7.1-7.4) and in vitreous humor from the rabbit's eye at  $37.0 \pm 1.0^\circ\text{C}$  for up to four weeks. The number of holes was

varied between 1 and 3. The tubes were loaded with crystal violet (CV) and ethinyl estradiol (EE). Linear release rates with  $R^2 > 0.9900$  were obtained for all groups with CV and EE. Release rates of  $7.8 \pm 2.5$ ,  $16.2 \pm 5.5$ , and  $22.5 \pm 6.0$  ng/day for CV and  $30.1 \pm 5.8$  ng/day for EE were obtained for small tubes (30  $\mu\text{m}$  hole diameter; 125  $\mu\text{m}$  tube diameter). For large tubes (362-542  $\mu\text{m}$  hole diameter; 1000  $\mu\text{m}$  tube diameter), a release rate of  $10.8 \pm 4.1$ ,  $15.8 \pm 4.8$  and  $22.1 \pm 6.7$   $\mu\text{g}/\text{day}$  was observed *in vitro* in PBS and a release rate of  $5.8 \pm 1.8$   $\mu\text{g}/\text{day}$  was observed *ex vivo* in vitreous humor.

The delivery system was also evaluated for its ability to produce a biologically significant amounts in cells stably transfected with an estrogen receptor/luciferase construct (T47D-KBluc cells). These cells are engineered to produce a constant luminescent signal in proportion to drug exposure. The average luminescence of  $1144.8 \pm 153.8$  and  $1219.9 \pm 127.7$  RLU/day, (RLU = Relative Luminescence Units), yet again indicating the capability of the device for long-term zero order release.

The polyimide device was characterized for biocompatibility. An automated goniometer was used to determine the contact angle for the device, which was found to be  $63.7 \pm 3.7$  degrees indicating that it is hydrophilic and favors cell attachment. In addition, after 72 h incubation with mammalian cells (RAW 267.4), a high cell distribution was observed on the device's surface. The polyimide tubes were also investigated for any signs of inflammation using inflammatory markers, TNF- $\alpha$  and IL-1 $\beta$ . No significant levels of either TNF- $\alpha$  or IL-1 $\beta$  were detected in polyimide device. The results indicated that polyimide tubes were biocompatible and did not produce an inflammatory response.

## Table of Contents

List of Tables .....	xviii
List of Figures .....	xxv
List of Figures .....	xxv
Statement of Objectives and Significance of Research .....	1
Chapter 1: Local Drug Delivery Devices for Long-term Zero Order	
Release .....	6
1.1 Need for a Drug Delivery System for Long-term Zero Order	
Release .....	6
1.2 Drug-Device Combination Products As Ideal Controlled Drug	
Delivery Systems .....	8
1.2.1 Ocusert <sup>®</sup> .....	9
1.2.2 Progestasert <sup>®</sup> .....	11
1.2.3 Norplant <sup>®</sup> .....	12
1.2.4 Osmotic Pumps (OROS <sup>®</sup> and DUROS <sup>®</sup> ) .....	13
1.2.5 Vitrasert <sup>®</sup> , Retisert <sup>®</sup> , and Iluvien <sup>®</sup> .....	15
1.3 Introduction to a Scalable Microperforated Drug Delivery	
Device .....	16

Chapter 2: Preliminary Work with Nanopores and Metal Surface .....	20
2.1 Introduction.....	20
2.2 Materials And Methods.....	23
2.2.1 Materials .....	23
2.2.2 Surface Analysis of Aluminum Coated Stainless Steel Tube 23	
2.2.3 Surface and Dimensional Analysis of Nanoporous Wafers.....	26
2.2.4 Drug Loading of Nanoporous wafers .....	28
2.2.5 Drug Release Study.....	29
2.3 Results And Discussion .....	29
2.3.1 Detection of Oxidative Degradation of Aluminum Coating.....	29
2.3.2 Dimensional Analysis of Nanopores .....	32
2.3.3 Surface Analysis of a Stent and Estimation of Volume of Pores on its Surface.....	33
2.3.4 Drug Release Study.....	35
2.4 Conclusion .....	38
Chapter 3: Designing and Fabrication of the Drug Delivery Device.....	39
3.1 Introduction.....	39

3.1.1 Drug Eluting Stents – Advantages and Disadvantages.....	40
3.1.2 Understanding Late Stent Thrombosis.....	41
3.1.3 Rationale for device development .....	42
3.2 Design of the Drug Eluting Stent.....	44
3.2.1 Material Considerations for the Manufacture of Stent Skeleton and Drug Delivery Device .....	47
3.3 Materials and Methods.....	49
3.3.1 Materials .....	49
3.3.2 Estimation of Appropriate Dimensions for the Device.....	49
3.3.3 Finite Element Analysis of the Stent Structure.....	52
3.3.4 Estimation of Hole Size .....	52
3.3.5 Coating of Polyimide Matrices with a Biocompatible Alloy .....	53
3.3.6 Characterization of Coating Composition .....	55
3.3.7 Fabrication of Holes on the Polyimide Matrix .....	56
3.4 Results and Discussion .....	58
3.4.1 Dimensions for the Stent and Drug Delivery Device .....	58
3.4.2 Finite Element Simulation of the Stent Design.....	58

3.4.3 Particle Size Distribution of Prednisolone to Estimate the Hole Diameter .....	62
3.4.4 Coating Characterization .....	64
3.4.5 Surface Analysis of Coated Polyimide Tubes .....	66
3.4.6 Analysis of Holes Manufactured by Photolithography.....	66
3.5 Conclusion .....	68
Chapter 4: Drug loading of the micro scalable perforated device .....	70
4.1 Introduction.....	70
4.1.1 Prednisolone.....	71
4.1.2 Ethinyl Estradiol .....	72
4.1.3 Crystal Violet.....	74
4.2 Materials and Methods.....	75
4.2.1 Materials .....	75
4.2.2 Polymorphism Characterization of Prednisolone and Ethinyl Estradiol .....	75
4.2.3 Fabrication of holes and drug loading .....	76
4.2.3.1 Drug loading with Prednisolone .....	76
4.2.3.2 Drug loading with Crystal Violet.....	77
4.2.3.3 Drug Loading with Ethinyl Estradiol.....	80

4.2.4 Statistical Analysis.....	81
4.3 Results and Discussion .....	81
4.3.1 Differential Scanning Calorimetry.....	81
4.3.2 Drug Loading Studies .....	85
4.3.2.1 Drug loading with Prednisolone .....	85
4.3.2.2 Drug loading with Crystal Violet.....	87
4.3.2.3 Drug loading with Ethinyl Estradiol .....	90
4.3.3 Capping and Sealing of the Tubes .....	92
4.4 Conclusion .....	93

Chapter 5: *In Vitro* Drug Release Studies to Evaluate the Micro Scalable

Perforated Device Capable of Long-Term Zero Order Drug Release .....	94
5.1 Introduction.....	94
5.2 Materials and Methods.....	96
5.2.1 Materials .....	96
5.2.2 <i>In vitro</i> drug release studies .....	96
5.2.2.1 Small Tubes .....	97
5.2.2.2 Large Tubes .....	97
5.2.2.3 Large Tubes without Holes.....	98
5.2.3 Statistical Analysis.....	98

5.3	Results and Discussion .....	99
5.3.1	Small Tubes .....	99
5.3.1.1	Method Validation .....	99
5.3.1.2	In vitro Drug Release Studies .....	101
5.3.2	Large Tubes .....	104
5.3.2.1	Method Validation .....	104
5.3.2.2	In vitro Drug Release Studies .....	106
5.3.3	Large Tubes without Holes .....	108
5.3.3.1	Method Validation .....	108
5.3.3.2	In vitro Drug Release Studies .....	108
5.3.4	Mechanism of Release Kinetics .....	111
5.4	Conclusion .....	114

Chapter 6: *Ex vivo* Drug Release Studies in Vitreous Humor from a

	Rabbit's Eye .....	116
6.1	Introduction .....	116
6.1.1	Intravitreal Drug Delivery .....	116
6.2	Methods .....	117
6.2.1	Materials .....	117
6.2.2	<i>In vitro</i> Drug Release Studies .....	117

6.3	Results and Discussion .....	118
6.4	Conclusion .....	120

Chapter 7: *In Vitro* Biocompatibility Evaluation of Cobalt-Chromium

	Alloy Coated and Uncoated Polyimide Matrices.....	121
7.1	Introduction.....	121
	7.1.1 Biocompatibility .....	121
	7.1.1.1 Cell Adhesion and Cell Attachment .....	121
	7.1.1.2 Inflammatory Studies.....	122
7.2	Materials and Methods.....	124
	7.2.1 Materials .....	124
	7.2.2 Contact Angle Measurement.....	124
	7.2.3 Cell Culture.....	125
	7.2.4 Inflammatory Studies.....	125
	7.2.4.1 Extraction of RNA by Cell Lysis- .....	125
	7.2.4.2 Two Step RT-PCR: Reverse Transcription of RNA to cDNA.....	125
7.3	Result and Discussion.....	126
	7.3.1 Hydrophilicity Studies .....	126
	7.3.2 Biocompatibility Studies.....	127

7.3.3 Inflammatory Studies.....	129
7.4 Conclusion .....	132
Chapter 8: <i>In Vitro</i> Dose Response Studies.....	133
8.1 Introduction.....	133
8.1.1 Luciferase.....	133
8.1.2 Reporter Gene Assay .....	134
8.2 Materials and Methods.....	136
8.2.1 Materials .....	136
8.2.2 Drug Release Studies .....	136
8.2.3 Dose Response Studies using Luciferase Gene Reporter Assay System.....	137
8.2.3.1 Method Validation .....	137
8.2.3.2 Dose Response Studies .....	137
8.2.4 Quantitative Estimation of Ethinyl Estradiol in Drug Release Samples using ELISA.....	138
8.3 Results and Discussion .....	138
8.3.1 Dose Response Study.....	138
8.3.2 Quantitative Analysis of Drug Release Samples .....	143
8.4 Conclusion .....	149

Chapter 9: Pharmaceutical Applications of the Scalable Microperforated	
Drug Delivery Device .....	151
9.1 Ocular Implant .....	151
9.2 Drug Eluting Stent .....	154
9.3 Management of Pain, Cancer and other Chronic Diseases .....	155
9.4 Neural or Brain Implant .....	157
Chapter 10: Conclusions .....	159
<i>Appendix I – Drug Release Study Data (Tables and Calculations for</i>	
<i>Chapters 2, 5, and 6).....</i>	164
<i>Appendix II – Dose Response Study Data (Tables and Calculations for</i>	
<i>Chapter 8) .....</i>	215
References.....	228
VITA.....	267

## List of Tables

Table 2.1:	Statistical Analysis of Nanoporous Wafers using Dimensions obtained from AFM .....	35
Table 2.2:	Drug Loading Data (N=3).....	37
Table 3.1:	Cobalt-Chromium L605 Alloy Composition.....	64
Table 3.2:	The coating composition obtained using EDS from the three separate batches of coated polyimide tubes. ....	65
Table 4.1:	Drug loading data of polyimide tubes loaded with prednisolone.....	86
Table 5.1:	The table illustrates the absorbance readings (A) used for the construction of standard curve. Intraday and interday precision was calculated by analyzing standard solutions at predetermined intervals.....	100
Table 5.2:	The table illustrates the absorbance readings (A) used for the construction of standard curve. Intraday and interday precision were calculated by analyzing standard solutions at predetermined intervals.....	105
Table 5.3:	The table illustrates the absorbance readings (A) used for the construction of standard curve. Intraday and interday precision were calculated by analyzing standard solutions at predetermined intervals.....	109

Table 8.1:	The table illustrates the standard absorbances (A) that were used to estimate the parameters a, b, and c for 20 micron group. ....	145
Table 8.2:	The table illustrates the standard absorbances (A) that were used to estimate the parameters a, b, and c for 30 micron group. ....	145
<b><i>Appendix I – Drug Release Study Data (Tables and Calculations for Chapters 2, 5, and 6)</i></b>		
Table 2.3:	Standard curve measurements for estimation of drug release data from the nanoporous wafers. ....	164
Table 2.4:	Drug release data from nanoporous wafer-1 loaded with methyl orange and 2-octyl cyanoacrylate as the drug polymer matrix. ....	164
Table 2.5:	Drug release data from nanoporous wafer-2 loaded with methyl orange and 2-octyl cyanoacrylate as the drug polymer matrix. ....	165
Table 2.6:	Drug release data from nanoporous wafer-3 loaded with methyl orange and 2-octyl cyanoacrylate as the drug polymer matrix. ....	165
Table 2.7:	Cumulative percentage of drug release data from the three nanoporous wafers. ....	166
Table 5.4:	Absorbance readings for ‘one hole’ group belonging to ‘small tubes’ .....	167

Table 5.5:	Absorbance readings for ‘two hole’ group belonging to ‘small tubes’ .....	168
Table 5.6:	Absorbance readings for ‘three hole’ group belonging to ‘small tubes’ .....	169
Table 5.7:	Cumulative amount of crystal violet released from ‘one hole’ group. The amount and cumulative amount values are in microgram units of weight. ....	170
Table 5.8:	Cumulative amount of crystal violet released from ‘two holes’ group. The amount and cumulative amount values are in microgram units of weight. ....	171
Table 5.9:	Cumulative amount of crystal violet released from ‘three holes’ group. The amount and cumulative amount values are in microgram units of weight. ....	172
Table 5.10:	Drug loading in ‘one hole’ group.....	173
Table 5.11:	Drug loading in ‘two holes’ group.....	173
Table 5.12:	Drug loading in ‘three holes’ group.....	173
Table 5.13:	Percentage cumulative drug released for ‘one hole’ group .....	174
Table 5.14:	Percentage cumulative drug released for ‘two holes’ group.....	175
Table 5.15:	Percentage cumulative drug released for ‘three holes’ group .....	176
Table 5.16:	Absorbance readings for ‘one small hole’ group belonging to ‘large tubes’ .....	177

Table 5.17:	Absorbance readings for ‘one big hole’ group belonging to ‘large tubes’ .....	179
Table 5.18:	Absorbance readings for ‘two holes’ group belonging to ‘large tubes’ .....	181
Table 5.19:	Cumulative amount of crystal violet released from ‘one small hole’ group belonging to ‘large tubes’. The amount and cumulative amount values are in microgram units of weight.....	183
Table 5.20:	Cumulative amount of crystal violet released from ‘one big hole’ group belonging to ‘large tubes’. The amount and cumulative amount values are in microgram units of weight.....	186
Table 5.21:	Cumulative amount of crystal violet released from ‘two holes’ group belonging to ‘large tubes’. The amount and cumulative amount values are in microgram units of weight.....	189
Table 5.22:	Drug loading data for ‘one small hole’ group.....	192
Table 5.23:	Drug loading data for ‘one big hole’ group. ....	193
Table 5.24:	Drug loading data for ‘two holes’ group.....	194
Table 5.25:	Percentage cumulative drug released for ‘one small hole’ group .....	195
Table 5.26:	Percentage cumulative drug released for ‘one big hole’ group .....	198

Table 5.27:	Percentage cumulative drug released for ‘two holes’ group.....	201
Table 5.28:	Absorbance readings (A) for ‘200 micron’ group belonging to ‘large tubes without holes’ .....	204
Table 5.29:	Absorbance readings (A) for ‘400 micron’ group belonging to ‘large tubes without holes’ .....	204
Table 5.30:	Absorbance readings (A) for ‘600 micron’ group belonging to ‘large tubes without holes’ .....	204
Table 5.31:	Cumulative amount of crystal violet released from ‘200 microns group. The amount and cumulative amount values are in microgram units of weight.....	205
Table 5.32:	Cumulative amount of crystal violet released from ‘400 microns’ group. The amount and cumulative amount values are in microgram units of weight.....	206
Table 5.33:	Cumulative amount of crystal violet released from ‘600 microns’ group. The amount and cumulative amount values are in microgram units of weight.....	207
Table 5.34:	Drug loading data for 200, 400, and 600 microns group.....	207
Table 5.35:	Percentage cumulative drug released for ‘200 microns’ group .....	208
Table 5.36:	Percentage cumulative drug released for ‘400 microns’ group .....	209
Table 5.37:	Percentage cumulative drug released for ‘600 microns’ group .....	210

Table 6.1:	The table illustrates the absorbance readings (A) used for the construction of standard curve. Intraday and interday precision was calculated by analyzing standard solutions at predetermined intervals.....	211
Table 6.2:	Absorbance readings for drug release study in phosphate buffered saline.....	212
Table 6.3:	Absorbance readings for drug release study in vitreous humor from the rabbit's eye.....	212
Table 6.4:	Cumulative amount of crystal violet released in phosphate buffered saline. The amount and cumulative amount values are in microgram units of weight.....	213
Table 6.5:	Cumulative amount of crystal violet released in vitreous humor. The amount and cumulative amount values are in microgram units of weight.....	214
Table 8.3:	Luminescence values (in relative luminescence units) from 20 micron group polyimide tubes .....	215

***Appendix II – Dose Response Study Data  
(Tables and Calculations for Chapter 8)***

Table 8.4:	Calculation of cumulative luminescence values from values in Table 8.3 .....	216
Table 8.5:	Luminescence values (in relative luminescence units) from 30 micron group polyimide tubes .....	217

Table 8.6:	Calculation of cumulative luminescence values from values in Table 8.5 .....	218
Table 8.7:	Absorbance values of the drug release samples belonging to the 20 micron group as obtained using ELISA.....	219
Table 8.8:	Concentration (ng/ml) of drug release samples belonging to 20 micron group obtained using ELISA.....	222
Table 8.9:	Original concentrations (ng/ml) for 20 micron group.....	222
Table 8.12:	Absorbance values of the drug release samples belonging to the 30 micron group as obtained using ELISA.....	223
Table 8.13:	Concentration (ng/ml) of drug release samples belonging to 30 micron group obtained using ELISA.....	226
Table 8.14:	Original concentrations (ng/ml) for 30 micron group.....	226
Table 8.15:	Amount of ethinyl estradiol released for 30 micron group.....	227
Table 8.16:	Cumulative amount of ethinyl estradiol released (ng) from 30 micron group over 30 days. ....	227

## List of Figures

Figure 1.1:	Zero-Order Release Curve .....	8
Figure 1.2:	A schematic diagram of Ocusert <sup>®</sup> . The pilocarpine core is sandwiched in between two polymeric membranes which control the release rate [19].....	10
Figure 1.3:	Progestasert <sup>®</sup> [31] .....	11
Figure 1.4:	Implantation procedure for Norplant <sup>®</sup> [40].....	12
Figure 1.5:	An elementary osmotic pump .....	14
Figure 1.6:	The push-pull osmotic delivery system .....	14
Figure 1.7:	A schematic diagram of Retisert <sup>®</sup> .....	16
Figure 1.8:	A schematic diagram of Iluvien <sup>®</sup> .....	16
Figure 1.9:	The drug delivery system with microholes on the surface. The holes are equidistant from each other and from the ends of the tubes. The size of the device and the perforations can be scaled to fit the need of the therapeutic application.....	17
Figure 2.1:	An aluminum coated stainless steel tube at 50X magnification .....	24
Figure 2.2:	An aluminum coated stainless steel tube at 50,000 X magnification .....	24
Figure 2.3:	The aluminum coating was fractured after treatment with PBS for seven days (Magnification: 100X) .....	25

Figure 2.4:	The fractured coating at 10,000 X magnification .....	25
Figure 2.5:	A skeleton design of a bare metal stent composed of 87 mini cylindrical rods .....	26
Figure 2.6:	SEM pictures of the stent were used to estimate the length of the cylindrical rods .....	27
Figure 2.7:	Silicone wafer (Magnification: 500,000 X) .....	27
Figure 2.8:	Gold coated silicone wafer (Magnification: 200,000 X) .....	28
Figure 2.9:	Nanoporous gold coated silicone wafer (Magnification: 200,000 X) .....	28
Figure 2.10:	XRD spectra of alumina coating (sample).....	30
Figure 2.11:	XRD spectra of alumina (standard) .....	31
Figure 2.12:	Elemental composition obtained from EDS shows high percentage of both aluminum and oxygen in the coating. ....	31
Figure 2.13:	Sharp peaks of oxygen and aluminum confirmed the presence of alumina in the sample.....	32
Figure 2.14:	The figure shows the nanopores as analyzed using AFM (a) - (Top) - The section analysis of 1 $\mu\text{m}^2$ area of the wafer using AFM shows top view of the nanopores as indicated by brown region and was used to analyze the depth of the pores (b) - (Bottom) - The particle analysis of 1 $\mu\text{m}^2$ area of the wafer using AFM shows horizontal view of the nanopores as indicated by the red region and	

	was used to analyze the length, width, and area of the pores in the wafers .....	34
Figure 2.15:	SEM picture of a nanoporous gold silicon wafer treated with methyl orange and cyanoacrylate. ....	36
Figure 2.16:	A cumulative % release profile of methyl orange from cyanoacrylate polymer matrix. Values are presented as mean with standard deviation, n = 3. ....	37
Figure 3.1:	A comparison of the two DES, Cypher and Taxus stents with their bare metal stent counterparts, BxVelocity and Express respectively 28 days after implantation. The bare metal stents are completely endothelialized whereas, the drug coated stents show incomplete endothelialization due to drug over exposure [118]. ....	42
Figure 3.2:	A design of the DES comprising of a stent skeleton mounted with perforated tubes. ....	45
Figure 3.3:	A sketch of the perforated microtube. The device consists of a micro tube with micro perforations on one side of its surface. The diameter of the device can range from several micrometers to millimeters. The hole size can range from 20 $\mu\text{m}$ to several hundred microns depending on the need of the application. ....	46
Figure 3.4:	The drug is released from the drug delivery device into the targeted site. ....	46

Figure 3.5:	Optimal diameter of the stent and the optimal distance between connectors was calculated using above SEM pictures.....	50
Figure 3.6:	SEM pictures used to estimate the length and width of the arms and connectors.....	51
Figure 3.7:	At t = 0 minutes, the electropolished stent ( <b>A</b> ) showed a smooth surface whereas the unpolished device's surface ( <b>B</b> ) was originally rougher. Blood exposure for 120 minutes resulted in cell deposition on few areas of the electropolished stent's surface ( <b>C</b> ). In contrast, the unpolished device developed a rough coating consisting of large amounts of cell deposition (mainly platelets and macrophages) and fibrin ( <b>D</b> ) [136]. .....	54
Figure 3.8:	Sputtering mechanism for coating of a metal ion onto a polyimide substrate [139] .....	55
Figure 3.9:	Holes are made on the surface of the polyimide matrix using photolithography techniques. ....	57
Figure 3.10:	Initial sketch of the stent that was designed. Here, the three nodes of the structure are marked with letters A, B, and C. The nodes serve as reference point to indicate any shortening of length after expansion.....	59
Figure 3.11:	The nodes A, B, and C become misaligned after expansion indicating uneven expansion and stent shortening.....	60

Figure 3.12:	The nodes of the stent struts were rounded to distribute the stress evenly during expansion. ....	60
Figure 3.13:	Even and symmetric expansion of the stent after modification of the initial design. ....	61
Figure 3.14:	A 3-D model of the design. ....	61
Figure 3.15:	Particle size distribution of prednisolone from three experiments obtained using Malvern Mastersizer. A 20 micron reference line is drawn to estimate the percentage of particles below that value. ....	63
Figure 3.16:	Polyimide surface without coating. Root mean square roughness is 0.97 nm. ....	67
Figure 3.17:	Polyimide surface after coating with Co-Cr L605 alloy. Root mean square roughness is 0.62 nm. ....	67
Figure 3.18:	Holes produced by photolithography on polyimide tubes. ....	68
Figure 4.1:	Molecular structure of prednisolone [158]. ....	72
Figure 4.2:	Molecular structure of ethinyl estradiol [175]. ....	73
Figure 4.3:	Molecular structure of crystal violet [187]. ....	74
Figure 4.4:	Drug loading using touhy borst adapter. ....	77
Figure 4.5:	Polyimide tubes with different number of holes on the surface. The holes are equidistant from each other and also from the ends of the tube. ....	78

Figure 4.6:	Large tubes without holes. Crystal violet was loaded into the tubes and one end was sealed using biocompatible glue and other end was left open for drug release. ....	80
Figure 4.7:	Prednisolone crystals after evaporation of alcohol .....	83
Figure 4.8:	Modulated differential scanning calorimetric (MDSC) thermogram of anhydrous prednisolone. ....	83
Figure 4.9:	Modulated differential scanning calorimetric (MDSC) thermogram of alcohol treated (ethanolates) prednisolone.....	84
Figure 4.10:	Comparison of modulated differential scanning calorimetric (MDSC) thermograms of untreated and alcohol treated anhydrous ethinyl estradiol. ....	85
Figure 4.11:	The circle region shows void spaces inside the polyimide tube loaded with prednisolone. The void spaces are indicated by black arrows and the drug filled regions are indicated by blue arrows. The white line at the centre is the reflection of the light.....	87
Figure 4.12:	Three group of polyimide tubes with one hole, two holes, and three holes respectively were loaded with crystal violet. Statistical significant difference was not observed between the groups. Results are reported as mean with standard deviation, $p > 0.05$ ( $n=7$ )......	88
Figure 4.13:	Drug loading in 'large tubes' was found to be uniform per unit length and statistical difference was not observed	

	amongst the groups. Results are reported as mean with standard deviation, $p > 0.05$ (n=12).....	89
Figure 4.14:	Drug loading in subsets belonging to ‘large tubes without holes’. Polyimide tubes with different diameters, 200 microns, 400 microns, and 600 microns respectively were loaded with crystal violet. The drug loading in 600 micron group was found to be significantly different than the other two groups. Results are reported as mean with standard deviation, *: $p < 0.05$ (n=4).....	90
Figure 4.15:	Drug (EE) loading in 20 and 30 micron tubes was found to be uniform with no statistical significant difference amongst the tubes with respect to each other. Results are reported as mean with standard deviation, $p > 0.05$ (n=7). .....	91
Figure 4.16:	Ethinyl estradiol loaded polyimide tube (bottom) in contrast to an empty tube (top). The region circled in red shows empty spaces left inside the tube after alcohol was evaporated indicating uneven distribution of drug. ....	91
Figure 5.1:	Standard curve for crystal violet solutions ( $y = 0.0984x + 0.0001$ ; $R^2 = 0.9996$ ) used for drug release studies of ‘Small Tubes’. Data is presented as mean with standard deviation.....	101
Figure 5.2:	Cumulative amount of drug released as a function of time. A constant amount of drug was released from the three	

	subsets exhibiting zero-order rate. Each curve represents seven tubes. Data is presented as mean with standard deviation.....	102
Figure 5.3:	Comparison of cumulative amount of CV released from the three groups after 28 days. A linear relationship between release rate and number of holes was observed. The release is $220.1 \pm 25.0$ , $455.7 \pm 95.6$ , and $628.9 \pm 128.2$ ng for one hole, two holes, and three holes group. Data is presented as mean with standard deviation.....	103
Figure 5.4:	Cumulative % of crystal violet released from the three subsets. Assuming zero order release, the total duration of drug release from one hole, two holes, and three holes subsets correspond to drug release of more than five years. Data is presented as mean with standard deviation. ....	104
Figure 5.5:	Standard curve for crystal violet solutions ( $R^2 = 0.9982$ ; $y = 0.1051x - 0.0262$ ) which was used in the drug release studies with 'Large Tubes'. Data is presented as mean with standard deviation. ....	106
Figure 5.6:	The release profile of CV from the three subsets. Each curve represents twelve tubes. Data is presented as mean with standard deviation. ....	107
Figure 5.7:	Standard curve for crystal violet solutions ( $y = 0.046x - 0.0026$ ; $R^2 = 0.9999$ ) used for drug release studies with	

	‘Large Tubes without Holes’. Data is presented as mean with standard deviation. ....	110
Figure 5.8:	Cumulative amount of crystal violet released from three groups with different hole sizes, 200, 400, and 600 microns. Each curve represents four tubes. Data is presented as mean with standard deviation.....	110
Figure 5.9:	The release of crystal violet from two holes is depicted. Release of drug from each hole is independent of the other. The regions where holes are present on the tube have been circled in red. The dimension of the tube is 1000 microns and the holes size is approximately 400 microns.....	111
Figure 5.10:	The cumulative amount of CV released from the three groups (200 microns, 400 microns, and 600 microns) is plotted for each day for seven days. As indicated by the equation of line, the drug release rates from the three groups obey a perfect quadratic relationship. Data is presented as mean with standard deviation.....	115
Figure 6.1:	Standard curve for crystal violet in vitreous humor ( $R^2 = 0.9974$ , $y = 0.0291x + 0.0005$ ). Data is presented as mean with standard deviation. ....	119
Figure 6.2:	Comparison of crystal violet release in PBS (circles) and vitreous humor (squares). Each curve represents six tubes.	

	A linear release was observed in both the mediums. Data is presented as mean with standard deviation. ....	120
Figure 7.1:	Contact angle measurements of untreated and alcohol treated polyimide film. Results are shown as mean with standard deviations (n= 5).....	127
Figure 7.2:	Uncoated (top) and coated (bottom) polyimide matrices. ....	128
Figure 7.3:	RAW cells adhered well to both the uncoated (top) and alloy coated (bottom) polyimide tubes .....	129
Figure 7.4:	Four different groups: Coated and uncoated polyimide, control and LPS treated cells were analyzed for expression of TNF- $\alpha$ using Real Time RT-PCR. Polyimide tubes showed significantly lesser expression of the inflammatory marker. Data is represented as mean with standard deviation. ....	131
Figure 7.5:	Four different groups: Coated and uncoated polyimide, control and LPS treated cells were analyzed for expression of IL-1 $\beta$ using Real Time RT-PCR. Polyimide tubes showed significantly lesser expression of the inflammatory marker. Data is represented as mean with standard deviation. ....	132
Figure 8.1	Mechanism of luciferase gene reporter system employed in the dose response study. (A) Ethinyl estradiol is released from the tubes into the PBS solution. (B) The cells are	

dosed with the drug solution. (C) The drug binds to the EE receptors. (D)The drug-receptor complex binds to the ERE and activates the luciferase reporter gene. Luminescence is produced on addition of luciferin. The luminescence (response) is produced in vitro as a function of amount of ethinyl estradiol released from the drug delivery device (dose).....135

Figure 8.3: Assessment of T47D-KBluc cells in presence of various controls. Vehicle = Negative Control with Dosing Media only; Background = Vehicle plus 1.0  $\mu$ M fulvestrant; Agonist is Positive Control (0.1nM E2); Antagonist is 0.1nM E2 plus 1.0  $\mu$ M fulvestrant. Data is presented as mean with standard deviation (n=3) .....140

Figure 8.4: Dose response of the T47D-KBluc cells with increasing concentrations of ethinyl estradiol (n=3). Data is presented as mean with standard deviation.....141

Figure 8.5: Dose-Response Data with 30 micron and 20 micron group. The cumulative luminescence response from cells was linear to the dosing samples from the two groups (30 microns:  $R^2 = 0.9965$  and 20 microns:  $R^2 = 0.9955$ ). Data is presented as mean with standard deviation ( n = 6 for 20 micron group; n = 7 for 30 micron group).....142

Figure 8.6:	A model standard curve for a typical competitive ELISA assay (solid line). The parameters a, b, and c are obtained using the logistic model. The dotted lines represent the family of curves illustrating the effect of the slope factor, b, on the linear portion of the curve. As 'b' increases the curve would become steeper and vice versa. The raw data are fitted to the logistic model. ....	144
Figure 8.7:	The standard curve for the 20 micron group was constructed and fitted using non linear regression logistic model. The solid line represents the curve fitting regression line. Blue squares represent the absorbance readings of the standard solutions, n=2. ....	146
Figure 8.8:	The standard curve for the 30 micron group was constructed and fitted using non linear regression logistic model. The solid line represents the curve fitting regression line. Blue squares represent the absorbance readings of the standard solutions, n=2. ....	146
Figure 8.9:	Cumulative Amount of EE released from 20 micron group over 30 days. The release profile exhibits a zero order kinetics with $R^2 = 0.9990$ . The slope of the line suggests the rate of EE release of $32.7 \pm 7.3$ ng/day. Data is presented as mean with standard deviation, n=6. ....	148

Figure 8.10:	Cumulative amount of EE released from 30 micron group over 30 days. The release profile exhibits a zero order kinetics with $R^2 = 0.9996$ . The slope of the line suggests the rate of EE release of $30.1 \pm 5.8$ ng/day. Data is presented as mean with standard deviation, n=7. ....	149
Figure 9.1:	Anatomy of the Eye [287].....	153
Figure 9.2:	The figure demonstrates the flexibility of the drug delivery which is capable of conforming to any shape and curvature and hence can be successfully used as an ophthalmic implant .....	153
Figure 9.3:	(Left) A bare metal stent. (Right) Drug delivery system (shown also in inset) can be mounted on top of the stent. The stent will open the clogged artery and the controlled release of drug from the device will prevent restenosis.....	155
Figure 9.4:	A transdermal patch containing multiple drug delivery devices.....	157

## **Statement of Objectives and Significance of Research**

Zero order drug release is defined as a mechanism wherein a drug is released at equal increments from the reservoir per unit time. Linear drug release profiles provide a more stable therapeutic drug level over time and therefore provide a more predictable clinical response. Ideal drug delivery processes would therefore be expected to exhibit zero-order kinetics.

This dissertation is the result of an effort to develop a micro scalable perforated drug delivery system that is capable of long-term zero order delivery of drugs locally to the desired site. As such the device may be useful for management of debilitating and chronic conditions that require long-term drug therapy. The device is manufactured from an impermeable and biocompatible material. In its most basic form, the medical device acts as a housing for the drug reservoir, and means for facilitating release of drug from the drug reservoir to an anatomical site. It has holes of various sizes penetrating the wall of the device allowing interaction of the drug with the surrounding environment. The release of the drug from the device is achieved without the use of a release control polymer or a membrane. Physicochemical parameters of the drug such as solubility, molecular weight, and density loaded inside the device influence the drug release. The holes on the surface of the device are fabricated in a symmetrical manner such that they are equidistant from each other and from the ends of the device. In addition, the size of the holes is comparatively lesser than the total device size which enables the drug release from each hole to be independent of each other. The delivery system should be able to

deliver a variety of pharmaceutical agents for treatment of various diseased states such as cancer, pain management, and for ophthalmic diseases.

The following specific aims were proposed:

1. Determine if nanoporous metal surfaces could be used as templates for drug delivery devices. The study was done as preliminary work to develop a novel drug eluting stent. This study was discontinued when problems with production occurred and evolved into the concept of diffusion of a drug across a hole present on the surface of a microtube.
2. Design and develop a drug delivery platform consisting of perforated microtubes that are capable of exhibiting zero-order drug release. The development process included selection of appropriate dimensions, material, and technique for its manufacture.
3. Develop methods for loading of the device using a model drug.
4. Perform *in vitro* drug release studies:
  - a. To evaluate the scalability of the micro perforated drug delivery system.
  - b. To evaluate the capability of the drug delivery system for long-term zero order drug release.
5. Perform *ex vivo* drug release studies in vitreous humor from the rabbit's eye.
6. Evaluate the micro perforated drug delivery system for a second drug, ethinyl estradiol, producing a biological response in T47D-KBluc cells using estrogen-responsive luciferase reporter system

Although considerable advancements have occurred in controlled release technology, oral and parenteral formulations still face challenges in delivering drugs

across a physiological barrier. For instance, blood-brain, blood-eye, and blood-cerebrospinal fluid barriers are very selective in regulating the type of molecules that can move across them. Therefore there is a need to be able to locally deliver drugs to these sites in a controlled manner.

Another problem commonly observed during management of chronic diseases such as diabetes, hypertension, and uveitis is the need for repeated and frequent dosing of the patient. For example, repeated injections that are required in management of Type 1 diabetes are inconvenient and painful to patients. As such, long-term therapies are generally inconvenient and generally result in patient noncompliance. Long-term therapies often result in patient noncompliance. Current interventional techniques have been developed that are capable of long-term release. However, these technologies can only last up to several days or months and need replacement thereafter.

Additionally, new advancements in drug discovery bring in new and complex molecules that are not compatible with the standard modes of drug delivery. For example, drugs based on proteins and peptides get denatured easily in the digestive environment when given by oral route. A solution to this problem would be to develop a drug delivery device that can also protect the drug under hostile physiological environments. At the same time, the device will also prevent release of toxic amounts of the drug in the body. Therefore, this dissertation is a result of a need of a drug delivery system that can provide following characteristics:

1. The device must be capable of long-term zero order drug release. This will ensure constant amounts of drugs being delivered to the desired site for prolonged periods.

2. The drug delivery device must reduce the need for repeated dosing. This translates into reduced healthcare costs, reduce hospital visits, and improve patient compliance.
3. The drug delivery should be implantable and capable of local drug delivery. This will reduce the problems associated with biological barriers, increase efficacy, and decrease side effects associated with conventional drug that are delivered to the entire body
4. The device should be able to be used for diverse diseased states, such as cancer and pain management and can be tailor made to deliver a variety of small molecules, proteins and peptides, biomarkers, and genetic material.
5. The drug delivery device should improve patient comfort by decreasing risk, pain, and inconvenience to the patient.
6. The device must be inert, robust, impermeable, and biocompatible protecting the body from leakage of the drug and inappropriate dosing.

The project was initiated with an aim to develop a polymer free drug delivery device with an emphasis on developing a DES. Since polymers, which were needed for controlled drug release, were causing vascular complications such as restenosis and thrombosis in stents, a polymer free system was envisioned. Nanoporous surfaces were evaluated for their capability to hold drugs. Although, nanoporous surfaces demonstrated promising results in drug elution, the novel idea of developing a micro-perforated drug delivery micro-device was further investigated.

The micro drug delivery system hence developed offers specific advantages -

1. It is free from initial burst release of drugs.
2. It can be manufactured from a variety of biocompatible materials.
3. It can be made from both metal and non metal surfaces keeping the metal to artery ratio minimal and thus inhibiting the prevalence of any immunogenic response from the body due to injury during device implantation.
4. As the device can be made from non-metal surfaces hence it is MRI safe.
5. The device after implantation should require minimal post surgical supervision.
6. It is scalable and the device size and the hole size can be tailor made to fit the requirements for management of a specific diseased states.
7. Due to its micro size and flexibility the device can be implanted at complex anatomical sites such as glands, eye, coronary arteries, and cerebro-spinal regions.

# **Chapter 1: Local Drug Delivery Devices for Long-term Zero Order**

## **Release**

### **1.1 NEED FOR A DRUG DELIVERY SYSTEM FOR LONG-TERM ZERO ORDER**

#### **RELEASE**

Oral, topical and inhalation are the oldest modes of drug administration. The modern era has witnessed development of alternate routes such as, systemic, intravitreal, and pulmonary delivery of drugs. The new and conventional routes of drug delivery have been well accepted due to many advantages that they offer. Tablets, capsules, eye drops, creams and lotions offer convenience and ease of use. Intravenous injections deliver drug directly into the blood stream achieving high bioavailability and less wastage and is essential for drugs that are not well absorbed by other routes. Pulmonary drug delivery enables delivery of poorly absorbed drugs, such as insulin and vasopressin for treatment of diabetes insipidus, without encountering the first pass hepatic metabolism [1, 2].

However, these popular modes of drug administration have limitations. Injections, intravenous or otherwise, are inconvenient, especially when repeated dosing is required to treat chronic conditions. In such circumstances, a patient is either required to return to a medical professional regularly or must learn to self inject (such as for diabetes mellitus). Apart from the discomfort and nuisance, there is also the risk of infection if the needle is not clean.

Topical delivery intended for dermal use has limited applications. Skin imposes physiochemical obstacles to drug permeation [3]. A drug has to be adequately lipophilic

to be passively delivered via the skin [4]. Eye drops, although convenient, are very inefficient as about 95% of the applied drug is lost to absorption by the conjunctiva and through tear drainage [5]. The absorbed drug is released into the blood stream, where it can have detrimental side effects elsewhere in the body. An important example would be timolol which is used to treat glaucoma [6] but may also causes side effects such as, bronchospasms, depression, and heart failure [7].

Oral delivery systems also offer convenience in administration but not all drugs can be given orally. Some drugs may not be properly absorbed through the stomach wall; may be degraded by the gastrointestinal tract; or may irritate the stomach causing unwanted side effect. Insulin, a protein based drug, is one such example that cannot be given orally since it would be degraded by proteolytic enzymes and therefore, must be given by injection [8]. Pulmonary drug delivery is very wasteful and associated with low efficiency and poor reproducibility, thus increasing the treatment expenditure [9].

In addition, these traditional methods of drug delivery more commonly result in patient non-compliance or discomfort when used for treating chronic diseases. In lieu of these limitations, efforts have been made to achieve optimized drug therapy by developing controlled drug delivery systems. A zero-order release rate is desirable because a constant amount of drug is released over a period of time (Figure 1.1). The drug dose to be administered can be calculated to remain in the therapeutic range without the fear of overdose or underdose.

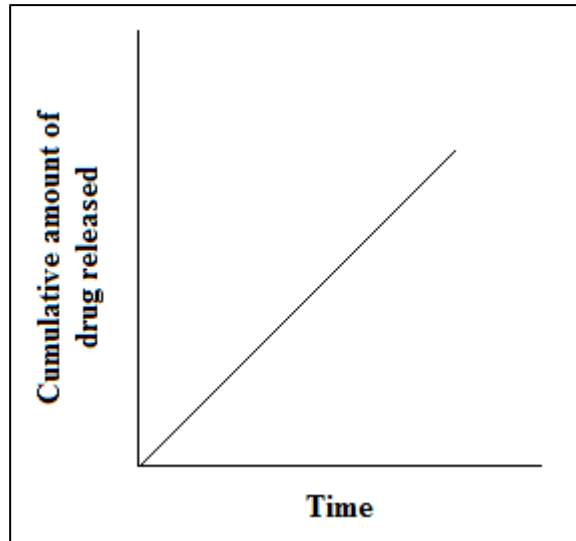


Figure 1.1: Zero-Order Release Curve

## **1.2 DRUG-DEVICE COMBINATION PRODUCTS AS IDEAL CONTROLLED DRUG DELIVERY SYSTEMS**

Targeted and controlled delivery of drugs is a relatively new technology. Drug device combination systems have their origins in mid 1960's when Dr. Judah Folkman first proposed the use of Silastic® tubing as an implant for prolonged drug therapy [10]. He accidentally discovered that when a silicone rubber tubing, which was used to supply blood to rabbits, is exposed to anesthetic gases, the rabbits fell asleep [11]. This observation gave him an idea to develop a reservoir type zero order drug delivery system. Folkman and other researchers have been interested in zero order and sustained release systems due to many advantages that they offer [12]:

1. Drug levels are continuously maintained at a desirable therapeutic range.

2. Adverse effects are reduced by targeting delivery to a specific site and avoiding distribution to unwanted tissues.
3. Dose of drug is decreased while mean residence time is increased.
4. A decrease in administered doses decreases patient trauma and improves patient compliance.
5. An inert and impermeable device protects the drug in the hostile environment.
6. Drugs that have short *in vivo* half-lives can be administered directly at the desired site.

Controlled drug delivery (CDD) devices have been designed as ingestible capsules, transdermal patches, implants, and ocular or vaginal inserts. In the following section, few of the commonly used zero-order drug delivery devices have been reviewed. The review will highlight the goal of this dissertation and will also help to understand the significance of CDD's as important therapeutic tools.

### **1.2.1 Ocusert<sup>®</sup>**

Ocusert<sup>®</sup> is a pilocarpine containing CDD device which was developed by Alza Corporation to treat glaucoma [13]. Alza Corporation, founded by Dr. Alejandro Zaffaroni in 1968, developed a zero-order CDD systems based on Folkman's observations [14]. This collaboration resulted in the development of world's first zero-order drug device combination product, called Ocusert<sup>®</sup> in the 1970's for treatment of

glaucoma. The device consists of Pilocarpine, a muscarinic agonist that decreases the intraocular pressure

Figure 1.2 illustrates the construction and dimension of Ocusert<sup>®</sup>. The device consists of a drug reservoir and a rate controlling membrane made of poly(ethylene-co-vinyl acetate) [15]. The device is placed in a manner similar to contact lenses. The Ocusert<sup>®</sup> system, continuously releases pilocarpine locally to the eye at a programmed rate of 20 -40  $\mu\text{g}$  per hour for seven days [16].. In comparison with the 2% or 4% eye drops of pilocarpine, the Ocusert<sup>®</sup> system proved effective in treatment of glaucoma but with fewer side effects [17, 18].

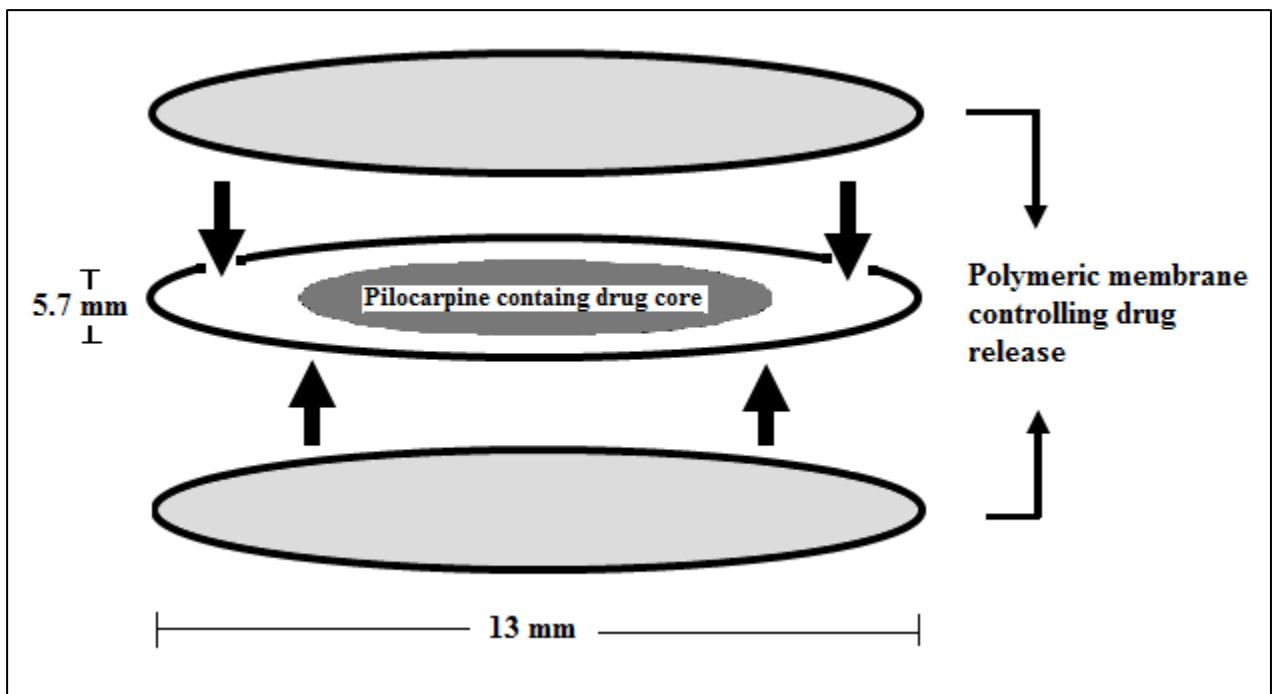


Figure 1.2: A schematic diagram of Ocusert<sup>®</sup>. The pilocarpine core is sandwiched in between two polymeric membranes which control the release rate [19]

### 1.2.2 Progestasert®

Progestasert®, an intrauterine device, is another CDD system which was developed by Alza Corporation [20]. As illustrated in Figure 1.3, the hollow stem of the T-shaped device serves as the reservoir for 38 mg progesterone. The hormone progesterone, is an important female reproductive hormone which is responsible for menstrual bleeding [21-23]. Progesterone makes the cervical mucus thicker and changes vaginal epithelium so that the sperm cannot reach the egg [24, 25]. The rate controlling membrane in the device is made of poly(ethylene-co-vinyl acetate) that provides an average release rate of 65 µg/day [20]. The device proved as an effective contraceptive device for at least one year [26-29]. In some countries such as France, Progestasert® is even approved for 18 months of use [30].

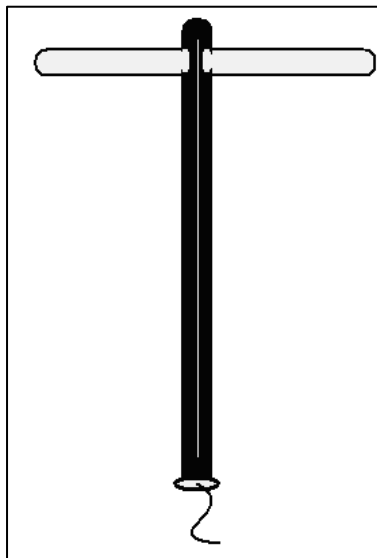


Figure 1.3: Progestasert® [31]

### 1.2.3 Norplant<sup>®</sup>

Norplant<sup>®</sup> is a levo-norgestrel subdermal implant consisting of a set of six small silastic capsules that are placed under the skin of a woman's upper arm (Figure 1.4). The implantation consists of a minor surgical procedure that lasts for 10-15 minutes. A local anesthetic is applied on the inside of the upper arm, and a small incision, about 2 mm long is made. The capsules are placed one at a time in a fan shape setting. Norplant<sup>®</sup> was developed by Population Council in 1983 as a direct extension of Dr. Folkmans findings of 1964 [32-35]. The Norplant<sup>®</sup> capsules are 34 mm long and 2.4 mm in diameter and contains 36 mg of levo-norgestrel [32]. The implant releases drug at a steady rate of 30  $\mu\text{g}/\text{day}$ . The implant was designed to last for up to five or six years [36]. The fertility can be restored within days of the implant removal and does not depend on duration of use [32, 36-39].

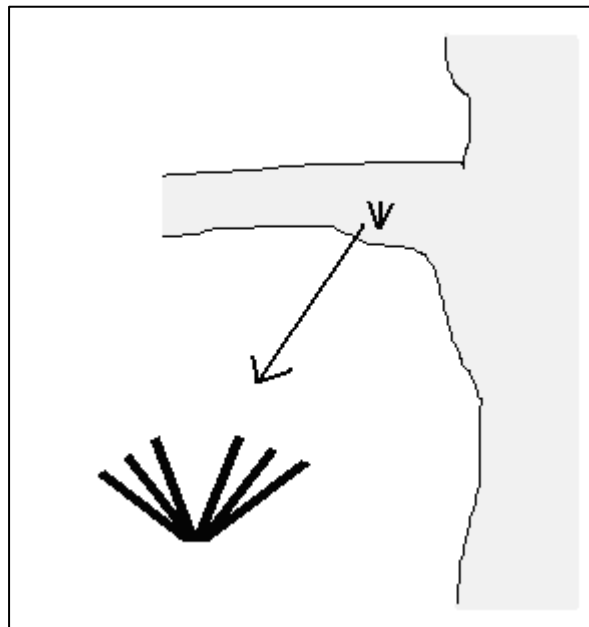


Figure 1.4: Implantation procedure for Norplant<sup>®</sup> [40]

#### 1.2.4 Osmotic Pumps (OROS<sup>®</sup> and DUROS<sup>®</sup>)

Development of osmotically controlled oral drug delivery systems (OROS<sup>®</sup>) was pioneered by Alza in 1980's and 1990's [14]. The simplest of such system is an elementary osmotic pump [41] wherein, a water soluble drug core is contained in a semi permeable membrane (Figure 1.5). The membrane is permeable to water but not to the drug molecules. An opening is drilled on the surface of the membrane to allow for drug release. As the water moves through the membrane due to osmosis, it pushes the drug out of the orifice. A similar system known as The OROS<sup>®</sup>/Push Pull System was designed by Alza to overcome the problem of delivering poorly soluble drugs. As illustrated in Figure 1.6, the OROS<sup>®</sup> system consists of a drug layer on top of an osmotically active push layer [41]. Pfizer used the push-pull osmotic technology to develop extended release tablets, namely Procardia XL (nifedipine) and Glucotrol XL (glipizide) for treatment of angina and high blood glucose, respectively. A single extended release tablet is capable of releasing the drug at a constant rate of over 24 hours [42-44]. The controlled delivery of the drugs into the gastrointestinal lumen using osmotic pumps is independent of pH or gastrointestinal motility.

Durect Inc. has used the OROS<sup>®</sup> technology to develop DUROS<sup>®</sup>, a 44 mm long and a 3.8 mm diameter osmotic implant made of titanium reservoir [45]. Developed for the delivery of leoprolide to treat prostate cancer, the DUROS<sup>®</sup> implant can hold 65 mg of the drug with a release rate of 120 µg/day for one year [46]. The implant can be used for site specific applications and can be scaled-up to hold 1000 mg of drug [45].

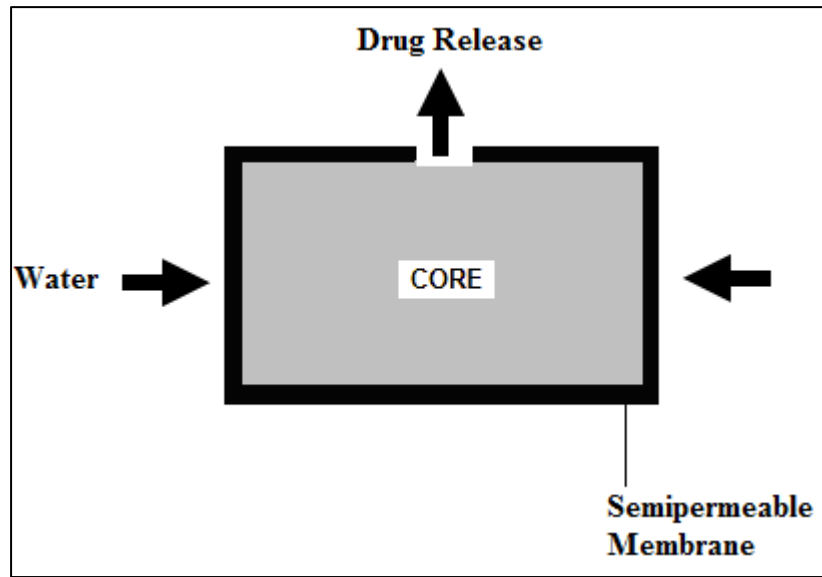


Figure 1.5: An elementary osmotic pump

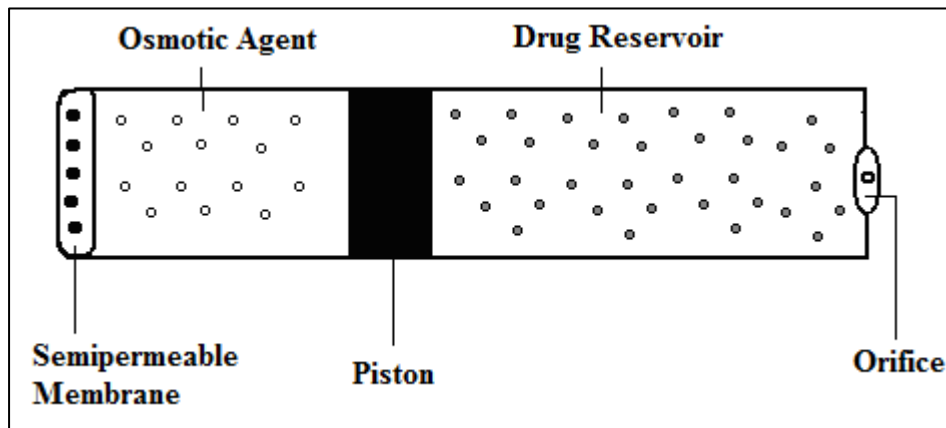


Figure 1.6: The push-pull osmotic delivery system

### 1.2.5 Vitrasert<sup>®</sup>, Retisert<sup>®</sup>, and Iluvien<sup>®</sup>

Vitrasert<sup>®</sup> and Retisert<sup>®</sup> are sustained release intraocular drug delivery devices marketed by Bausch & Lomb. The underlying technology was developed by Control Delivery Systems which was acquired by pSivida Corp. in 2005 [47]. Bausch & Lomb obtained the licensing rights of the devices in 2005 [48]. Vitrasert<sup>®</sup> was approved by FDA in 1996 whereas, Retisert<sup>®</sup> (Figure 1.7) which is a second generation reservoir style implant to Vitrasert<sup>®</sup> was approved by FDA in April 2005 [49-51]. Vitrasert<sup>®</sup> delivers ganciclovir for the treatment of cytomegalovirus retinitis, whereas Retisert<sup>®</sup> contains fluocinolone acetonide for the treatment of uveitis [52-54].

Each Vitrasert<sup>®</sup> Implant contains 4.5 mg of ganciclovir, and is designed to release the drug over a period of 5 to 8 month [55]. Retisert<sup>®</sup> consists of a compressed drug pellet in a silicone elastomeric cup, holds 0.59 mg of drug, and has nominal dimensions of 3 mm x 2 mm x 5 mm [56]. The implant is surgically placed into the vitreous humor. As the water enters through the orifice on the cup, the drug dissolves and diffuses out of the device with a constant release rate of approximately two years.

Iluvien<sup>®</sup>, is a third generation eye drug delivery systems designed for treatment of diabetic macular edema is currently in its Phase III clinical trials [57]. The device was licensed to Alimera Sciences in 2008 [58]. The device holds 2 mg of fluocinolone acetonide and measure 3.5 mm in length and 0.37 mm in diameter and releases 0.23 µg/day for three years [59]. Figure 1.8, illustrates a schematic diagram of Iluvien<sup>®</sup>.

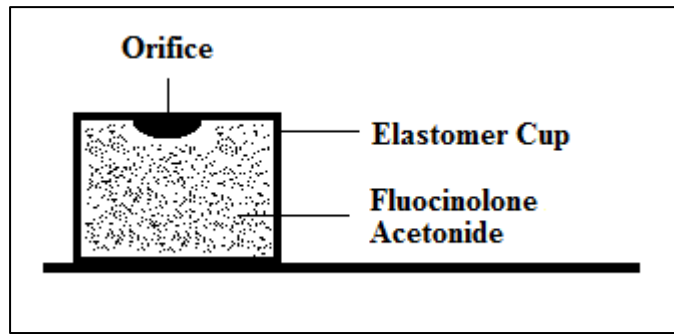


Figure 1.7: A schematic diagram of Retisert<sup>®</sup>

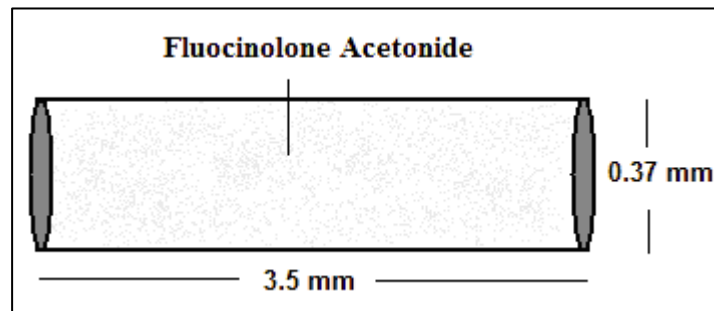


Figure 1.8: A schematic diagram of Iluvien<sup>®</sup>

### 1.3 INTRODUCTION TO A SCALABLE MICROPERFORATED DRUG DELIVERY DEVICE

The chronological review of previous drug delivery devices has pointed out one common fact. Over the years, the dimension of the device has decreased and the duration of release has increased. The constant reduction in size has improved immunological responses, biocompatibility, and reduced side effects associated with earlier devices [60, 61].

As a focus of this dissertation, a novel drug delivery system has been developed that can be fabricated in variable shapes and sizes. The device consists of an impermeable reservoir provided with microperforation through which the drug diffuses. If the drug has appropriate solubility, it will diffuse out through the holes following zero order kinetics. Figure 1.9 illustrates one such example of the device. The device is scalable and can measure as thin as a human hair [62] or bigger in size. The rate of drug release can range from several days to several years by manipulating the number of holes, size of the holes, size of the tube, length of the tube, drug density inside the tube, and solubility of the drug. The drug delivery system is multifunctional as it can be used for management of several diseased states depending on the drug loaded inside the device.

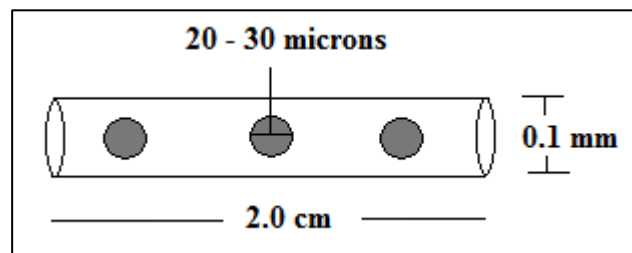


Figure 1.9: The drug delivery system with microholes on the surface. The holes are equidistant from each other and from the ends of the tubes. The size of the device and the perforations can be scaled to fit the need of the therapeutic application

The following chapters discuss the historical events that led to the development of the microperforated drug delivery system of Figure 1.9. The perforated device was being developed as a component of a drug eluting stent (DES). The idea of developing the perforated system as a general purpose drug delivery device was serendipitous as the

drug release studies (Chapter 5) suggested that the perforated tubes can be extended to other diseased states as well. However, before the perforated device was designed, the initial research efforts were focused exclusively on developing a DES. To achieve this goal, a nanoporous metal surface was characterized which could be potentially used to manufacture next generation DES. The nanoporous surfaces were developed in collaboration with Setagon Inc. The nanopores were loaded with a model drug and *in vitro* release studies were performed. Although extended release was observed, the primary objective to obtain zero order drug release rates was not achieved using the nanopores. This preliminary work with the nanoporous surfaces has been summarized in Chapter 2 of this dissertation.

The work with nanoporous surfaces was discontinued as a better idea of developing a DES composed of perforated microtubes (of Figure 1.9) was envisioned. The idea was to mount the drug releasing perforated microtubes on the stent skeleton (Figure 3.2, Chapter 3). Since, fabrication of the stent skeleton from a metal alloy was more of an engineering challenge than a pharmaceutical task; it was decided to fabricate the stent skeleton commercially. Accordingly, initial efforts were concentrated solely on developing and characterizing the drug eluting perforated tubes that could later be used with the stent skeleton. A step by step developmental process has been summarized in Chapter 3 with respect to designing of the stent, finding appropriate dimensions for both the stent and the perforated tubes, and fabrication of holes on the microtubes.

Once, the holes were fabricated on the microtubes, the next step was to load the tubes with drugs. Hence, in Chapter 4 drug loading data using different techniques and different drugs has been summarized.

The next step was to evaluate the drug loaded perforated tubes for their capability to produce zero order release rates. The delivery system was evaluated *in vitro* in phosphate buffered saline (PBS) and *ex vivo* in vitreous humor from the rabbit's eye. The corresponding drug release data has been summarized in Chapters 5 and 6. The release studies indicate that the perforated tube is capable of delivering drugs at zero order for long periods of time ranging from several months to several years. These results were unexpected and suggested that the perforated tubes by themselves are efficient drug delivery systems that can be used for management of diverse diseased states that require long-term therapy.

Hence, the focus of the dissertation has now broadened and involves development of a general purpose device and is not limited to merely DES, which now can be one of its many applications. The various therapeutic applications of the device have been summarized in Chapter 9 of this dissertation. Most of these applications require the device to be implanted. Since the success or failure of an implantable device greatly depends on how it interacts with the body, *in vitro* biocompatibility evaluation was performed and has been summarized in Chapter 7. In Chapter 8 of this dissertation, further proof of concept has been provided by evaluating the device's capability to release biologically significant doses in luciferase transfected cells.

## **Chapter 2: Preliminary Work with Nanopores and Metal Surface**

### **2.1 INTRODUCTION**

The research project was started with a goal to develop a novel drug eluting stent (DES). The idea was to manufacture a DES made up of a nanoporous metal surface, with nanopores acting as drug reservoirs. The initial efforts with nanoporous surfaces will be discussed in the present chapter. The reasons for investigating a nanoporous surfaces to improve drug delivery methods may be better understood after the following review of current developments in drug delivery methods.

Current targeted therapy is centered around nanoparticles which may help to decrease the drug toxicity by improving target specificity and delivery efficiency [63-66]. A popular example is Abraxane®, an albumin bound nanoparticles form of paclitaxel, which is free from solubilizers, shows excellent efficacy, and is less toxic than the original drug [67, 68].

While the earlier research has been focused on development of drugs, present methodologies target development of the delivery device itself [69-71]. Local delivery of a drug to a specific site enhances the safety and efficacy by improving its bioavailability and decreasing the side effects. In addition, an implantable drug delivery device offers various advantages such as maintenance of therapeutics blood levels, improved patient compliance, less wastage of drug, and avoidance of a repeated administration [72].

The past few years have witnessed advancements in nanotechnology. Nanorobots capable of treatment, prophylaxis, and diagnosis represent the next generation of drug

delivery devices [73, 74]. Carbon nanotubes have been developed to seek and destroy tumor cells [75]. Accordingly, conventional drug delivery devices such as stents, ocular implants, and nasal devices are also being fabricated as nano devices for better delivery of proteins, DNA, enzymes, and other biological materials. Recently, Martin et al tailored the width of microfabricated nanochannels to solute size and to control diffusion kinetics of macromolecules [76].

A nanoporous metal surface offers one such improvisation possibility for DES and was characterized for its drug loading and drug release capabilities. The drug can be loaded into the nanopores either as nanoparticles in solution form, or as a polymer-drug system. These pores can either be built directly on a surface or a nanoporous membrane can be adhered to the surface of an implant or a drug delivery device (e.g. stent).

Inorganic materials, such as aluminum and gold were evaluated as suitable surface materials to develop nanopores. Both aluminum and gold, have been extensively used in development of novel nano-diagnostic tools [77, 78]. They are known to improve the mechanical stability while maintaining the required biocompatibility and being soft materials, they also offer ease in fabrication [79-81].

Hence, initial efforts were directed towards evaluation of stainless steel and aluminum as prospective coating materials for future development of implant with depots on its surface. Stainless steel itself is biocompatible and offers good material properties [82-85]. However, in vitro testing of aluminum coating revealed oxidative instability in phosphate buffer. Hence, gold coating which is biologically inert [86, 87] was selected for fabrication of nanopores. The fabrication of the nanopores was undertaken by Nanomedsystems, (formerly Setagon, Inc.) (Charlottesville, VA, USA).

Nanopores were fabricated using photolithography techniques. Fabrication of nanostructures by lithography has been explained in detail in literature [88, 89]. Briefly, silicon wafers were coated with a combination of gold and silver. A photomask was used to transfer the pattern onto the wafer and a layer of photosensitive polymer (photo-resist) was applied using spin coating technique. The wafers were then exposed to ultraviolet light. The mask protects the portion of the wafer it covers, whereas, the uncovered part gets etched by light. Silver, which was used as a sacrificial material was precipitated out leaving nanopores behind.

The next step was to estimate the volume of the pores. Accordingly, nanopores were physically characterized using scanning electron microscopy (SEM) and atomic force microscopy (AFM). The dimensions of the nanopores were estimated and the measurements were used to determine the total volume of pores available for drug loading and the capability of a nanoporous surface as a suitable drug carrier. For purpose of estimation, a bare metal stent, was used as a reference. Hence, the volume of nanopores if they were built on a stent surface was calculated.

The drug loading capacity of nanopores was analyzed using a solution of 2 – octyl cyanoacrylate and methyl orange as the drug-polymer matrix. Methyl Orange (4-dimethylaminoazobenzene-4'-sulfonic acid, sodium salt) is a pH indicator commonly used in titrations [90]. Methyl orange was chosen as the model drug because it has sharp end point and gives a prominent color in solution, which assisted in its analysis both visually and spectrophotometrically. A solution of 2-octyl cyanoacrylate was used as the polymer matrix. Poly (2-octyl cyanoacrylate) is approved by FDA and is being currently used as a tissue adhesive [91]. Several articles in literature have suggested the use of

poly(alkylcyanoacrylates) as the drug carrier [92-94]. The drug-polymer mixture was loaded into the nanopores. The role of the polymer here is to control the release of methyl orange from nanopores, which would otherwise release quickly owing to its high solubility. The present investigation has also been recently published [95].

## **2.2 MATERIALS AND METHODS**

### **2.2.1 Materials**

Aluminum coated stainless steel tubes, bare silicon wafers, gold coated silicon wafers, and nanoporous gold-coated silicon wafers were obtained from Nanomedsystems, (formerly Setagon, Inc.) (Charlottesville, VA, USA). A bare metal stent (Palmaz-Schatz® Balloon-expandable stent, Size = 15 x 3.0 mm) was obtained from The University of Texas Health Sciences Centre, (San Antonio, TX, USA). Methyl Orange was obtained from Fisher Scientific (Pittsburgh, PA, USA). Band-Aid ® Brand Liquid Bandage, containing 2-octyl cyanoacrylate as the active ingredient, was obtained from the local CVS store (Austin, TX, USA).

### **2.2.2 Surface Analysis of Aluminum Coated Stainless Steel Tube**

Aluminum was selected for coating, as it is a soft metal and would thus facilitate drilling of pores. The durability of aluminum coated stainless steel tube was tested by immersing the tube in phosphate buffer saline (PBS, pH 7.4) for seven days. Scanning electron microscope (SEM) pictures of tubes were taken before (Figure 2.1 and 2.2) and after (Figures 2.3 and 2.4,) the PBS treatment using a Hitachi S-4500II microscope. As

illustrated in Figures 2.3 and 2.4, fractured coating with signs of corrosion was observed. The X-ray diffraction spectrometry (XRDS) and energy dispersive spectrometry (EDS) were used to detect if corrosion (alumina) was responsible for coating fracture.

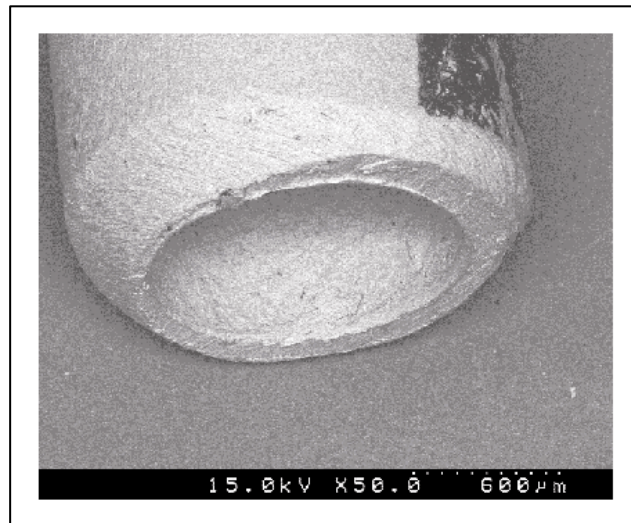


Figure 2.1: An aluminum coated stainless steel tube at 50X magnification

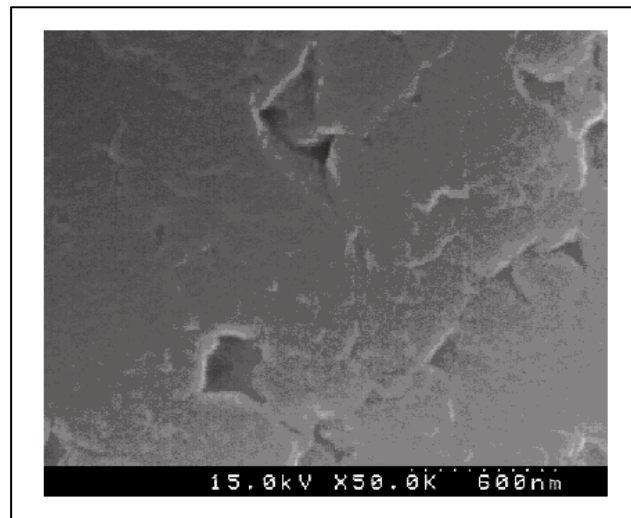


Figure 2.2: An aluminum coated stainless steel tube at 50,000 X magnification

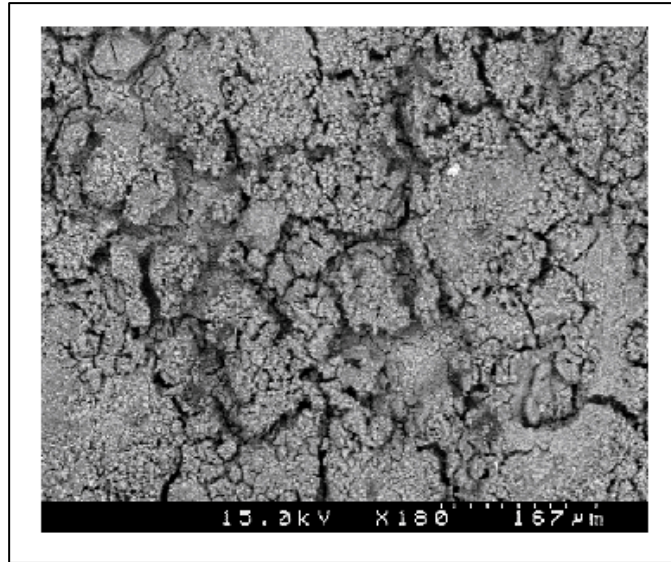


Figure 2.3: The aluminum coating was fractured after treatment with PBS for seven days (Magnification: 100X)

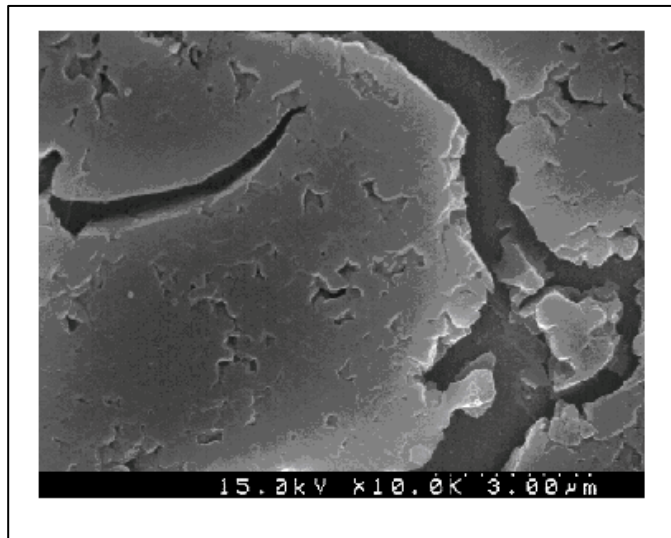


Figure 2.4: The fractured coating at 10,000 X magnification

### 2.2.3 Surface and Dimensional Analysis of Nanoporous Wafers

The bare metal stent was characterized using a Hitachi S – 4500II Scanning electron microscope. The stent is made of 87 mini cylindrical rods (Figure 2.5). The length, width, and thickness of the rods were estimated from SEM micrographs (Figure 2.6). Three wafers from each group of wafers were selected and their surface morphology was compared using the SEM (Figure 2.7, 2.8, & 2.9). Dimensional analysis of the nanoporous wafers were performed using SEM and atomic force microscopy (AFM). The AFM topographic images of the nanoporous wafers were analyzed using the ‘particle analysis’ and the ‘section analysis’ commands yielding length, width, area of the pores and depth of the pores, respectively. The software used in AFM was Nanoscope 5.12b48 and the cantilever used was of 300 kHz frequency.

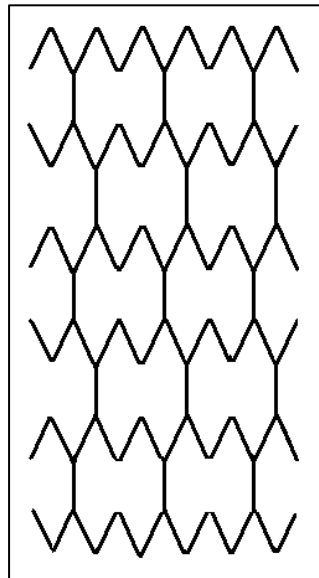


Figure 2.5: A skeleton design of a bare metal stent composed of 87 mini cylindrical rods

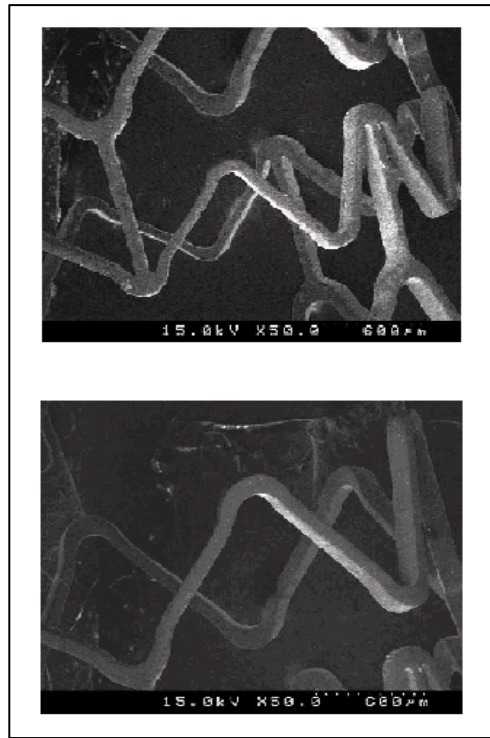


Figure 2.6: SEM pictures of the stent were used to estimate the length of the cylindrical rods

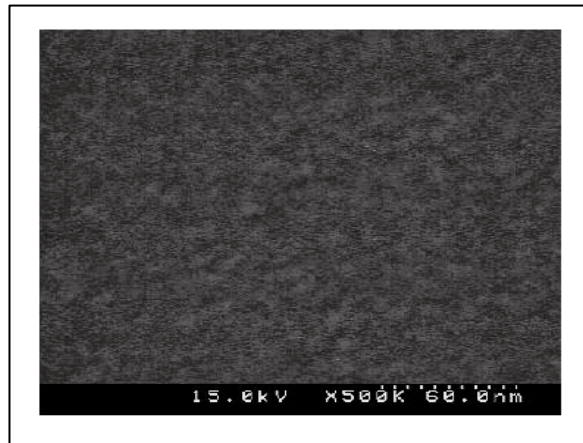


Figure 2.7: Silicone wafer (Magnification: 500,000 X)

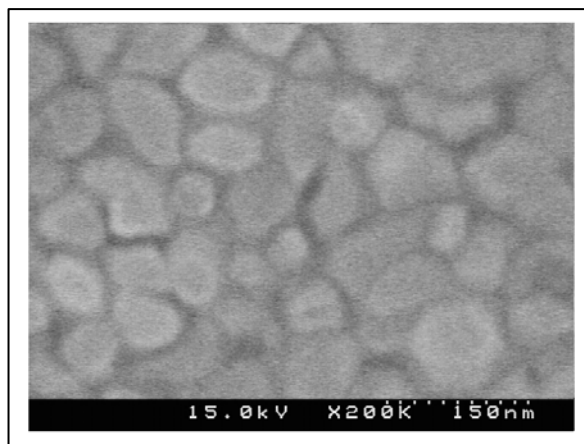


Figure 2.8: Gold coated silicone wafer (Magnification: 200,000 X)

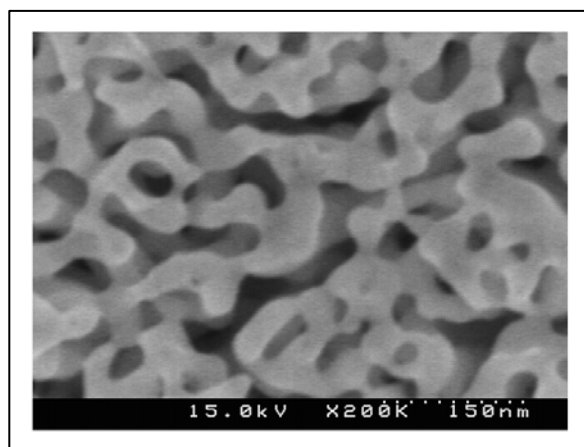


Figure 2.9: Nanoporous gold coated silicone wafer (Magnification: 200,000 X)

#### 2.2.4 Drug Loading of Nanoporous wafers

Three nanoporous wafers were weighed gravimetrically and a thin layer of an ethanolic solution of methyl orange was applied onto the surface. The silicon gold nanoporous surface was inert to alcohol. Afterwards, ethanol was evaporated using a heat gun. The wafers were weighed again to determine the amount of methyl orange loaded

onto each wafer. The gravimetric method proved to be accurate and precise in the weight range loaded in the nanoporous surface. A drop of 2-octyl cyanoacrylate solution was then applied onto the wafer followed by the addition of a drop of water for polymerization of the monomer. The weight of cyanoacrylate added was estimated using the weight difference of the drug loaded wafers before and after application of the cyanoacrylate. SEM pictures were then taken.

### **2.2.5 Drug Release Study**

The *in vitro* drug release study was performed in a non stirred environment according to a previously published method [96]. The drug loaded wafers were immersed in a vial containing 10 ml of distilled water. After each 24 hr period, the solution was collected and retained for absorbance measurements to assure even dispersion of the compound, placed in a clean quartz cuvette and its absorbance measured at 464 nm against a blank standard.

## **2.3 RESULTS AND DISCUSSION**

### **2.3.1 Detection of Oxidative Degradation of Aluminum Coating**

After immersing in PBS for seven days, the aluminum coating appeared to be fractured and corroded. The corrosion of aluminum which occurs due to its oxidation results in the formation of alumina,  $\text{Al}_2\text{O}_3$ . The detection of corrosion in the form of alumina was analyzed by X-Ray Diffraction Spectrometry (XRDS). However, XRDS didn't prove to be effective in detecting corrosion because of the amorphous nature of the

sample (coating). As illustrated in Figures 2.10 and 2.11, the XRD spectra obtained from sample didn't match with the standard.

In the next step, energy dispersive spectrometry (EDS) was used to analyse the alumina coating because by coupling SEM with EDS, it is possible to obtain the precise elemental composition of the material. As illustrated in Figure 2.12, high percentages of both aluminum (13.63%) and oxygen (57.83%) were obtained. Sharp peaks of aluminum and oxygen in the EDS spectra further confirmed the presence of alumina and hence corrosion in the sample (Figure 2.13). As a result, due to chemical and mechanical instability in the physiological environment, alumina was rejected as the coating material.

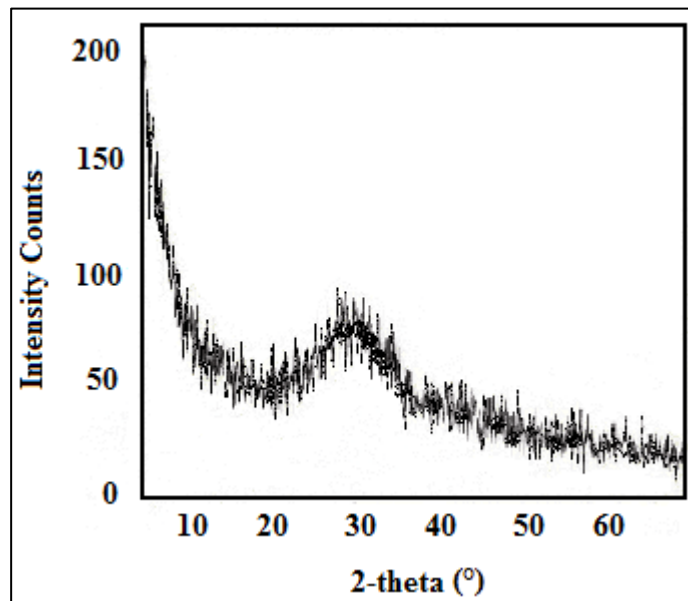


Figure 2.10: XRD spectra of alumina coating (sample)

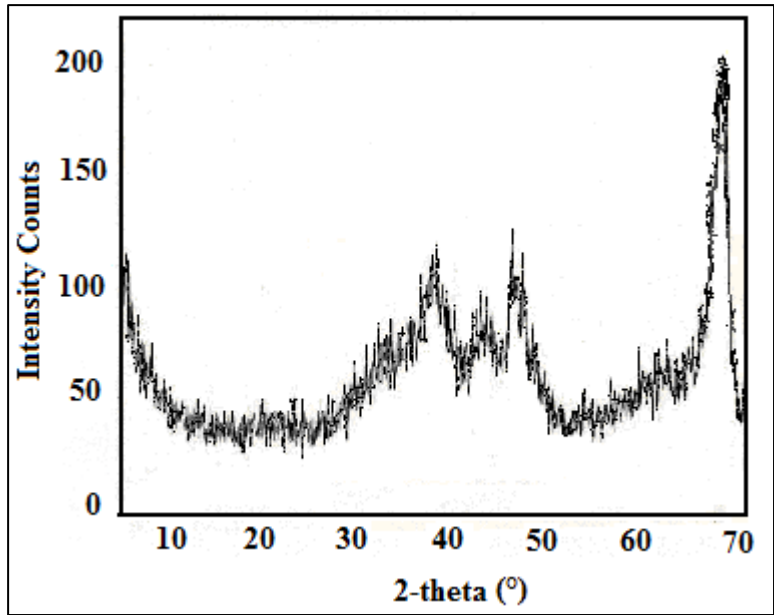


Figure 2.11: XRD spectra of alumina (standard)

Sample is unpolished X-Ray corrections may be approximate.  
 Sample is uncoated  
 The element used for optimization was Phosphorous  
 Spectrum processing:  
 No peaks omitted  
 Processing option: All elements analyzed (Normalised)  
 Number of iterations = 7  
 Standard:  
 C CaCO3 1-Jun-1999 12:00 AM  
 O SiO2 1-Jun-1999 12:00 AM  
 Na Albite 1-Jun-1999 12:00 AM  
 Al Al2O3 1-Jun-1999 12:00 AM  
 P GaP 1-Jun-1999 12:00 AM  
 K MAD-10 Feldspar 1-Jun-1999 12:00 AM  
 Ca Wollastonite 1-Jun-1999 12:00 AM

Element	AppConc.	Intensity Corrn.	Wt%	Wt% Sigma	Atomic %
C K	54.25	0.2864	12.30	1.33	18.05
O K	601.28	0.6753	57.83	1.10	63.71
Na K	18.02	0.5600	2.09	0.21	1.60
Al K	143.62	0.6841	13.63	0.38	8.91
P K	179.56	1.0074	11.58	0.36	6.59
K K	9.44	0.9600	0.64	0.08	0.29
Ca K	27.72	0.9326	1.93	0.12	0.85
<b>Totals</b>			<b>100.00</b>		

Figure 2.12: Elemental composition obtained from EDS shows high percentage of both aluminum and oxygen in the coating.

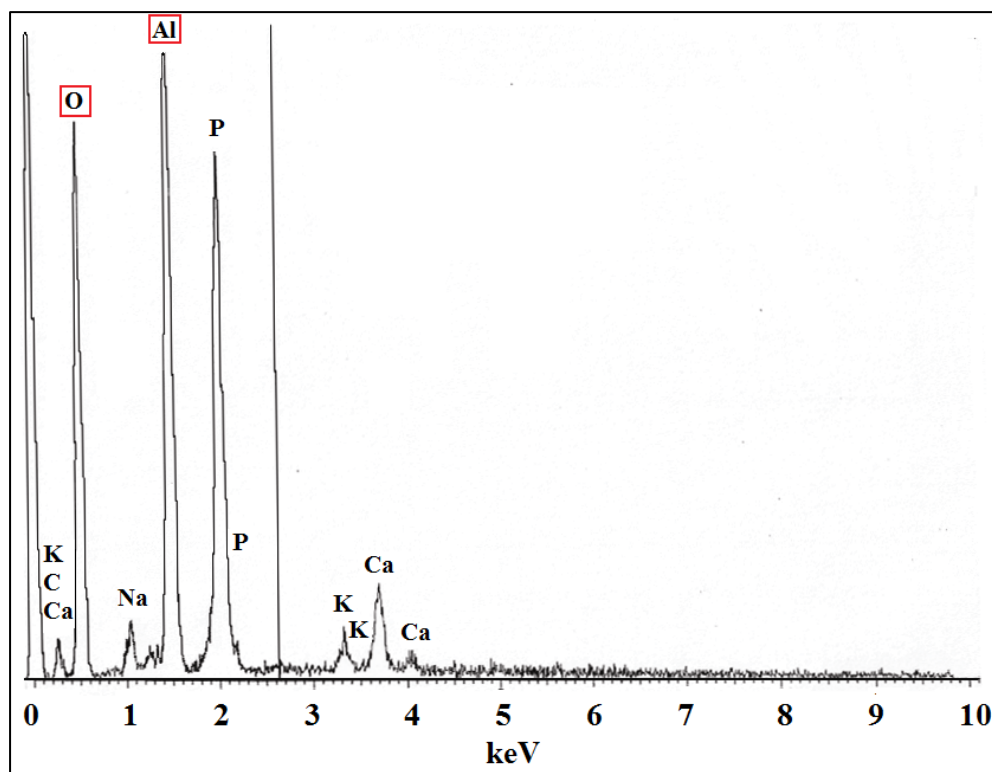


Figure 2.13: Sharp peaks of oxygen and aluminum confirmed the presence of alumina in the sample.

### 2.3.2 Dimensional Analysis of Nanopores

The length and width of nanopores can be measured manually from SEM pictures of nanoporous gold coated silicon wafers. However, depth could not be ascertained using SEM. Estimation of depth of the pores is an important criterion in determining the exact volume available for drug loading. Hence, the wafers were analyzed again using AFM. Figures 2.14 (a) and 2.14 (b) illustrate, analysis of depth and area of the pores in  $1 \mu\text{m}^2$  area of the wafer. Table 2.1 represents the statistical data of the three nanoporous wafers analyzed by AFM. The data indicates uniformity as all the analytical measurements have

relative standard error below 20 %. The SEM pictures suggest the pores to be cylindrical in shape. Hence the volume was estimated using the equation:

$$\text{Volume of a cylinder} = (\text{Area of Base}) \times \text{Depth} \quad (1)$$

In the calculations, area of base and depth were obtained from particle analysis in AFM (Table 2.1). Thus,

$$\begin{aligned} \text{Volume of Pores} &= (1.32 \times 10^3 \text{ nm}^2) \times (26.9 \text{ nm}) \\ &= 3.55 \times 10^4 \text{ nm}^3 \end{aligned}$$

Hence,  $1 \mu\text{m}^2$  of wafer surface contains on an average  $3.55 \times 10^4 \text{ nm}^3$  of pore volume which can also be translated as the volume of pores available per unit  $\mu\text{m}$  of length. (2)

### **2.3.3 Surface Analysis of a Stent and Estimation of Volume of Pores on its Surface**

The calculations are based on the design of a commercially available bare metal stent (Figures 2.5 & 2.6, previously mentioned in Section 2.2.3). The stent is cylindrical in shape with open ends. It is made up of 87 mini cylindrical rods, which have void spaces in between. Figure 2.6 indicated the length of the cylindrical rods as 1.30 mm. Hence,

$$\begin{aligned} \text{Total length available on stent for fabrication of nanopores} &= 87 \times 1.30 \text{ mm} \\ &= 0.113 \text{ m} \end{aligned} \quad (3)$$

Hence, total volume of pores available on entire length of the stent can be given

by = (Volume of pores/ $\mu\text{m}$ ) x (Total length of stent)

=  $(3.55 \times 10^4 \text{ nm}^3 / \mu\text{m}) \times (0.113 \text{ m})$

=  $4.01 \times 10^9 \text{ nm}^3$ , which is the volume available for drug loading.

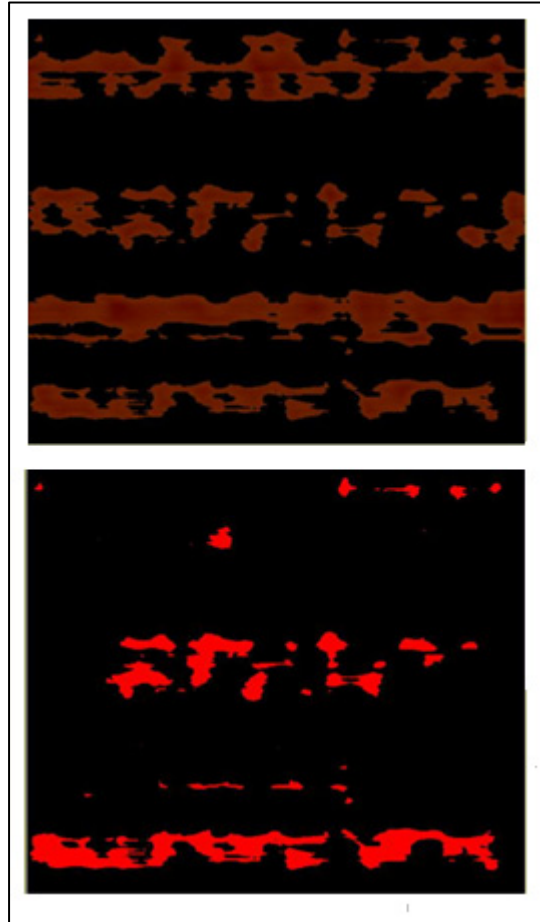


Figure 2.14: The figure shows the nanopores as analyzed using AFM (a) - (Top) - The section analysis of  $1 \mu\text{m}^2$  area of the wafer using AFM shows top view of the nanopores as indicated by brown region and was used to analyze the depth of the pores (b) - (Bottom) - The particle analysis of  $1 \mu\text{m}^2$  area of the wafer using AFM shows horizontal view of the nanopores as indicated by the red region and was used to analyze the length, width, and area of the pores in the wafers

Table 2.1: Statistical Analysis of Nanoporous Wafers using Dimensions obtained from AFM

	Area (nm <sup>2</sup> )	Diameter (nm)	Length (nm)	Width (nm)	Depth (nm)
Wafer 1	1440.2	27.2	57.1	14.4	23.0
Wafer 2	1448.4	32.3	72.6	17.4	30.5
Wafer 3	1063.5	22.5	53.3	12.8	27.4
Average	1317.4	27.3	61.0	14.9	26.9
SD	219.9	4.9	10.2	2.3	3.8
% CV	16.7	17.9	16.7	15.6	14.0

### 2.3.4 Drug Release Study

The aim of this study was to test the drug loading capacity of nanopores and the effectiveness of poly (2-octylcyanoacrylate) as an extended release polymer matrix. Figure 2.15 illustrates a nanoporous wafer loaded with methyl orange and polymer. The drug loading data is illustrated in Table 2.2. A uniform w/w ratio of methyl orange and cyanoacrylate,  $0.70 \pm 0.04$  was applied to the wafers. A single coat of polymer and model drug on the untreated wafer resulted in 7 days of drug release. Average cumulative percentage release of  $88.1 \pm 5.0$  %, equivalent to  $220 \pm 97$   $\mu\text{g/day}$  of methyl orange, was released for first 7 days (Figure 2.16). The drug delivery study can be extended to other

polymer as well. The polymers may be bioadhesive which will allow the implant to deliver the drug to the targeted site. Certain patients may be hypersensitive to polymers [97]. In such cases, biodegradable or bioabsorbable polymers may be used which gets completely metabolized after elution of the drug leaving the metal alone. The device later gets endothelialized preventing further complications such as thrombosis and platelet activation.



Figure 2.15: SEM picture of a nanoporous gold silicon wafer treated with methyl orange and cyanoacrylate.

Table 2.2: Drug Loading Data (N=3).

	Weight of Wafer in mg	Weight of Methyl Orange loaded ( D ), in mg	Weight of cyanoacrylate added ( C ), in mg	Ratio of D:C
Wafer 1	34.0	2.5	3.6	0.7
Wafer 2	30.6	1.5	2.4	0.6
Wafer 3	33.9	1.2	1.9	0.6

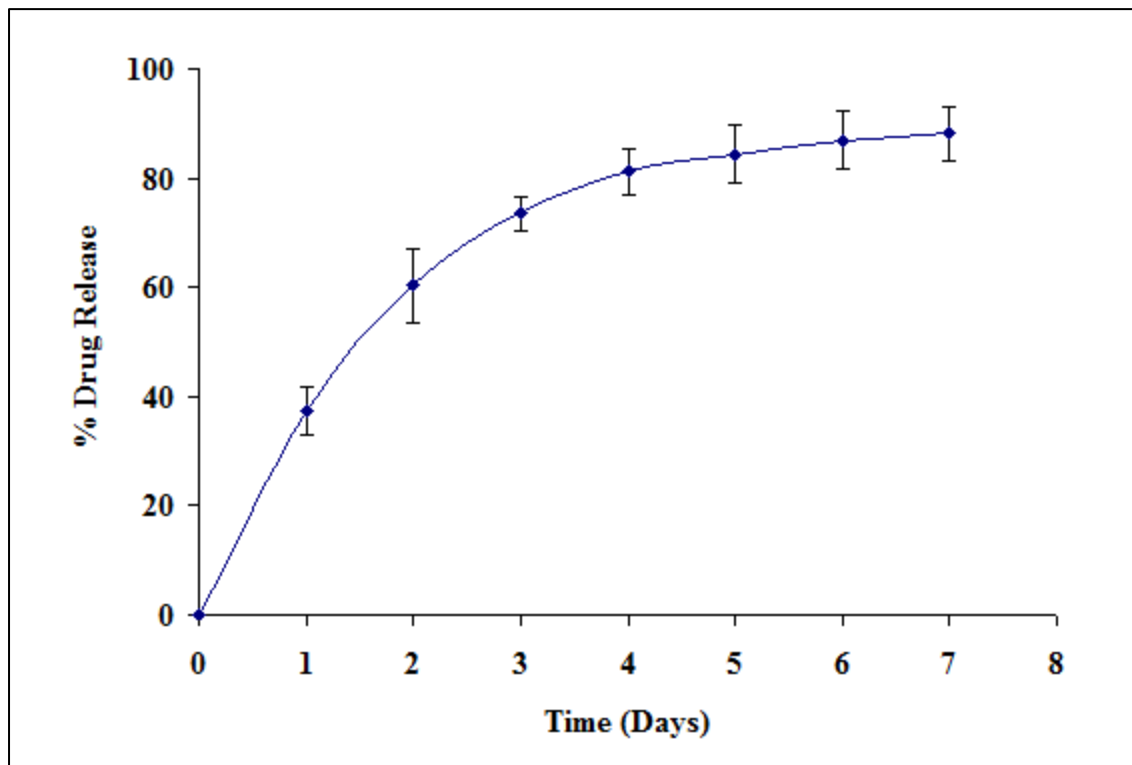


Figure 2.16: A cumulative % release profile of methyl orange from cyanoacrylate polymer matrix. Values are presented as mean with standard deviation, n = 3.

## 2.4 CONCLUSION

Aluminum was found to be unsuitable for making implants due to its chemical and mechanical instability in the physiological environment. Gold proved to be an effective material for the fabrication of nanopores. The volume calculations indicate that nanopores offer significant volume for the purpose of drug loading. They can be fabricated in different patterns and by different techniques, to meet the volume requirements of a certain application. The standard metric techniques such as SEM and AFM have proven to be useful tools in analyzing nano features. Poly (2- octyl cyanoacrylate) can be successfully used to prolong methyl orange release from nanoporous surface, metals, and probably other surfaces. They may either be used alone or in conjunction with other polymers for drug delivery.

The preliminary work with nanopores was discontinued because of reports in literature which pointed to problems arising in implants due to polymers [97, 98]. In addition the primary objective to obtain zero order drug release rates was not accomplished. Therefore, other concepts of develop a polymer free DES were researched. A new stent was designed that was composed of two parts - the stent skeleton and the perforated microtubes. The following chapter discusses the various steps that were involved in designing of the stent and its fabrication.

## Chapter 3: Designing and Fabrication of the Drug Delivery Device

### 3.1 INTRODUCTION

As the initial studies with nanopores did not meet the primary objective of producing zero order drug release rate, a new stent was designed that consisted of perforated microtubes that can be built in or mounted on the stent itself. Although originally designed to be part of the drug eluting stent (DES), the perforated tubes later on demonstrated that they can also be used as independent drug delivery systems. This observation was made after the *in vitro* drug release studies of Chapter 5 revealed that the perforated tubes are capable of long-term drug release ranging from several months to years. A chronological description that explains the advancement of the perforated tubes from merely being a component of a DES to being currently developed as a general purpose drug delivery device has been discussed in the present and following chapters.

Before discussing the long-term drug delivery capability of the perforated drug delivery system, it is important to understand the dimensional and material considerations that were involved during the device development. The device design and fabrication have been discussed in this chapter.

The present chapter also discusses the initial motives and reasons to develop the perforated tubes as part of the DES. The following discussion involves a review of prophylactic use of DES in medical practice; their complications; and advantages of a polymer free DES in reducing these complications.

### 3.1.1 Drug Eluting Stents – Advantages and Disadvantages

The first generation DES, the CYPHER<sup>TM</sup> Sirolimus Eluting Coronary Stent (Johnson & Johnson) and the Paclitaxel Eluting TAXUS<sup>TM</sup> Stent (Boston Scientific) were introduced in 2003 and 2004, respectively to prevent restenosis (renarrowing of the coronary artery) after stent deployment [99, 100]. Since their inception, DES have significantly reduced the rate of clinical restenosis as compared to bare metal stents (BMS) and conventional balloon angioplasty [101-105]. An ideal DES was visualized to possess following characteristics:

1. Polymers should allow ideal drug release.
2. Drugs should inhibit vascular smooth cell proliferation and inflammation and prevent restenosis.
3. The stents becomes part of the vasculature to prevent any late inflammations / thrombosis.
4. The stent should allow collateral circulation. Collaterals are blood vessels that are formed by angiogenesis and which act as a bypass to supply blood flow to ischemic regions due to stenosis of epicardial arteries [106, 107].

However, even before the introduction of first commercial DES, Virmani *et al* suggested that the potential problem with DES may arise due to the “nonerodable thick polymer sleeve, very high concentration of the active drug, extended release kinetics, loose stent architecture, and inhomogeneous drug delivery” [108]. These problems tend to be associated with late stent thrombosis (LST) which renarrows the arteries increasing the risk of myocardial infarction [109-112].

### **3.1.2 Understanding Late Stent Thrombosis**

The mechanisms of restenosis and LST associated with DES have recently been reviewed [113] and polymers that have been used for release control have been associated with the DES failure. Under mechanical stress such as during implantation of stents, polymers might crack leading to injury to arterial wall. Injury activates platelet aggregation and blood clotting leading to LST. Cracking of polymer may also lead to drug dumping at the injured arterial site delaying the healing of the stent (endothelialization). The incomplete endothelialized stent becomes a site for platelet adhesion increasing the probability of LST.

Hypersensitivity to polymers might incite inflammation reactions. Due to allergy, a marked activation of inflammatory cells such as leucocytes at the site of stent has been observed [114]. Leukocyte have also been linked to the formation of neointimal hyperplasia along with platelet adhesion indicating the central role of inflammation in both restenosis and LST [115-117]. As illustrated in Figure 3.1, the dose dumping in DES leads to delayed healing or incomplete endothelialization of the stent structure. The exposed site becomes a probable target for platelet adhesion and auto-immune response, which may lead to LST.

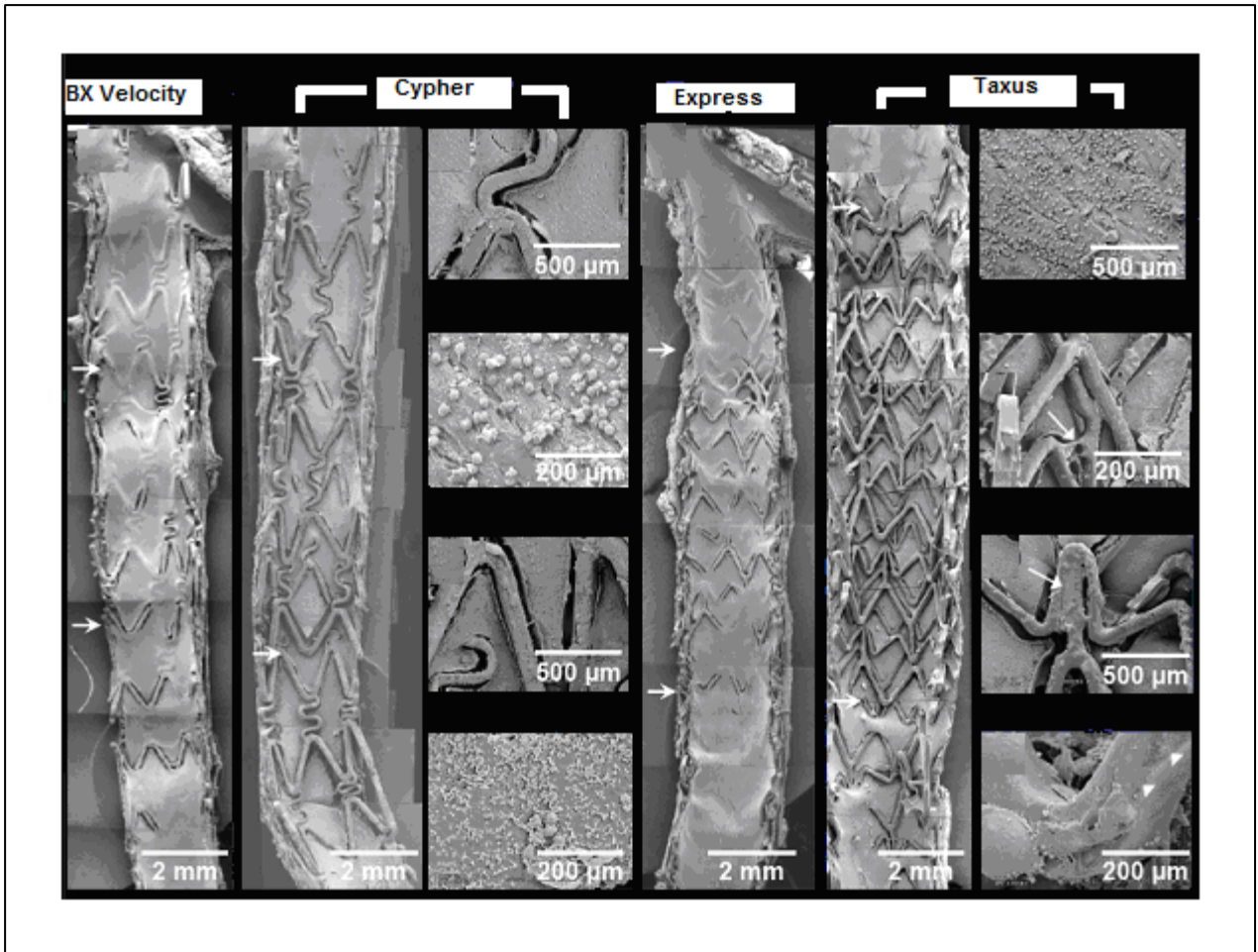


Figure 3.1: A comparison of the two DES, Cypher and Taxus stents with their bare metal stent counterparts, BxVelocity and Express respectively 28 days after implantation. The bare metal stents are completely endothelialized whereas, the drug coated stents show incomplete endothelialization due to drug over exposure [118].

### 3.1.3 Rationale for device development

A plethora of new DES's have been introduced after TAXUS™ and CYPHER™ stents. The next generation stents have shown some promising results. However, most of these stents were conceptualized before the discovery of LST and its implications. The latest FDA approved stents, such as XIENCE™ (Abbott Vascular) and ENDEAVOR™

(Medtronic) are still questionable for their long-term usage. Hence, there is a need of a stent system that does not require a polymer to control drug release. Such system should be capable of delivering a combination of drugs at concentrations sufficient to inhibit restenosis without delaying the healing of the stent.

Material considerations, surface characteristics, and appropriate size of the device were some of the factors that were kept in mind while designing the device. A drug delivery device in general and a coronary stent specifically, should exhibit the following characteristics [119-121].

1. It should limit recoil and should not shrink back after it has been expanded and deployed.
2. It should be flexible to pass through circuitous vessels.
3. It should be opaque to X-ray and other radiations (radiopacity).
4. It should have sufficient radial strength. The device should be able to withstand the inner radial pressure of the artery. However, it should not be too stiff as to cause damage to the arterial wall.
5. It should have low profile and a low metal to artery ratio. A low surface area of the stent ensures less damage to the inner wall of the vessel and less thrombus or platelet formation.
6. The material used to manufacture the device should be biocompatible, hemocompatible, and should not propagate thrombus formation.
7. The device should be electro polished to remove surface roughness. A mirror finish helps to reduce the platelet adhesion when the device comes in contact with the blood.

8. As polymers have been known to be the genesis of restenosis and LST, a polymer free DES would be ideal.

### **3.2 DESIGN OF THE DRUG ELUTING STENT**

Keeping the above ideal characteristics in mind a new stent was designed (Figure 3.2). The stent was designed after a comprehensive research of limitations of past and present stents and the improvements that can be incorporated in their design. However, that discussion is focused on engineering aspects of the design and will be a deviation from the main theme of this dissertation. As illustrated in the figure, the stent consists of two components – stent skeleton and perforated microtubes mounted on top of the skeleton. The stent skeleton would serve as the scaffold to keep the artery open whereas, the drug delivery device would release the anti-restenosis drug. The design of the perforated tubes is based on the principle of simple diffusion. A programmed release is desired from the perforated microtubes, such that the device is capable to release drugs for at least 28 days at a controlled rate. Figure 3.2, illustrates a sketch of the design. The device consists of a hollow drug reservoir with holes on the surface. The drug travels from inside of the reservoir to the outside into the dissolution medium following its concentration gradient.

As illustrated in Figure 3.3, the tube is the drug reservoir with holes on the surface. The drug travels from inside of the reservoir to the outside into the dissolution medium following its concentration gradient. A sink condition outside the device enables zero order release and is the driving force for drug release. When the device comes in contact with an anatomical site the drug is released into the site (Figure 3.4).

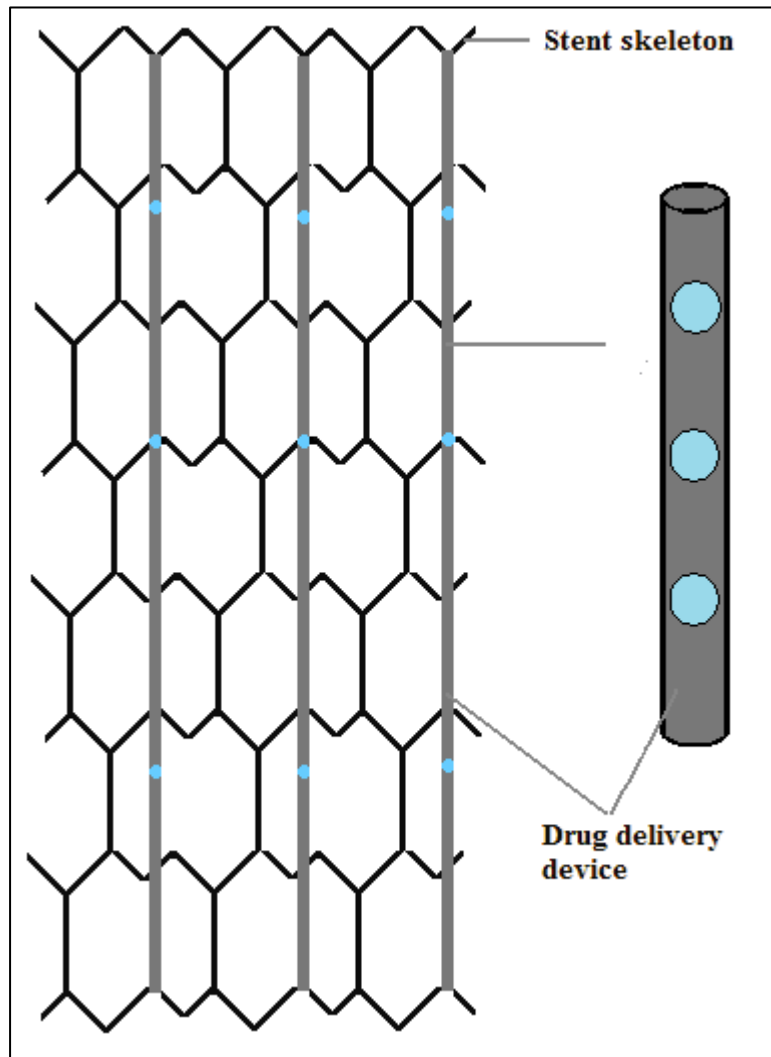


Figure 3.2: A design of the DES comprising of a stent skeleton mounted with perforated tubes.

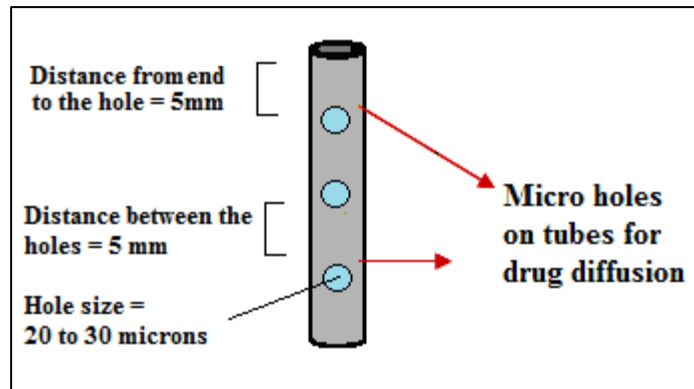


Figure 3.3: A sketch of the perforated microtube. The device consists of a micro tube with micro perforations on one side of its surface. The diameter of the device can range from several micrometers to millimeters. The hole size can range from 20  $\mu\text{m}$  to several hundred microns depending on the need of the application.

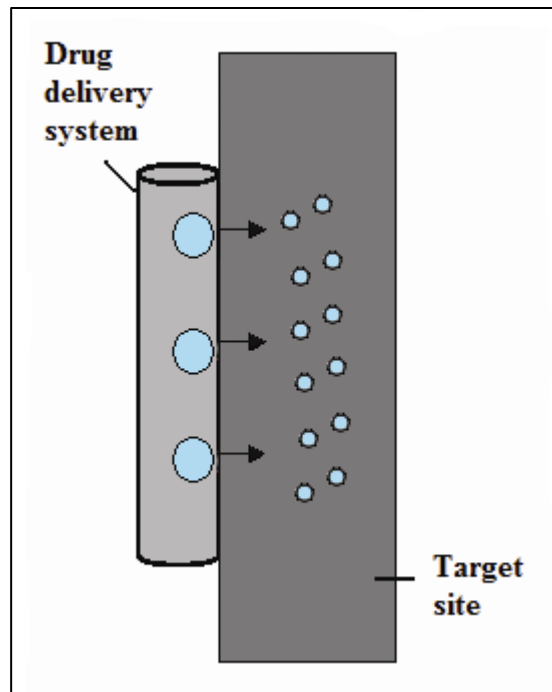


Figure 3.4: The drug is released from the drug delivery device into the targeted site.

### **3.2.1 Material Considerations for the Manufacture of Stent Skeleton and Drug Delivery Device**

Current DES consists of drugs which are embedded and released from within (matrix) or surrounded by and released through (reservoir) polymers. An example of reservoir type system is the CYPHER stent. The polymer matrix consists of parylene C (poly-(p-xylelene) polymer with one repeat chlorine group per repeat unit), polyethylene-co-vinyl acetate (PEVA) and poly n-butyl methacrylate (PBMA) [122]. A combination of the two polymers mixed with Sirolimus (67%/33%) makes up the basecoat formulation which is applied to a parylene C treated stent. A drug-free topcoat of PBMA polymer is applied to the stent surface to control the release kinetics of Sirolimus. The drug/polymer coating is adhered to the entire surface (i.e., luminal and abluminal) of the stent. The TAXUS Express stent, serves as an example of matrix type system where, the only inactive ingredient is poly(styrene-b-isobutylene-b-styrene), a tri-block copolymer [123]. The polymer is mixed with the drug Paclitaxel and then applied to the entire surface of the stent.

However, the polymers have been associated with the problems of LST. Hence, there is a need for a polymer free stent which is capable of controlled release of drugs. The Cobalt Chromium–L605 alloy was selected as the material of choice to manufacture the stent skeleton of Figure 3.2. The alloy is ideal for stent manufacture because of the following desirable properties that it possess [124-126].

1. It is biocompatible and corrosion resistant.

2. The density and elastic modulus of L605 are better than 316L stainless steel (another popular stent material). Elastic modulus is the mathematical value of a substance's tendency to be deformed non-permanently when a force is applied to it. It is obtained as the stress / strain ratio.
3. Its high density and high radial strength allows thinner struts, radiopacity, and high elastic modulus, which limits recoil and improves flexibility.
4. Thinner struts allow lower profile.
5. L605 is non-ferromagnetic and thus MRI (Magnetic Resonance Imaging) safe.

Polyimide was selected to manufacture the drug delivery device because:

1. It is inert, corrosion resistant, and chemical resistant [127].
2. It exhibits high mechanical toughness and thermal stability [127].
3. Because of its high degree of ductility and inherently low coefficient of thermal expansion, polyimide can be readily implemented into a variety of microelectronic applications [128, 129].
4. It has a high tensile strength and tensile elongation which facilitates the placement of a polyimide matrix through the tortuous blood vessels to the desired site of location [130, 131].
5. Polyimides are hemocompatible, biocompatible, and can be used for invasive clinical applications [132].

### **3.3 MATERIALS AND METHODS**

#### **3.3.1 Materials**

A bare metal stent (Palmaz-Schatz® Balloon-expandable stent, Size = 15 x 3.0 mm) was obtained from The University of Texas Health Sciences (San Antonio, TX, USA). Prednisolone was obtained from Sigma-Aldrich (St. Louis, MO, USA). Polyimide tubings were obtained from Microlumen Inc (Tampa, FL, USA). All reagents used for photolithography process were provided by the clean room facility in Micro-electronics research centre, located in the J.J. Pickle research centre, The University of Texas at Austin (Austin, TX, USA).

#### **3.3.2 Estimation of Appropriate Dimensions for the Device**

In order to obtain the dimensions for the different components of stent illustrated in Figure 3.2, a reference stent, Palmaz-Schatz stent, was analyzed by SEM (Figure 3.5 & 3.6). The different parts of the stent, such as length and width of the connectors, diameter of the stent, diameter of the drug delivery tubes, were manually estimated to calculate the appropriate dimensions for the novel DES.

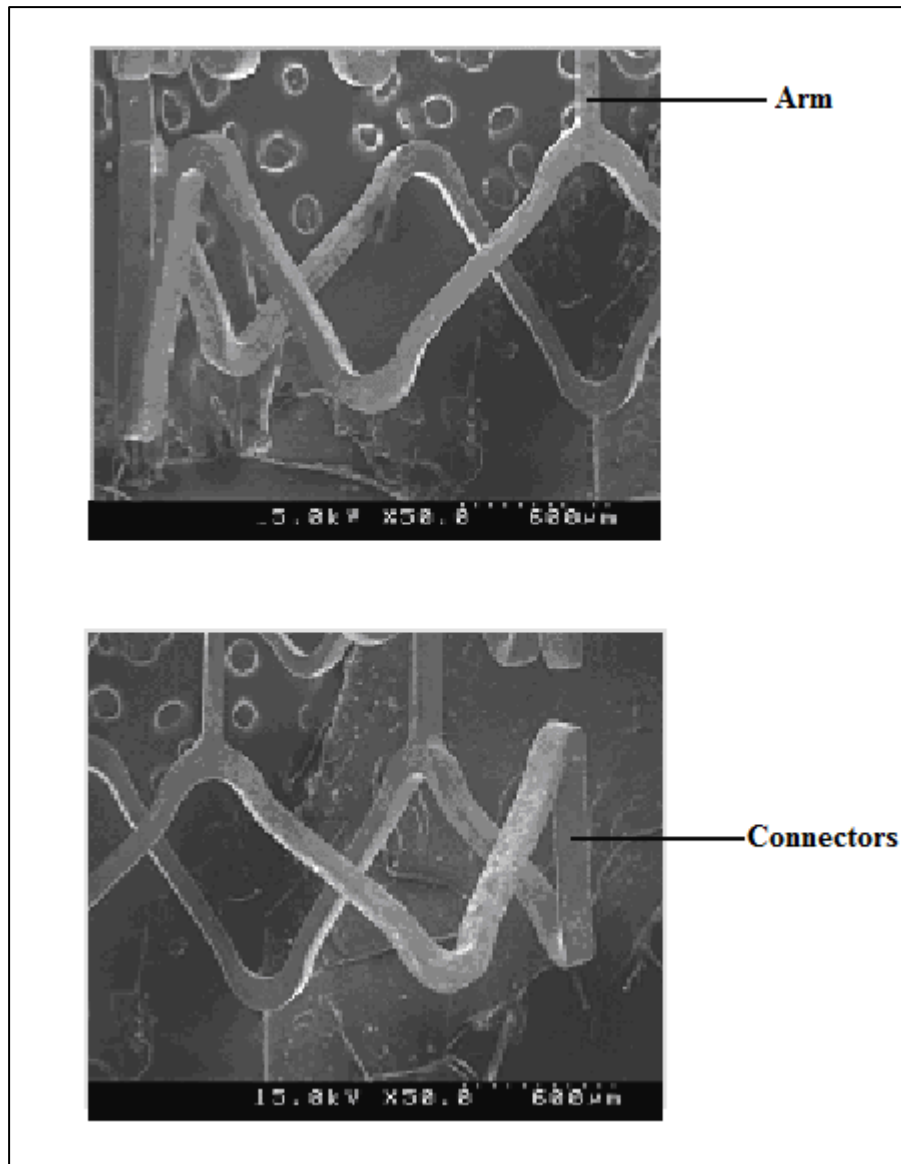


Figure 3.5: Optimal diameter of the stent and the optimal distance between connectors was calculated using above SEM pictures

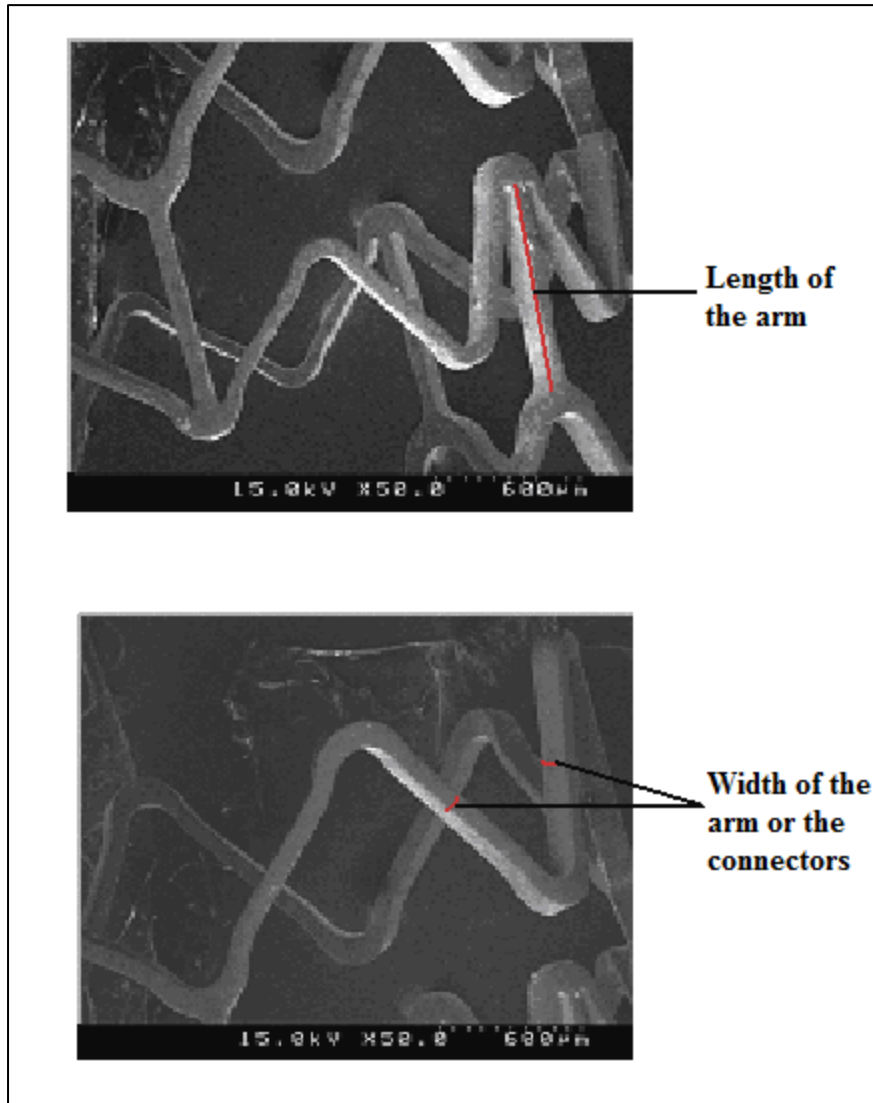


Figure 3.6: SEM pictures used to estimate the length and width of the arms and connectors

### **3.3.3 Finite Element Analysis of the Stent Structure**

Finite Element Method (FEM) allows design of a mechanical structure to be developed and optimized before it is manufactured [133]. Hence, the design of Figure 3.2, was corroborated using FEM. The early detection of limitations in designs avoids unnecessary cost in development of the prototype. The FEM was used to study the stent expansion and possible shortcomings of the design such as, stent shortening, lack of flexibility, and uneven distribution of stress.

### **3.3.4 Estimation of Hole Size**

After the dimensional considerations of the stent skeleton were taken into account, the next step was to develop the perforated drug delivery system. Although the tubes were commercially available, the holes still needed to be fabricated on them. Two important features were taken into consideration while deciding for an appropriate hole size. Firstly, the holes should not be blocked by the red blood cells, whose size ranges from 8 to 10 microns. Secondly, the hole should be big enough to allow drug molecules in solution or suspension to diffuse out of the holes. Hence, the next step was to determine particle size for a model drug, prednisolone. The particle size distribution of a poorly water soluble drug, prednisolone [134, 135] was measured using Malvern Mastersizer 2000 ((Malvern Instruments, Ltd., Worcestershire, UK)), to estimate the appropriate hole size. A nominal amount of prednisolone powder was dispersed in deionized water and added to the Malvern apparatus, with recirculation and sonication,

until a percent obscuration of between 9% - 12% was acquired. When using the Malvern particle sizer, data is obtained as volume data (percentage frequency of cumulative volume).

### **3.3.5 Coating of Polyimide Matrices with a Biocompatible Alloy**

The polyimide tubes were coated with L605 alloy to impart exterior toughness along with surface smoothness. As illustrated in Figure 3.7, a rough surface is more prone to platelet activation (precursor for inflammation and thrombogenicity) as compared to a polished surface [136]. The coating of polyimide matrix with Co-Cr alloy enabled us to lower the surface roughness making the polymer more suitable for *in vivo* use.

The coating methodology has been described elsewhere in detail [137, 138]. Briefly, polyimide tubes were coated with the alloy using dc magnetron sputtering of metals. The substrate to be coated (polyimide tube) is placed between two electrodes in air, at high vacuum. The sputtering system consists of a vacuum chamber, which is filled with argon gas. The cathode consists of a target made out of metals that need to be deposited (such as cobalt, chromium, nickel, etc). A high voltage is used to ionize the gas which then strikes the cathode forcing it to cast off metal particles on the substrate as an adherent film. An example of sputtering mechanism is shown in Figure 3.8. Here, the cobalt is extracted from the cathode and dislodged to the substrate as a metal film.

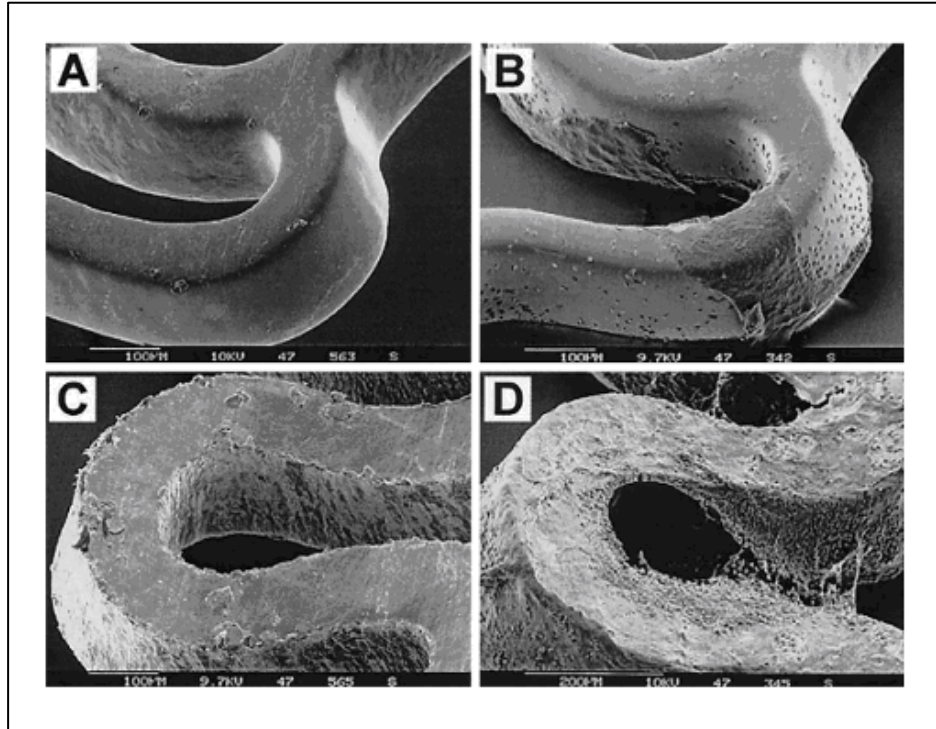


Figure 3.7: At  $t = 0$  minutes, the electropolished stent (A) showed a smooth surface whereas the unpolished device's surface (B) was originally rougher. Blood exposure for 120 minutes resulted in cell deposition on few areas of the electropolished stent's surface (C). In contrast, the unpolished device developed a rough coating consisting of large amounts of cell deposition (mainly platelets and macrophages) and fibrin (D) [136].

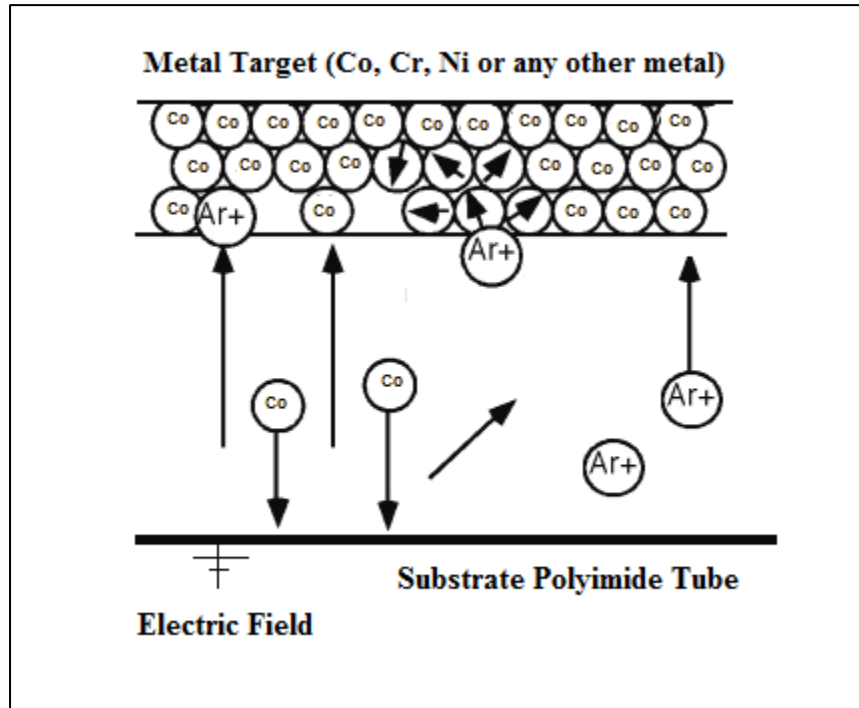


Figure 3.8: Sputtering mechanism for coating of a metal ion onto a polyimide substrate [139]

### 3.3.6 Characterization of Coating Composition

The composition of the biocompatible alloy coating was characterized using Electron Dispersive X-ray Spectrophotometer (EDS). EDS is an analytical technique that employs X-rays to reveal the elemental composition of the specimen. As the X-ray bombards the specimen, it emits spectra that are specific for an element. Hence, in the case of a metal alloy sample, the resultant spectrum provided a fingerprint representation of its composition and thus its identity. The thickness of the deposited film was evaluated using the Molecular Force Probe 3D (MFP-3D) Atomic force microscopy (Asylum Research, Santa Barbara, California).

### **3.3.7 Fabrication of Holes on the Polyimide Matrix**

The holes can be produced by either laser drilling or photolithography techniques. Initially laser drilling was used to fabricate the microholes on the microtubes, however a more economical and practical method amenable to mass production was developed using photolithographic techniques. The lithography process which has been used to fabricate holes has been covered in our United States Provisional Patent Application (61/225,309 and 61/225,352). The technology to fabricate micro-structures on planar silicon wafers is well developed. The patents define the methods which can be used to fabricate micro-structures such as micro holes on non planar surfaces, for example, polyimide tubes.

A step by step illustration is shown in Figure 3.9. Briefly, the polyimide matrix is coated with chromium metal and placed on nano trenches (grooves) made previously on a silicone wafer. A layer of photoresist is applied by spin coating at 4800 rpm for 60 seconds. The photoresist coated matrix is baked for few minutes at 100°C to remove off any excess solvent. A photomask is generated from a premade data file. The photoresist is exposed to ultraviolet light through the photomask, and the pattern from the mask is imprinted onto the photoresist. The pattern is dry etched to the underlying chromium layer and to the polyimide surface. Reactive ion etching is used to remove both the chromium layer and the polyimide surface producing holes. The surface of the polyimide covered with photoresist remains unharmed. The FEM analysis of the stent design, coating of the tubes, and photolithography were conducted in collaboration with Dr. Paul Ho and his graduate students at the Pickle Research Center (The University of Texas at Austin).

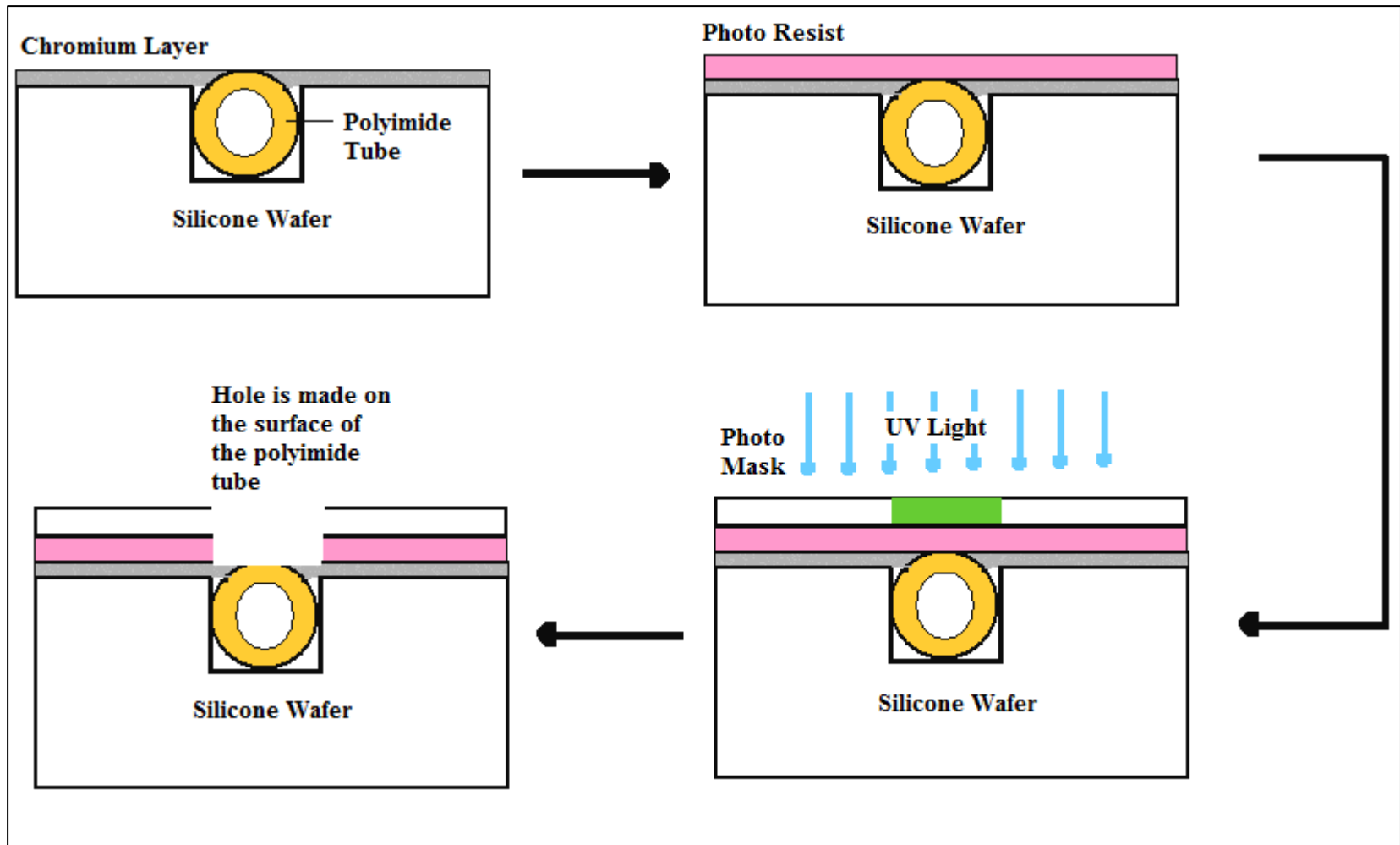


Figure 3.9: Holes are made on the surface of the polyimide matrix using photolithography techniques.

## **3.4 RESULTS AND DISCUSSION**

### **3.4.1 Dimensions for the Stent and Drug Delivery Device**

From the dimensional analysis of Figures 3.5 & 3.6 (illustrated previously in section 3.3.2), inside diameter of the stent was found to be 3.5 mm. Distance between the connectors and length and width of the arms were 0.96 mm 1.46 mm, and 80  $\mu\text{m}$ , respectively. The length of the reference stent was 15 mm. The stents' diameter and length can range from 2.0 - 4.0 mm and 8.0 – 28.0 mm, respectively, depending on size of the coronary artery and extent of blockage [140]. In accordance to these results, the dimensions of the various components of Figure 3.4 were selected. For the stent skeleton which is made of Co-Cr alloy, width of the stent struts and length and diameter of the stent were selected as 80  $\mu\text{m}$ , 21 mm, and 3 mm respectively. For the drug delivery device which is made of polyimide tube, a length of the tubes is 20 mm was selected. A slightly larger size tubes (OD=165 $\mu\text{m}$ ; ID=125  $\mu\text{m}$ ) were selected to achieve effective drug loading.

### **3.4.2 Finite Element Simulation of the Stent Design**

The Finite Element Method revealed few drawbacks in the initial design (Figure 3.10). During expansion, the sharp angles between the arms and the connectors lead to stent shortening. The expanded stent also had uneven distribution of stress points, which may cause recoil under arterial pressure (Figure 3.11). However, by making slight

modification in the design of the stent, significant improvements were achieved (Figures 3.12 & 3.13). The sharp angles in the initial design were replaced with smooth rounded curves. The stent shortening was decreased and the stress was evenly distributed along the stent structure resulting in uniform expansion. A 3D model further reveals the uniformity in structure after design modification (Figure 3.14).

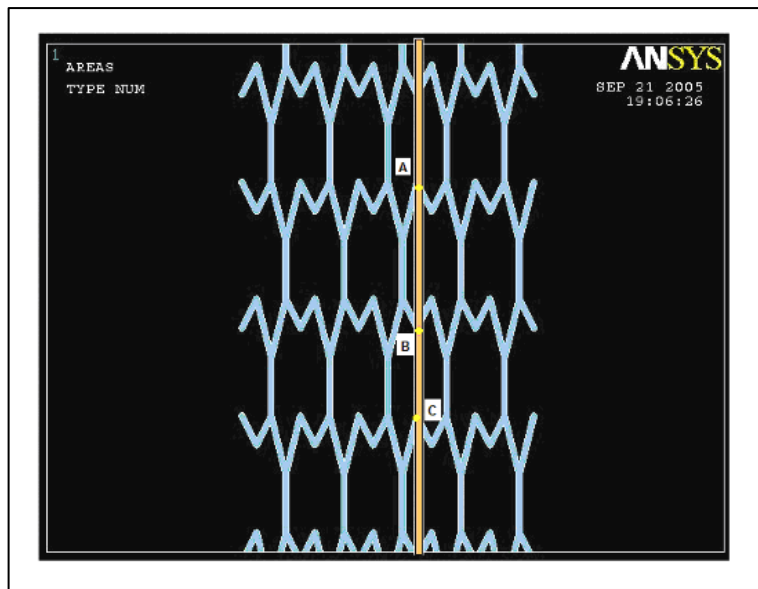


Figure 3.10: Initial sketch of the stent that was designed. Here, the three nodes of the structure are marked with letters A, B, and C. The nodes serve as reference point to indicate any shortening of length after expansion.

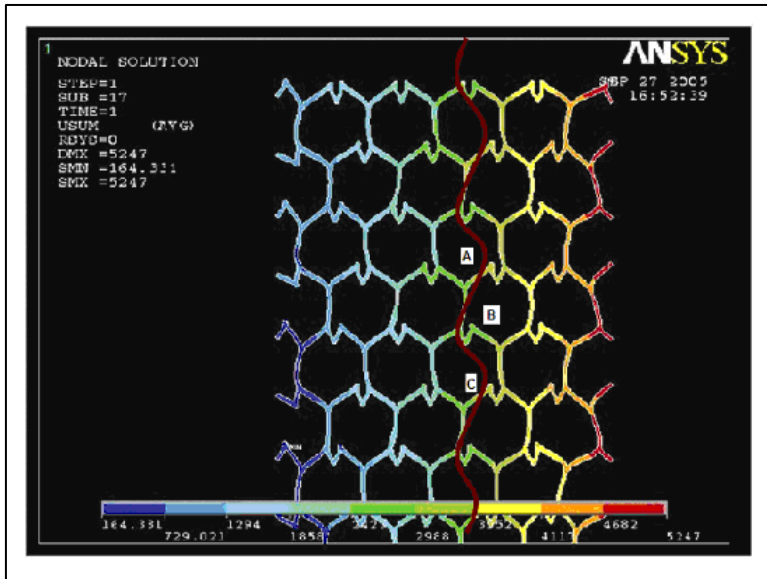


Figure 3.11: The nodes A, B, and C become misaligned after expansion indicating uneven expansion and stent shortening.

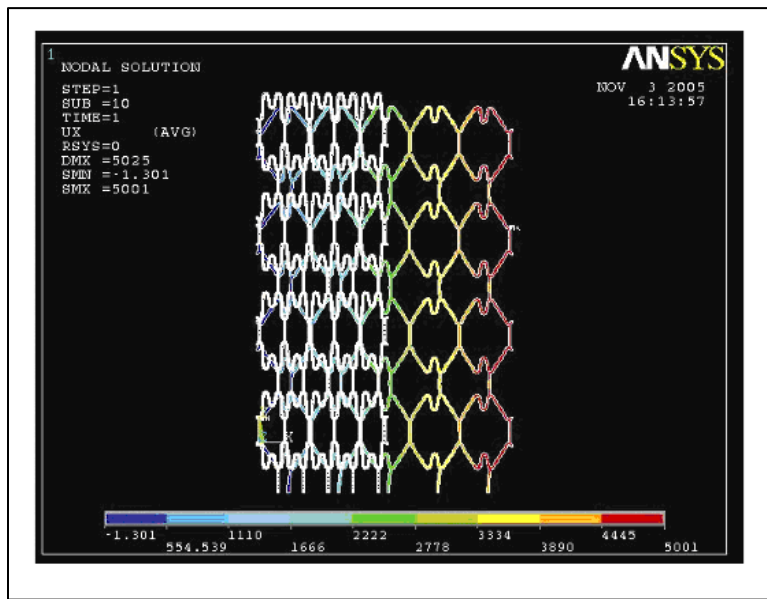


Figure 3.12: The nodes of the stent struts were rounded to distribute the stress evenly during expansion.



Figure 3.13: Even and symmetric expansion of the stent after modification of the initial design.

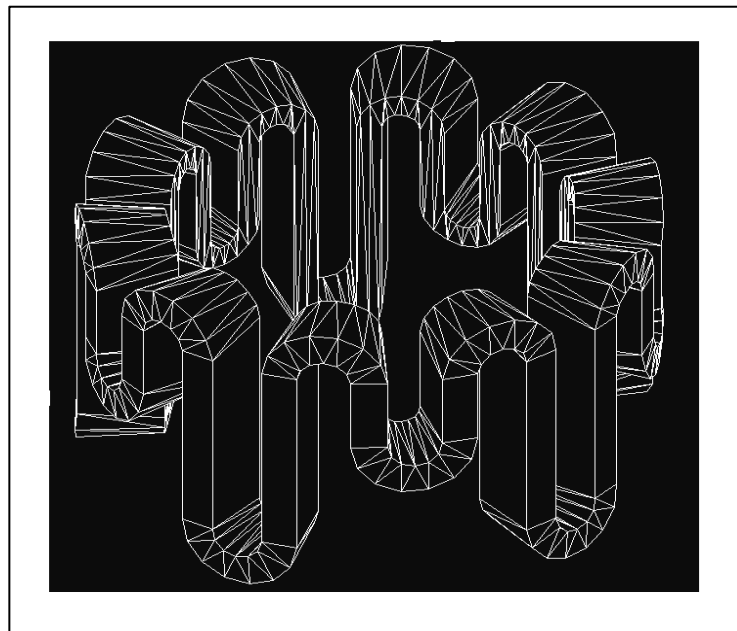


Figure 3.14: A 3-D model of the design.

### 3.4.3 Particle Size Distribution of Prednisolone to Estimate the Hole Diameter

The particle size experiment was performed in triplicate to estimate the particle size of prednisolone using water as the dispersion medium. As also reported previously in literature [141, 142], the data in Figure 3.15 is presented as three separate trials instead of the customary presentation of average with standard deviations. Li *et al* have mentioned that “although the results from the Malvern Mastersizer show particle mean size, and volume distribution can be reconstructed with acceptable accuracy, however, the recovery of standard deviation is sensitive to noise effect and can be very large as compared to the experimental data” [143]. Hence, it is more suitable to present the data as separate trials rather than average cumulative value. Figure 3.15, illustrates the results that were obtained from the three experiments. More than 80% of the particles lie within the 20  $\mu\text{m}$  range. Hence, a range of 20 - 40  $\mu\text{m}$  was selected as the suitable size for holes which will allow substantial drug release if prednisolone was loaded inside the device. The range gives a starting value for manufacturing of holes on the surface of the tubes, which could be increased or decreased afterwards depending on the application, duration of release, and drug characteristics.

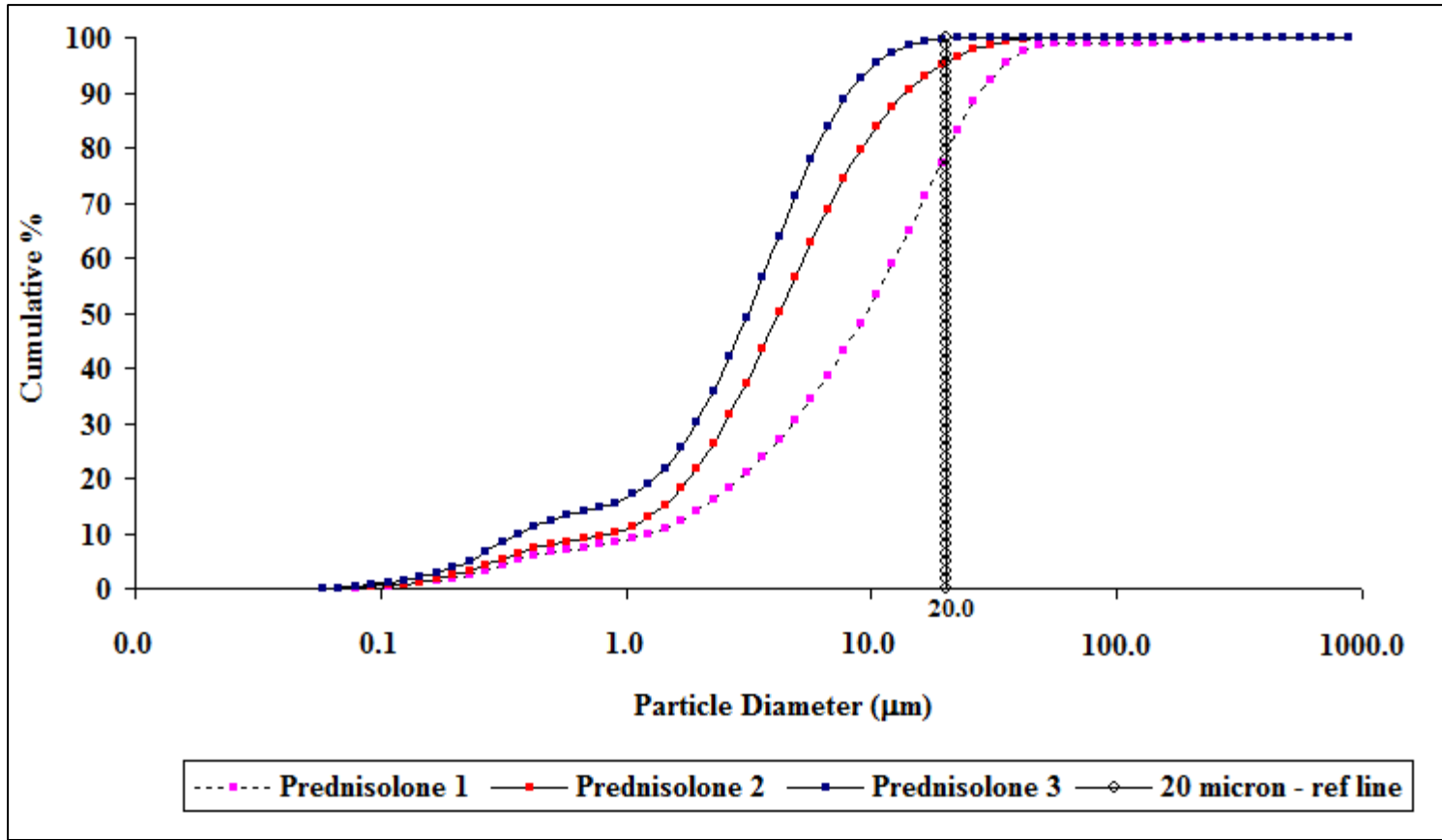


Figure 3.15: Particle size distribution of prednisolone from three experiments obtained using Malvern Mastersizer. A 20 micron reference line is drawn to estimate the percentage of particles below that value.

### 3.4.4 Coating Characterization

The exact composition of cobalt-chromium L605 alloy (Table 3.1) was obtained from a commercial website [144], specializing in alloy manufacture, and was used as standard. Three different batches of polyimide tubes were coated and coating composition was analyzed using EDS. As illustrated in Table 3.2, the experimental values were close to the standard values.

Table 3.1: Cobalt-Chromium L605 Alloy Composition

<b>Element</b>	<b>Nominal Composition in Percent</b>
Cobalt (Co)	50.0
Chromium (Cr)	20.0
Tungsten (W)	15.0
Nickel (Ni)	10.0
Iron (Fe)	3.0
Manganese (Mn)	2.0

Table 3.2: The coating composition obtained using EDS from the three separate batches of coated polyimide tubes.

<b>Elements</b>	<b>Batch 1 (%)</b>	<b>Batch 2 (%)</b>	<b>Batch 3 (%)</b>	<b>Average (%)</b>	<b>S.D.</b>	<b>%C.V.</b>
Cobalt (Co)	56.1	48.9	53.2	52.7	3.6	6.9
Chromium (Cr)	17.6	21.6	19.2	19.3	2.2	11.4
Tungsten (W)	17.9	19.3	16.5	17.9	1.5	8.3
Nickel (Ni)	5.1	5.0	7.0	5.7	1.1	19.2
Iron (Fe)	1.8	2.7	2.4	2.3	0.5	21.5
Manganese (Mn)	1.5	2.5	1.8	1.9	0.5	27.0

### **3.4.5 Surface Analysis of Coated Polyimide Tubes**

The atomic force microscope was used to analyse the surface characteristics because it is non damaging and has a three dimensional resolution. With this technique, it is possible to view and measure the textures and surface roughness in the nanometer range without any surface treatment [145]. Using the Molecular Force Probe 3D AFM, surface topography and roughness was investigated. From the investigation of  $1.0 \mu\text{m}^2$  area, the initial root mean square (RMS) roughness of polyimide surface was found to be 0.97 nm (Figure 3.16). However, as illustrated in Figure 3.17, after coating the polyimide tubes with 30 nm of L605 alloy, the RMS roughness decreased to 0.62 nm making the surface very smooth.

### **3.4.6 Analysis of Holes Manufactured by Photolithography**

Initially laser drilling was used to fabricate the microholes in the microtubes, however a more economical and practical method amenable to mass production was developed using photolithographic techniques. In addition, with photolithography it is also possible to produce high quality cuts with a relatively fast turn around. Figure 3.18 illustrates holes that were produced on the polyimide tube using photolithography. The holes were very uniform without any jagged edges with an average size of  $34.6 \pm 6.3 \mu\text{m}$  (n=36). The holes produced by laser drilling had an average size of  $32.9 \pm 1.7 \mu\text{m}$  (n=45).

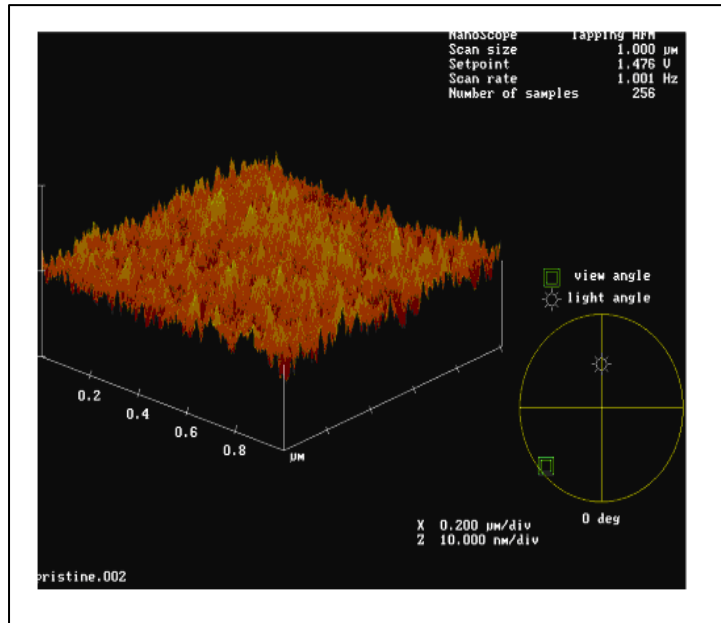


Figure 3.16: Polyimide surface without coating. Root mean square roughness is 0.97 nm.

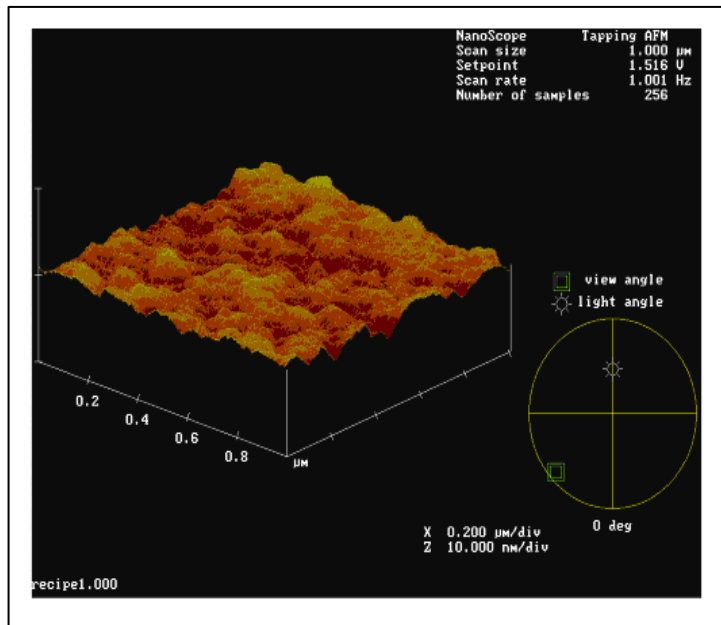


Figure 3.17: Polyimide surface after coating with Co-Cr L605 alloy. Root mean square roughness is 0.62 nm.

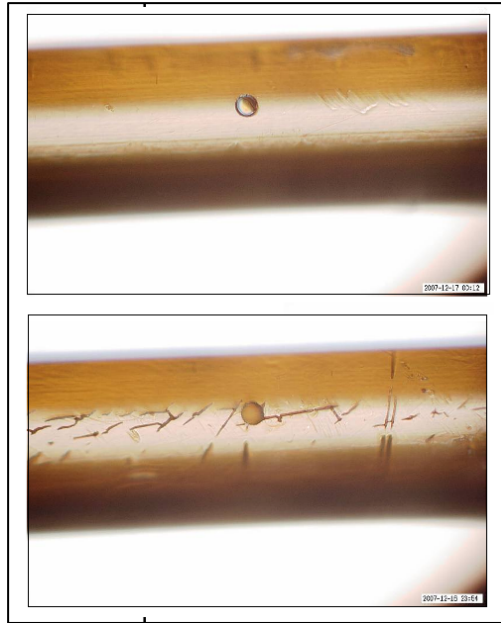


Figure 3.18: Holes produced by photolithography on polyimide tubes.

### 3.5 CONCLUSION

It has taken significant time to manufacture the drug delivery device (polyimide micro tubes with holes). Although a simple manufacturing procedure has been described, but the actual process involved multiple steps with several method modifications. The Finite Element Method approved the initial design of the stent structure with slight modifications. The dimensions of both the stent and the drug delivery device were successfully estimated, which can be applied to produce a prototype. The coating of the polymer matrix with the biocompatible alloys reduced surface roughness encouraging the use of the device as an implant. The coating did not fracture after it was bent. Micro fabrication of polyimide matrices with photolithography and laser drilling yielded perforations between 25 – 40  $\mu\text{m}$  size ranges.

After the holes were fabricated on the perforated tubes, the next step was to load the perforated microtubes with drug. The following chapter discusses the drug loading methodologies and data of the perforated polyimide tubes with different drugs.

Even though the project was initiated to develop a polymer free DES, the preliminary *in vitro* drug release data (discussed in Chapter 5) suggested that the drug delivery device can be used for multiple applications such as management of pain, cancer, and ophthalmic diseases. From that point onwards, the focus has been on the development and the evaluation of the micro scalable perforated device as a general purpose drug delivery device.

## **Chapter 4: Drug loading of the micro scalable perforated device**

### **4.1 INTRODUCTION**

After fabrication of holes on the perforated microtube the next step in the development process was to load the perforated tubes with drugs. Drug loading is an important consideration because the way the drug is packed inside a reservoir greatly influences the drug release [146]. A loosely packed device with void spaces inside it may cause faster release as well as batch variations. A tightly packed device on the other hand ensures content uniformity and homogenous distribution of the drug.

Drug loading of a micro device is challenging and commonly used powder feeder and filling methods are not suitable. The size also limits the use of other mechanical and electrical loading methods such as vacuum suction and voltage pulse [147]. Loading the micro tubes with hydrogels might seem like a plausible solution. Hydrogels are frequently used in controlled release systems because they are biocompatible and their swelling level can be easily manipulated to occupy the entire space inside the device [148]. However, duration and rate of drug release is dependent on hydrogel properties such as swellability, drug holding capability, and drug polymer interactions [148-150].

An effective loading method was achieved with a high density suspension or a supersaturated solution of the drugs using micro syringes, touhy borst adapters, or capillary action. For this reason, solubility of the drug becomes an important factor in drug loading and selection of a model drug. However, other techniques such as the ones used for filling HPLC columns with stationary phases might also be used to fill the

microtubes. Three model drugs were used to validate the drug loading technique, namely prednisolone, ethinyl estradiol, and crystal violet.

#### **4.1.1 Prednisolone**

Prednisolone is a synthetic adrenocortical steroid drug metabolically interconvertible with prednisone [151, 152]. It is a potent anti-inflammatory and immuno-suppressant agent [153-156]. Prednisolone is soluble in methanol and dioxane, very slightly soluble in water, and one gram of the drug dissolves in about 30 ml of alcohol [157]. Figure 4.1 illustrates the molecular structure of prednisolone ((11 $\beta$ )-11,17,21-trihydroxypregna-1,4-diene-3,20-dione) [158].

Prednisolone induces anti-inflammatory effect by inhibiting leukotriene production [159], and promoting cellular release of lipocortin-1 [160] which prevents synthesis of prostaglandins' precursor arachidonic acid [161]. It also blocks the release of inflammatory mediators such as neutrophils, macrophages, mastocytes [162, 163], and cytokines (interleukin-5, interleukin-8) [164]. Prednisolone is used in ophthalmics as an ointment or an eye drop to treat ocular inflammation [134, 165-168]. It is also used in post-operative eye surgery [169, 170]. Due to its inflammatory properties, prednisolone has also found its use in stents as an anti-restenosis drug [171]. Restenosis is a result of two major mechanisms, inflammation and cell proliferation at the site of injury in the stented artery. Drugs such as paclitaxel and sirolimus are being currently used in drug eluting stents to prevent scar-tissue growth and neointima formation. A novel drug, TRM-484, consisting of nanoparticles of prednisolone has reduced smooth muscle cell (SMC)

proliferation and macrophage migration *in vitro* [172]. The nanoparticles act on site specific targeting areas of injury at systemic concentrations without inducing the side effects associated with oral delivery.

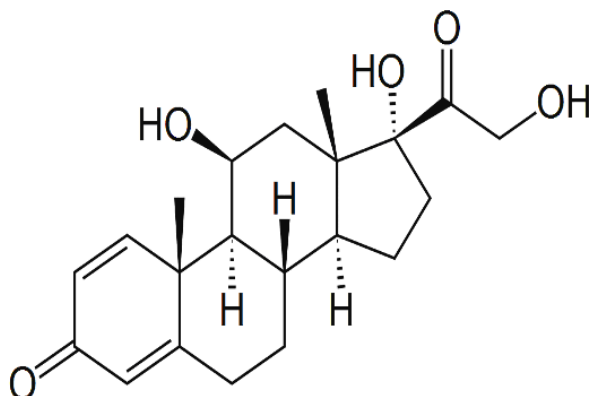


Figure 4.1: Molecular structure of prednisolone [158].

#### 4.1.2 Ethinyl Estradiol

Ethinyl Estradiol (EE or  $17\alpha$ -ethynylestradiol) is the synthetic analogue of the estrogenic steroid estradiol, which was synthesized in 1938 in Berlin [173]. EE is most commonly used in contraceptives and is at least 20 times as potent in oral doses than the natural estradiol hormone [174]. The IUPAC name of EE is 17-ethynyl-13-methyl-7,8,9,11,12,13,14,15,16,17-decahydro-6H-cyclopenta-a phenanthrene- 3,17-diol, and its molecular structure has been illustrated in Figure 4.2 [175]. It is soluble in vegetable oils, alkali hydroxides, practically insoluble in water and 1 part of the drug dissolves in 6 parts

of ethanol [157]. Amongst estrogens, EE was selected as the model drug because it has better alcohol solubility, which facilitated drug loading.

Apart from their contraceptive action, estrogens are also known as augmenters of vascular endothelial growth factor (VEGF), which in turn promotes VEGF dependent angiogenesis [176]. Angiogenesis is a natural process which involves growth of new blood vessels and aids in natural growth and development, as well as in wound healing [177]. In contrast, angiogenesis is also involved in the proliferation of tumors [178]. However, current investigations have focused on therapeutic angiogenesis to manage ischemic heart diseases and peripheral artery diseases [179-182]. These studies are focusing on the creation of new blood vessels to bypass the blocked arterial sites. A local delivery of EE to the blocked site hence, might serve as another potential and novel use.

Estradiol eluting stents have also shown promising long-term results due to their ability to promote endothelial cell growth at the stenting site [183]. As previously discussed, endothelialization is important for the stent to become part of the vasculature and prevent future complications, in form of restenosis and late stent thrombosis.

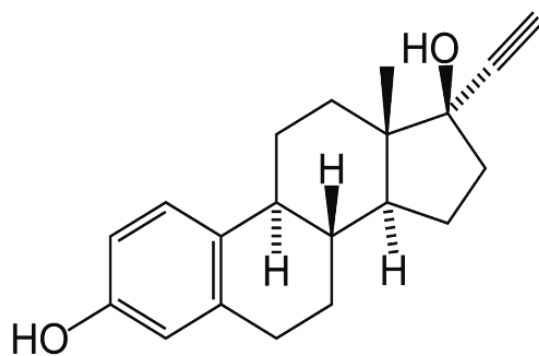


Figure 4.2: Molecular structure of ethinyl estradiol [175].

### 4.1.3 Crystal Violet

Crystal violet (CV or gentian violet) is an antifungal agent which is also commonly used in cell culture techniques as a staining agent [184, 185]. Crystal violet was chosen as the model drug because it gives a prominent color in the solution due to its high molar extinction coefficient [186]. Figure 4.3 illustrates the molecular structure of crystal violet (N-(4-(Bis(4-(dimethylamino)phenyl)methylene)-2,5-cyclohexadien-1-ylidene)-N-methylmethanaminium chloride) [187]. The solubility of crystal violet is 0.2% in water and 14% in ethanol [157]. An aqueous solution of crystal violet shows maximum absorption at 590 nm.

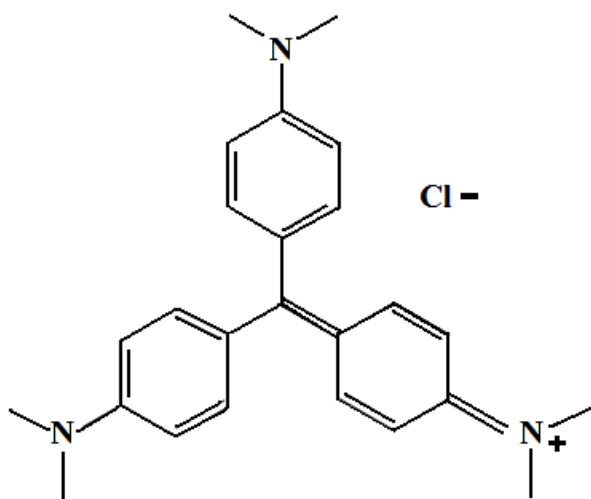


Figure 4.3: Molecular structure of crystal violet [187].

## **4.2 MATERIALS AND METHODS**

### **4.2.1 Materials**

Prednisolone, ethinyl estradiol, crystal violet, and phosphate buffered saline (PBS) were obtained from Sigma-Aldrich (St. Louis, MO, USA). Different size polyimide tubes were obtained from Microlumen Inc. (Tampa, FL, USA). Touhy Borst adapters were obtained from Qosina (Edgewood, NY, USA). N-butyl cyanoacrylate (referred in text as superglue) was obtained from a local convenient store. Bioglue™ was obtained from Cryolife Inc. (Kennesaw, GA, USA). Medical grade steel wires were obtained from Small Parts Inc. (Miramar, FL, USA). Heat shrink polyolefin tubings (3.0 mm diameter) were obtained from Altex (San Antonio, TX, USA).

### **4.2.2 Polymorphism Characterization of Prednisolone and Ethinyl Estradiol**

As ethanolic drug solutions were used for drug loading, there was a possibility of formation of solvates and other polymorphs of the compounds. Accordingly, polymorphic studies were performed. Briefly, excess amount of anhydrous prednisolone and ethinyl estradiol were dissolved in ethanol, by heating to 80°C. The solutions were allowed to stand overnight to evaporate the alcohol. Following day, alcohol treated prednisolone and ethinyl estradiol were analyzed using a Digital Microscope KH-7700 (Hirox Inc., River Edge, New Jersey). Afterwards, 5 - 10 mg of original anhydrous samples and alcohol treated samples were weighed into aluminum pans and sealed. A modulated differential scanning calorimetry (MDSC) (TA Instruments, New Castle, DE,

USA) was used to analyze the samples. A nitrogen atmosphere with a heating rate of 3°C/min over a temperature range of -20–110°C and a modulation rate of 1°C/min was used. The glass transition temperature was determined as the midpoint of the transition using Universal V3.0G software.

### **4.2.3 Fabrication of holes and drug loading**

A standard procedure was developed to load the polyimide tubes. The tubes were cut manually into desired length. The exact length of the tubes was measured using a digital caliper (Ted Pella Inc., Redding, CA, USA). The weight of the empty tube before and after drug loading was measured using Thermo-Gravimetric Analyzer (TGA-7, Perkin Elmer Inc., Waltham, MA, USA). The tubes were loaded with a suspension, solution, or powder.

#### ***4.2.3.1 Drug loading with Prednisolone***

Twelve polyimide micro tubes (length = 15 mm; I.D. = 125 µm) were loaded with ethanolic suspension of prednisolone using touhy borst adapters attached to a syringe (Figure 4.4). This was the first attempt to test drug loading on microtubes and hence these tubes did not have any holes on the surface. Briefly, an ethanolic suspension of prednisolone was prepared by adding 200 mg of prednisolone to 0.5 ml ethanol. A 1 ml syringe, which was attached to the touhy borst adapter, was filled with the high density suspension. The polyimide tube was screwed tightly to the other end of the adapter, and

the prednisolone suspension was injected into the tube. Afterwards, the ethanol was evaporated by allowing the tubes to stand overnight. The final weight was analyzed using TGA-7 and pictures were taken using Hirox Digital Microscope KH-7700.

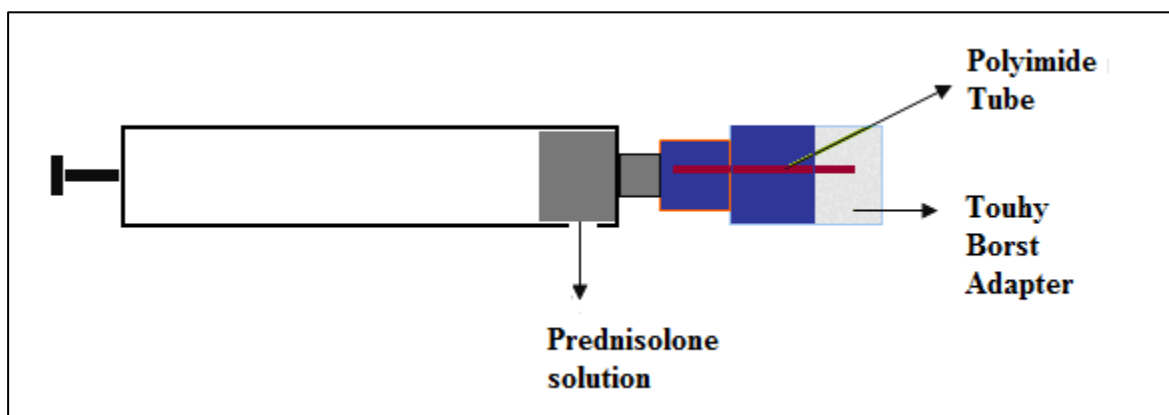


Figure 4.4: Drug loading using touhy borst adapter.

#### ***4.2.3.2 Drug loading with Crystal Violet***

##### **4.2.3.2.1 Small tubes**

Polyimide tubes (I.D.= 125  $\mu\text{m}$ , referred to in text as small tubes) were cut to 20 mm in length. Three subsets of perforated polyimide tubes having a one hole, two holes, or three holes through the tube's surface were prepared (Figure 4.5). The holes can be produced by either laser drilling or photolithography techniques. The holes were placed at even distances on the tubes with respect to each other and also with respect to the tube ends. The average hole size of all the three groups was  $32.9 \pm 1.7 \mu\text{m}$  ( $n = 45$ ).

Loading of these microtubes was achieved using a highly concentrated solution of CV in ethanol (400 mg/ml), prepared by heating to 80 °C. Drug loading of the solution inside the perforated tubes was achieved using capillary action. The tubes were allowed to stand overnight at room temperature to evaporate the alcohol. The ends of the tubes were plugged with a stainless steel wire (120  $\mu\text{m}$  diameter) (Small Parts Inc., Miramar, FL, USA) and sealed with biocompatible glue. The tubes were prepared for the drug release studies as described in Chapter 5.

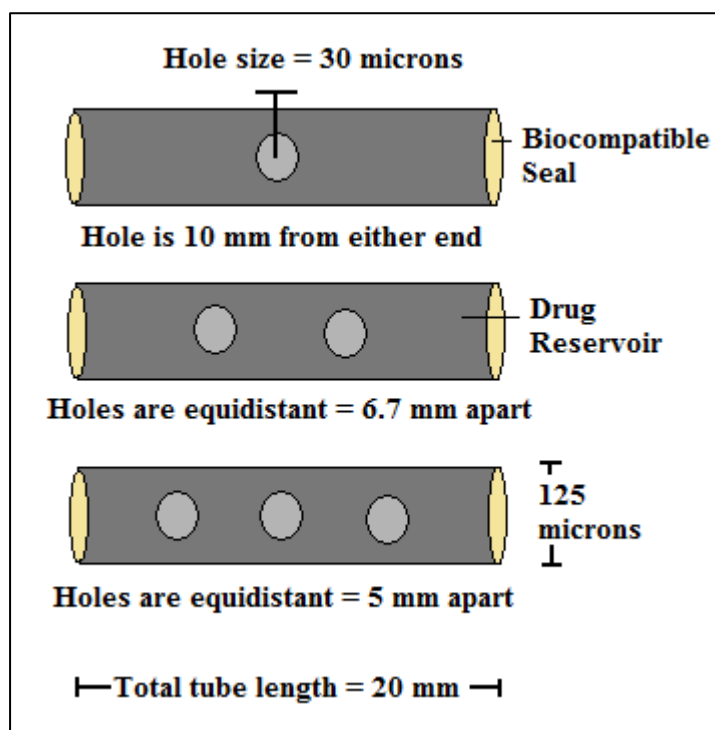


Figure 4.5: Polyimide tubes with different number of holes on the surface. The holes are equidistant from each other and also from the ends of the tube.

#### **4.2.3.2.2 Large tubes**

A larger polyimide tubes (I.D. = 1000 microns, referred to in text as large tubes) for releasing larger amounts of CV were used. The holes were manually drilled using drill bits. Three subsets were prepared differing from each other in either number of holes or size of the holes. For the first subset, 10 mm tubes were cut in length and a single hole was fabricated at the center using a 300 micron drill bit; the second subset had two holes on 15 mm tubes; and the third subset consisted of one bigger size hole drilled using a 450 micron size drill bit on 10 mm tubes.

The large perforated tubes were tightly packed with CV powder and placed on a glass slide with a piece of polyolefin tubes on its ends. A propane lighter was used to apply heat from the other side of the glass slide. The polyolefin tubes shrank due to heat and were immediately crimped to ensure proper sealing of the CV loaded tubes. The tubes were prepared for the drug release studies described in Chapter 5.

#### **4.2.3.2.3 Large tubes without holes**

Another set of polyimide tubes (length = 10 mm) without any holes but with different diameters, ranging from 200 to 600 microns (referred to in text as ‘large tubes without holes’) were used (Figure 4.6). The tubes were used to study the release rates as a function of hole size. The tubes were loaded with concentrated solution of CV as previously discussed. One end of the tubes was sealed with biocompatible glue after drug loading. The tubes were prepared for the drug release studies as described in Chapter 5.

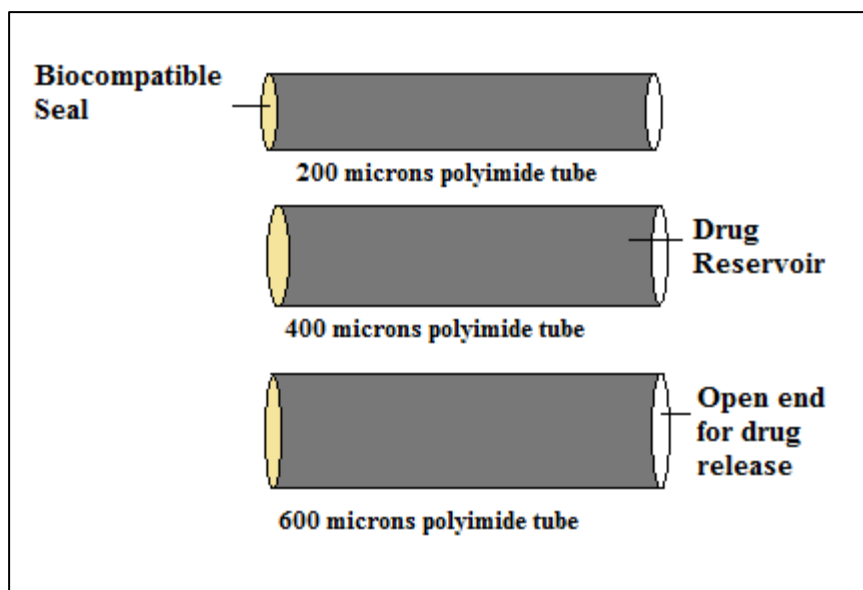


Figure 4.6: Large tubes without holes. Crystal violet was loaded into the tubes and one end was sealed using biocompatible glue and other end was left open for drug release.

#### ***4.2.3.3 Drug Loading with Ethinyl Estradiol***

Two groups of tubes (I.D. = 125  $\mu\text{m}$ ), with three holes on the surface were used. The two groups differed in the size of the holes,  $20.1 \pm 1.1 \mu\text{m}$  ( $n = 27$ ) and  $33.3 \pm 1.7 \mu\text{m}$  ( $n = 21$ ), respectively. The two groups have been referred to in text as 20 micron and 30 micron groups. The tubes were loaded with ethinyl estradiol using the drug loading method similar to CV. Briefly; a 160 mg/ml ethanolic solution of EE was prepared by heating to 80°C. Drug loading was achieved using capillary method. Alcohol was evaporated and ends sealed using stainless steel wire and biocompatible glue. For estimation of homogeneity of distribution inside the tubes, an uncoated tube was loaded with ethinyl estradiol and observed using Nikon TE2000-E confocal microscope and

Metamorph 7.6 software (Molecular Devices, Sunnyvale, CA). The tubes were prepared to study the biological response from the device as described in Chapter 8.

#### **4.2.4 Statistical Analysis**

Levene's test was used to assess the homogeneity of variance in various groups. One way ANOVA with post hoc analysis using Tukey-HSD test (equal variance assumed) or Games Howell test (equal variances not assumed) through SPSS statistical software was used to analyze difference within the groups with respect to hole size and drug loading.

### **4.3 RESULTS AND DISCUSSION**

#### **4.3.1 Differential Scanning Calorimetry**

Differential Scanning Calorimetry (DSC) is a common analytical technique which is used to detect the presence of different polymorphs in a sample. Polymorphism is the ability of a drug to exist in more than one crystalline forms [188]. Polymorphs have their own distinct melting points and hence different glass transition temperatures will indicate respective polymorphs. In pseudo-polymorphism, the different crystal types are formed as a result of hydration or solvation from a particular solvent [189]. Different polymorphic forms of a particular drug may differ in solubility and potency and hence may also vary in dissolution rates, safety, and efficacy. However, similar phenomenon may or may not be observed with pseudo polymorphs [190].

During drug loading, a suspension or a solution of the drug was prepared in ethanol and the alcohol was evaporated after the tubes were loaded with the drug. This may have led to formation of different polymorphs such as desolvates, hydrates or even polymorphic inter conversions such as from crystalline to amorphous or vice versa. [190]. Additionally, there is evidence in literature that suggests that pseudo-polymorphism can be induced by solvents such as water, ethanol, and methanol [191, 192] and solvates of both prednisolone and ethinyl estradiol have been observed in different solvents [189, 190]. Figure 4.7 illustrates an example of prednisolone crystal structure which was obtained while evaporation of alcohol.

The aim of this study was to investigate whether any solvates formed by dissolution of drug in ethanol exhibited any polymorphic properties. Figure 4.8 and 4.9 illustrate the thermograms of anhydrous prednisolone and alcohol treated prednisolone, respectively. Figure 4.10 illustrates the combined thermograms of treated and untreated samples of EE. There was no significant difference found between the treated and untreated groups with respect to the glass transition temperature, in both prednisolone (untreated = 240.34 °C; alcohol treated = 238.88 °C) and EE (untreated = 185.35 °C; alcohol treated = 185.56 °C) suggesting that no true polymorphs were formed with alcohol treatment.

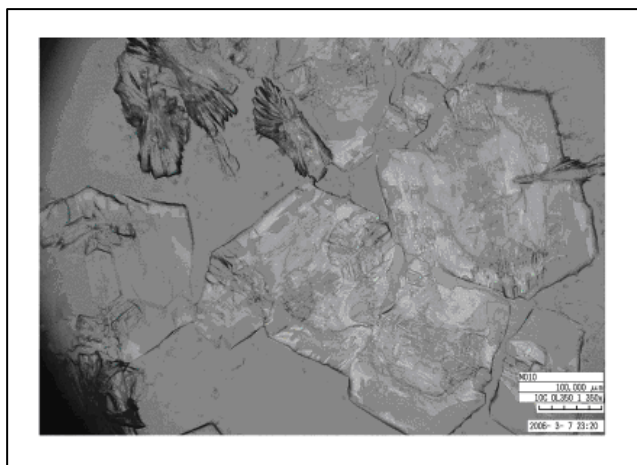


Figure 4.7: Prednisolone crystals after evaporation of alcohol

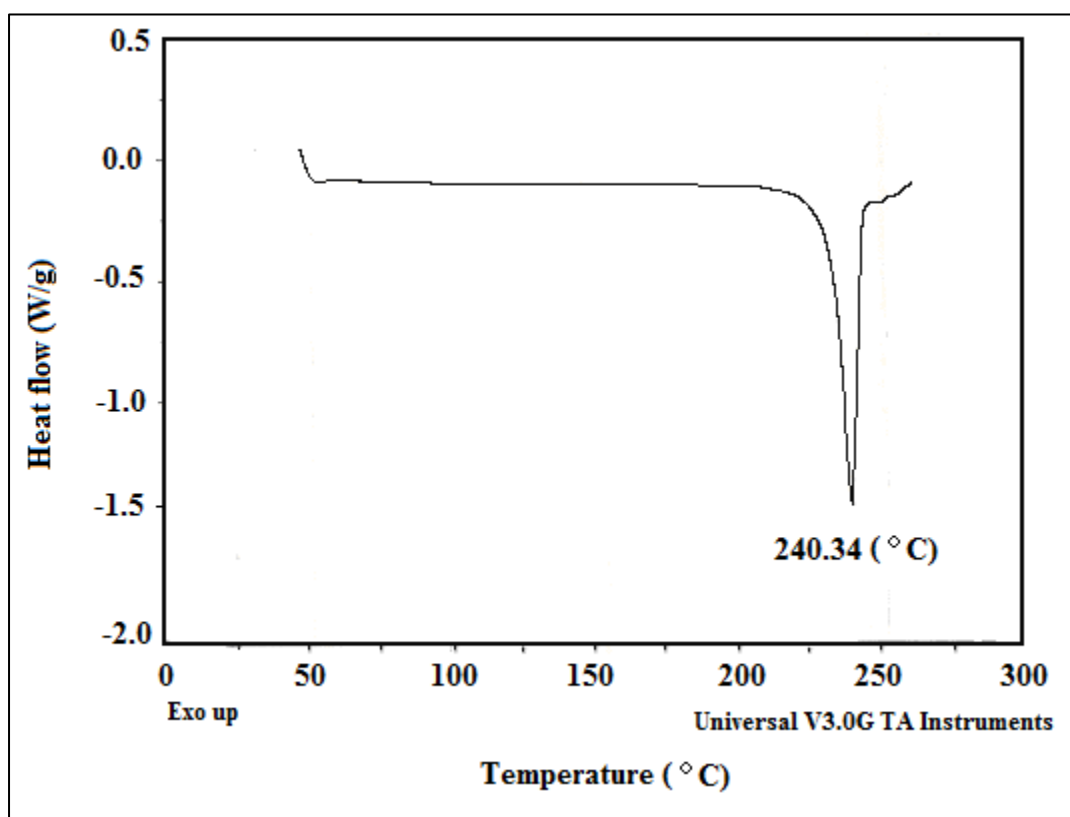


Figure 4.8: Modulated differential scanning calorimetric (MDSC) thermogram of anhydrous prednisolone.

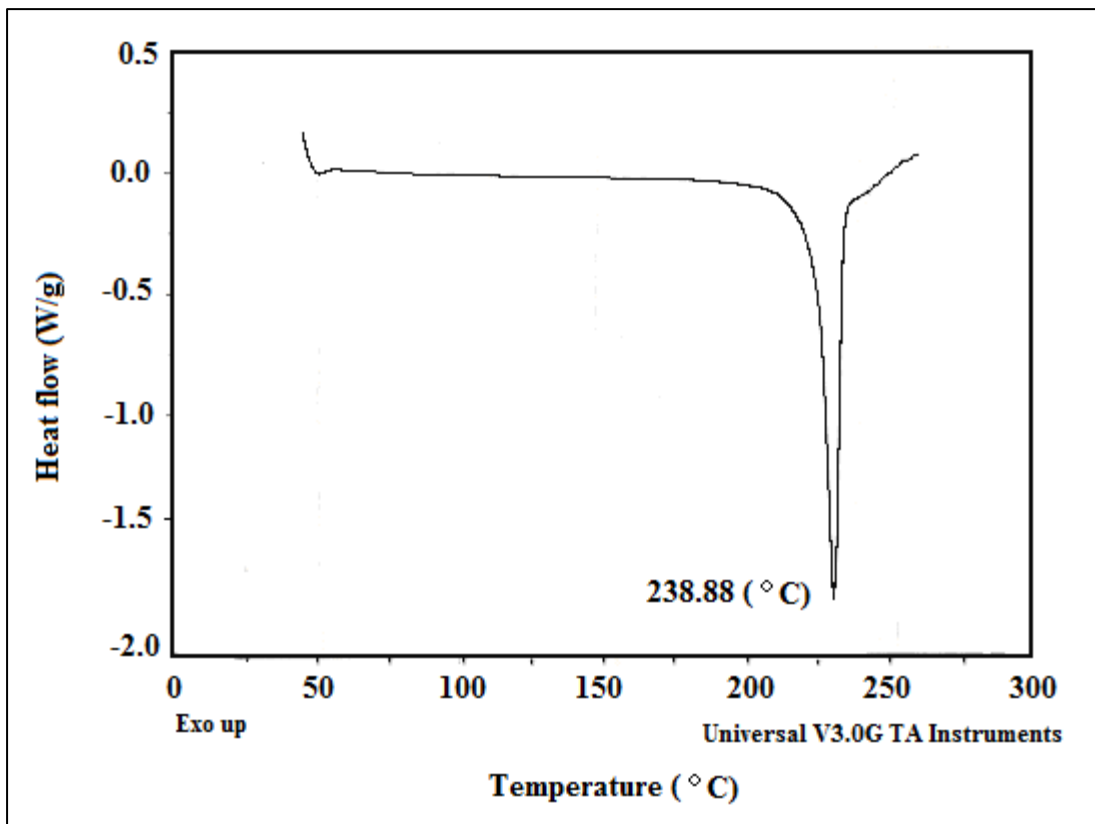


Figure 4.9: Modulated differential scanning calorimetric (MDSC) thermogram of alcohol treated (ethanolates) prednisolone.

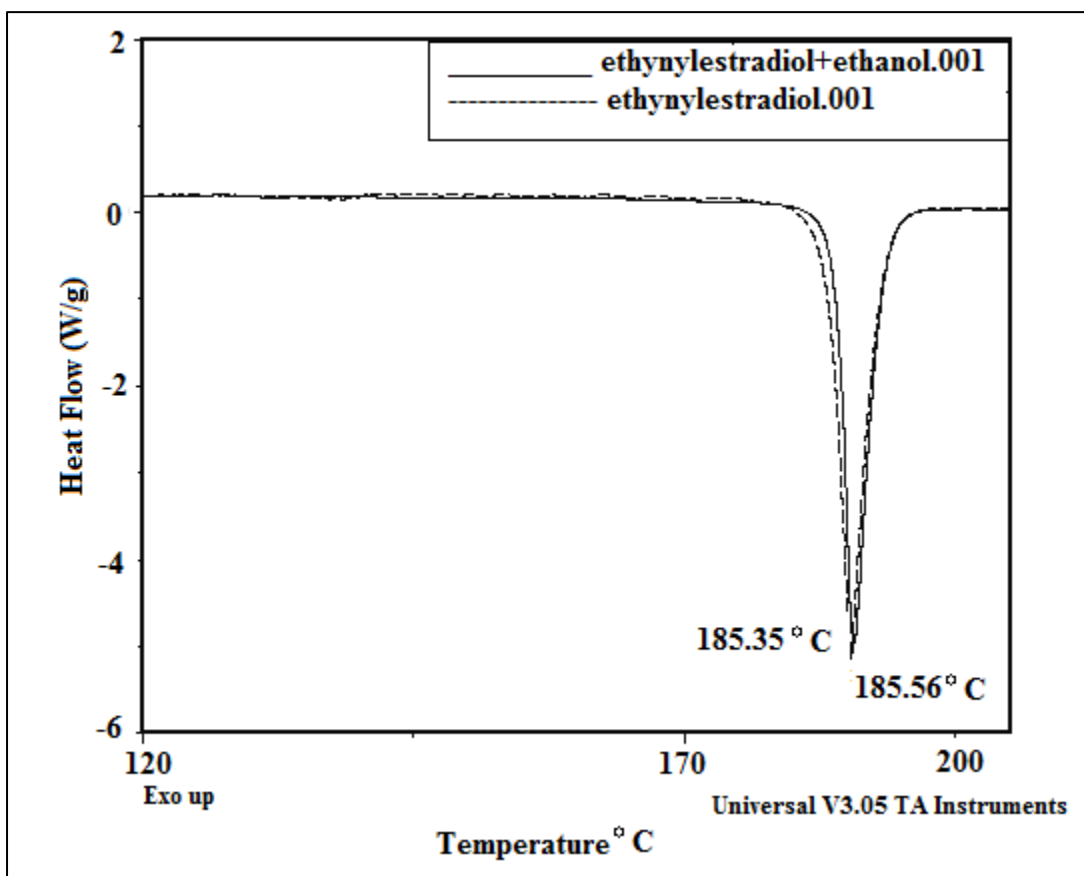


Figure 4.10: Comparison of modulated differential scanning calorimetric (MDSC) thermograms of untreated and alcohol treated anhydrous ethinyl estradiol.

## 4.3.2 Drug Loading Studies

### 4.3.2.1 Drug loading with Prednisolone

The drug loading data of prednisolone for twelve polyimide tubes is illustrated in Table 4.1. As shown in the table, a net amount of  $87.6 \pm 11.7 \mu\text{g}$  of prednisolone was loaded into the tubes. The amount of drug loaded per unit length of the tube was  $5.7 \pm 0.7 \mu\text{g}/\text{mm}$ . The net amount of drug loaded indicated content uniformity amongst all the

tubes whereas, amount of drug loaded per unit length indicates the homogeneity of drug distribution inside the tube. The low coefficient of variance (%CV) suggested that all the tubes were loaded uniformly. However, micrographs of prednisolone loaded tubes (Figure 4.11) showed void spaces suggesting an uneven distribution of drug inside the tube.

Table 4.1: Drug loading data of polyimide tubes loaded with prednisolone.

Tube	Length (mm) (A)	Initial Weight ( $\mu\text{g}$ ) (B)	Weight after 24 hrs ( $\mu\text{g}$ ) (C)	Net amount of drug loaded ( $\mu\text{g}$ ) (C-B)	Amount of drug loaded per unit length ( $\mu\text{g}/\text{mm}$ ) (C-B)/A
1	15.5	210.0	293.0	83.0	5.4
2	14.7	200.0	279.0	79.0	5.4
3	15.5	212.0	316.0	104.0	6.7
4	14.6	197.0	284.0	87.0	5.9
5	15.2	210.0	277.0	67.0	4.4
6	15.6	214.0	291.0	77.0	4.9
7	15.2	209.0	290.0	81.0	5.3
8	15.3	214.0	305.0	91.0	5.9
9	15.9	217.0	310.0	93.0	5.8
10	16.6	224.0	333.0	109.0	6.6
11	15.0	208.0	293.0	85.0	5.7
12	15.6	214.0	309.0	95.0	6.1

<b>Average</b>	87.6	5.7
<b>S.D.</b>	11.7	0.7
<b>% C.V.</b>	13.4	11.4

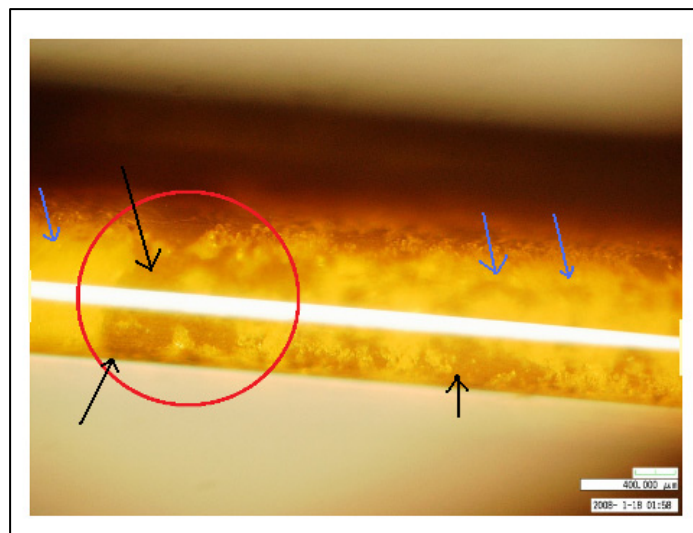


Figure 4.11: The circle region shows void spaces inside the polyimide tube loaded with prednisolone. The void spaces are indicated by black arrows and the drug filled regions are indicated by blue arrows. The white line at the centre is the reflection of the light.

### 4.3.2.2 Drug loading with Crystal Violet

#### 4.3.2.2.1 Small tubes

The average diameter of one hole, two holes, and three holes group was measured as  $32.5 \pm 1.5$ ,  $32.3 \pm 1.0$ , and  $33.3 \pm 1.7$   $\mu\text{m}$ , respectively. Each group consisted of seven tubes and therefore  $n = 7$ , 14, and 21 for the three groups. The combined average diameter of the holes was measured as  $32.9 \pm 1.7$   $\mu\text{m}$  for the three groups ( $n = 45$ ). An average of  $127.1 \pm 11.9$   $\mu\text{g}$  of CV was loaded in all the three groups. The drug loading data is illustrated in Figure 4.12. Statistical significant difference were not observed amongst the three groups with respect to hole size or drug loading,  $p > 0.05$ .

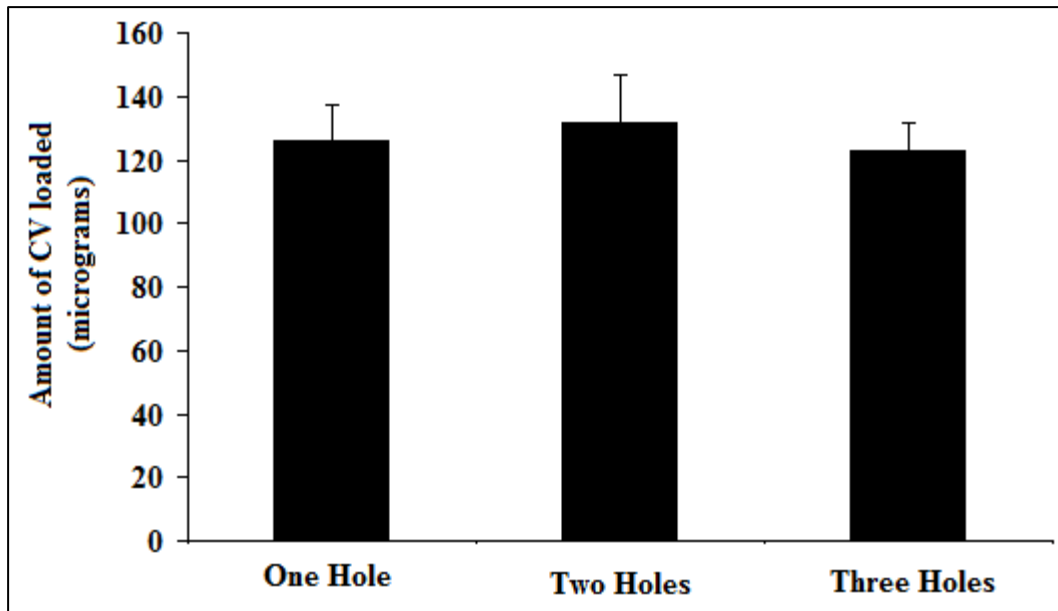


Figure 4.12: Three group of polyimide tubes with one hole, two holes, and three holes respectively were loaded with crystal violet. Statistical significant difference was not observed between the groups. Results are reported as mean with standard deviation,  $p > 0.05$  ( $n=7$ ).

#### 4.3.2.2.2 Large tubes

Three subsets of large holes were prepared - The first subset consisted of one hole ( $365.3 \pm 16.7 \mu\text{m}$ ); the second subset consisted of two holes ( $362.4 \pm 23.1 \mu\text{m}$ ); and the third subset consisted of one bigger size hole ( $542.6 \pm 26.3 \mu\text{m}$ ). The average amount of CV loaded per unit length in the groups was  $5.3 \pm 0.3$ ,  $5.2 \pm 0.3$ , and  $5.4 \pm 0.3 \text{ mg/cm}$ , respectively. The drug loading data is illustrated in Figure 4.13. Statistical analysis for drug loading did not yield any significant difference amongst the groups,  $p > 0.05$ .

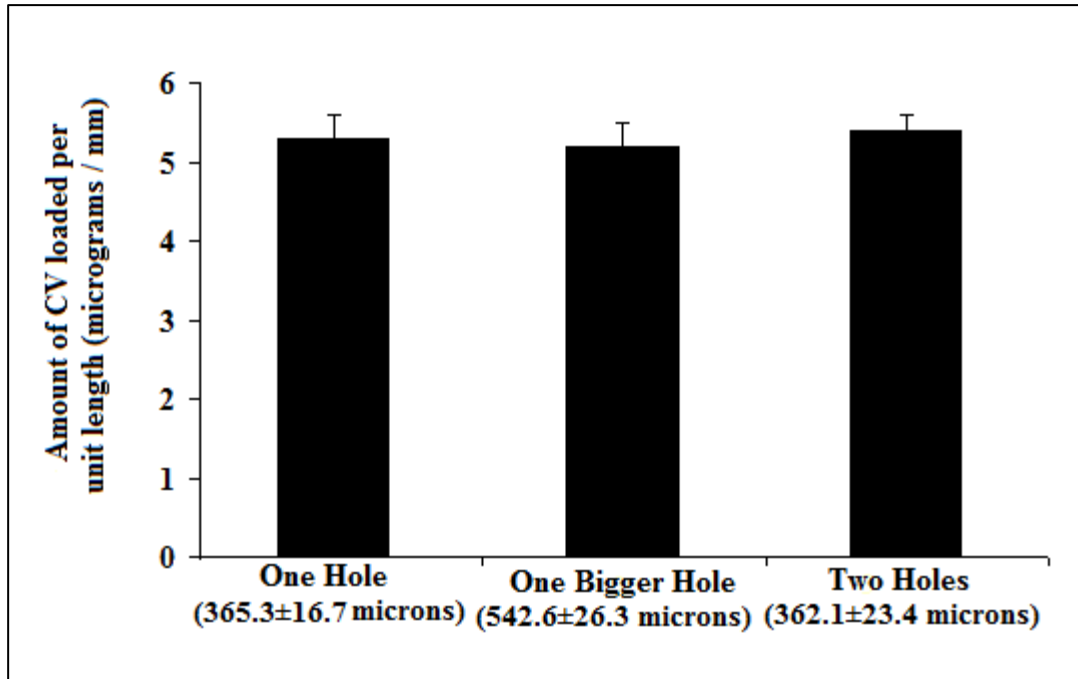


Figure 4.13: Drug loading in ‘large tubes’ was found to be uniform per unit length and statistical difference was not observed amongst the groups. Results are reported as mean with standard deviation,  $p > 0.05$  ( $n=12$ ).

#### 4.3.2.2.3 Large tubes without holes

Polyimide tubes with different sizes (I.D. = 200, 400, and 600  $\mu\text{m}$ ) were loaded with crystal violet. The length of all the tubes was 10 mm. The drug loading data was standardized by calculating the average amount of crystal violet loaded in each group per unit volume. The drug loading data is illustrated in Figure 4.14. Drug loading in 600 micron group was significantly different than the other two groups,  $p < 0.05$ .

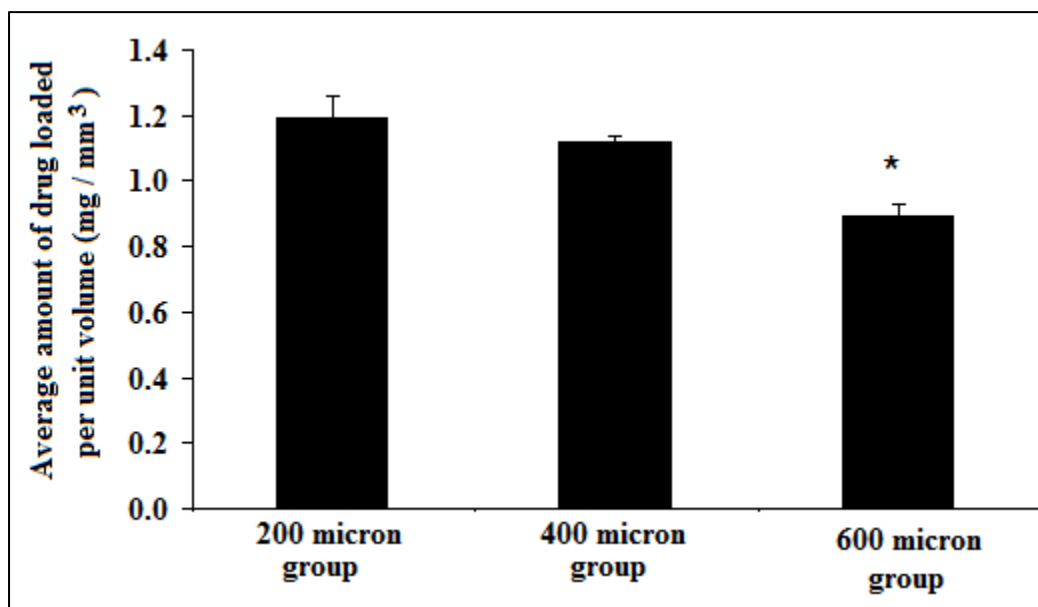


Figure 4.14: Drug loading in subsets belonging to ‘large tubes without holes’. Polyimide tubes with different diameters, 200 microns, 400 microns, and 600 microns respectively were loaded with crystal violet. The drug loading in 600 micron group was found to be significantly different than the other two groups. Results are reported as mean with standard deviation, \*:  $p < 0.05$  ( $n=4$ ).

#### 4.3.2.3 Drug loading with Ethinyl Estradiol

Two groups of polyimide microtubes (I.D. = 125  $\mu\text{m}$ ; length = 20 mm) with three equidistant holes on the surface were prepared. The hole diameter in the two groups were  $20.0 \pm 1.1$  ( $n = 27$ ) and  $33.3 \pm 1.7$   $\mu\text{m}$  ( $n = 21$ ), respectively. The two groups have been referred to in text as 20 micron and 30 micron groups. The average amount of EE loaded in the 20 and 30 micron groups were  $51.7 \pm 4.8$  and  $57.9 \pm 9.9$   $\mu\text{g}$ , respectively. The drug loading data is illustrated in Figure 4.15. Statistical difference in drug loading was not observed between the two groups,  $p > 0.05$ . Figure 4.16 shows a polyimide tube before and after loading with EE. The empty spaces within the drug loaded tube suggest that

although the drug loaded tubes are equivalent in weight but they may have uneven distribution.

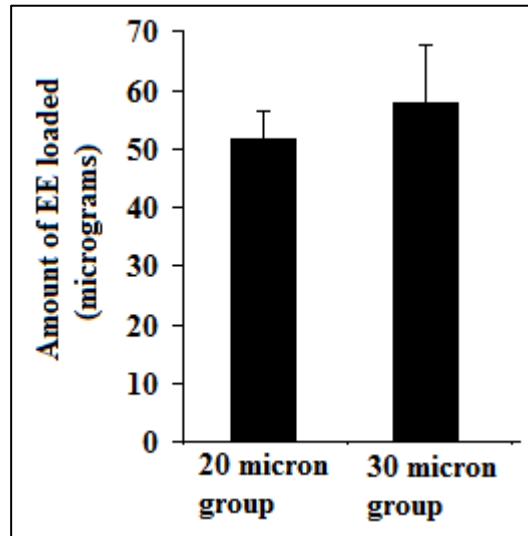


Figure 4.15: Drug (EE) loading in 20 and 30 micron tubes was found to be uniform with no statistical significant difference amongst the tubes with respect to each other. Results are reported as mean with standard deviation,  $p > 0.05$  ( $n=7$ ).

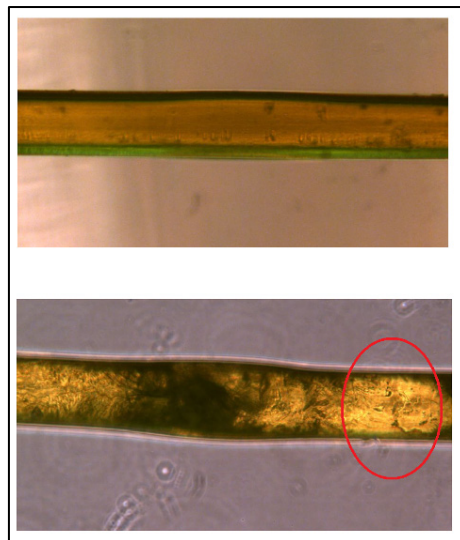


Figure 4.16: Ethinyl estradiol loaded polyimide tube (bottom) in contrast to an empty tube (top). The region circled in red shows empty spaces left inside the tube after alcohol was evaporated indicating uneven distribution of drug.

### 4.3.3 Capping and Sealing of the Tubes

*Superglue* - Higher alkyl group cyanoacrylates, such as n-butyl cyanoacrylate and n-octyl cyanoacrylate, are used as tissue adhesives and form a tough bond with the surface of contact [193]. During initial studies, superglue was evaluated as one of the sealants. The glue was found to degrade slowly in the aqueous environment. In addition, removal of glue at the end of the experiment was tedious.

*Bioglue<sup>TM</sup>* - Bioglue is composed of albumin and glutaraldehyde. Once in contact, the two components completely polymerize within two minutes [194]. Since its launch in 1998, bioglue has been widely used in various medical procedures such as cardiovascular surgery, thoracic surgery, and as a spinal dural sealant [195-198]. Bioglue was used to seal the ends of 'large tube without holes'. For 'small tubes' and tubes loaded with ethinyl estradiol a cap was made to seal the ends. A size bigger polyimide tube (ID = 170  $\mu\text{m}$ ) was taken and cut into 5 mm pieces. One end of this cap was blocked using a stainless steel wire (ID = 125  $\mu\text{m}$ ) and a bioglue. The cap was placed over the end of the drug loaded tubes and sealed using a bioglue. The caps were dipped in ethanol in order to clean them and to ensure that there is no drug leakage. The ethanol also served as a dehydrating agent for the albumin-glutaraldehyde complex which further enhanced the bonding strength.

*Heat Shrink Tubes* – Heat shrink tubes were used to cap the 'large tubes'. On application of heat the tubes shrank and formed a leak proof cap over the drug loaded tubes.

#### **4.4 CONCLUSION**

The three model drugs with variable solubilities in alcohol and water were successfully loaded into the tubes. Prednisolone and ethinyl estradiol did not form any true polymorphs and are suitable for drug loading and drug release studies. Content uniformity was achieved across various groups but homogenous drug distribution within the micro device is still desired. The variation in drug distribution might affect drug release and be a probable contributor to the variability in results. The tubes with diameter greater than 400 microns can be manually packed with drug powder. The capillary force is the simplest and most feasible drug loading method for microtubes in a laboratory setting. However, other techniques such as the ones used for filling HPLC columns with solids might also be used to fill the microtubes. Lastly, the methods developed to cap and seal the ends of the tubes were successful in preventing any leakage of the drug.

## **Chapter 5: *In Vitro* Drug Release Studies to Evaluate the Micro Scalable Perforated Device Capable of Long-Term Zero Order Drug Release**

### **5.1 INTRODUCTION**

After the successful fabrication of holes on the tube's surface and drug loading of the tubes, the next step in the development process was to evaluate the perforated tubes for their capability to produce zero order release rates. In this chapter, the *in vitro* drug release studies using the drug loaded tubes from Chapter 4 have been summarized. The perforated drug delivery system was also tested for its scalability by using different sized tubes varying in hole numbers and hole size. Additionally, the perforated system was also tested in a different dissolution medium, rabbit's vitreous humor (Chapter 6). The drug release data in all the studies indicated that a perforated microtube is capable of producing zero order drug release for prolonged periods ranging from months to years. Concentration gradient of the drug was observed to be the main driving force for drugs diffusion. After chance discovery of these results, it became evident that the perforated tubes are not limited for use in just drug eluting stents (DES) and can be applied to other applications as well. Hence, current efforts are now dedicated to develop a general purpose drug delivery device, where DES can be one of its several applications.

The perforated tube also offers several advantages over other diffusion controlled reservoir type devices. In general, such devices are known to yield zero order release rates due to the concentration gradient maintained across the membrane [199]. However,

membrane effects such as ‘boundary layer problem’, ‘burst effect’, and ‘membrane rupture’ have been described, which may become rate controlling steps [200]. A boundary layer problem arises when drug release is stalled due to drug saturation at the membrane [201]. A burst effect may be observed when a device, which is stored for a long time, exhibits rapid release due to prior accumulation of drug at the membrane [200], and similar occurrence is also seen with polymer controlled drug delivery systems [202]. Membrane rupture may result in drug dumping causing toxicity concerns [203]. The present investigation presents a potential solution to these problems because the perforated tubes do not require membrane to control drug release and hence are potentially free from membrane related effects.

In this chapter, the *in vitro* drug release is presented demonstrating long-term zero order drug release from the perforated tubes. It was observed that the drug release from the device is dependent on the solubility of the drug, the distance between the holes, and the area available for drug diffusion. The diffusion area in turn is dependent on the number of holes and the size of the holes. Since, the size of the holes is very small as compared to the total device size and the distance between the holes, the release rate from each hole is independent from each other as long as the basic conditions of solubility and sink conditions are met.

A series of experiments were designed to determine the release rates from the perforated microtubes. Different sized microtubes were used to study the effect of device size. The number of holes, size of the holes, and the distance between holes were varied to study their effect on drug release. The triphenylmethane dye, crystal violet (CV) was selected as the model drug. It is a commonly used biological staining agent with anti-

fungal properties [204] and high molar extinction coefficient, making it easily detectable spectrophotometrically even at very low concentrations [205, 206]. Polyimide was used because it is biocompatible, chemically inert, and widely used in fabrication of implantable micro electrodes [207-209].

## **5.2 MATERIALS AND METHODS**

### **5.2.1 Materials**

Polyimide tubes were obtained from Microlumen Inc. (Tampa, FL, USA). Crystal violet was obtained from Sigma-Aldrich (St. Louis, MO, USA). Bioglue™, a biocompatible glue, was obtained from Cryolife (Kennesaw, GA, USA). Microvials (0.3 ml) were obtained from Perkin-Elmer (Waltham, MA, USA). Glass vials (2.0 ml) were obtained from Agilent (Santa Clara, CA, USA). Borosilicate Glass tubes (10.0 ml) were obtained from Fisher Scientific (Pittsburgh, PA, USA). Drill bits of different sizes (Dremel®, Racine, WI, USA) were obtained from HobbyTown (San Antonio, TX, USA).

### **5.2.2 *In vitro* drug release studies**

The three groups of crystal violet loaded tubes (small tubes, large tubes, and large tubes without holes) as described in Chapter 4 were evaluated for their capability of long-term and zero order release *in vitro*.

### **5.2.2.1 Small Tubes**

The CV loaded tubes were placed in microvials containing 0.3 ml of phosphate buffered saline (PBS, 0.01 M phosphate, pH 7.4). A blank polyimide tube was used as an experimental control. The vials were placed on a drug dissolution apparatus having a dip rate of 30-32 dips per minute. The apparatus was connected to a water bath maintained at  $37.0 \pm 1.0^\circ\text{C}$ , for the duration of study. The method was developed in accordance to the method proposed by Varian Inc for *in vitro* testing of drug delivery devices [210]. Aliquots were withdrawn every two days and replenished with fresh buffer. The collected samples were analyzed spectrophotometrically at 590 nm to estimate the amount of CV released. A standard curve was prepared from standard solutions of crystal violet in PBS at concentrations of 0.05, 0.08, 0.16, 0.24, 0.28, and 0.30  $\mu\text{g}/\text{ml}$ , respectively.

### **5.2.2.2 Large Tubes**

A similar but simpler dissolution method was developed for the larger tubes. Briefly, the CV loaded tubes were transferred to glass vials containing 1.5 ml of PBS (0.01 M phosphate, pH 7.1). The glass vials were put on a rocker with a rocking rate of 46-48 oscillations per minute and maintained inside an incubator ( $37.0 \pm 1.0^\circ\text{C}$ ) for the entire duration of study. Empty polyimide tubes and CV loaded non-perforated polyimide tubes with heat shrink caps were used as experimental controls. Samples were withdrawn at regular intervals and assayed as for small tubes. A standard curve was prepared from standard solutions of crystal violet in PBS at concentrations of 0.1, 0.2, 1.0, 5.0, 10.0, 15.0 and 20.0  $\mu\text{g}/\text{ml}$ , respectively.

### **5.2.2.3 Large Tubes without Holes**

Crystal violet loaded tubes were placed in borosilicate glass tubes containing 3.0 ml of PBS (0.01 M phosphate, pH 7.4). A blank polyimide tube and a crystal violet loaded polyimide tubes with both ends sealed were used as experimental controls. The glass tubes were sealed and placed inside the incubator maintained at  $37.0 \pm 1.0^\circ\text{C}$  in a static environment (non-moving) to see if any drug is released in absence of any agitation. The solution was changed at regular intervals, sampled, and assayed as for 'small tubes' and 'large tubes'. A standard curve was prepared from standard solutions of crystal violet in PBS at concentrations of 0.2, 0.5, 1.0, 5.0, 10.0, and 15.0  $\mu\text{g}/\text{ml}$ , respectively.

### **5.2.3 Statistical Analysis**

Levene's test was used to access the homogeneity of variance in various groups. One way ANOVA with post hoc analysis using Tukey-HSD test (equal variance assumed) or Games Howell test (equal variances not assumed) through SPSS statistical software was previously used to analyze difference amongst the subsets with respect to hole size and drug loading. Linear regression analysis was performed on the cumulative release data and F-statistics was used to estimate the association between the amount of release and time points. A difference of p value  $< 0.05$  was considered significant.

## 5.3 RESULTS AND DISCUSSION

### 5.3.1 Small Tubes

#### 5.3.1.1 Method Validation

The analytical methods were developed and validated as per the FDA Guidelines for Bioanalytical Method Validation [211]. The absorbance data used for constructing the standard curve for the ‘small tubes’ is illustrated in Table 5.1. The data was collected for three days 3 times a day to estimate interday and intraday precision. The limit of detection (LOD) was found to be 0.05 µg/ml. The LOD for crystal violet was tested at 0.02, 0.03, and 0.04µg/ml. The analyte peak obtained at all the three concentrations was debatable and without any visual precision. On the contrary, at 0.05 µg/ml the peak for crystal violet could be detected and quantified. Thus, a limit of quantification (LOQ) of 0.05 µg/ml, for crystal violet was assigned. The mean absorbance value for LOQ did not exceed 20% of the coefficient of variation (CV). For remaining concentrations, %CV did not exceed 15% over the entire data range suggesting good precision. As illustrated in Figure 5.1, a linear relationship ( $R^2 = 0.9996$ ;  $y = 0.0984x + 0.0001$ ) was observed over the selected concentration range.

Table 5.1: The table illustrates the absorbance readings (A) used for the construction of standard curve. Intraday and interday precision was calculated by analyzing standard solutions at predetermined intervals.

Nominal Conc. ( $\mu\text{g/ml}$ )	DAY 1	DAY 2	DAY 3	Average Absorbance (A)	SD	%CV
0.0	0.000 0.000 0.000	0.000 0.000 0.000	0.000 0.000 0.000	0.000	0.000	n.a
0.05	0.005 0.004 0.005	0.006 0.006 0.004	0.004 0.005 0.005	0.005	0.001	15.99
0.08	0.008 0.006 0.008	0.009 0.009 0.008	0.007 0.009 0.008	0.008	0.001	12.50
0.16	0.017 0.015 0.017	0.015 0.015 0.017	0.014 0.017 0.018	0.016	0.001	8.47
0.20	0.021 0.017 0.023	0.018 0.022 0.019	0.019 0.023 0.018	0.020	0.002	11.46
0.24	0.026 0.022 0.024	0.024 0.024 0.026	0.024 0.023 0.021	0.024	0.002	6.90
0.30	0.030 0.028 0.031	0.032 0.029 0.030	0.030 0.028 0.026	0.029	0.002	6.15

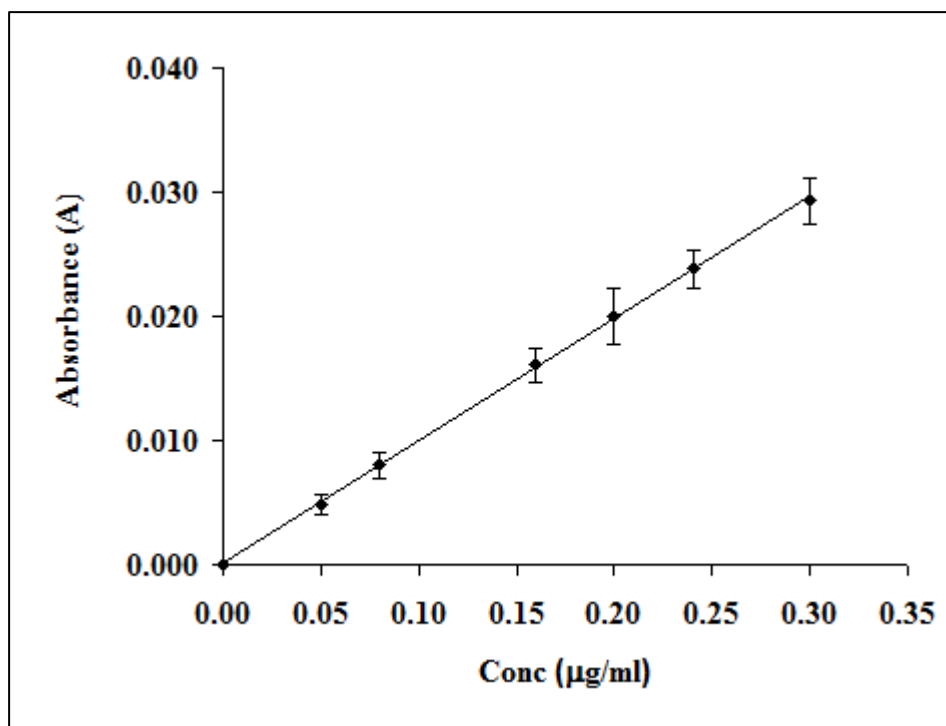


Figure 5.1: Standard curve for crystal violet solutions ( $y = 0.0984x + 0.0001$ ;  $R^2 = 0.9996$ ) used for drug release studies of ‘Small Tubes’. Data is presented as mean with standard deviation.

### 5.3.1.2 *In vitro Drug Release Studies*

Crystal violet *in vitro* release from the microtubes was monitored for 28 days (Figure 5.2). The three subsets differed only in the number of holes on the surface, namely one hole, two holes, and three holes. The release of CV was linear with  $R^2$  values of 0.9945, 0.9998, and 0.9998 for the three subsets. The F-statistics,  $F(1,28)$ ,  $p < 0.05$ , revealed a close association between the amount of drug released and time, confirming the linearity in release. The average amount of CV released was  $7.8 \pm 2.5$ ,  $16.2 \pm 5.5$ , and  $22.5 \pm 6.0$  ng/day for one hole, two holes, and three holes, respectively. The data suggests a linear

relationship between drug release and number of holes. As illustrated in Figure 5.3, the release rate increased linearly with increasing numbers of holes. These results suggest that in a multiple hole setting the release of drug from one hole is independent of the other. Assuming a constant rate of release from each hole, the amount of drug released when correlated to the total amount of drug loaded, suggests a total duration of release of more than 5 years. Figure 5.4 illustrates the cumulative % of CV released in 28 days and can be used as a reference for extrapolation of duration of drug release.

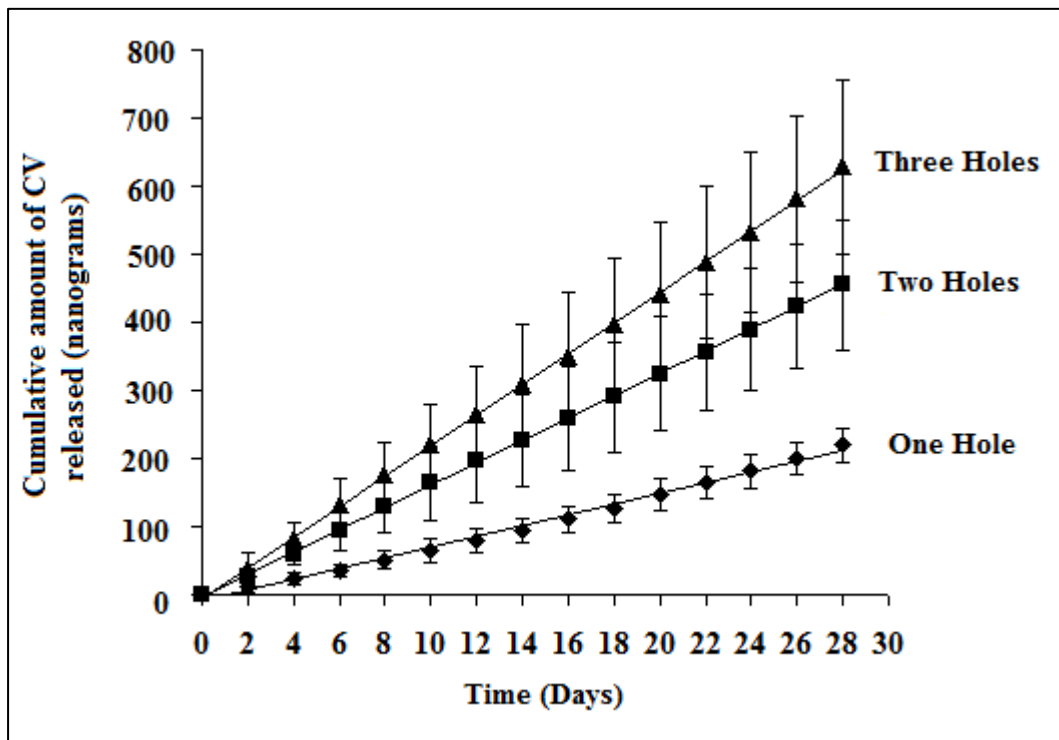


Figure 5.2: Cumulative amount of drug released as a function of time. A constant amount of drug was released from the three subsets exhibiting zero-order rate. Each curve represents seven tubes. Data is presented as mean with standard deviation.

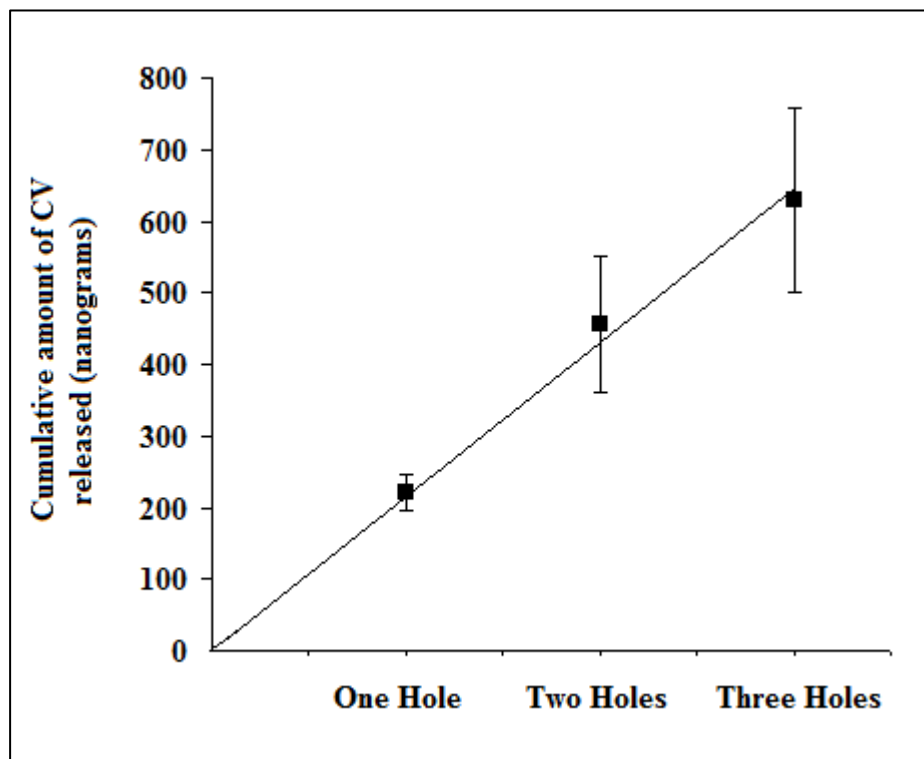


Figure 5.3: Comparison of cumulative amount of CV released from the three groups after 28 days. A linear relationship between release rate and number of holes was observed. The release is  $220.1 \pm 25.0$ ,  $455.7 \pm 95.6$ , and  $628.9 \pm 128.2$  ng for one hole, two holes, and three holes group. Data is presented as mean with standard deviation.

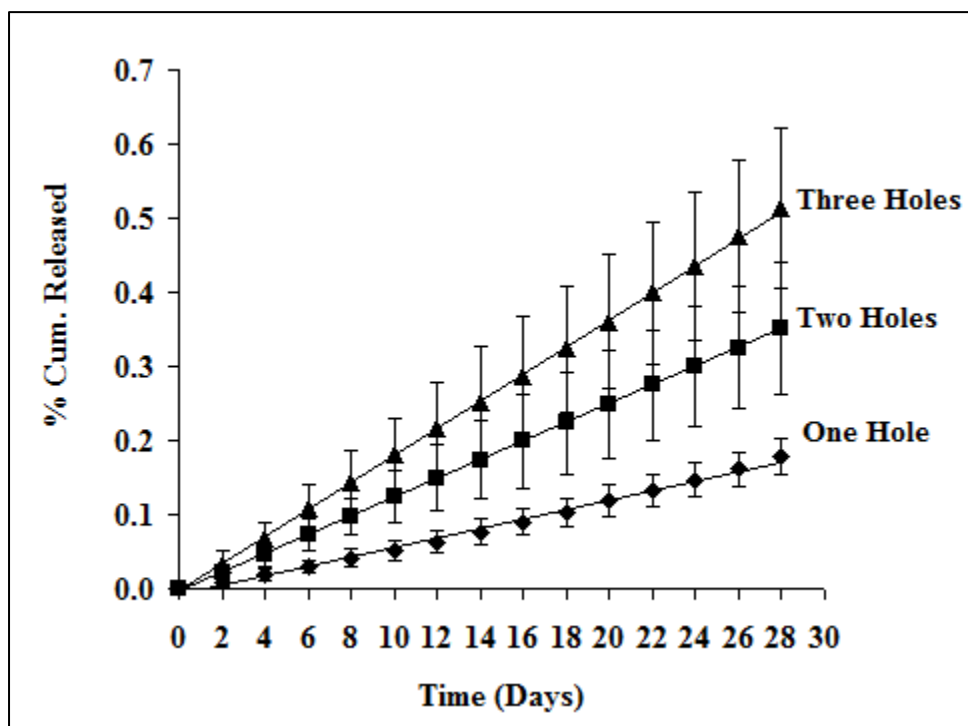


Figure 5.4: Cumulative % of crystal violet released from the three subsets. Assuming zero order release, the total duration of drug release from one hole, two holes, and three holes subsets correspond to drug release of more than five years. Data is presented as mean with standard deviation.

### 5.3.2 Large Tubes

#### 5.3.2.1 Method Validation

The standard curve data for the ‘large tubes’ is illustrated in Table 5.2. Interday and intraday precisions were calculated as for the ‘small tubes’. As illustrated in Figure 5.5, a linear relationship ( $R^2 = 0.9982$ ;  $y = 0.1051x - 0.0262$ ) was observed over the selected concentration range indicating accurate results. However, the %CV value for the three lowest concentrations was well above 15% as specified by the FDA. The poor precision of the instrument in measuring the absorbance may have contributed to some variation in the drug release results.

Table 5.2: The table illustrates the absorbance readings (A) used for the construction of standard curve. Intraday and interday precision were calculated by analyzing standard solutions at predetermined intervals.

<b>Nominal Conc. (µg/ml)</b>	<b>Day 1</b>	<b>Day 2</b>	<b>Day 3</b>	<b>Average Absorbance (A)</b>	<b>SD</b>	<b>% CV</b>
<b>0.00</b>	0.000 0.000 0.000	0.000 0.000 0.000	0.000 0.000 0.000	0.000	0.000	n/a
<b>0.10</b>	0.007 0.005 0.004	0.003 0.003 0.003	0.003 0.005 0.005	0.004	0.001	30.06
<b>0.20</b>	0.022 0.015 0.011	0.009 0.009 0.008	0.008 0.009 0.010	0.011	0.005	41.85
<b>1.00</b>	0.074 0.051 0.048	0.047 0.047 0.048	0.046 0.047 0.047	0.051	0.009	17.86
<b>5.00</b>	0.497 0.464 0.459	0.455 0.451 0.448	0.444 0.443 0.442	0.456	0.017	3.73
<b>10.00</b>	1.052 1.015 1.003	0.992 0.981 0.975	0.972 0.969 0.961	0.991	0.029	2.89
<b>15.00</b>	1.701 1.642 1.619	1.607 1.592 1.581	1.579 1.568 1.561	1.606	0.044	2.75
<b>20.00</b>	2.196 2.121 2.088	2.063 2.042 2.030	2.022 2.003 1.999	2.063	0.064	3.10

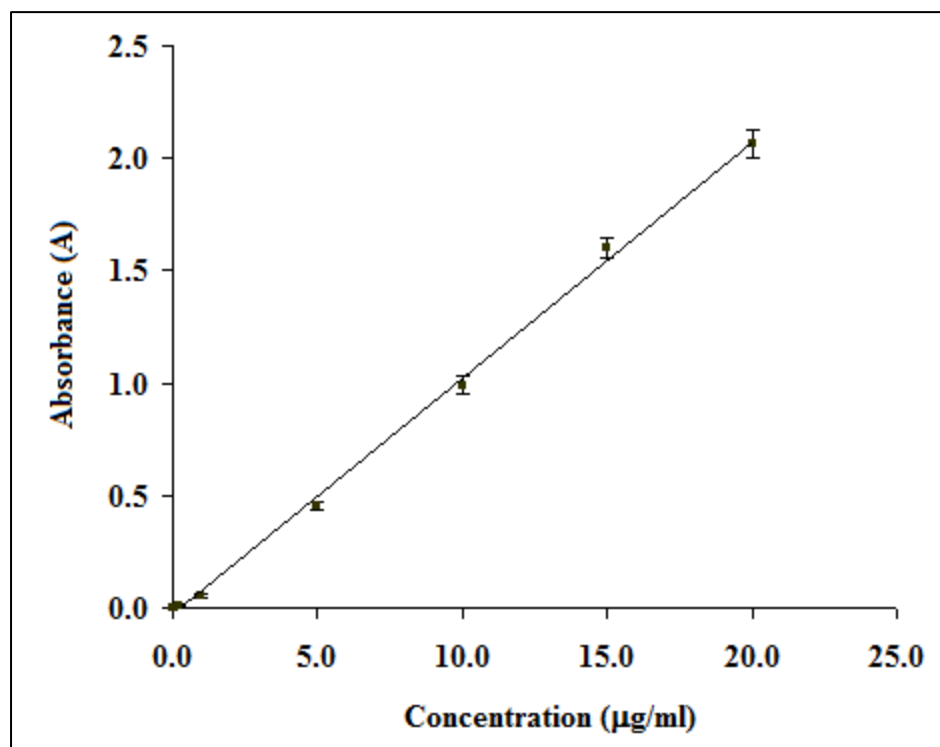


Figure 5.5: Standard curve for crystal violet solutions ( $R^2 = 0.9982$ ;  $y = 0.1051x - 0.0262$ ) which was used in the drug release studies with 'Large Tubes'. Data is presented as mean with standard deviation.

### 5.3.2.2 *In vitro Drug Release Studies*

Three subsets of large holes were prepared: The first subset consisted of one hole ( $365.3 \pm 16.7 \mu\text{m}$ ); the second subset consisted of two holes ( $362.4 \pm 23.1 \mu\text{m}$ ); and the third subset consisted of one bigger size hole ( $542.6 \pm 26.3 \mu\text{m}$ ). The coefficient of variation for hole size measurement for each of the three groups was less than five percent. The gravimetric analysis yielded the average amount of CV loaded per unit length in the groups as  $5.3 \pm 0.3$ ,  $5.2 \pm 0.3$ ,

and  $5.4 \pm 0.2$  mg/cm, respectively. Statistical analysis for drug loading did not yield any significant difference amongst the groups,  $p > 0.05$ .

The rate of CV release from loaded tubes was obtained as previously described (Figure 5.6). The kinetics of crystal violet was found to be linear. The  $R^2$  was found to be 0.9958, 0.9947, and 0.9979 for the 365.3, 362.1, and 542.6  $\mu\text{m}$  holes respectively. The linearity of the release was further confirmed by F test,  $F(1, 56)$ ,  $p < 0.05$ . The average amount of  $10.8 \pm 4.1$ ,  $15.8 \pm 4.8$  and  $22.1 \pm 6.7$   $\mu\text{g}$  /day of CV were released from the three sets. The release data yet again suggest a linear relationship between number of holes and drug release. The release data suggests the total duration of release of approximately one year or longer from the three groups.

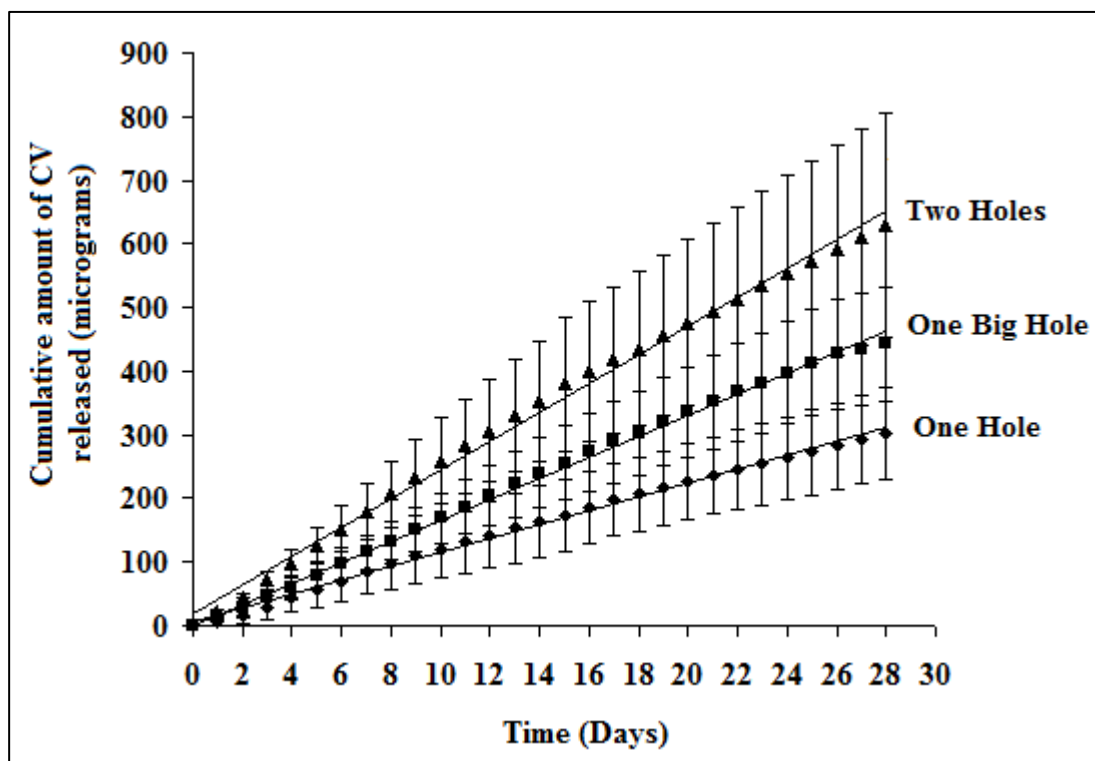


Figure 5.6: The release profile of CV from the three subsets. Each curve represents twelve tubes. Data is presented as mean with standard deviation.

### **5.3.3 Large Tubes without Holes**

#### ***5.3.3.1 Method Validation***

Table 5.3 illustrates the absorbance data which was used to construct the standard curve for 'Large Tubes without Holes'. The interday and intraday precision was calculated as described previously. A linear relationship ( $R^2 = 0.9999$ ;  $y = 0.046x - 0.0026$ ) was observed over the selected concentration range indicating accurate results. (Figure 5.7)

#### ***5.3.3.2 In vitro Drug Release Studies***

The cumulative amount of crystal violet released from the three groups (n=4 in each set) is illustrated in Figure 5.8. A near zero-order release kinetics was observed as indicated by the  $R^2$  value of 0.9667, 0.9695, and 0.9355 for 200, 400, and 600 microns group respectively. The linearity of the release was further confirmed by F test, F (1, 14),  $p < 0.05$ . The drug release studies were successfully conducted in the static environment confirming that the concentration gradient is the single main driving force for the drug release.

Table 5.3: The table illustrates the absorbance readings (A) used for the construction of standard curve. Intraday and interday precision were calculated by analyzing standard solutions at predetermined intervals.

<b>Nominal Conc. (<math>\mu\text{g/ml}</math>)</b>	<b>DAY 1</b>	<b>DAY 2</b>	<b>DAY 3</b>	<b>Average</b>	<b>SD</b>	<b>%CV</b>
<b>0.0</b>	0.000	0.000	0.000	0.000	0.000	0.00
	0.000	0.000	0.000			
	0.000	0.000	0.000			
<b>0.20</b>	0.009	0.009	0.008	0.008	0.002	22.06
	0.006	0.010	0.007			
	0.005	0.008	0.006			
<b>0.50</b>	0.022	0.019	0.019	0.018	0.002	12.50
	0.018	0.020	0.018			
	0.014	0.019	0.016			
<b>1.00</b>	0.042	0.051	0.038	0.041	0.007	16.85
	0.038	0.038	0.038			
	0.032	0.053	0.037			
<b>5.00</b>	0.235	0.266	0.223	0.227	0.017	7.36
	0.224	0.212	0.224			
	0.217	0.233	0.211			
<b>10.00</b>	0.434	0.465	0.485	0.461	0.022	4.77
	0.456	0.442	0.486			
	0.429	0.475	0.479			
<b>15.00</b>	0.699	0.699	0.694	0.686	0.034	4.90
	0.691	0.691	0.699			
	0.632	0.632	0.737			

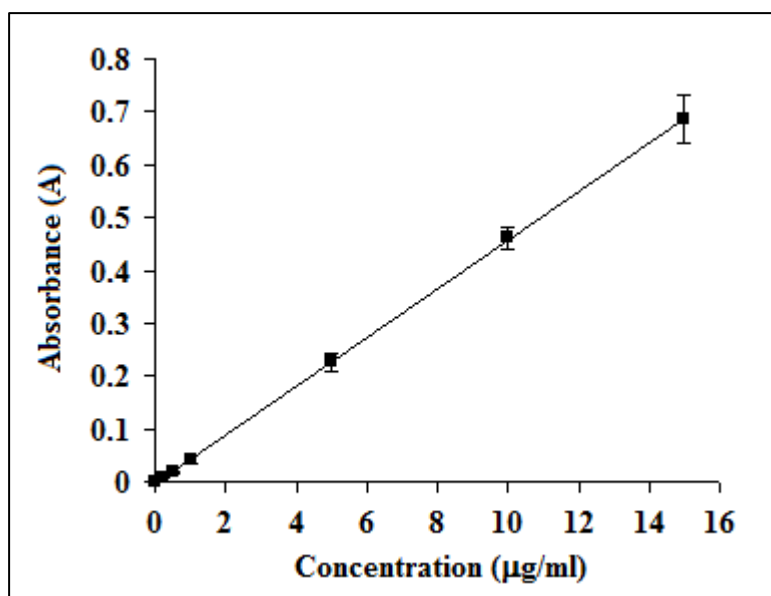


Figure 5.7: Standard curve for crystal violet solutions ( $y = 0.046x - 0.0026$ ;  $R^2 = 0.9999$ ) used for drug release studies with ‘Large Tubes without Holes’. Data is presented as mean with standard deviation.

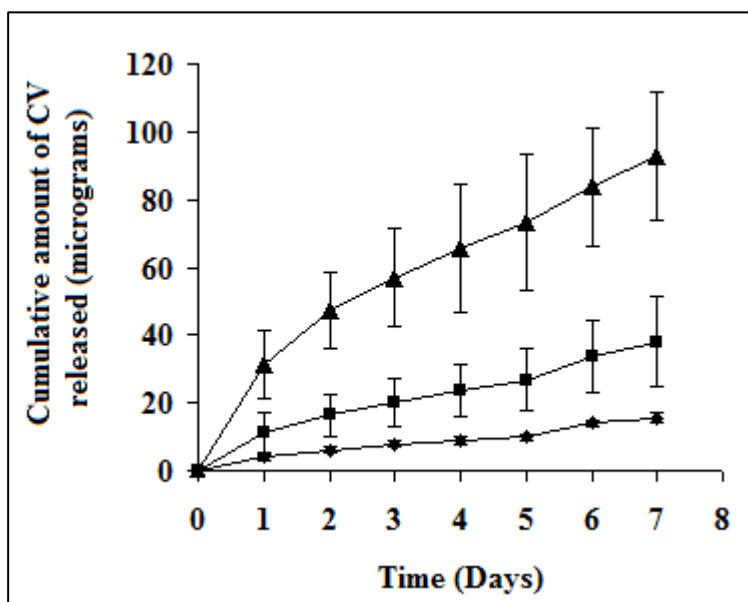


Figure 5.8: Cumulative amount of crystal violet released from three groups with different hole sizes, 200, 400, and 600 microns. Each curve represents four tubes. Data is presented as mean with standard deviation.

### 5.3.4 Mechanism of Release Kinetics

The release of crystal violet through a hole on a polyimide tube is illustrated in Figure 5.9. The drug release from the device can be explained by drug dissolution due to surface erosion of the drug at the hole/drug solvent interface. The impermeable tube protects the enclosed drug and the hole allows for exposure of small amounts of drug inside the tube. The exposed drug layer is solubilised by the solvent and the solution diffuses out. Drug release is controlled by various factors such as, surface area of the drug that is exposed, solubility of the drug, drug loading, and drug packing. The exposed surface area is dependent on the number of holes and size of the holes on the surface.

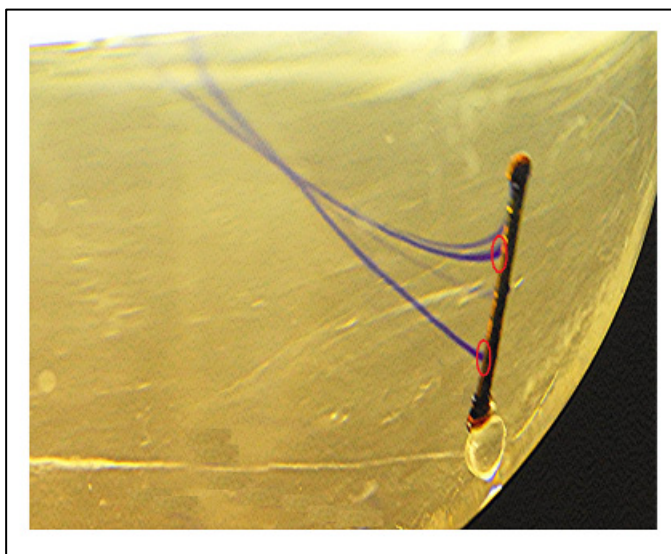


Figure 5.9: The release of crystal violet from two holes is depicted. Release of drug from each hole is independent of the other. The regions where holes are present on the tube have been circled in red. The dimension of the tube is 1000 microns and the holes size is approximately 400 microns.

**Mathematical Model** -The Noyes Whitney's equation for dissolution is given by:

$$\frac{dM}{dT} = \frac{D}{L} \cdot (C_s - C) \cdot A \quad (1)$$

where,  $\frac{dM}{dT}$ , D, L,  $C_s$ , C, and A are rate of drug dissolution, diffusion coefficient of the drug, diffusion layer thickness, solubility of the drug, concentration of the drug in dissolution medium, and area available for dissolution.

For a perforated device, with 'n' number of microholes; A will be the area of each hole. In addition, the concentration of the drug inside the device is greater than in the medium rendering sink conditions,  $C \ll C_s$ . Thus, for a perforated device loaded with drug, equation (1) is reduced to

$$\frac{dM}{dT} = \frac{D}{L} \cdot C_s \cdot A \cdot n \quad (2)$$

**Apparent Permeability Coefficient** - The apparent permeability coefficients (D/L), can be calculated from equation (2). For one hole ( $365.3 \pm 16.7 \mu\text{m}$ ) and one bigger sized hole ( $542.6 \pm 26.3 \mu\text{m}$ ) subsets in large tubes, D/L were calculated as  $6.08 \times 10^{-5}$  cm/sec and  $4.01 \times 10^{-5}$  cm/sec, respectively. For the one hole group in small tubes ( $32.9 \pm 1.7 \mu\text{m}$ ), the D/L was calculated as  $5.7 \times 10^{-6}$  cm/sec. The difference in D/L values obtained from large tubes and small tubes may be attributed to the difference in ratio of hole size with respect to the device size in two groups. A greater ratio will lead to faster diffusion and vice versa as also suggested by the D/L values. For a multi-hole setting, it is my observation that the hole diameter should be comparatively smaller than the device diameter and also to the distance between the adjacent holes.

***Influence of number of holes (n) and size of the holes (r) on release rates*** - For a particular

drug, D, L, and Cs are constant. Hence,  $\frac{dM}{dT} \propto A$  (3)

The area available for dissolution depends on number of holes (n) and size of the holes (r), in which case,

$$\frac{dM}{dT} \propto n \cdot \pi \cdot r^2 \quad (4)$$

Equation (4) shows influence of the two parameters ‘n’ and ‘r’ on release rate. The *in vitro* studies with different size perforated polyimide tubes (Figures 5.3 and 5.6) have established a linear relationship between drugs release rates and number of holes,

$$\frac{dM}{dT} \propto n \quad (5)$$

According to equation (4), release rate also follow a quadratic relationship as a function of hole size,

$$\frac{dM}{dT} \propto r^2$$

For the perforated system to obey this rule, the amount of drug released from ‘one big hole’ subset should be twice than that released from the ‘one small hole’ subset in the large tubes. On comparison of the release rates, we obtain a ratio of 1.46, which is close to the ideal value. In addition, the ‘Large Tubes without Holes’ were also employed to study the effect of hole size on release rates. Hence, three groups with one open end and differing only in the diameter of the tubes (200, 400, and 600 microns) were used. On plotting the cumulative amount of drug released from the three groups every day, we observed that the amount of drug released, increased as a factor of  $(r)^2$  (Figure 5.10). Hence, the groups follow a quadratic

relationship as is evident by the equations of line for each day, which are in the form:  $y = a.x^2 + bx + c$ , and their corresponding  $R^2$  values which are close to 1.000.

#### 5.4 CONCLUSION

The drug release data indicated that microperforated microtubes are capable of long-term zero order drug release. Hence, the development process of the device is not limited to DES and is being developed for other applications as well. The microperforated microtube delivery system is scalable and produces long-term zero order kinetics without the use of a polymer or a membrane. While polyimide tubing was used in this study, any impermeable and biocompatible material of any shape can be used. The *in vitro* release rates were found to be proportional to the exposed surface area of the drug. They were linear as a function of number of holes and proportional to the square of radii of holes. Drug release from the device depends on the drug's solubility, drug loading, drug packing, number of holes, and hole size. The concentration gradient across the hole is the main driving force for release of drug from the perforated device. The rate and extent of drug release may be tailored by manipulating the size of the reservoir, number of holes, hole size, and drug solubility. The equidistant holes acted independently and the drug release from each hole was distinctive. It should be possible to use such a device for local and controlled delivery of drugs; as a protective carrier to transport labile drugs; and as an implant for treatment of various chronic conditions.

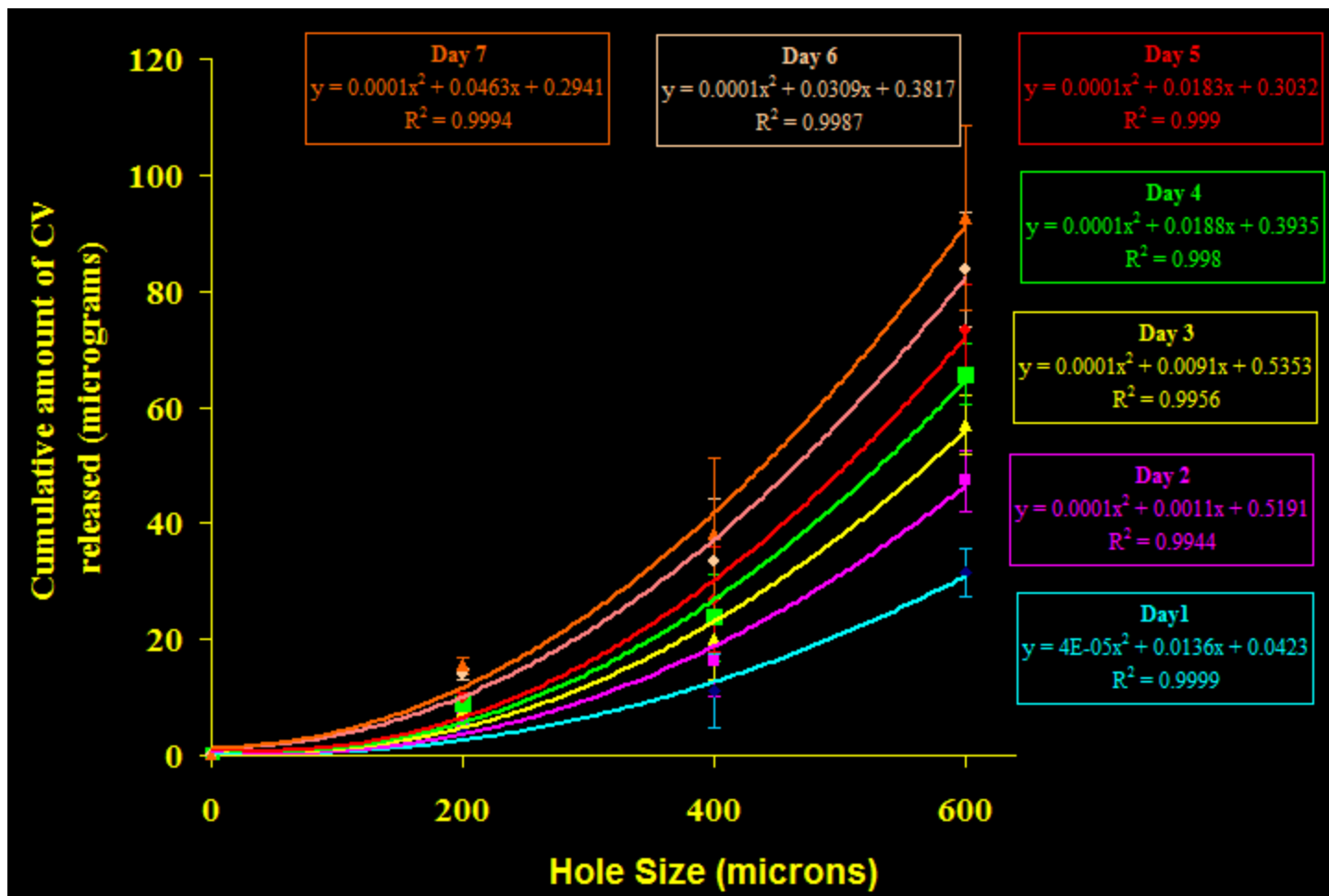


Figure 5.10: The cumulative amount of CV released from the three groups (200 microns, 400 microns, and 600 microns) is plotted for each day for seven days. As indicated by the equation of line, the drug release rates from the three groups obey a perfect quadratic relationship. Data is presented as mean with standard deviation.

## **Chapter 6: *Ex vivo* Drug Release Studies in Vitreous Humor from a Rabbit's Eye.**

### **6.1 INTRODUCTION**

#### **6.1.1 Intravitreal Drug Delivery**

The in vitro drug release data from the perforated tubes in phosphate buffered saline (PBS) suggested that the perforated microtubes are capable of long-term zero order release and can be used for management of diverse diseased states. One such possible application of the device is to treat diseases related to posterior segment of the eye. This is the area behind the lens and consists of vitreous humor, retina, choroid, sclera, and the optic nerve [212]. While treating a posterior disorder of the eye, vitreous humor becomes the desired location for drug delivery due to its contact with other parts. Drug delivery to the posterior chamber by non-invasive method is difficult because of blood-eye barrier and hence invasive methods such as intravitreal injections are commonly employed [213]. However, management of an ophthalmic disorder using invasive methods cause patient distress and may also lead to injuries due to frequent penetration into the eye.

To overcome this problem, implantable drug delivery systems have been developed, which are capable of long-term delivery of constant amounts of drug in vitreous [52, 56]. These devices have proved to be beneficial in the treatment of chronic conditions such as uveitis and cytomegalovirus retinitis, minus the drawbacks associated with traditional drug delivery methods.

The drug delivery device described here provides another option for long term drug delivery. The aim of the following study was to evaluate the long-term and zero

order drug release capability of the device in vitreous, which has been previously tested in the phosphate buffer.

## **6.2 METHODS**

### **6.2.1 Materials**

Rabbit's vitreous humor was obtained from Pel-Freez Biologicals (Rogers, AR, USA). Sodium azide was obtained from Mallinckrodt (Hazelwood, MO, USA). Polyimide tubes were obtained from Microlumen Inc. (Tampa, FL, USA). Crystal violet was obtained from Sigma-Aldrich (St. Louis, MO, USA). Heat shrink polyolefin tubing (3.0 mm diameter) was obtained from Altex (San Antonio, TX, USA).

### **6.2.2 *In vitro* Drug Release Studies**

The study was undertaken to investigate the influence of a biological fluid on the rate of drug release from the perforated microtubes. Rabbit's vitreous humor was centrifuged at 1900 rpm for 2 min and the supernatant was collected and diluted with PBS (0.01M, pH 7.1) to provide a 1:1 v/v dilution. Sodium azide (0.05% w/v) was added to inhibit microbial growth. Crystal violet loaded polyimide tubes with 'One Small Hole' belonging to 'Large Tubes' groups were preserved after the drug release studies of Chapter 5. The twelve tubes were divided into two groups. One group was transferred to glass vials containing 1.0 ml of PBS (0.01 M phosphate, pH 7.1) and the other to glass vials containing 1.0 ml of diluted vitreous humor. The glass vials were put on a rocker with a rocking rate of 46-48 oscillations/min and maintained inside an incubator ( $37.0 \pm$

1.0°C) for the entire duration of study. Empty polyimide tubes and CV loaded non-perforated polyimide tubes with heat shrink caps were used as experimental controls. Samples were withdrawn at regular intervals and assayed spectrophotometrically at 590 nm.

A standard curve was constructed from standard solutions of crystal violet in vitreous humor at concentrations of 1.0, 2.0, 3.0, 5.0, 6.0, 8.0, and 10.0, µg/ml, respectively. A standard curve of Figure 5.5 was used for the PBS group.

### **6.3 RESULTS AND DISCUSSION**

The drug release data from previously conducted drug release studies (Chapter 5) indicated that the variation in the release data during the first few days was higher than the following days. This was attributed to the differences in surface erosion of the drug through the holes in different tubes. However, after several days its release was standardized and all the tubes started behaving in a similar fashion leading to reduction in standard deviation. It is due to this reason that the once yearly histrelin implant Vantas, is stored in saline and hence primed and standardized before its use [214]. Hence, CV loaded perforated tubes belonging to 'Large Tubes', which have been previously used, were reused in this study. A standard curve was constructed in vitreous humor. The interday and intraday precision was calculated as described previously. As illustrated in Figure 6.1, a linear relationship ( $R^2 = 0.9974$ ,  $y = 0.0291x + 0.0005$ ) was observed over the selected concentration range indicating accurate results.

The release kinetics of crystal violet was found to be linear in both PBS and vitreous humor (Figure 6.2). The  $R^2$  was found to be 0.9986 and 0.9909 for the phosphate buffered and vitreous humor groups, respectively. The linearity of the release was further confirmed by F test,  $F(1, 14)$ ,  $p < 0.05$ . The average amount of  $8.5 \pm 2.2$  and  $5.8 \pm 1.8$   $\mu\text{g}/\text{day}$  of CV was released from the two groups, respectively. The greater viscosity of vitreous humor due to presence of hyaluronic acid and collagen may have resulted in slower release [215]. Other factors such as molecular weight of the drug and drug-protein binding may also influence the rate of drug release [216].

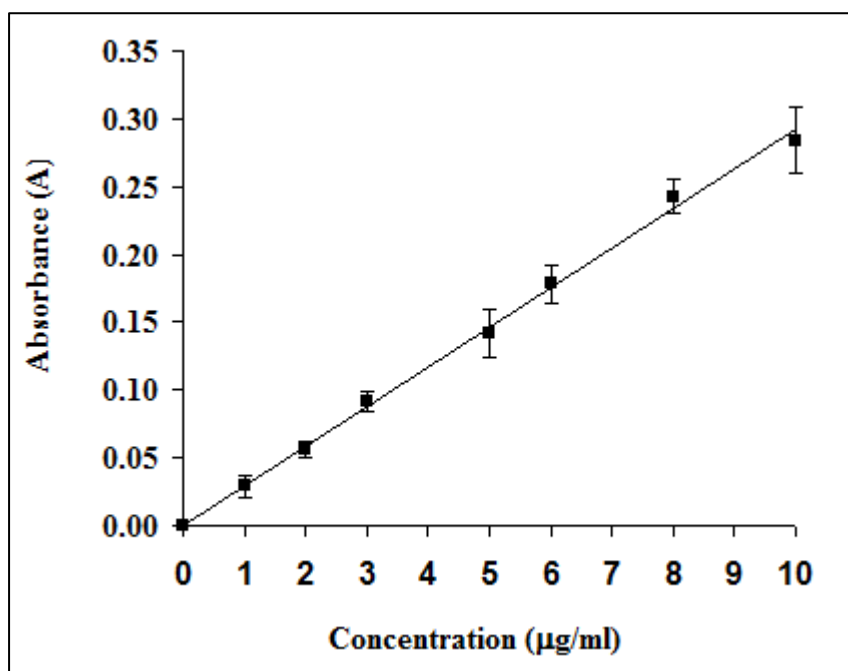


Figure 6.1: Standard curve for crystal violet in vitreous humor ( $R^2 = 0.9974$ ,  $y = 0.0291x + 0.0005$ ). Data is presented as mean with standard deviation.

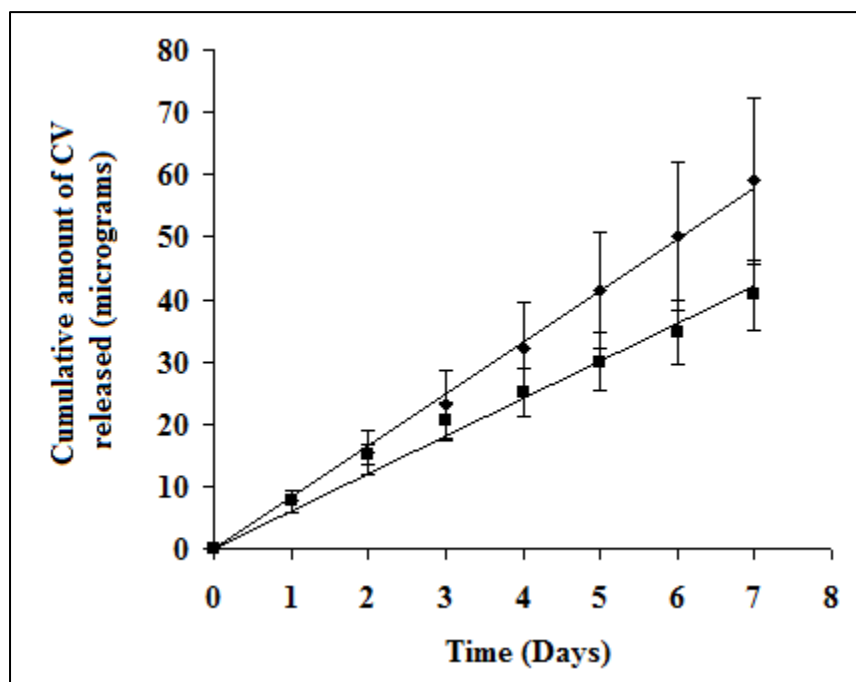


Figure 6.2: Comparison of crystal violet release in PBS (circles) and vitreous humor (squares). Each curve represents six tubes. A linear release was observed in both the mediums. Data is presented as mean with standard deviation.

#### 6.4 CONCLUSION

The perforated drug delivery system was successfully tested *ex vivo* in vitreous humor obtained from the rabbit's eyes. The drug release data supported the previous data obtained in PBS. The device was yet again found capable of delivering drugs at zero order for prolonged periods and hence can be potentially used as an ophthalmic implant. As the device would be implanted inside the body lumen, the next step in the development process was to test its biocompatibility and make sure that the device does not incite any inflammatory responses.

## **Chapter 7: *In Vitro* Biocompatibility Evaluation of Cobalt-Chromium Alloy Coated and Uncoated Polyimide Matrices**

### **7.1 INTRODUCTION**

#### **7.1.1 Biocompatibility**

##### ***7.1.1.1 Cell Adhesion and Cell Attachment***

Biocompatibility of an implanted drug delivery device refers to acceptability of the device by the surrounding tissues. The body has a tendency to attack anything it considers ‘non-self’. Therefore, it is important that the biomaterial promotes cell adhesion on its surface, which is the first sign of body’s acceptability to the implant. Poor adhesion may lead to loss of contact between the implant and tissue, often followed by complications that may cause implant failure. In a previously published study, a hydrophilic surface was shown to facilitate cell attachment and adhesion as compared to a hydrophobic surface [217]. The wettability of a poor hydrophilic material can be improved by reducing the surface roughness, altering the surface charge, or by other surface treatment methods such as, oxygen plasma treatment of a polymeric surface and application of CO<sub>2</sub> laser [218-223]. Fluorinated polyimides, which are an example of chemically modified polyimide, are known to promote cell adhesion on their surface and possess excellent biomedical properties [224, 225].

In biocompatibility studies, the wettability of the coated and uncoated polyimide surfaces was evaluated using the contact angle measurement and by incubating the devices with mammalian cells to observe the extent of cell attachment and/ or cytotoxicity.

#### ***7.1.1.2 Inflammatory Studies***

Implantable medical devices may remain inside the body for a long time ranging from weeks to years and as such they are always in contact with bodily fluids. Chemical or mechanical nature of the device may irritate the surrounding tissues resulting in unwanted inflammation, platelet activation and clotting at the implant site [226]. Although inflammation initiates the healing process in tissues, chronic inflammation due to a non-compliant material may result in poor wound healing, and may trigger immunogenic responses [227-229]. When macrophages encounter a foreign object too large to be phagocytosed, such as an implant, the macrophages experience ‘frustrated phagocytosis’ [230]. They fuse to form larger foreign body giant cells composed of individual macrophages. Macrophages and foreign body giant cells adhere to the surface of an implant and remain for the duration of its presence. The foreign body reaction can lead to chronic pain and device rejection and failure. Since blood and its components are also involved in the early inflammation process, thrombosis may also occur [231, 232].

Chronic inflammation is characterized by the infiltration of mononuclear immune cells (monocytes, macrophages, lymphocytes, and plasma cells), tissue destruction, and attempts at healing, which include angiogenesis and fibrosis [233-237]. Macrophages

play a key role in inflammation by releasing pro-inflammatory cytokines and forming foam cells in sub-endothelial lesions [238-240]. The cytokines serve as biochemical clues or biomarkers [241, 242]. Of these, tumor necrosis factor-alpha (TNF- $\alpha$ ), interleukins (IL-1, IL-6), monocyte chemoattractant protein-1 (MCP-1), and macrophage inhibitory protein (MIP-1), serve as key inflammatory regulators [243-247]. Interleukin-1 $\beta$  (IL-1 $\beta$ ) and TNF- $\alpha$  are two major cytokines that rise to relatively high levels during systemic inflammation [248].

As initial screening of biomaterials in animal models can be expensive and impractical, *in vitro* assays in suitable cell lines are developed as they can hasten the material development, increase the economic efficiency, and decrease the number of animals required for the biocompatibility assessment [249]. Recent studies have proposed various *in vitro* screening methods to assess the cytotoxicity and the pro-inflammatory potential of a biomedical materials in RAW 264.7 (mouse leukemic monocyte macrophage cell line) [250-252]. In the studies, the Co-Cr L605 alloy coated and uncoated polyimide tubes were co-cultured with RAW 264.7 cells. The release of inflammatory markers, TNF- $\alpha$  and IL-1 $\beta$ , was used as an indicator of the material's potential to elicit a pro-inflammatory response.

## **7.2 MATERIALS AND METHODS**

### **7.2.1 Materials**

Uncoated polyimide tubes were obtained from Microlumen Inc. (Tampa, FL, USA). Coated tubes were prepared in collaboration with Dr. Paul Ho's group using sputtering method as previously described in Chapter 3.

### **7.2.2 Contact Angle Measurement**

Contact Angle was measured using the FTA 200 Automated Goniometer (First Ten Angstroms, Portsmouth, VA, USA) that had preinstalled FTA 32 Video 2.0 software. The instrument was coupled to a CCD camera (Sanyo, Model VCB-3512T) .A 3 ml syringe was used for the study and the pump out speed was set at 1.5  $\mu\text{l}/\text{sec}$ . For, untreated group, a polyimide film was cut and a drop of water was placed automatically using the Goniometer and the contact angle reading was taken. The process was repeated 5 times. For alcohol treated group, the polyimide film was first washed with acetone and then thoroughly with ethanol. After drying, the contact angle measurements were taken as with untreated tubes.

### **7.2.3 Cell Culture**

The mouse macrophage cell line RAW 264.7 cells were cultivated in 10% bovine calf serum in  $\alpha$ -MEM medium. Coated and uncoated polyimide matrices were placed on a 48 well plate and  $5 \times 10^5$  dissociated RAW 267.4 cells were seeded to each well. Cells grown on plastic were treated with 10  $\mu$ g/ml lipopolysaccharide (LPS) for 3 hrs and few wells were left untreated. The LPS treated and the untreated cells served as positive and negative controls respectively, for production of inflammatory mediators [252]. After 72 hrs of incubation, the tubes and associated cells were removed from the well and rinsed thoroughly with phosphate buffered saline (PBS).

### **7.2.4 Inflammatory Studies**

#### ***7.2.4.1 Extraction of RNA by Cell Lysis-***

The samples were lysed using the Cell to cDNA II Kit™ (Ambion®) solution prior to reverse transcription of RNA. The procedure was followed as described in the manufacturer's protocol.

#### ***7.2.4.2 Two Step RT-PCR: Reverse Transcription of RNA to cDNA***

The RT-PCR steps were processed as per the manufacturer's protocol using 18S as an endogenous normalizer and TNF- $\alpha$  and IL-1 $\beta$  as inflammatory markers. One microgram of total RNA from lysed cells was converted to cDNA using random primers and Superscript III reverse transcriptase according to the manufacture's instruction

(Invitrogen™ Life Technologies, Carlsbad, CA, USA). Real-time PCR was performed on a LightCycler® System (Roche Diagnostics, Indianapolis, IN, USA) with 18S, TNF- $\alpha$  and IL-1 $\beta$  primer sets, which were from TaqMan® Gene Expression Assays (Applied Biosystems, Foster City, CA, USA). Relative quantification was acquired by comparative C<sub>T</sub> method.

Inflammatory markers, TNF- $\alpha$  and IL-1 $\beta$  primers, were normalized to the expression level of 18S for each sample. A normalizer corrects the gene expression data for differences in cellular input, RNA quality, and RT efficiency between samples [253]. Hence, 18 S was used as an internal control to normalize the signal value of each sample.

## **7.3 RESULT AND DISCUSSION**

### **7.3.1 Hydrophilicity Studies**

If a surface is strongly hydrophilic, water will completely spread on its surface and contact angle will be between 0-30 degrees. Less strongly hydrophilic solids will have a contact angle up to 90°. If the solid surface is hydrophobic, the contact angle will be larger than 90°. On highly hydrophobic surfaces, such as Teflon, the surfaces have water contact angles as high as 150° or even nearly 180°. As seen in Figure 7.1, the contact angles for both the alcohol treated and untreated groups, were close to each other and remained under 90° in both the cases. Hence, polyimide is a hydrophilic and possibly a biocompatible material.

### 7.3.2 Biocompatibility Studies

Optical images of coated and uncoated polyimide tubes were recorded, before treating them with cells, using a phase inverted microscope which was coupled to a MetaMorph Imaging Software (Molecular Devices, Sunnyvale, CA, USA). After 72 hours of incubation with RAW cells, polyimide matrices were analyzed again using the phase inverted microscope. Figures 7.2 and 7.3 illustrate polyimide tubes before and after the incubation period. A high growth of RAW cells was seen in coated and uncoated surfaces confirming biocompatibility of alloy coated or uncoated polyimide tubes. The results from the biocompatibility testing of polyimide tubes were in accordance to the cytotoxicity testing guidelines as provided by the ISO-10993 international standards and FDA Guidance for toxicological evaluation of medical devices [254-256].

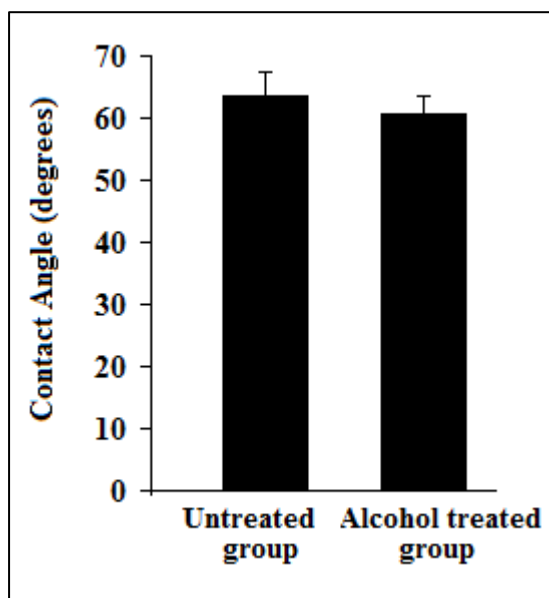


Figure 7.1: Contact angle measurements of untreated and alcohol treated polyimide film. Results are shown as mean with standard deviations (n= 5).

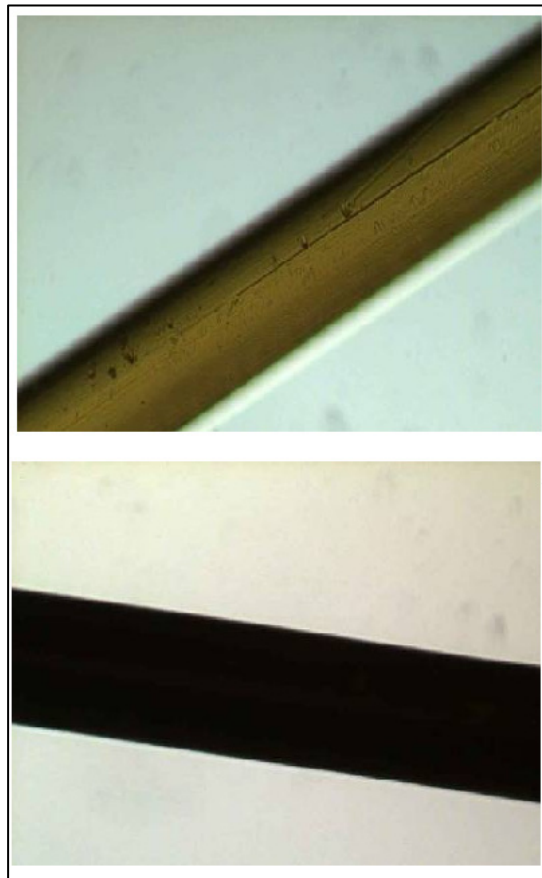


Figure 7.2: Uncoated (top) and coated (bottom) polyimide matrices.

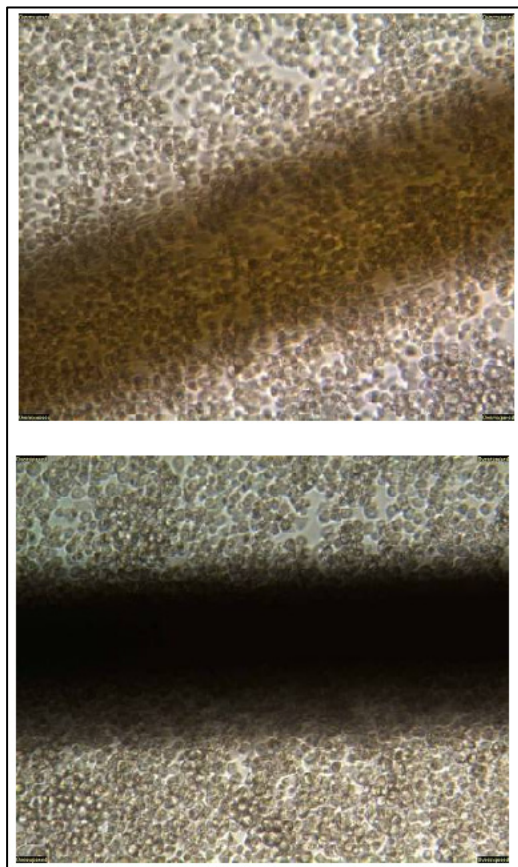


Figure 7.3: RAW cells adhered well to both the uncoated (top) and alloy coated (bottom) polyimide tubes

### 7.3.3 Inflammatory Studies

Although polyimide tubes were found to be biocompatible, it was necessary to ascertain that the polyimide would also not incite any inflammatory response when it would be implanted inside the body lumen. To evaluate possible inflammatory stimulation by coated and uncoated polyimide, the induction of the inflammatory mediators TNF  $\alpha$  and IL-1 $\beta$  were investigated. The gene expression levels of these

inflammatory biomarkers were measured using the RT-PCR technique which can amplify the amount of gene (protein) expressed so that the levels can be quantitatively measured. To standardize the amount of gene expressed, an endogenous biomarker (18 S) was used as an internal standard. The comparative  $C_T$  method or the  $\Delta\Delta C_T$  method has been employed to determine the expression levels of TNF- $\alpha$  and IL-1  $\beta$ . This involves calculating the ratio ( $C_T$  values) of the sample of interest (TNF, IL) with the internal standard (18S).

As illustrated in Figures 7.4 and 7.5, the gene expression levels of TNF- $\alpha$  and IL-1 $\beta$  respectively was lower for coated and uncoated polyimide matrices in comparison to LPS treated cells (positive control) and similar to growth on plastic surfaces that are non-inflammatory. The expression efficiency in the figures is represented as fold induction. In addition, the level of expression of both TNF- $\alpha$  and IL-1 $\beta$  in coated was lower than in the uncoated matrices, which suggests that the Co-Cr alloy coating can be further useful in reducing the inflammatory response of the polyimide matrices.

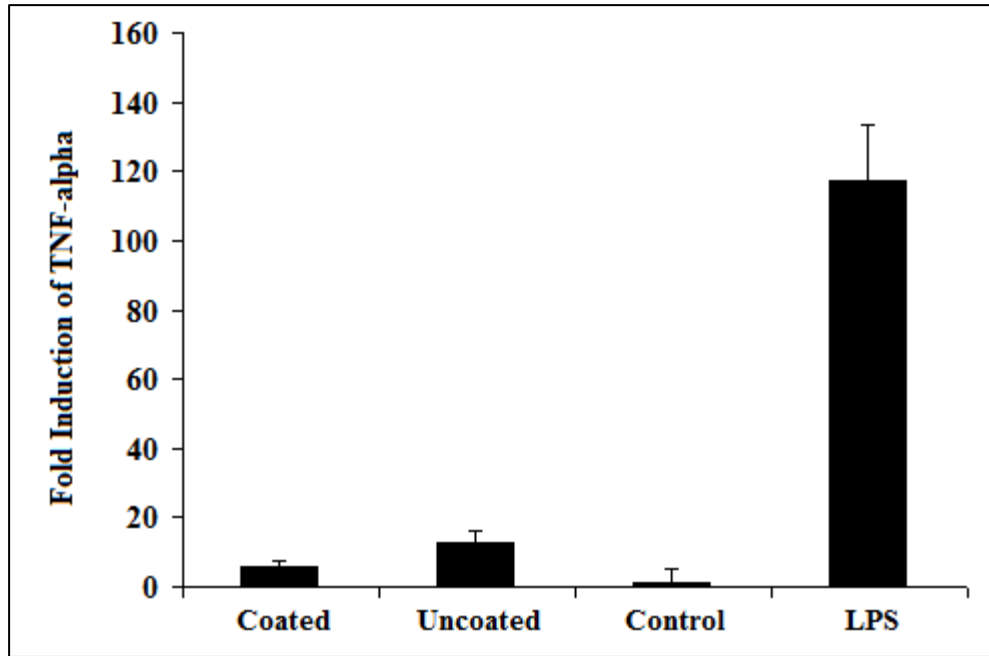


Figure 7.4: Four different groups: Coated and uncoated polyimide, control and LPS treated cells were analyzed for expression of TNF- $\alpha$  using Real Time RT-PCR. Polyimide tubes showed significantly lesser expression of the inflammatory marker. Data is represented as mean with standard deviation.

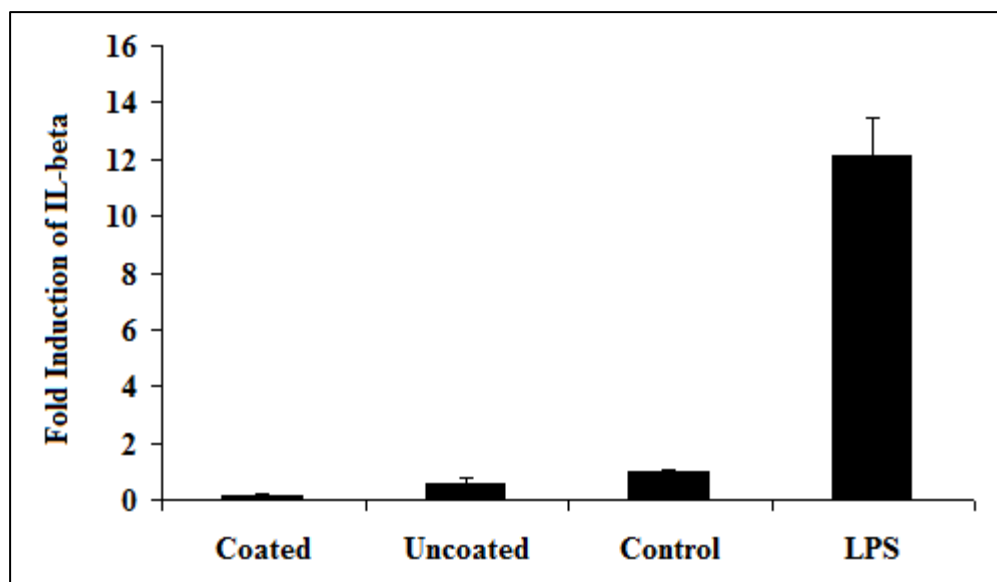


Figure 7.5: Four different groups: Coated and uncoated polyimide, control and LPS treated cells were analyzed for expression of IL-1 $\beta$  using Real Time RT-PCR. Polyimide tubes showed significantly lesser expression of the inflammatory marker. Data is represented as mean with standard deviation.

#### 7.4 CONCLUSION

Cobalt-chromium alloy coated and uncoated polyimide matrices showed no signs of cytotoxicity or stimulation of inflammatory mediators *in vitro*. A contact angle study of alcohol treated and untreated polyimide films indicated the hydrophilicity and hence the biocompatibility of polyimide material. The biocompatibility was confirmed after the observation that RAW 267.4 cells adhered well to both the coated and uncoated polyimide matrices. Even after incubation for 72 h, no significant levels of either TNF- $\alpha$  or IL-1  $\beta$  were detected in coated and uncoated tubes while very large amounts were stimulated by LPS in 3 h at the mRNA level. The results indicate that coated or uncoated polyimide tubes do not produce an inflammatory response.

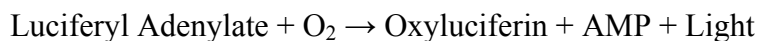
## Chapter 8: *In Vitro* Dose Response Studies

### 8.1 INTRODUCTION

#### 8.1.1 Luciferase

The purpose of this study was to determine if a newly developed perforated drug delivery system could deliver a biologically significant dose of a drug. The device was loaded with ethinyl estradiol (EE) and release from the device was confirmed using cells stably transfected with an estrogen receptor/luciferase construct (T47D-KBluc cells). A luminescence signal from the device in proportion to the drug released was considered as a biologically significant response. The amount of EE present in the drug release samples was also quantitatively measured using ELISA.

Luciferase is a general name of enzymes found in the insect firefly, *Photinus pyralis* that helps it to produce luminescence [257]. It's official name is Photinus-luciferin 4-monooxygenase and is also known as firefly luciferase and *Photinus pyralis* luciferase [258]. The production of luminescence, in the form of yellow-green light, involves oxidation of the pigment, luciferin, in presence of magnesium and adenosine tri phosphate (ATP) [259]. This reaction, which is catalyzed by luciferase, would otherwise be very slow. The luminescent reaction consists of two steps [260]:



The luminescence product, oxyluciferin is supplied as the substrate luciferin for next light emission [261]. The oxyluciferin is transformed to 2-cyano-6-hydroxybenzothiazole, which is later condensed to luciferin [261, 262]. Luciferase genes can be transfected into cells or living organisms and used as a reporter gene to access their transcriptional activity [263].

### **8.1.2 Reporter Gene Assay**

Reporter genes utilizing luciferase have become very popular in molecular biology and in biomedical and pharmaceutical research to study gene expression. In a reporter gene assay, regulatory sequence of interest is combined with a reporter gene and subsequently assayed via modulation of suitable transcription factors [264]. The reporter gene is further linked to a promoter, which activates or suppresses its expression [265]. As mammalian cells have no endogenous luciferases, their use in reporter systems produce very sensitive signals with very little noise.

A recently published paper by Wilson *et al* proposed a sensitive and specific method to detect estrogenic activity using a luciferase gene reporter system [266]. The method lead to the development of the T47D-KBluc cell line, which naturally express estrogen receptor (ER) alpha and beta, and are stably transfected with a triplet ERE (estrogen-responsive elements)–promoter–luciferase reporter gene construct. These cells are very sensitive to minute amounts of estrogenic compounds. In the present study, the method proposed by Wilson *et al* [266] was adopted to determine if a newly developed perforated drug delivery system could deliver a biologically significant dose of a drug. The different steps involved in the study are illustrated in Figure 8.1. Briefly, ethinyl estradiol is released from the device to the saline solution. The

T47D-KBluc cells are dosed with the estrogenic solution. As the compounds enter the cell, it binds to estrogen receptor. The drug-receptor complex binds to the ERE on the reporter gene construct and activates the luciferase reporter gene. The luciferase activity is assayed by measuring the light produced using a illuminometer.

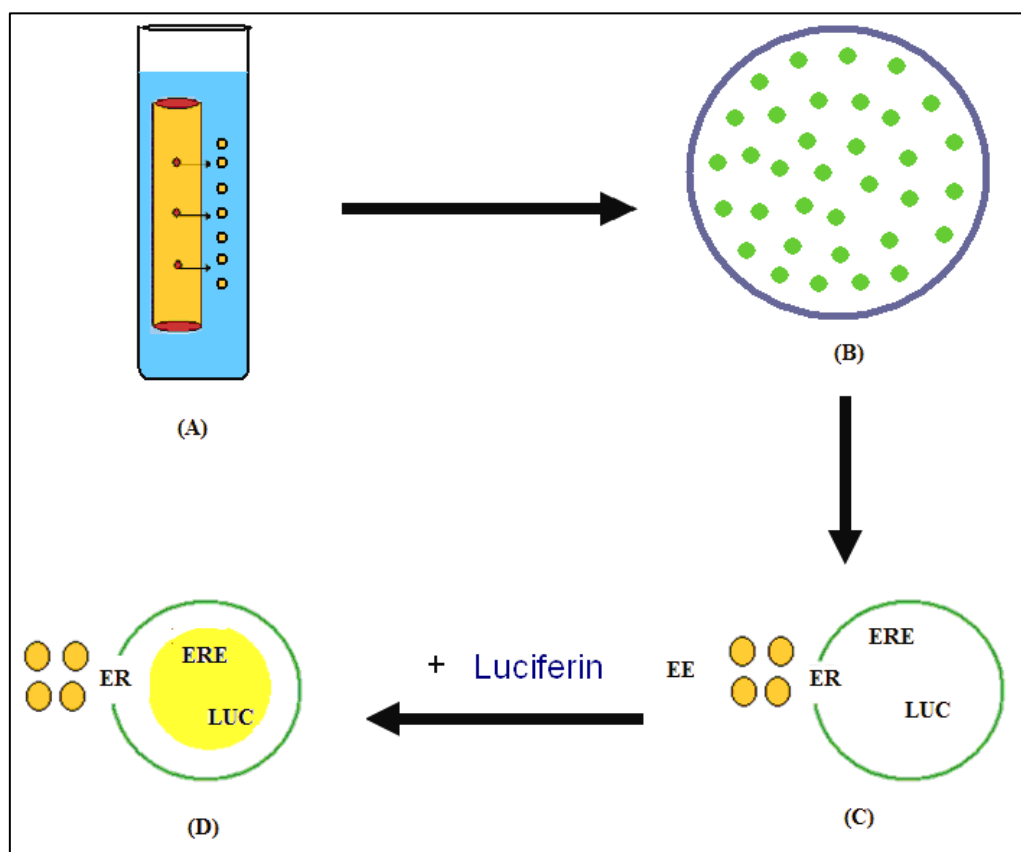


Figure 8.1 Mechanism of luciferase gene reporter system employed in the dose response study. (A) Ethinyl estradiol is released from the tubes into the PBS solution. (B) The cells are dosed with the drug solution. (C) The drug binds to the EE receptors. (D) The drug-receptor complex binds to the ERE and activates the luciferase reporter gene. Luminescence is produced on addition of luciferin. The luminescence (response) is produced in vitro as a function of amount of ethinyl estradiol released from the drug delivery device (dose).

## **8.2 MATERIALS AND METHODS**

### **8.2.1 Materials**

17 $\beta$ -Estradiol (E2, 99%), 17 $\alpha$ -ethynylestradiol (EE, $>98\%$ ), and the anti-estrogen, ICI 182780 (fulvestrant), were purchased from Sigma-Aldrich (St. Louis, MO, USA). Polyimide tubes were purchased from Microlumen Inc. (Tampa, FL, USA). The T47D-KBluc cell line was obtained from ATCC (Manassa, VA, USA). Ethynylestradiol ELISA kit was purchased from Abraxis Kits (Warminster, PA, USA).

### **8.2.2 Drug Release Studies**

The two groups of polyimide tubes, namely the 20 and 30 micron groups were loaded with ethinyl estradiol as previously discussed in Chapter 4. EE loaded tubes were placed in micro vials containing 0.3 ml of PBS (0.01 M phosphate, pH 7.4). A blank polyimide tube was used as an experimental control. The glass vials were put on a rocker with a rocking rate of 46-48 oscillations/min and maintained inside an incubator ( $37.0 \pm 1.0^{\circ}\text{C}$ ) for the entire duration of study. Samples were withdrawn every 5 days and replenished with fresh buffer for 30 days. The aliquots were stored at  $-20^{\circ}\text{C}$ .

### **8.2.3 Dose Response Studies using Luciferase Gene Reporter Assay System**

#### ***8.2.3.1 Method Validation***

Dosing media was prepared using 5% dextran-charcoal treated FBS. Standard solutions of EE were prepared using Dimethyl sulfoxide (DMSO) and dosing media at concentrations of  $10^{-7}$ ,  $10^{-8}$ ,  $10^{-9}$ ,  $10^{-10}$ ,  $10^{-11}$ ,  $10^{-12}$ ,  $10^{-13}$ ,  $10^{-14}$ , and  $10^{-15}$  M. Cells were screened by running following controls on each plate - agonist positive (0.1nM E2), negative (vehicle that is dosing media only), antagonist (0.1nM E2 plus 1.0  $\mu$ M fulvestrant), and background (vehicle plus 1.0  $\mu$ M fulvestrant). The DMSO concentration did not exceed 0.1%. The standard solutions and controls were tested in triplicate.

#### ***8.2.3.2 Dose Response Studies***

T47D-KBluc cells (ATCC, Manassa, VA, USA) were grown in 10% DMEM and  $10^4$  cells per well were seeded into 96-well multiplate and allowed to attach overnight. They were shifted to 5% dextran-charcoal treated fetal bovine serum (Hyclone, Logan, UT, USA) without antibiotic supplement one week prior to assay. The cells were then dosed with standard solutions and diluted aliquots (1:100 dilutions in PBS) from drug release study for 24 h. Following dosing and incubation, the cells were lysed and luciferase activity quantified using a luminometer (Turner Biosystems, Sunnyvale, CA, USA).

#### **8.2.4 Quantitative Estimation of Ethinyl Estradiol in Drug Release Samples using ELISA**

The drug release samples from 20 and 30 micron group were quantitatively estimated for EE using the ethinyl estradiol ELISA Kit, according to the protocol suggested by the manufacturer. Briefly, samples were diluted using 10% (v/v) methanol of the highest purity. The antigen-enzyme conjugate powder was reconstituted with 7 ml of buffer solution. A 100  $\mu$ l of EE standards (or sample) was mixed with a 100  $\mu$ l of conjugate solution and 100  $\mu$ l of the mixture was added to the coated microplate included in the kit. After sufficient incubation time, a 100  $\mu$ l of color solution was added followed by addition of 100  $\mu$ l of stop solution after 30 minutes. The standard and sample absorbance was measured using a spectrophotometer at 450 nm. The standard curve for a competitive binding assay has a negative slope. The standard curve data was fitted to the non linear regression logistic model using XLSTAT software version 2009.5.01 and the concentration of EE in the unknowns was determined by interpolation. Duplicate assays were performed for each standard and sample.

### **8.3 RESULTS AND DISCUSSION**

#### **8.3.1 Dose Response Study**

The purpose of this study was to determine if a newly developed perforated drug delivery system could deliver a biologically significant dose of a drug. The device was loaded with ethinyl estradiol (EE) and release from the device was confirmed using cells stably transfected with an estrogen receptor/luciferase construct (T47D-KBluc cells).

The T47 D-KBluc cells provided a sensitive and specific dose response method for evaluation of the drug delivery device. During the study, it was essential to run controls on every plate because various factors may contribute to high background activation levels in cells dosed only with the vehicle [266, 267]. For example presence of steroids or antibiotics in the media may contribute to high levels of background estrogenicity. The background levels were significantly brought down by growing the cells in charcoal stripped and antibiotic free medium (Figure 8.3).

A plot of standard solution of ethinyl estradiol revealed that the maximum estrogenic activity was seen at  $10^{-10}$  M (Figure 8.4). This is in agreement with the previously published work using similar dose response methods [266, 267]. The portion of the standard curve ranging from  $10^{-10}$  M to  $10^{-6}$  M is mostly linear and can be used for estimation of EE concentrations in the sample.

The *in vitro* release of EE in PBS quantified by biological stimulation of luciferase activity exhibited a linear relationship between luminescence and the amount of EE released into PBS (Figure 8.5). The average luminescence produced from 20 and 30 micron groups was measured in relative luminescence units (RLU) as  $5724 \pm 701.89$  and  $6099 \pm 590.92$  RLU every five days or  $1144.8 \pm 153.8$  and  $1219.9 \pm 127.7$  RLU/day, corresponding to  $10^{-6} - 10^{-7}$  M EE/day. The statistical analysis using one way anova did not yield any significant difference between the release rates of two groups,  $p > 0.005$ . The linear rate observed for cumulative luminescence as illustrated in Figure 8.6 indicated zero order release of EE.

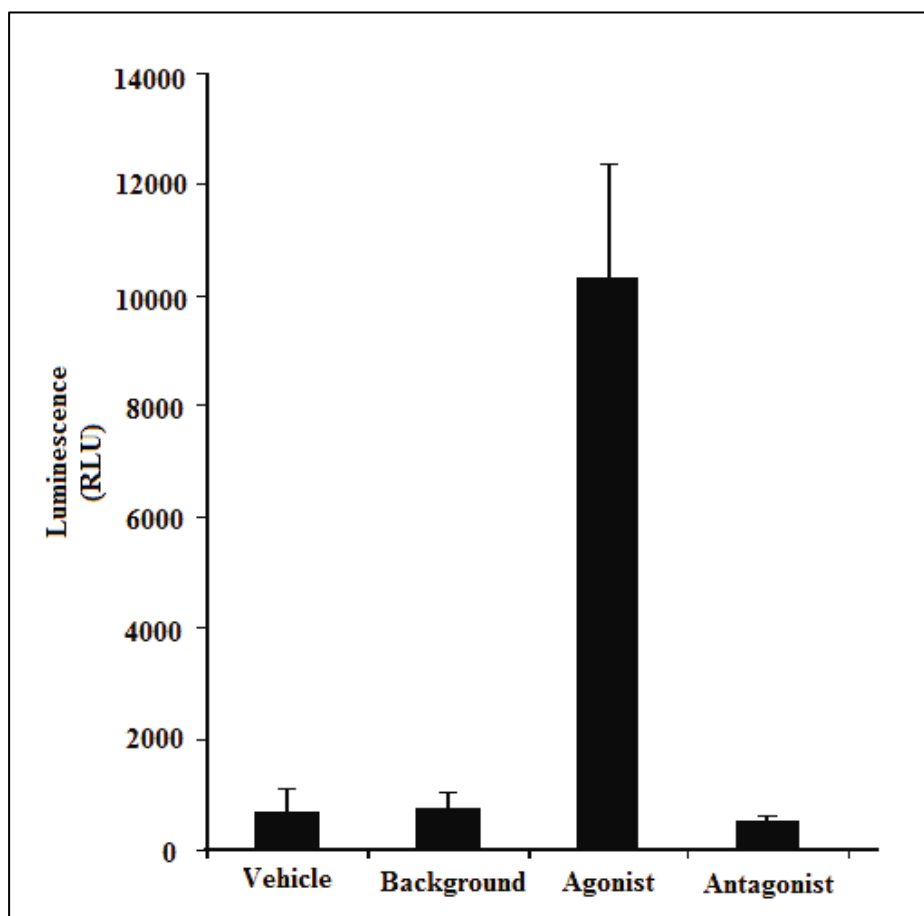


Figure 8.3: Assessment of T47D-KBluc cells in presence of various controls. Vehicle = Negative Control with Dosing Media only; Background = Vehicle plus 1.0  $\mu$ M fulvestrant; Agonist is Positive Control (0.1nM E2); Antagonist is 0.1nM E2 plus 1.0  $\mu$ M fulvestrant. Data is presented as mean with standard deviation (n=3)

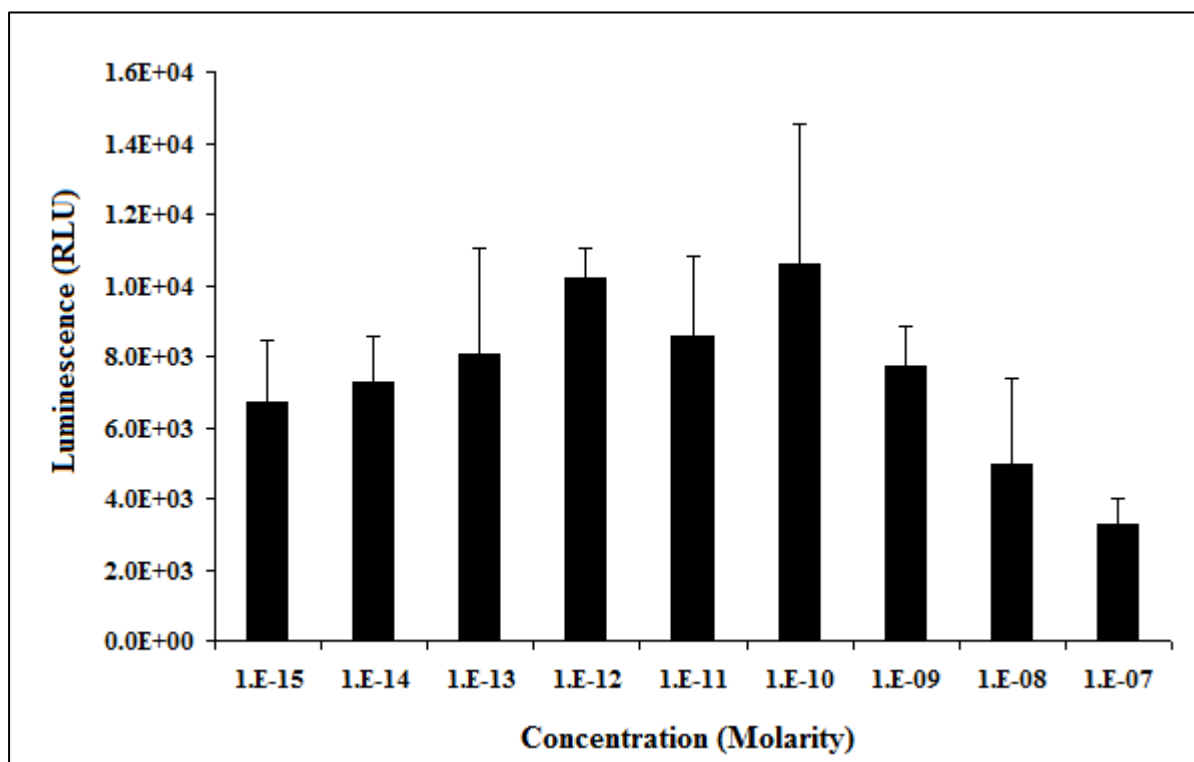


Figure 8.4: Dose response of the T47D-KBluc cells with increasing concentrations of ethinyl estradiol (n=3). Data is presented as mean with standard deviation.

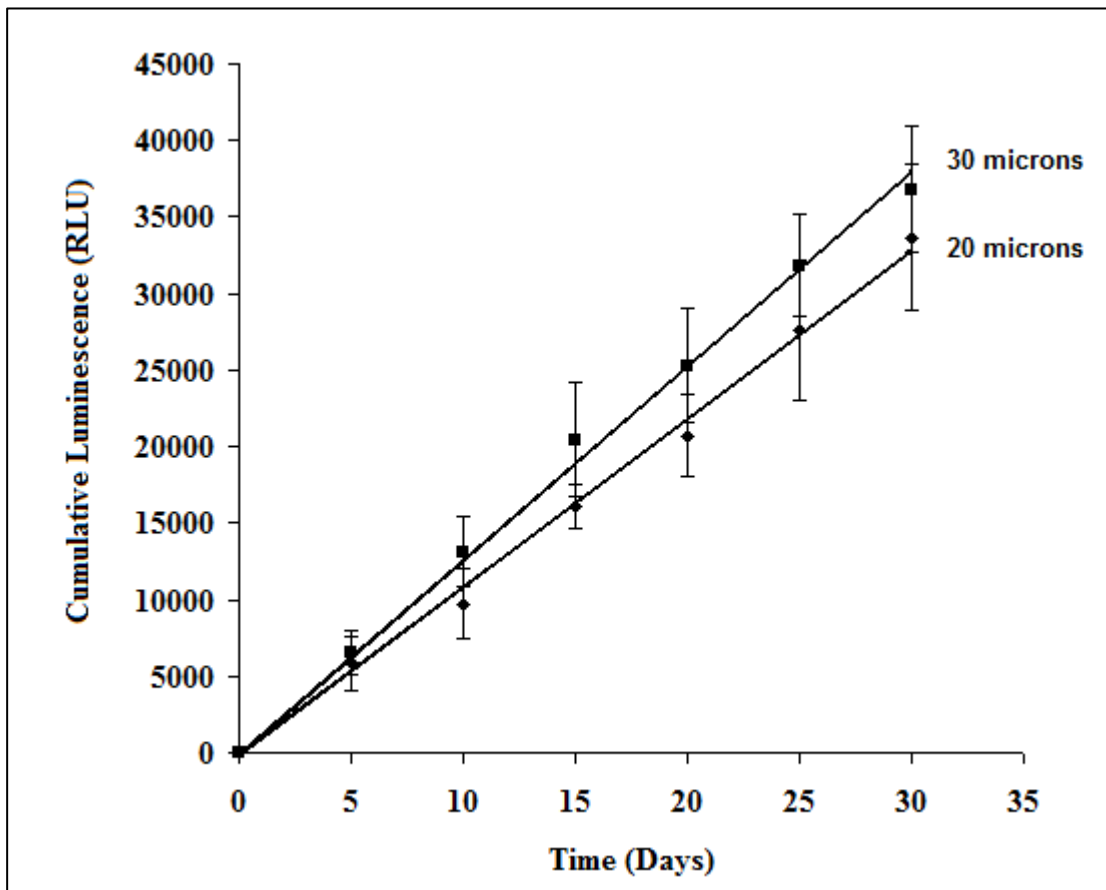


Figure 8.5: Dose-Response Data with 30 micron and 20 micron group. The cumulative luminescence response from cells was linear to the dosing samples from the two groups (30 microns:  $R^2 = 0.9965$  and 20 microns:  $R^2 = 0.9955$ ). Data is presented as mean with standard deviation (  $n = 6$  for 20 micron group;  $n = 7$  for 30 micron group).

### 8.3.2 Quantitative Analysis of Drug Release Samples

Another assay, ELISA, was employed for the quantitative determination of EE in the drug release samples. The ELISA test is based on the competitive reaction where EE competes with the antigen-enzyme conjugate for a limited number of binding sites of specific antibodies immobilized on the surface of the wells [268]. The reaction is concentration dependent, wherein, a higher concentration of EE relative to the antigen-enzyme conjugate leads to a predominant binding of EE to the antibody and vice versa. The antigen-enzyme-antibody complex catalyzes the conversion of the substrate (color solution) to a colored product. After a sufficient incubation period, the reaction is stopped by addition of sulphuric acid (stop solution). Hence, a sample with higher concentration of EE than the antigen-enzyme conjugate will bound more to the antibody producing a less intense color and a lower absorbance.

#### *Selection of the analytical model -*

Non-linear regression logistic models are often recommended for fitting ELISA calibration curves due to their sigmoidal shape [269, 270]. The three parameter logistic equation is given by:

$$Y = \frac{(a)}{(1 + (X/c)^b)} \quad (1)$$

Where, X and Y are the concentration and absorbance of analyte, respectively, and the three parameters a, b, and c are defined as the absorbance at zero concentration, slope factor, and the midrange concentration. Figure 8.6 illustrates the three parameters which are obtained using the logistic model. The linear portion of the curve is the most reliable part for analyzing experimental data. The family of curves as illustrated in the figure represents the effect of the

slope factor 'b' on the linear portion. A greater value of 'b' leads to a steeper curve resulting in a narrow concentration range available for sample analysis, and vice versa.

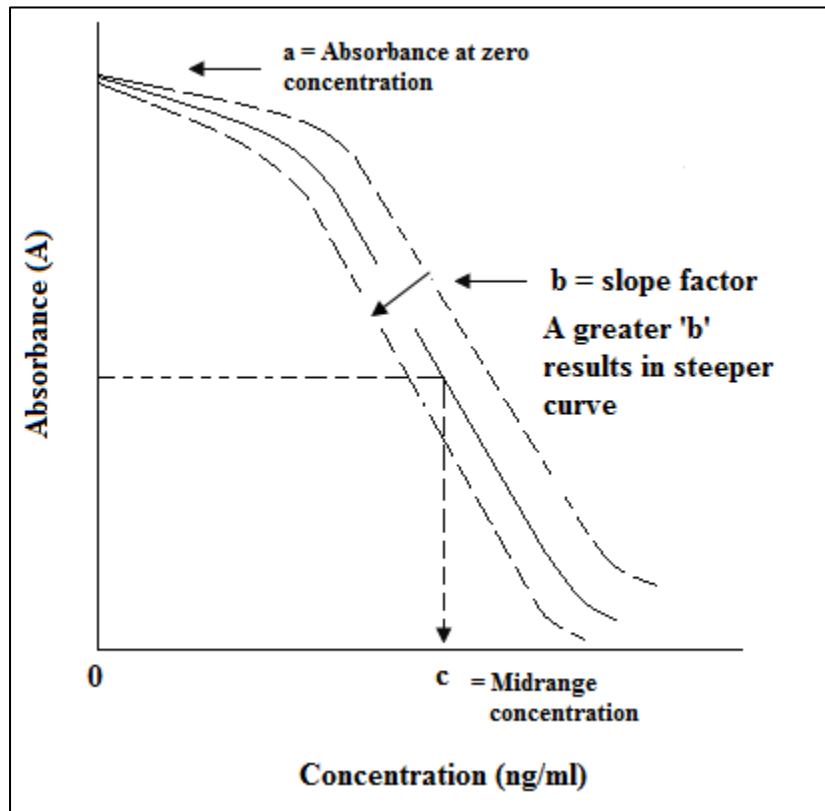


Figure 8.6: A model standard curve for a typical competitive ELISA assay (solid line). The parameters a, b, and c are obtained using the logistic model. The dotted lines represent the family of curves illustrating the effect of the slope factor, b, on the linear portion of the curve. As 'b' increases the curve would become steeper and vice versa. The raw data are fitted to the logistic model.

Tables 8.1 and 8.2 represent the absorbance data for standards for the two groups. When this data is fitted to a non linear logistic model using the XLSTAT software (version 2009.5.01), the three parameters a, b, and c are obtained as 1.757 absorbance units, 1.153, and 0.140 ng/ml for the 20 micron group and 1.400 absorbance units, 1.103, and 0.164 ng/ml for the 30 micron group. The logistic model also yields the standard curves which are illustrated in Figures 8.7 and 8.8.

Table 8.1: The table illustrates the standard absorbances (A) that were used to estimate the parameters a, b, and c for 20 micron group.

Concentration (ng/ml)	Average Absorbance (A)	SD	%CV
0.00	1.752	0.074	4.22
0.05	1.374	0.014	1.02
0.15	0.918	0.008	0.88
0.50	0.435	0.004	0.94
3.00	0.176	0.005	3.01

Table 8.2: The table illustrates the standard absorbances (A) that were used to estimate the parameters a, b, and c for 30 micron group.

Concentration (ng/ml)	Average Absorbance (A)	SD	%CV
0.00	1.400	0.050	3.57
0.05	1.088	0.000	0.00
0.15	0.739	0.021	2.84
0.50	0.353	0.013	3.68
3.00	0.083	0.008	9.63

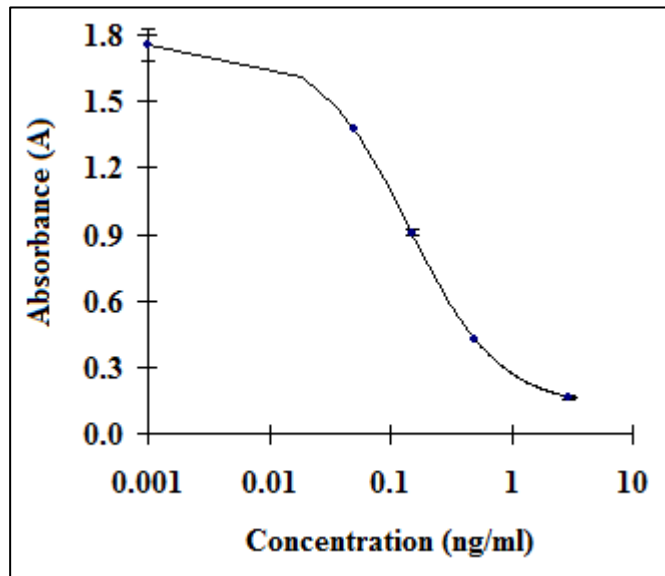


Figure 8.7: The standard curve for the 20 micron group was constructed and fitted using non linear regression logistic model. The solid line represents the curve fitting regression line. Blue squares represent the absorbance readings of the standard solutions, n=2.

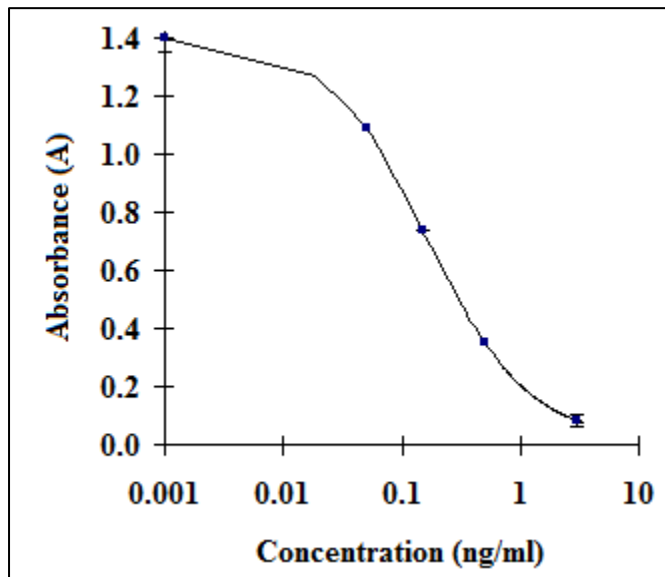


Figure 8.8: The standard curve for the 30 micron group was constructed and fitted using non linear regression logistic model. The solid line represents the curve fitting regression line. Blue squares represent the absorbance readings of the standard solutions, n=2.

The drug release data from 20 micron and 30 micron groups (Figures 8.9 and 8.10) indicates a greater release of EE from 20 micron group ( $32.7 \pm 7.3$  ng/day) as compared to the 30 micron group ( $30.1 \pm 5.8$  ng/day) . These results were not expected. It has been reported that while running multiple kits to analyse large number of samples, small errors introduced during analysis of each kit may result in % CV of 20-60% amongst the kits [271-273]. These errors may be due to pipetting volumes of analyte, antigen, antibody and substrate solutions, and incubation time for color development [271]. Accordingly, only a rough concentration estimate has been possible using ELISA. Although the results obtained from each analysis show intra-kit precision, the kits may lack in inter-kit precision. However, there may be other factors such as effects of drug loading and hydrodynamic changes occurring during drug release that we are not aware of and which may affect the drug release.

Nevertheless, zero order drug release profiles with  $R^2$  values of 0.9997 and 0.9999 were obtained for both the groups, respectively, and are illustrated in Figs 8.9 and 8.10. The linearity of the release was further confirmed by F test,  $F(1, 12)$ ,  $p < 0.05$ . The release data suggests the total duration of release of approximately three years or longer from the two groups.

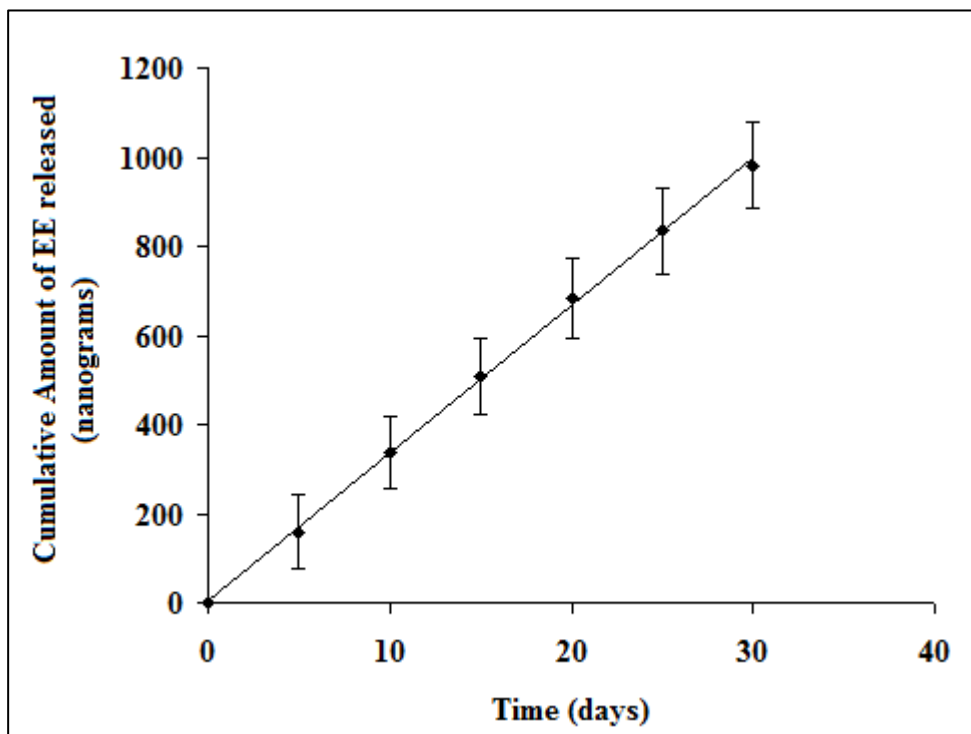


Figure 8.9: Cumulative Amount of EE released from 20 micron group over 30 days. The release profile exhibits a zero order kinetics with  $R^2 = 0.9990$ . The slope of the line suggests the rate of EE release of  $32.7 \pm 7.3$  ng/day. Data is presented as mean with standard deviation,  $n=6$ .

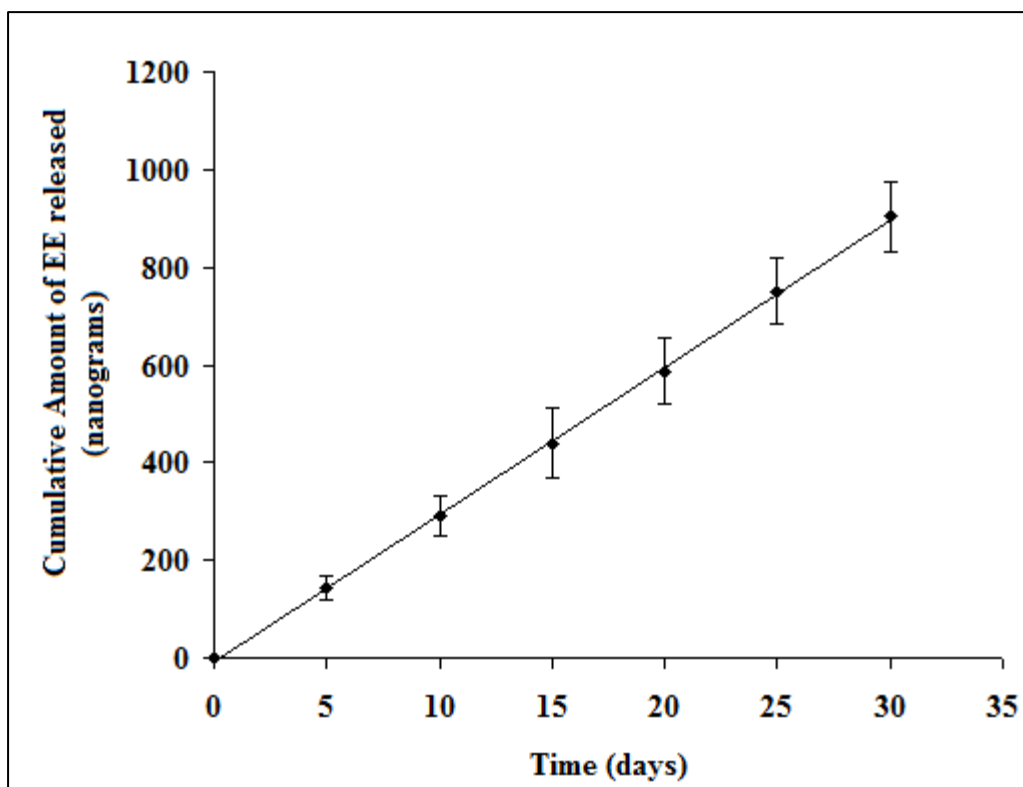


Figure 8.10: Cumulative amount of EE released from 30 micron group over 30 days. The release profile exhibits a zero order kinetics with  $R^2 = 0.9996$ . The slope of the line suggests the rate of EE release of  $30.1 \pm 5.8$  ng/day. Data is presented as mean with standard deviation,  $n=7$ .

#### 8.4 CONCLUSION

T47D-KBluc cells provided a sensitive and specific estrogen-responsive luciferase reporter system to quantify a biologically relevant amount of EE released into saline. The cells produced a luminescent signal in proportion to drug exposure. ELISA was used to estimate the amount of EE in the samples. ELISA is a popular analytical technique that is used in various fields such as pharmacy, biotechnology, and environmental science. Previous reports in literature suggest that errors introduced during

the analytical procedure may compound the error while analyzing unknown samples. The % difference between the two groups with respect to the amount of EE released is less than 10% and can be attributed to experimental error with ELISA as also described by previously published reports. This may explain the greater release of EE from 20 micron groups as compared to the 30 micron group. Nevertheless, the goal of the study was achieved as the delivery system yet again exhibited a zero order release over the 30 day period. Assuming a constant rate of release, the delivery system was found to be capable of releasing EE for more than three years.

## **Chapter 9: Pharmaceutical Applications of the Scalable Microperforated Drug Delivery Device**

The drug delivery system can be used for treatment of diverse chronic diseased states.

### **9.1 OCULAR IMPLANT**

The drug delivery system can be used as an ophthalmic implant or as an insert for treatment of ophthalmic diseases. Patients suffering from retinopathy, glaucoma, and age related macular degeneration (the three leading causes of blindness) [274-276] may benefit from delivery of drug by such a device.

Retinopathy refers to damage to the retina of the eye caused by non-ocular complications such as diabetes and hypertension [277, 278]. Diabetes leads to build up of plaque, hard exudates, edema, and hemorrhage of the retinal blood vessels resulting in their occlusion and leakage [279]. When left unchecked, the proliferating retinopathy may cause complete blindness. Glaucoma is a group of diseases that damage optic nerve and cause blindness [280]. An increasing intraocular pressure is a significant risk factor in progression of glaucoma. Age related macular degeneration (AMD) is a disease associated with aging that steadily diminishes central vision [281-283]. As illustrated in Figure 9.1, macula is the central area of the retina that processes fine details such as while reading or driving. AMD can be classified into two types. An abnormal growth of retinal blood vessels around the macula causes Wet AMD. The neovessels are unstable and may leak, raising the macula from its normal position [283]. In another type of AMD, which

is known as dry AMD, light sensitive cells in macula gradually breakdown, blurring the central vision [283].

Other major causes of blindness are cytomegalovirus (CMV) retinitis and endophthalmitis. CMV retinitis is a viral inflammation of the retina of the eye. It is a sight-threatening disease associated with late-stage AIDS (Acquired Immuno Deficiency Syndrome) [284]. Endophthalmitis involves inflammation of the intraocular cavities (i.e., the aqueous or vitreous humor) usually caused by infection [285].

All the aforementioned diseases relate to the posterior segment of the eye. Ophthalmic diseases associated with the posterior section present treatment challenges due to its inaccessible location [286]. Currently, approximately 90% of all ophthalmic drugs are delivered using eye drops. Although convenient and easy to use, eye drops are very inefficient, as 95% of the drug go waste to pre-corneal loss [213]. Figure 9.2 illustrates the flexibility of the drug delivery system developed. The device is capable of conforming to any shape and curvature and hence can be readily placed in the eye and used for long-term delivery of drugs.

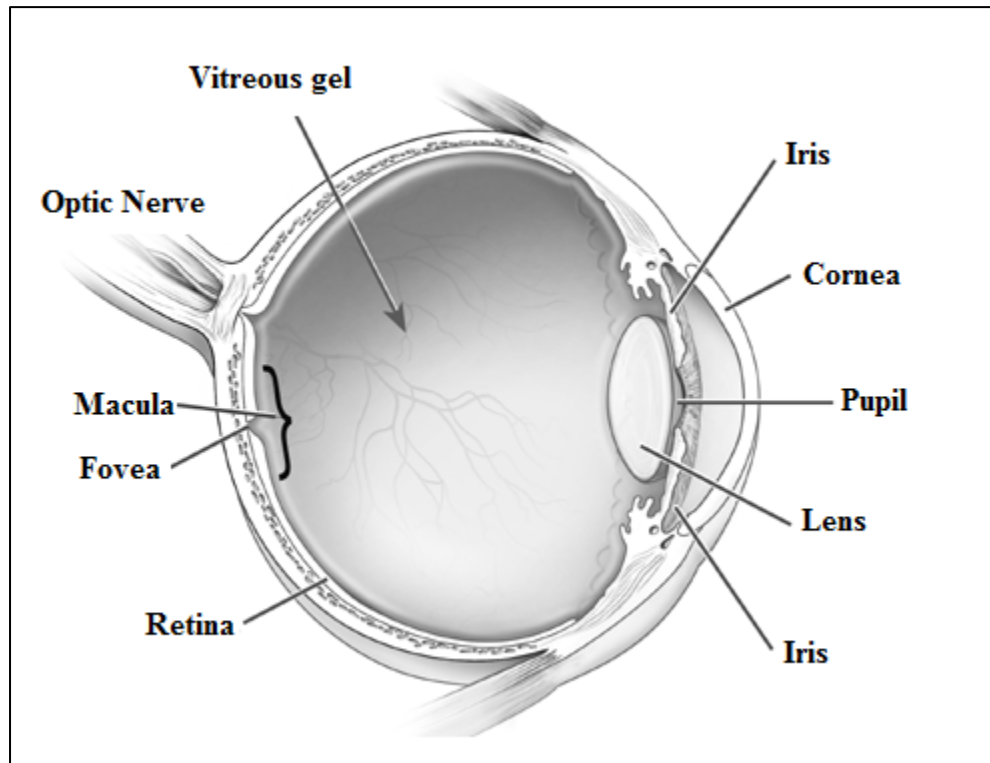


Figure 9.1: Anatomy of the Eye [287]

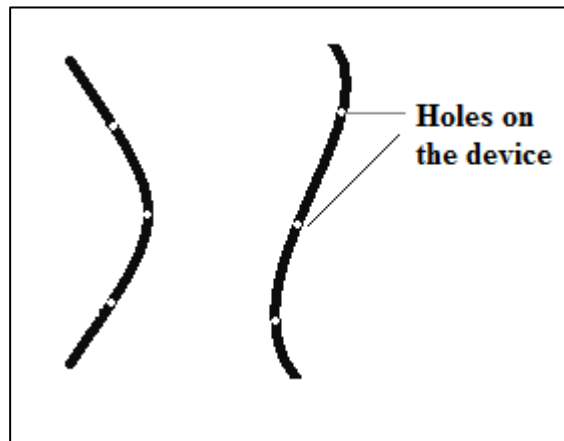


Figure 9.2: The figure demonstrates the flexibility of the drug delivery which is capable of conforming to any shape and curvature and hence can be successfully used as an ophthalmic implant

## 9.2 DRUG ELUTING STENT

The drug delivery system can also be built in as part of a drug eluting stent (DES) for treatment of renal, coronary, or intracranial atherosclerosis. Atherosclerosis is the narrowing of an artery due to build up of plaque [288]. Stents are mesh like cylindrical structures which are inserted into the affected artery to unclog it. However, injury to the implanted site at the time of placement triggers cellular mechanisms causing re-blockage [289]. This process of reoccurrence of stenosis or occlusion is known as restenosis. At present, a drug-polymer system, which is coated on the stent surface, is used to prevent restenosis. The polymer controls the drug release and the drug itself inhibits the restenosis causing cellular mechanisms. However, initial burst effect of drug, uneven coating of drug-polymer system, allergic reaction to polymer, and breakage of polymer while implantation leads to subsequent complications known as late stent thrombosis [111, 290].

The novel drug delivery system can be either mounted on the stent skeleton or built in along with the stent (Figure 9.3). The device offers several advantages over current DES because it is free from polymer and capable of zero order release of drugs. Hence cytotoxic dose dumping and complications due to polymer can be avoided.

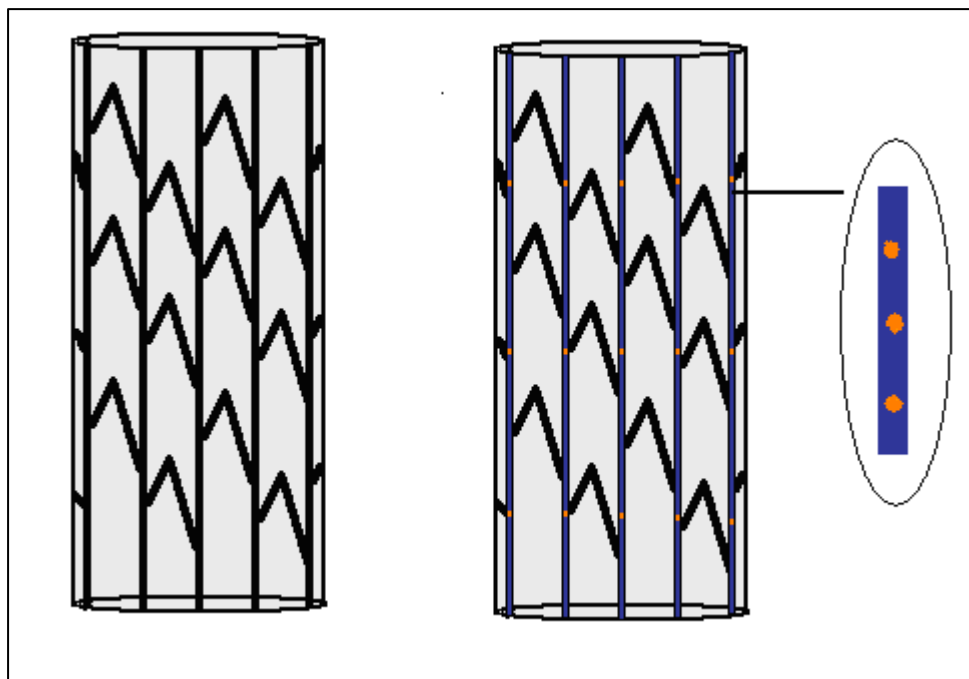


Figure 9.3: (Left) A bare metal stent. (Right) Drug delivery system (shown also in inset) can be mounted on top of the stent. The stent will open the clogged artery and the controlled release of drug from the device will prevent restenosis

### 9.3 MANAGEMENT OF PAIN, CANCER AND OTHER CHRONIC DISEASES

Management of several diseases such as chronic pain, cancer, diabetes, hypertension, require long-term drug therapy which may sometime last life-long. Many such diseases require repeated dosing to the patient. Chronic pain can be any or combination of the following - burn pain, dental/facial pain, migraine headache pain, musculoskeletal pain, neuropathic pain, obstetrical pain, surgical and trauma pain [291-294]. Additionally, there's pain associated with progressing diseases such as cancer, HIV, and arthritis, where the severity of pain increases with the proliferation of the disease.

Current drug delivery regimens revolve around oral administration of analgesics, drug infusion at the site, or intrathecal pumps and intraspinal catheters. Intrathecal is an

adjective which is used to describe devices or treatments related to spinal cord [295]. As previously discussed, oral drugs may have poor bioavailability and require multiple dosing. A need for frequent injections such as to control muscular or dental pain can also be distressful and costly to patients. Intrathecal injections, pumps, and catheters have been used in past for spinal anesthesia and analgesic delivery [296, 297]. Here, drugs are delivered directly to the cerebrospinal fluid that surrounds the spinal cord. The intrathecal methods have improved the quality of life of people by significantly reducing disability related to pain [298]. However, large amount of systemic narcotic exposure introduces several complications and may also lead to drug addiction [299]. Recent literature suggests implantable drug delivery systems as ideal candidates for pain management as they decrease the side effects and increase the treatment efficacy [300].

Cancer treatment usually involves systemic or oral administration of chemotherapeutic drugs. Although these drugs are beneficial in controlling the tumor spread, they are also associated with severe side effects such as hair loss, nausea, bone marrow depression, and memory changes [301]. A valid approach to decrease these side effects would be to deliver constant amount of drugs locally.

The novel drug delivery system offers one such solution for replacement of present chronic pain management methods and cancer treatment. The device can be implanted at the desired site or used transdermally. Figure 9.4 demonstrates one such scenario where multiple devices loaded with different drugs are placed on a transdermal patch. Each device on the patch acts independently, delivering different drugs. The said example also illustrates the possibility of combination therapy with the device.

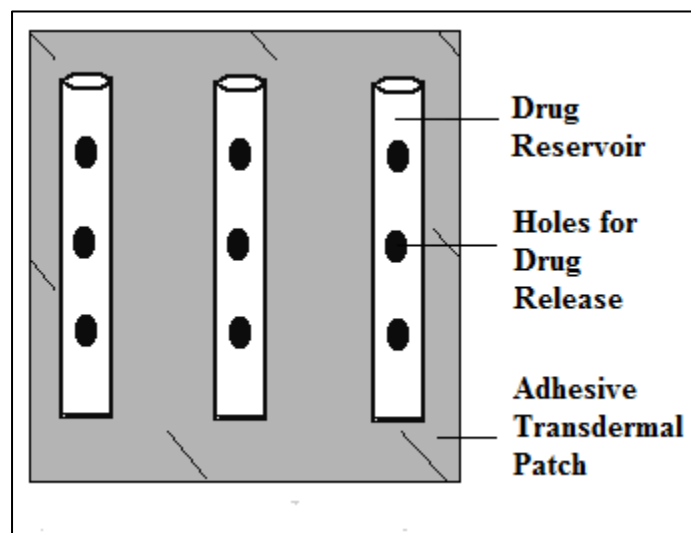


Figure 9.4: A transdermal patch containing multiple drug delivery devices

#### 9.4 NEURAL OR BRAIN IMPLANT

The novel drug delivery system can also be used as a brain or neural implant for the treatment of diseases of the central nervous system such as Parkinsonism and brain tumor. A similar example of an implantable system used for managing brain tumor is Gliadel® (Eisai Inc.). It is a biodegradable wafer, which is implanted at the tumor site after the tumor has been surgically removed [302]. The wafer, which is loaded with the drug carmustine, kills the surrounding tumor cells and prevent their re-occurrence [303].

The drug delivery system developed may also enable drug-gene combination therapy, wherein, anti-cancer drugs can be combined with small interfering RNA's (siRNA) and delivered to the tumor site. RNA interference technology can be used to silence a specific oncogene in tumor cells bringing about cell death [304]. The tumor

targeted delivery of siRNA presents a safer and more effective method for cancer therapies [305].

The drug delivery system can also be used for treatment of Parkinsonism and related disorders. Parkinson's disease is a degenerative disorder of the central nervous system that is caused by low levels of dopamine and characterized by impaired speech, and motor skills such as poor posture, tremors, and slowness in movement [306]. The treatment usually involves systemic administration of the dopamine precursor, Levo-dopa (L-dopa), because dopamine itself cannot cross the blood brain barrier. [307]. L-dopa is converted into dopamine in the dopaminergic neurons by L-aromatic amino acid decarboxylase [308]. However, the high systemic concentration of levodopa triggers the feedback inhibition mechanism by L-dopa decarboxylase and only 1-5% of L-dopa enters the dopaminergic neurons. Although L-Dopa is administered in combination with decarboxylase inhibitors, such as Carbidopa [309] but the problem of low bioavailability still remains. In such a scenario, the novel drug delivery system offers suitable replacement for existing therapies as significant amounts of L-dopa or dopamine can be delivered directly at the desired site.

## Chapter 10: Conclusions

The work of this dissertation has led us to following conclusions:

1. Aluminum was found to be unsuitable for making implants as it degraded in the physiological environment. After immersing in phosphate buffer saline for seven days, the aluminum coating appeared to be fractured and corroded. A high percentage of both aluminum (13.63%) and oxygen (57.83%) were obtained using EDS. However, nanopores were successfully made on gold layer which is chemically inert. Poly (2- octyl cyanoacrylate) was successfully evaluated as an extended release polymer. The length, width, depth, diameter, and area of the nanopores were found to be  $60.0 \pm 10.9$  nm,  $14.9 \pm 2.3$  nm,  $26.9 \pm 3.8$  nm,  $27.3 \pm 4.9$  nm, and  $1317.4 \pm 219.9$  nm<sup>2</sup>, respectively. A  $1 \mu\text{m}^2$  of wafer surface was estimated to hold  $3.55 \times 10^4$  nm<sup>3</sup> of pore volume. A bare metal stent was analyzed using SEM and it was estimated that a total pore volume of  $4.0 \times 10^9$  nm<sup>3</sup> would be available for drug loading if the stent is made using the nanoporous surface. In vitro drug release study using 2 - octyl cyanoacrylate and methyl orange as the drug-polymer matrix was conducted and after 7 days  $88.1 \pm 5.0$  % drug was released. The rate and extent of the drug release can be altered by using varying amounts of drug and varying the polymer layer. The initial work with nanodepots led to the current concept that instead of loading drug into the pores, we can load the drug inside a matrix with pores (or holes) on its surface.

2. The polyimide tubes were successfully coated with a biocompatible cobalt-chromium L605 alloy using sputtering method. The alloy coating was tested using EDS and was found to contain  $52.7 \pm 3.6$  % of cobalt,  $19.3 \pm 2.2$  % of chromium,  $17.9 \pm 1.5$  % of tungsten, nickel  $5.7 \pm 1.1$  %,  $2.3 \pm 0.5$  % of iron, and  $1.9 \pm 0.5$  % of manganese, which conformed to the commercial standards. The coating was found durable to mechanical stress and it helped to reduce the surface roughness. An investigation of  $1.0 \mu\text{m}^2$  area, of polyimide surface before and after coating revealed a reduction in root square mean surface roughness of 0.97 to 0.62 nm. Micro fabrication of polyimide matrices with photolithography yielded perforations between 25 – 40 micron size ranges.

3. Even though the perforated microdevice was essentially developed as part of a drug eluting stent, it can also be applied to other therapeutic and prophylactic treatments. The Finite Element Analysis revealed feasibility of the stent design. The development of the device as a drug eluting stent was not continued due to time constraint and manufacturing limitations. The perforated device was hence developed as a general drug delivery housing matrix.

4. Prednisolone, ethinyl estradiol and crystal violet were successfully loaded inside the tubes using different drug loading techniques. DSC analysis was used to investigate formation of any pseudo-polymorphs or true polymorphs for prednisolone and ethinyl estradiol in presence of alcohol. There was no significant difference found between the treated and untreated groups with respect to the glass transition temperature, in both prednisolone (untreated =  $240.3$  °C; alcohol treated =  $238.9$  °C) and EE (untreated =

185.4 °C; alcohol treated = 185.6 °C) suggesting that no true polymorphs were formed with alcohol treatment.

Drug loading using concentrated solutions ensured content uniformity across various groups. An average of  $127.1 \pm 11.9$   $\mu\text{g}$  of CV was loaded in all the small tubes with one, two, and three holes. For large tubes with one hole ( $365.3 \pm 16.7$   $\mu\text{m}$ ); two holes ( $362.4 \pm 23.1$   $\mu\text{m}$ ); and one bigger size hole ( $542.6 \pm 26.3$   $\mu\text{m}$ ) the average amount of CV loaded per unit length in the groups was  $5.3 \pm 0.3$ ,  $5.2 \pm 0.3$ , and  $5.4 \pm 0.2$   $\text{mg}/\text{cm}$ , respectively. The average amount of EE loaded in small tubes with 20 and 30 micron holes, the drug loading was measured as  $51.7 \pm 4.8$  and  $57.9 \pm 9.9$   $\mu\text{g}$ , respectively. However, in tubes where alcohol was used as drug loading solvent, homogenous distribution of the drug was not achieved. This is due to the fact that as the alcohol evaporates, it leaves void spaces, which cause erratic distribution of drug inside the device. An ideal drug loaded tube would have tightly packed drug powder in it. The variation in drug distribution was found to effect drug release study in the 600 micron group (large tubes with holes). We envision the limitations in drug loading procedure to be more of a simple engineering problem rather than a pharmaceutical problem. Several technologies such as those used for filling micro capillary columns in HPLC can be used to fill microtubes.

5. A series of drug release studies revealed that the perforated microtubes are scalable and can be successfully used for long-term zero order drug release. Polymers or membrane are not required to control release rates. Linear release rates with  $R^2 > 0.9900$

were obtained for all groups with CV and EE. For small tubes (30 $\mu$ m hole diameter; 125 $\mu$ m tube diameter) release rate of  $30.1 \pm 5.8$  ng/day was obtained for EE loaded tubes. and release rates of  $7.8 \pm 2.5$ ,  $16.2 \pm 5.5$ , and  $22.5 \pm 6.0$  ng/day were obtained for CV loaded tubes with one hole, two holes, and three holes respectively. The drug release was found to increase additively with increase in the number of holes. For large tubes (1000  $\mu$ m tube diameter) with holes, a release rate of  $10.8 \pm 4.1$ ,  $15.8 \pm 4.8$  and  $22.1 \pm 6.7$   $\mu$ g/day was observed *in vitro* in PBS and a release rate of  $5.8 \pm 1.8$   $\mu$ g/day was observed *ex vivo* in vitreous humor. The release rates were linear as a function of number of holes and proportional to the area of diffusion. Drug release from the device also depends on the drug's solubility, drug loading, and drug packing. The drug release in static environment does not differ greatly from the dynamic environment suggesting that the concentration gradient is the main driving force that causes the drug to move out of the device. Hence, a sink condition is always desired.

6. Cobalt-chromium L605 alloy coated and uncoated polyimide tubes, which were found to be non-inflammatory, non-cytotoxic, and biocompatible. A contact angle of  $63.7 \pm 3.7$  degrees was obtained for the device indicating that it is hydrophilic and favors cell attachment. After 72 h incubation with RAW 267.4 mouse cells, uniform cell distribution was observed on the polyimide surface. The polyimide matrices also did not induce significant expression of inflammatory markers such as TNF- $\alpha$  and IL-1 $\beta$  proving that it is biocompatible and non cytotoxic.

7. T47D-KBluc cells provided a sensitive and specific estrogen-responsive luciferase reporter system to quantify a biologically relevant amount of EE released into saline. The cells produced a luminescent signal in proportion to drug exposure. The average luminescence produced from 20 and 30 micron groups was  $1144.8 \pm 153.8$  and  $1219.9 \pm 127.7$  RLU/day. With ELISA, the amount of EE in the samples was quantitatively determined. It was estimated that with 20 micron and 30 micron groups  $32.7 \pm 7.3$  and  $30.1 \pm 5.8$  ng/day of EE was released, respectively. The discrepancy in the amount of EE released from the two groups was attributed to the lack of inter kit precision.

8. In conclusion, a novel drug delivery device has been devised and evaluated. The micro perforated micro delivery system can be used for long-term treatment of debilitating and chronic diseased states such as ocular diseases, cerebral diseases, and cancer or pain management. The simplicity of device's design and mechanism of function makes it economically viable. The low cost can be transferred to patients which can make otherwise expensive treatments affordable. Other advantages offered by the device would be: overcoming repeated dosing, improved patient compliance, improved health care, reduce hospital visits, reduced health care cost, and better quality of life for the patients.

**Appendix I – Drug Release Study Data (Tables and Calculations for Chapters 2, 5, and 6)**

Table 2.3: Standard curve measurements for estimation of drug release data from the nanoporous wafers.

Concentration (µg/ml)	Absorbance (A)
0.0	0.000
4.0	0.286
8.0	0.573
12.0	0.860
16.0	1.150
20.0	1.429

Standard Curve Equation => Absorbance (A) = 0.0716 \* Concentration (µg/ml) + 0.0003; R<sup>2</sup> = 1.000

Table 2.4: Drug release data from nanoporous wafer-1 loaded with methyl orange and 2-octyl cyanoacrylate as the drug polymer matrix.

Time (days)	Dilution (X)	Absorbance (A)	Conc (µg/ml)	Amount (µg)	Cumulative Amount (µg)	Cumulative % of drug released
0	0	0	0	0	0	0
1	4x	1.503	21.0	840.8	840.8	33.6
2	3x	1.371	19.2	575.2	1416.1	56.6
3	2x	1.694	23.7	473.8	1889.9	75.6
4	1x	1.879	26.3	262.8	2152.7	86.1
5	1x	0.736	10.3	102.9	2255.7	90.2
6	1x	0.354	5.0	49.5	2305.2	92.2
7	1x	0.128	1.8	17.9	2323.1	92.9

Table 2.5: Drug release data from nanoporous wafer-2 loaded with methyl orange and 2-octyl cyanoacrylate as the drug polymer matrix.

Time (days)	Dilution (X)	Absorbance (A)	Conc (µg/ml)	Amount (µg)	Cumulative Amount (µg)	Cumulative % of drug released
0	0	0	0	0	0	0
1	4x	1.131	15.8	632.7	632.7	42.2
2	3x	0.921	12.9	386.4	1019.2	67.9
3	2x	0.376	5.3	105.2	1124.3	75.0
4	1x	0.360	5.0	50.3	1174.7	78.3
5	1x	0.130	1.8	18.2	1192.9	79.5
6	1x	0.204	2.9	28.5	1221.4	81.4
7	1x	0.147	2.1	20.6	1242.0	82.8

Table 2.6: Drug release data from nanoporous wafer-3 loaded with methyl orange and 2-octyl cyanoacrylate as the drug polymer matrix.

Time (days)	Dilution (X)	Absorbance (A)	Conc (µg/ml)	Amount (µg)	Cumulative Amount (µg)	Cumulative % of drug released
0	0	0	0	0	0	0
1	4x	0.785	11.0	439.2	439.2	36.6
2	3x	0.560	7.8	235.0	674.1	56.2
3	2x	0.585	8.2	163.6	837.8	69.8
4	1x	0.787	11.0	110.1	947.8	79.0
5	1x	0.371	5.2	51.9	999.7	83.3
6	1x	0.308	4.3	43.1	1042.8	86.9
7	1x	0.135	1.9	18.9	1061.7	88.5

Table 2.7: Cumulative percentage of drug release data from the three nanoporous wafers.

<b>Time (days)</b>	<b>Cumulative % of methyl orange from wafer 1</b>	<b>Cumulative % of methyl orange from wafer 2</b>	<b>Cumulative % of methyl orange from wafer 3</b>	<b>Average cumulative %</b>	<b>S.D.</b>
0	0.0	0.0	0.0	0.0	0.0
1	33.6	42.2	36.6	37.5	4.4
2	56.6	68.0	56.2	60.3	6.7
3	75.6	75.0	69.8	73.5	3.2
4	86.1	78.4	79.0	81.2	4.3
5	90.2	79.6	83.3	84.4	5.4
6	92.2	81.5	86.9	86.9	5.4
7	92.9	82.9	88.5	88.1	5.0

Table 5.4: Absorbance readings for 'one hole' group belonging to 'small tubes'

Tube No.	Days															Average	SD	%CV
	0	2	4	6	8	10	12	14	16	18	20	22	24	26	28			
1	0.000	0.004	0.004	0.004	0.005	0.007	0.011	0.009	0.006	0.008	0.009	0.008	0.007	0.008	0.008	0.007	0.002	30.69
2	0.000	0.003	0.006	0.003	0.003	0.004	0.005	0.006	0.007	0.007	0.007	0.007	0.008	0.008	0.008	0.006	0.002	32.71
3	0.000	0.002	0.002	0.004	0.004	0.002	0.004	0.006	0.005	0.005	0.007	0.006	0.006	0.008	0.008	0.005	0.002	41.71
4	0.000	0.003	0.007	0.007	0.009	0.003	0.005	0.006	0.007	0.007	0.005	0.007	0.007	0.006	0.009	0.006	0.002	28.89
5	0.000	0.009	0.004	0.003	0.004	0.007	0.005	0.005	0.006	0.005	0.006	0.007	0.006	0.006	0.007	0.006	0.002	26.96
6	0.000	0.004	0.008	0.006	0.007	0.004	0.004	0.007	0.006	0.005	0.008	0.006	0.007	0.005	0.006	0.006	0.001	23.36
7	0.000	0.003	0.003	0.008	0.010	0.008	0.004	0.004	0.008	0.006	0.010	0.007	0.006	0.007	0.009	0.007	0.002	36.21
<b>Avg.</b>	0.000	0.004	0.005	0.005	0.006	0.005	0.005	0.006	0.006	0.006	0.007	0.007	0.007	0.007	0.008			
<b>SD</b>	0.000	0.002	0.002	0.002	0.003	0.002	0.003	0.002	0.001	0.001	0.002	0.001	0.001	0.001	0.001			
<b>%CV</b>	0.00	57.74	45.15	40.00	45.13	46.19	46.18	25.62	15.18	19.78	23.13	10.06	11.26	17.72	13.61			

Table 5.5: Absorbance readings for 'two hole' group belonging to 'small tubes'

Tube No.	Days															Average	SD	%CV
	0	2	4	6	8	10	12	14	16	18	20	22	24	26	28			
1	0.000	0.011	0.014	0.021	0.012	0.015	0.019	0.020	0.020	0.016	0.015	0.012	0.015	0.014	0.014	0.015	0.003	22.21
2	0.000	0.015	0.015	0.010	0.010	0.015	0.016	0.013	0.015	0.014	0.014	0.013	0.013	0.013	0.015	0.013	0.002	14.32
3	0.000	0.006	0.008	0.007	0.013	0.014	0.014	0.013	0.013	0.015	0.013	0.014	0.013	0.014	0.014	0.011	0.003	25.56
4	0.000	0.004	0.017	0.020	0.018	0.013	0.014	0.015	0.009	0.009	0.013	0.010	0.011	0.011	0.013	0.012	0.004	35.12
5	0.000	0.013	0.012	0.005	0.009	0.005	0.005	0.006	0.006	0.008	0.009	0.010	0.010	0.011	0.009	0.008	0.003	34.08
6	0.000	0.011	0.005	0.008	0.008	0.007	0.007	0.008	0.009	0.011	0.013	0.013	0.011	0.014	0.011	0.009	0.003	29.48
7	0.000	0.011	0.013	0.026	0.021	0.026	0.011	0.008	0.013	0.011	0.012	0.015	0.013	0.013	0.013	0.014	0.006	40.53
<b>Avg.</b>	0.000	0.010	0.012	0.014	0.013	0.014	0.012	0.012	0.012	0.012	0.013	0.012	0.012	0.013	0.013			
<b>SD</b>	0.000	0.004	0.004	0.008	0.005	0.007	0.005	0.005	0.005	0.003	0.002	0.002	0.002	0.001	0.002			
<b>%CV</b>	0.00	37.94	34.69	59.72	37.16	49.95	40.35	41.15	38.16	25.46	14.86	15.31	13.87	10.46	16.19			

Table 5.6: Absorbance readings for ‘three hole’ group belonging to ‘small tubes’

Tube No.	Days															Average	SD	%CV
	0	2	4	6	8	10	12	14	16	18	20	22	24	26	28			
1	0.000	0.024	0.018	0.025	0.021	0.016	0.024	0.020	0.017	0.019	0.017	0.019	0.018	0.017	0.020	0.020	0.003	14.76
2	0.000	0.004	0.009	0.009	0.009	0.009	0.007	0.007	0.011	0.013	0.011	0.013	0.013	0.015	0.012	0.010	0.003	29.41
3	0.000	0.026	0.015	0.018	0.018	0.021	0.017	0.017	0.017	0.018	0.018	0.018	0.019	0.020	0.021	0.019	0.003	14.03
4	0.000	0.016	0.016	0.017	0.012	0.016	0.011	0.016	0.019	0.017	0.018	0.019	0.018	0.021	0.017	0.017	0.003	15.74
5	0.000	0.016	0.016	0.020	0.019	0.013	0.019	0.019	0.015	0.014	0.014	0.016	0.014	0.016	0.019	0.016	0.002	14.27
6	0.000	0.008	0.022	0.013	0.018	0.019	0.018	0.021	0.015	0.017	0.019	0.021	0.017	0.021	0.020	0.018	0.004	21.17
7	0.000	0.009	0.019	0.029	0.024	0.025	0.022	0.018	0.019	0.021	0.022	0.022	0.018	0.021	0.017	0.020	0.005	22.45
<b>Avg.</b>	0.000	0.015	0.016	0.019	0.017	0.017	0.017	0.017	0.016	0.017	0.017	0.018	0.017	0.019	0.018			
<b>SD</b>	0.000	0.008	0.004	0.007	0.005	0.005	0.006	0.005	0.003	0.003	0.004	0.003	0.002	0.003	0.003			
<b>%CV</b>	0.00	56.14	24.56	36.34	29.82	30.94	35.50	27.70	17.31	16.29	20.94	16.62	13.69	14.04	16.97			

Table 5.7: Cumulative amount of crystal violet released from ‘one hole’ group. The amount and cumulative amount values are in microgram units of weight.

Days	Tube1		Tube2		Tube3		Tube4		Tube5		Tube6		Tube7		Average Cum. Amt	SD	%CV
	Amt	Cum. Amt.															
0	0.000	0.000	0.000	0.000	0.000	0.000	0.000	0.000	0.000	0.000	0.000	0.000	0.000	0.000	0.000	0.000	n.a
2	0.010	0.010	0.008	0.008	0.005	0.005	0.008	0.008	0.024	0.024	0.010	0.010	0.008	0.008	0.010	0.006	59.215
4	0.010	0.021	0.016	0.023	0.005	0.010	0.018	0.026	0.010	0.034	0.021	0.031	0.008	0.015	0.023	0.008	36.788
6	0.010	0.031	0.008	0.031	0.010	0.020	0.018	0.044	0.008	0.041	0.016	0.047	0.021	0.036	0.036	0.009	25.704
8	0.013	0.044	0.008	0.039	0.010	0.031	0.024	0.068	0.010	0.052	0.018	0.065	0.026	0.062	0.051	0.014	27.745
10	0.018	0.062	0.010	0.049	0.005	0.036	0.008	0.075	0.018	0.070	0.010	0.075	0.021	0.083	0.064	0.017	26.120
12	0.029	0.091	0.013	0.062	0.010	0.046	0.013	0.088	0.013	0.083	0.010	0.086	0.010	0.094	0.078	0.018	22.573
14	0.024	0.114	0.016	0.077	0.016	0.062	0.016	0.104	0.013	0.096	0.018	0.104	0.010	0.104	0.094	0.018	19.516
16	0.016	0.130	0.018	0.096	0.013	0.075	0.018	0.122	0.016	0.112	0.016	0.119	0.021	0.125	0.111	0.020	17.657
18	0.021	0.151	0.018	0.114	0.013	0.087	0.018	0.140	0.013	0.124	0.013	0.132	0.016	0.140	0.127	0.021	16.675
20	0.024	0.174	0.018	0.132	0.018	0.106	0.013	0.153	0.016	0.140	0.021	0.153	0.026	0.166	0.146	0.023	15.723
22	0.021	0.195	0.018	0.150	0.016	0.121	0.018	0.171	0.018	0.158	0.016	0.169	0.018	0.185	0.164	0.024	14.759
24	0.018	0.213	0.021	0.171	0.016	0.137	0.018	0.190	0.016	0.174	0.018	0.187	0.016	0.200	0.182	0.025	13.531
26	0.021	0.234	0.021	0.192	0.021	0.158	0.016	0.205	0.016	0.189	0.013	0.200	0.018	0.219	0.200	0.024	12.116
28	0.021	0.255	0.021	0.213	0.021	0.179	0.024	0.229	0.018	0.208	0.016	0.216	0.024	0.242	0.220	0.025	11.339

Standard Curve Equation: Absorbance (A) = 0.0984 (Conc in µg/ml) + 0.0001 was used in the calculations.

Table 5.8: Cumulative amount of crystal violet released from ‘two holes’ group. The amount and cumulative amount values are in microgram units of weight.

Days	Tube1		Tube2		Tube3		Tube4		Tube5		Tube6		Tube7		Average Cum. Amt	SD	%CV
	Amt	Cum. Amt.															
0	0	0		0	0	0	0	0	0	0	0	0	0	0	0	0	n.a
2	0.029	0.029	0.039	0.039	0.016	0.016	0.010	0.010	0.034	0.034	0.029	0.029	0.029	0.029	0.027	0.010	38.319
4	0.037	0.066	0.039	0.079	0.021	0.036	0.045	0.055	0.031	0.066	0.013	0.042	0.034	0.063	0.058	0.015	25.432
6	0.055	0.121	0.026	0.105	0.018	0.055	0.053	0.108	0.013	0.078	0.021	0.063	0.068	0.131	0.094	0.029	31.150
8	0.031	0.152	0.026	0.131	0.034	0.089	0.047	0.155	0.024	0.102	0.021	0.083	0.055	0.187	0.128	0.039	30.053
10	0.039	0.192	0.039	0.170	0.037	0.126	0.034	0.189	0.013	0.115	0.018	0.102	0.068	0.255	0.164	0.054	32.897
12	0.050	0.242	0.042	0.212	0.037	0.162	0.037	0.226	0.013	0.128	0.018	0.120	0.029	0.284	0.196	0.061	31.201
14	0.053	0.294	0.034	0.247	0.034	0.196	0.039	0.265	0.016	0.143	0.021	0.141	0.021	0.305	0.227	0.068	29.896
16	0.053	0.347	0.039	0.286	0.034	0.230	0.024	0.289	0.016	0.159	0.024	0.164	0.034	0.339	0.259	0.077	29.647
18	0.042	0.389	0.037	0.323	0.039	0.270	0.024	0.312	0.021	0.180	0.029	0.193	0.029	0.368	0.291	0.081	27.821
20	0.039	0.428	0.037	0.359	0.034	0.304	0.034	0.346	0.024	0.203	0.034	0.227	0.031	0.399	0.324	0.084	25.983
22	0.031	0.459	0.034	0.393	0.037	0.341	0.026	0.372	0.026	0.230	0.034	0.261	0.039	0.438	0.356	0.086	24.116
24	0.039	0.499	0.034	0.428	0.034	0.375	0.029	0.401	0.026	0.256	0.029	0.290	0.034	0.472	0.389	0.090	23.108
26	0.037	0.536	0.034	0.462	0.037	0.411	0.029	0.430	0.029	0.285	0.037	0.327	0.034	0.507	0.422	0.091	21.556
28	0.037	0.572	0.039	0.501	0.037	0.448	0.034	0.464	0.024	0.308	0.029	0.356	0.034	0.541	0.456	0.096	20.970

Standard Curve Equation: Absorbance (A) = 0.0984 (Conc in µg/ml) + 0.0001 was used in the calculations.

Table 5.9: Cumulative amount of crystal violet released from ‘three holes’ group. The amount and cumulative amount values are in microgram units of weight.

Days	Tube1		Tube2		Tube3		Tube4		Tube5		Tube6		Tube7		Average Cum. Amt	SD	%CV
	Amt	Cum. Amt.															
0	0.000	0.000	0.000	0.000	0.000	0.000	0.000	0.000	0.000	0.000	0.000	0.000	0.000	0.000	0.000	0.000	n.a
2	0.063	0.063	0.010	0.010	0.068	0.068	0.042	0.042	0.042	0.042	0.021	0.021	0.024	0.024	0.039	0.022	56.524
4	0.047	0.110	0.024	0.034	0.039	0.108	0.042	0.084	0.042	0.084	0.058	0.079	0.050	0.073	0.082	0.025	31.134
6	0.066	0.176	0.024	0.057	0.047	0.155	0.045	0.129	0.053	0.137	0.034	0.113	0.076	0.150	0.131	0.038	29.205
8	0.053	0.229	0.018	0.076	0.045	0.200	0.042	0.171	0.050	0.187	0.055	0.168	0.047	0.197	0.175	0.048	27.651
10	0.042	0.271	0.024	0.099	0.055	0.255	0.042	0.213	0.034	0.221	0.050	0.218	0.066	0.263	0.220	0.058	26.472
12	0.063	0.334	0.018	0.117	0.045	0.300	0.029	0.242	0.050	0.271	0.047	0.265	0.058	0.321	0.264	0.072	27.411
14	0.063	0.397	0.018	0.136	0.045	0.344	0.029	0.270	0.050	0.321	0.050	0.315	0.058	0.379	0.309	0.087	28.236
16	0.045	0.442	0.029	0.164	0.045	0.389	0.050	0.320	0.039	0.360	0.039	0.355	0.050	0.429	0.351	0.093	26.400
18	0.050	0.492	0.034	0.198	0.047	0.436	0.045	0.365	0.037	0.397	0.045	0.399	0.055	0.484	0.396	0.099	24.945
20	0.045	0.536	0.029	0.227	0.047	0.484	0.047	0.412	0.037	0.433	0.050	0.449	0.058	0.542	0.441	0.106	24.112
22	0.050	0.586	0.034	0.261	0.047	0.531	0.050	0.462	0.042	0.475	0.055	0.504	0.058	0.600	0.489	0.113	23.100
24	0.047	0.634	0.034	0.295	0.050	0.581	0.047	0.509	0.037	0.512	0.045	0.549	0.047	0.647	0.532	0.118	22.098
26	0.045	0.678	0.039	0.335	0.053	0.633	0.055	0.565	0.042	0.554	0.055	0.604	0.055	0.702	0.582	0.122	20.941
28	0.053	0.731	0.031	0.366	0.055	0.689	0.045	0.609	0.050	0.604	0.053	0.657	0.045	0.747	0.629	0.128	20.385

Standard curve equation: Absorbance (A) = 0.0984 (Conc in µg/ml) + 0.0001 was used in the calculations.

Table 5.10: Drug loading in ‘one hole’ group

<b>Tubes</b>	<b>Drug loaded (<math>\mu\text{g}</math>)</b>
T1	115.0
T2	134.0
T3	117.0
T4	126.0
T5	125.0
T6	113.0
T7	138.0
<b>Average</b>	124.0
<b>SD</b>	9.6
<b>% CV</b>	7.7

Table 5.11: Drug loading in ‘two holes’ group

<b>Tubes</b>	<b>Drug loaded (<math>\mu\text{g}</math>)</b>
T1	117.0
T2	116.0
T3	120.0
T4	144.0
T5	131.0
T6	132.0
T7	160.0
<b>Average</b>	131.4
<b>SD</b>	16.1
<b>% CV</b>	12.2

Table 5.12: Drug loading in ‘three holes’ group

<b>Tubes</b>	<b>Drug loaded (<math>\mu\text{g}</math>)</b>
T1	110.0
T2	123.0
T3	126.0
T4	121.0
T5	119.0
T6	122.0
T7	139.0
<b>Average</b>	122.6
<b>SD</b>	8.7
<b>% CV</b>	7.1

Table 5.13: Percentage cumulative drug released for 'one hole' group

Days	Tube1		Tube2		Tube3		Tube4		Tube5		Tube6		Tube7		Average %- Cum. Rel	SD	%CV
	Cum. Amt.	% Cum Rel															
0	0.000	0.000	0.000	0.000	0.000	0.000	0.000	0.000	0.000	0.000	0.000	0.000	0.000	0.000	0.000	0.000	n.a
2	0.010	0.009	0.008	0.006	0.005	0.004	0.008	0.006	0.024	0.019	0.010	0.009	0.008	0.006	0.008	0.005	59.153
4	0.021	0.018	0.023	0.017	0.010	0.009	0.026	0.021	0.034	0.027	0.031	0.028	0.015	0.011	0.019	0.007	38.951
6	0.031	0.027	0.031	0.023	0.020	0.017	0.044	0.035	0.041	0.033	0.047	0.041	0.036	0.026	0.029	0.008	27.755
8	0.044	0.038	0.039	0.029	0.031	0.026	0.068	0.054	0.052	0.041	0.065	0.058	0.062	0.045	0.042	0.012	28.225
10	0.062	0.054	0.049	0.036	0.036	0.030	0.075	0.060	0.070	0.056	0.075	0.067	0.083	0.060	0.052	0.013	25.673
12	0.091	0.079	0.062	0.046	0.046	0.039	0.088	0.070	0.083	0.066	0.086	0.076	0.094	0.068	0.063	0.015	23.611
14	0.114	0.099	0.077	0.058	0.062	0.053	0.104	0.082	0.096	0.077	0.104	0.092	0.104	0.075	0.077	0.017	22.123
16	0.130	0.113	0.096	0.071	0.075	0.064	0.122	0.097	0.112	0.089	0.119	0.106	0.125	0.090	0.090	0.018	19.579
18	0.151	0.131	0.114	0.085	0.087	0.075	0.140	0.111	0.124	0.100	0.132	0.117	0.140	0.102	0.103	0.019	18.603
20	0.174	0.152	0.132	0.099	0.106	0.090	0.153	0.122	0.140	0.112	0.153	0.136	0.166	0.121	0.119	0.021	17.671
22	0.195	0.170	0.150	0.112	0.121	0.104	0.171	0.136	0.158	0.127	0.169	0.149	0.185	0.134	0.133	0.022	16.711
24	0.213	0.186	0.171	0.128	0.137	0.117	0.190	0.151	0.174	0.139	0.187	0.166	0.200	0.145	0.147	0.023	15.651
26	0.234	0.204	0.192	0.143	0.158	0.135	0.205	0.163	0.189	0.152	0.200	0.177	0.219	0.158	0.162	0.023	14.241
28	0.255	0.222	0.213	0.159	0.179	0.153	0.229	0.182	0.208	0.166	0.216	0.191	0.242	0.175	0.178	0.023	13.082

Calculations were performed using values from Table 5.7 and the drug loading data in Table 5.10

Table 5.14: Percentage cumulative drug released for ‘two holes’ group

Days	Tube1		Tube2		Tube3		Tube4		Tube5		Tube6		Tube7		Average % Cum. Rel	SD	%CV
	Cum. Amt.	% Cum Rel															
0	0.000	0.000	0.000	0.000	0.000	0.000	0.000	0.000	0.000	0.000	0.000	0.000	0.000	0.000	0.000	0.000	n.a.
2	0.029	0.025	0.039	0.034	0.016	0.013	0.010	0.007	0.034	0.026	0.029	0.022	0.029	0.018	0.021	0.009	42.876
4	0.066	0.056	0.079	0.068	0.036	0.030	0.055	0.038	0.066	0.050	0.042	0.032	0.063	0.039	0.045	0.014	30.802
6	0.121	0.103	0.105	0.090	0.055	0.046	0.108	0.075	0.078	0.060	0.063	0.047	0.131	0.082	0.072	0.022	30.415
8	0.152	0.130	0.131	0.113	0.089	0.074	0.155	0.108	0.102	0.078	0.083	0.063	0.187	0.117	0.097	0.025	26.083
10	0.192	0.164	0.170	0.147	0.126	0.105	0.189	0.131	0.115	0.088	0.102	0.077	0.255	0.159	0.124	0.035	28.044
12	0.242	0.206	0.212	0.183	0.162	0.135	0.226	0.157	0.128	0.098	0.120	0.091	0.284	0.177	0.150	0.044	29.301
14	0.294	0.251	0.247	0.213	0.196	0.164	0.265	0.184	0.143	0.110	0.141	0.107	0.305	0.190	0.174	0.053	30.256
16	0.347	0.296	0.286	0.246	0.230	0.192	0.289	0.200	0.159	0.121	0.164	0.125	0.339	0.212	0.199	0.063	31.453
18	0.389	0.332	0.323	0.278	0.270	0.225	0.312	0.217	0.180	0.137	0.193	0.146	0.368	0.230	0.224	0.069	30.694
20	0.428	0.366	0.359	0.310	0.304	0.253	0.346	0.240	0.203	0.155	0.227	0.172	0.399	0.249	0.249	0.073	29.335
22	0.459	0.393	0.393	0.339	0.341	0.284	0.372	0.259	0.230	0.175	0.261	0.198	0.438	0.274	0.274	0.076	27.506
24	0.499	0.426	0.428	0.369	0.375	0.312	0.401	0.279	0.256	0.195	0.290	0.220	0.472	0.295	0.299	0.080	26.824
26	0.536	0.458	0.462	0.398	0.411	0.343	0.430	0.299	0.285	0.217	0.327	0.248	0.507	0.317	0.326	0.083	25.593
28	0.572	0.489	0.501	0.432	0.448	0.373	0.464	0.322	0.308	0.235	0.356	0.269	0.541	0.338	0.351	0.089	25.247

Calculations were performed using values from Table 5.8 and the drug loading data in Table 5.11

Table 5.15: Percentage cumulative drug released for ‘three holes’ group

Days	Tube1		Tube2		Tube3		Tube4		Tube5		Tube6		Tube7		Average % Cum. Rel	SD	%CV
	Cum. Amt.	% Cum Rel	Cum. Amt.	% Cum Rel	Cum. Amt.	% Cum Rel	Cum. Amt.	% Cum Rel	Cum. Amt.	% Cum Rel	Cum. Amt.	% Cum Rel	Cum. Amt.	% Cum Rel			
0	0.000	0.000	0.000	0.000	0.000	0.000	0.000	0.000	0.000	0.000	0.000	0.000	0.000	0.000	0.000	0.000	n.a
2	0.063	0.057	0.010	0.008	0.068	0.054	0.042	0.035	0.042	0.035	0.021	0.017	0.024	0.017	0.032	0.019	59.376
4	0.110	0.100	0.034	0.027	0.108	0.086	0.084	0.069	0.084	0.071	0.079	0.065	0.073	0.053	0.067	0.023	34.574
6	0.176	0.160	0.057	0.047	0.155	0.123	0.129	0.106	0.137	0.115	0.113	0.092	0.150	0.108	0.107	0.034	31.844
8	0.229	0.208	0.076	0.061	0.200	0.159	0.171	0.141	0.187	0.157	0.168	0.138	0.197	0.142	0.144	0.043	30.270
10	0.271	0.246	0.099	0.081	0.255	0.202	0.213	0.176	0.221	0.185	0.218	0.179	0.263	0.189	0.180	0.050	27.730
12	0.334	0.304	0.117	0.095	0.300	0.238	0.242	0.200	0.271	0.227	0.265	0.217	0.321	0.231	0.216	0.062	28.864
14	0.397	0.361	0.136	0.110	0.344	0.273	0.270	0.223	0.321	0.269	0.315	0.258	0.379	0.272	0.253	0.075	29.813
16	0.442	0.402	0.164	0.134	0.389	0.309	0.320	0.265	0.360	0.302	0.355	0.291	0.429	0.308	0.287	0.080	27.839
18	0.492	0.447	0.198	0.161	0.436	0.346	0.365	0.302	0.397	0.333	0.399	0.327	0.484	0.348	0.324	0.085	26.247
20	0.536	0.488	0.227	0.185	0.484	0.384	0.412	0.341	0.433	0.364	0.449	0.368	0.542	0.390	0.360	0.090	25.090
22	0.586	0.533	0.261	0.212	0.531	0.421	0.462	0.382	0.475	0.399	0.504	0.413	0.600	0.431	0.399	0.096	23.953
24	0.634	0.576	0.295	0.240	0.581	0.461	0.509	0.421	0.512	0.430	0.549	0.450	0.647	0.465	0.435	0.100	22.975
26	0.678	0.617	0.335	0.272	0.633	0.503	0.565	0.467	0.554	0.466	0.604	0.495	0.702	0.505	0.475	0.103	21.652
28	0.731	0.664	0.366	0.298	0.689	0.546	0.609	0.504	0.604	0.508	0.657	0.538	0.747	0.537	0.514	0.109	21.288

Calculations were performed using values from Table 5.9 and the drug loading data in Table 5.12

Table 5.16: Absorbance readings for ‘one small hole’ group belonging to ‘large tubes’

Tubes	Days																
	1	2	3	4	5	6	7	8	9	10	11	12	13	14	15	16	17
<b>T1</b>	2.001	1.839	1.233	2.021	1.138	1.005	1.392	1.282	1.189	0.986	0.799	0.923	0.875	0.747	0.690	0.817	0.872
<b>T2</b>	0.429	0.457	0.485	0.731	0.440	0.444	0.614	0.452	0.531	0.569	0.557	0.605	0.750	0.643	0.621	0.925	0.661
<b>T3</b>	0.475	0.530	0.648	1.307	0.846	1.012	1.368	0.921	1.177	1.141	0.976	1.045	1.078	1.088	0.980	0.831	1.028
<b>T4</b>	0.604	0.646	0.829	1.314	0.921	0.981	1.229	0.935	1.094	0.877	0.788	0.838	0.755	0.780	0.819	0.918	0.812
<b>T5</b>	0.452	0.632	0.802	0.996	0.821	1.059	1.160	0.860	1.043	0.965	1.001	1.011	0.918	0.865	0.920	0.800	0.800
<b>T6</b>	0.570	0.760	0.849	1.210	0.820	1.064	1.130	0.822	0.940	0.835	0.740	0.791	0.767	0.760	0.674	0.768	0.724
<b>T7</b>	0.056	0.158	0.625	1.323	0.941	1.118	1.366	0.985	1.073	0.910	0.847	1.017	0.885	0.766	0.652	0.693	0.738
<b>T8</b>	0.064	0.138	0.117	1.092	0.790	1.116	0.918	0.700	0.860	0.777	0.523	0.589	0.521	0.501	0.752	0.793	0.745
<b>T9</b>	0.256	0.277	0.263	0.352	0.258	0.327	0.375	0.275	0.306	0.297	0.229	0.288	0.307	0.301	0.814	0.768	0.742
<b>T10</b>	0.597	0.954	1.153	1.493	1.023	1.135	1.179	0.930	0.998	0.826	0.683	0.858	0.799	0.671	0.781	0.892	0.789
<b>T11</b>	0.059	1.287	1.242	1.705	1.048	1.331	1.513	0.986	1.058	0.903	0.702	0.752	0.800	0.738	0.624	0.828	0.678
<b>T12</b>	0.253	0.257	0.294	0.390	0.300	0.355	0.400	0.293	0.316	0.389	0.346	0.389	0.409	0.391	0.723	0.758	0.738
<b>Average</b>	0.485	0.661	0.712	1.161	0.779	0.912	1.054	0.787	0.882	0.790	0.683	0.759	0.739	0.688	0.754	0.816	0.777
<b>SD</b>	0.521	0.502	0.379	0.494	0.291	0.337	0.391	0.304	0.318	0.249	0.234	0.246	0.221	0.212	0.114	0.069	0.098
<b>%CV</b>	107.49	75.92	53.27	42.55	37.35	36.94	37.14	38.64	36.05	31.56	34.30	32.46	29.95	30.77	15.15	8.45	12.59

Table 5.16 continues on next page -

Tubes	Days											Average	SD	% CV
	18	19	20	21	22	23	24	25	26	27	28			
<b>T1</b>	0.387	0.414	0.522	0.560	0.409	0.427	0.605	0.622	0.594	0.525	0.588	1.165	0.426	36.53
<b>T2</b>	0.485	0.787	0.737	0.534	0.648	0.466	0.486	0.474	0.479	0.629	0.475	0.583	0.134	23.05
<b>T3</b>	0.750	0.809	0.792	0.766	0.673	0.764	0.822	0.898	0.804	0.885	0.797	0.968	0.245	25.31
<b>T4</b>	0.799	0.862	0.904	0.839	0.714	0.731	0.767	0.757	0.810	0.786	0.819	0.891	0.185	20.78
<b>T5</b>	0.698	0.618	0.806	0.885	0.701	0.550	0.687	0.793	0.845	0.802	0.832	0.889	0.169	19.06
<b>T6</b>	0.622	0.651	0.653	0.661	0.567	0.568	0.591	0.599	0.591	0.571	0.585	0.837	0.164	19.63
<b>T7</b>	0.611	0.718	0.654	0.711	0.733	0.625	0.679	0.718	0.765	0.762	0.745	0.833	0.345	41.49
<b>T8</b>	0.568	0.597	0.570	0.588	0.555	0.550	0.615	0.563	0.713	0.706	0.648	0.647	0.312	48.19
<b>T9</b>	0.363	0.361	0.385	0.364	0.313	0.302	0.349	0.319	0.344	0.316	0.320	0.379	0.193	50.92
<b>T10</b>	0.752	0.764	0.724	0.699	0.670	0.644	0.721	0.700	0.767	0.750	0.698	0.927	0.224	24.12
<b>T11</b>	0.504	0.533	0.615	0.644	0.699	0.645	0.765	0.698	0.817	0.640	0.768	0.956	0.388	40.61
<b>T12</b>	0.590	0.547	0.535	0.626	0.519	0.496	0.526	0.523	0.579	0.539	0.536	0.412	0.164	39.88
<b>Average</b>	0.594	0.638	0.658	0.656	0.600	0.564	0.634	0.639	0.676	0.659	0.651	0.790	0.153	19.36
<b>SD</b>	0.141	0.157	0.144	0.141	0.132	0.130	0.135	0.156	0.157	0.156	0.156	0.293	0.136	46.38
<b>%CV</b>	23.81	24.65	21.91	21.44	22.00	23.09	21.28	24.48	23.30	23.67	24.03	38.858	23.397	60.21

Table 5.17: Absorbance readings for ‘one big hole’ group belonging to ‘large tubes’

Tubes	Days																
	1	2	3	4	5	6	7	8	9	10	11	12	13	14	15	16	17
<b>T1</b>	0.235	0.645	0.606	0.643	0.630	0.628	0.640	0.677	0.727	0.678	0.662	0.661	0.623	0.529	0.529	0.435	0.557
<b>T2</b>	0.417	0.493	0.510	0.536	0.526	0.659	0.604	0.532	0.541	0.510	0.518	0.545	0.495	0.528	0.528	0.431	0.460
<b>T3</b>	0.132	0.305	0.309	0.328	0.368	0.411	0.401	0.423	0.417	0.376	0.395	0.423	0.356	0.470	0.470	0.376	0.341
<b>T4</b>	0.563	0.612	0.632	0.659	0.850	0.862	0.791	0.706	0.593	0.619	0.629	0.621	0.737	0.671	0.671	0.555	0.713
<b>T5</b>	0.508	0.619	0.628	0.659	0.721	1.011	0.905	0.838	0.982	0.981	0.830	0.899	0.866	0.910	0.910	0.732	0.548
<b>T6</b>	0.876	0.370	0.384	0.400	0.893	0.527	0.880	0.662	0.794	0.786	0.674	0.783	0.637	0.792	0.792	0.648	0.745
<b>T7</b>	0.545	0.427	0.435	0.456	0.579	0.589	0.589	0.507	0.550	0.538	0.544	0.532	0.567	0.588	0.588	0.531	0.512
<b>T8</b>	0.526	0.330	0.347	0.361	0.444	0.379	0.372	0.327	0.339	0.335	0.329	0.369	0.367	0.427	0.427	0.414	0.451
<b>T9</b>	0.319	0.735	0.735	0.760	0.502	0.767	0.610	0.724	0.761	0.665	0.650	0.632	0.766	0.761	0.761	0.666	0.746
<b>T10</b>	0.621	0.548	0.572	0.598	0.541	0.553	0.683	0.662	0.671	0.550	0.539	0.624	0.577	0.521	0.521	0.535	0.471
<b>T11</b>	0.748	0.509	0.533	0.555	0.541	0.746	0.752	0.633	0.642	0.622	0.679	0.749	0.581	0.761	0.761	0.663	0.636
<b>T12</b>	0.419	0.311	0.330	0.344	0.386	0.399	0.381	0.381	0.399	0.470	0.482	0.495	0.496	0.467	0.467	0.457	0.465
<b>Average</b>	0.492	0.492	0.502	0.525	0.582	0.628	0.634	0.589	0.618	0.594	0.578	0.611	0.589	0.619	0.619	0.537	0.554
<b>SD</b>	0.208	0.144	0.139	0.145	0.167	0.194	0.182	0.155	0.185	0.176	0.138	0.152	0.152	0.156	0.156	0.118	0.130
<b>%CV</b>	42.22	29.36	27.74	27.56	28.69	30.93	28.75	26.27	29.94	29.69	23.85	24.81	25.86	25.17	25.17	21.92	23.53

Table 5.17 continues on next page -

Tubes	Days											Average	SD	% CV
	18	19	20	21	22	23	24	25	26	27	28			
<b>T1</b>	0.401	0.635	0.598	0.617	0.492	0.344	0.472	0.416	0.507	0.403	0.546	0.594	0.116	19.51
<b>T2</b>	0.452	0.521	0.470	0.491	0.414	0.416	0.468	0.503	0.488	0.523	0.555	0.520	0.057	10.94
<b>T3</b>	0.321	0.528	0.374	0.329	0.293	0.320	0.321	0.337	0.318	0.296	0.316	0.371	0.078	21.17
<b>T4</b>	0.703	0.692	0.666	0.616	0.622	0.508	0.557	0.539	0.586	0.647	0.481	0.676	0.091	13.51
<b>T5</b>	0.810	0.847	0.542	0.809	0.738	0.533	0.550	0.790	0.756	0.824	0.765	0.797	0.159	19.94
<b>T6</b>	0.640	0.590	0.695	0.597	0.714	0.445	0.658	0.559	0.534	0.599	0.559	0.685	0.173	25.19
<b>T7</b>	0.484	0.499	0.484	0.530	0.438	0.482	0.483	0.437	0.452	0.476	0.470	0.534	0.052	9.83
<b>T8</b>	0.440	0.524	0.508	0.407	0.741	0.605	0.637	0.628	0.445	0.475	0.455	0.385	0.055	14.38
<b>T9</b>	0.537	0.760	0.585	0.424	0.676	0.718	0.685	0.641	0.384	0.406	0.411	0.680	0.118	17.40
<b>T10</b>	0.469	0.464	0.434	0.349	0.302	0.298	0.297	0.378	0.267	0.385	0.425	0.576	0.059	10.28
<b>T11</b>	0.521	0.551	0.497	0.462	0.526	0.652	0.650	0.675	0.619	0.692	0.573	0.654	0.088	13.53
<b>T12</b>	0.425	0.425	0.381	0.395	0.390	0.407	0.377	0.447	0.420	0.470	0.473	0.421	0.059	14.12
<b>Average</b>	0.517	0.586	0.520	0.502	0.529	0.477	0.513	0.529	0.481	0.516	0.502			
<b>SD</b>	0.138	0.125	0.102	0.139	0.166	0.133	0.133	0.135	0.134	0.149	0.111			
<b>%CV</b>	26.72	21.39	19.70	27.64	31.36	27.77	25.94	25.55	27.79	28.95	22.09			

Table 5.18: Absorbance readings for ‘two holes’ group belonging to ‘large tubes’

Tubes	Days																
	1	2	3	4	5	6	7	8	9	10	11	12	13	14	15	16	17
<b>T1</b>	0.728	1.044	1.176	1.256	0.887	0.787	0.673	0.763	0.802	0.743	0.585	0.564	0.595	0.604	0.461	0.514	0.509
<b>T2</b>	0.660	0.861	0.985	1.035	1.003	1.070	1.064	0.917	1.013	0.916	0.937	0.888	0.871	0.917	0.789	0.857	0.807
<b>T3</b>	0.748	0.804	0.738	0.762	1.108	1.052	1.115	0.867	1.006	0.858	0.960	0.951	1.039	0.717	0.574	0.619	0.572
<b>T4</b>	0.684	0.895	0.642	0.681	0.730	1.099	0.830	0.942	0.939	0.902	0.771	0.809	0.905	0.586	0.504	0.779	0.740
<b>T5</b>	0.720	0.988	1.108	1.275	1.091	1.146	1.087	1.086	0.988	1.126	0.957	0.891	0.928	0.962	0.582	0.557	0.789
<b>T6</b>	0.677	0.814	0.986	1.047	1.502	1.153	1.254	1.056	1.275	0.943	0.951	1.216	1.219	1.223	0.877	1.077	1.073
<b>T7</b>	0.544	0.852	1.049	1.126	0.881	0.741	0.810	0.916	0.925	0.857	0.866	0.862	0.767	0.595	0.442	0.458	0.454
<b>T8</b>	0.815	0.723	0.638	0.567	0.774	0.631	0.653	0.725	0.633	0.631	0.682	0.556	0.451	0.645	0.574	0.608	0.582
<b>T9</b>	0.633	0.796	0.673	0.707	0.559	0.642	0.701	0.710	0.716	0.686	0.567	0.702	0.705	0.325	0.263	0.331	0.264
<b>T10</b>	0.937	0.872	0.998	1.052	0.968	1.041	1.400	1.173	1.118	1.189	0.900	1.043	1.110	0.699	0.637	0.658	0.646
<b>T11</b>	0.515	0.695	0.802	0.840	0.722	0.679	0.709	0.736	0.590	0.544	0.574	0.690	0.539	0.702	0.477	0.463	0.505
<b>T12</b>	0.648	0.742	0.848	0.862	0.832	0.763	1.139	0.907	0.883	0.868	0.893	0.829	0.883	0.633	0.759	0.787	0.795
<b>Average</b>	0.716	0.930	1.049	1.170	1.235	1.293	1.418	1.446	1.530	1.559	1.588	1.692	1.770	1.739	1.688	1.824	1.903
<b>SD</b>	0.113	0.103	0.188	0.231	0.243	0.209	0.254	0.151	0.198	0.188	0.160	0.191	0.233	0.227	0.170	0.205	0.211
<b>%CV</b>	15.77	11.06	17.92	19.75	19.68	16.17	17.90	10.41	12.96	12.03	10.07	11.26	13.15	13.06	10.06	11.25	11.10

Table 5.18 continues on next page –

Tubes	Days											Average	SD	% CV
	18	19	20	21	22	23	24	25	26	27	28			
<b>T1</b>	0.547	0.565	0.545	0.542	0.484	0.52	0.501	0.486	0.514	0.532	0.483	0.747	0.232	31.01
<b>T2</b>	0.773	0.827	0.921	0.809	0.738	0.838	0.761	0.866	0.762	0.857	0.797	0.917	0.107	11.72
<b>T3</b>	0.621	0.676	1.004	0.883	0.855	0.855	0.592	0.555	0.852	0.89	0.849	0.852	0.18	21.1
<b>T4</b>	0.744	0.778	0.536	0.469	0.449	0.475	0.725	0.482	0.483	0.487	0.475	0.79	0.149	18.83
<b>T5</b>	0.559	0.603	0.817	0.534	0.726	0.786	0.778	0.764	0.537	0.778	0.781	0.958	0.199	20.75
<b>T6</b>	1.095	1.264	1.159	1.057	0.777	1.032	1.039	0.814	1.006	1.078	1.049	1.079	0.198	18.39
<b>T7</b>	0.43	0.706	0.553	0.443	0.582	0.605	0.646	0.435	0.589	0.735	0.43	0.773	0.207	26.72
<b>T8</b>	0.591	0.656	0.485	0.589	0.564	0.578	0.584	0.454	0.586	0.487	0.59	0.64	0.087	13.62
<b>T9</b>	0.251	0.279	0.326	0.26	0.304	0.306	0.261	0.259	0.247	0.277	0.343	0.587	0.176	30.02
<b>T10</b>	0.7	0.76	0.995	0.998	0.994	0.935	0.961	0.942	0.921	0.705	0.945	0.967	0.214	22.17
<b>T11</b>	0.562	0.504	0.541	0.387	0.482	0.568	0.502	0.587	0.507	0.494	0.481	0.634	0.116	18.29
<b>T12</b>	0.575	0.836	0.605	0.751	0.51	0.521	0.733	0.541	0.52	0.785	0.77	0.828	0.113	13.71
<b>Average</b>	1.958	2.112	2.191	2.209	2.267	2.386	2.468	2.476	2.579	2.7	2.769			
<b>SD</b>	0.204	0.235	0.26	0.253	0.197	0.216	0.21	0.204	0.216	0.224	0.227			
<b>%CV</b>	10.43	11.13	11.88	11.43	8.7	9.07	8.51	8.24	8.38	8.29	8.22			

Table 5.19: Cumulative amount of crystal violet released from ‘one small hole’ group belonging to ‘large tubes’. The amount and cumulative amount values are in microgram units of weight.

Days	Tube1		Tube2		Tube3		Tube4	
	Amt	Cum. Amt.						
0	0.000	0.000	0.000	0.000	0.000	0.000	0.000	0.000
1	28.932	28.932	6.497	6.497	7.153	7.153	8.994	8.994
2	26.620	55.553	6.896	13.393	7.938	15.091	9.594	18.588
3	17.971	73.524	7.296	20.689	9.622	24.714	12.206	30.794
4	29.218	102.742	10.807	31.496	19.028	43.741	19.127	49.921
5	16.616	119.358	6.654	38.149	12.448	56.189	13.519	63.440
6	14.717	134.075	6.711	44.860	14.817	71.007	14.375	77.814
7	20.241	154.316	9.137	53.997	19.898	90.905	17.914	95.729
8	18.671	172.987	6.825	60.822	13.519	104.423	13.718	109.447
9	17.343	190.330	7.952	68.775	17.172	121.596	15.988	125.435
10	14.446	204.776	8.495	77.269	16.658	138.254	12.891	138.325
11	11.777	216.554	8.324	85.593	14.304	152.558	11.620	149.946
12	13.547	230.101	9.009	94.601	15.288	167.846	12.334	162.280
13	12.862	242.963	11.078	105.679	15.759	183.605	11.149	173.429
14	11.035	253.998	9.551	115.230	15.902	199.507	11.506	184.935
15	10.222	264.220	9.237	124.467	14.361	213.868	12.063	196.998
16	12.034	276.254	13.576	138.043	12.234	226.102	13.476	210.474
17	12.819	289.073	9.808	147.851	15.046	241.147	11.963	222.437
18	5.897	294.971	7.296	155.147	11.078	252.225	11.777	234.214
19	6.283	301.253	11.606	166.753	11.920	264.146	12.676	246.891
20	7.824	309.077	10.892	177.645	11.677	275.823	13.276	260.167
21	8.366	317.443	7.995	185.640	11.306	287.129	12.348	272.515
22	6.211	323.655	9.622	195.263	9.979	297.108	10.564	283.079
23	6.468	330.123	7.025	202.287	11.278	308.386	10.807	293.886
24	9.009	339.131	7.310	209.598	12.106	320.492	11.321	305.206
25	9.251	348.382	7.139	216.736	13.190	333.682	11.178	316.384
26	8.852	357.234	7.210	223.947	11.849	345.531	11.934	328.319
27	7.867	365.101	9.351	233.298	13.005	358.536	11.592	339.911
28	8.766	373.867	7.153	240.451	11.749	370.284	12.063	351.973

Standard curve equation: Absorbance (A) = 0.1051 (Conc in µg/ml) - 0.0262 was used in the calculations

Table 5.19 continues on next page -

Days	Tube5		Tube6		Tube7		Tube8	
	Amt	Cum. Amt.						
0	0.000	0.000	0.000	0.000	0.000	0.000	0.000	0.000
1	6.825	6.825	8.509	8.509	1.173	1.173	1.287	1.287
2	9.394	16.219	11.221	19.730	2.629	3.802	2.343	3.631
3	11.820	28.039	12.491	32.221	9.294	13.096	2.044	5.675
4	14.589	42.628	17.643	49.864	19.256	32.352	15.959	21.634
5	12.091	54.719	12.077	61.941	13.804	46.156	11.649	33.283
6	15.488	70.207	15.559	77.500	16.330	62.486	16.302	49.584
7	16.930	87.137	16.501	94.002	19.870	82.356	13.476	63.060
8	12.648	99.785	12.106	106.108	14.432	96.788	10.364	73.424
9	15.260	115.045	13.790	119.897	15.688	112.476	12.648	86.072
10	14.147	129.191	12.291	132.188	13.362	125.837	11.463	97.536
11	14.660	143.852	10.935	143.124	12.462	138.300	7.838	105.374
12	14.803	158.655	11.663	154.787	14.889	153.188	8.780	114.154
13	13.476	172.130	11.321	166.108	13.005	166.193	7.810	121.964
14	12.719	184.850	11.221	177.328	11.306	177.500	7.524	129.488
15	13.504	198.354	9.993	187.322	9.679	187.179	11.107	140.595
16	11.792	210.146	11.335	198.657	10.265	197.443	11.692	152.286
17	11.792	221.937	10.707	209.363	10.907	208.350	11.007	163.293
18	10.336	232.273	9.251	218.615	9.094	217.444	8.480	171.774
19	9.194	241.467	9.665	228.280	10.621	228.066	8.894	180.668
20	11.877	253.344	9.694	237.973	9.708	237.774	8.509	189.177
21	13.005	266.349	9.808	247.781	10.521	248.295	8.766	197.943
22	10.379	276.728	8.466	256.247	10.835	259.130	8.295	206.238
23	8.224	284.951	8.480	264.728	9.294	268.424	8.224	214.461
24	10.179	295.130	8.809	273.537	10.065	278.489	9.151	223.613
25	11.692	306.822	8.923	282.460	10.621	289.110	8.409	232.022
26	12.434	319.256	8.809	291.268	11.292	300.402	10.550	242.572
27	11.820	331.076	8.523	299.792	11.249	311.652	10.450	253.022
28	12.248	343.324	8.723	308.515	11.007	322.658	9.622	262.644

Table 5.19 continues on next page -

Days	Tube9		Tube10		Tube11		Tube12		Average	SD	%CV
	Amt	Cum. Amt.	Cum. Amt								
0	0.000	0.000	0.000	0.000	0.000	0.000	0.000	0.000	0.000	0.000	n.a
1	4.028	4.028	8.894	8.894	1.216	1.216	3.985	3.985	7.291	7.435	101.978
2	4.327	8.355	13.990	22.884	18.742	19.958	4.042	8.027	17.103	13.701	80.113
3	4.127	12.482	16.830	39.714	18.100	38.058	4.570	12.597	27.633	18.085	65.446
4	5.398	17.880	21.682	61.396	24.708	62.766	5.940	18.537	44.580	23.924	53.665
5	4.056	21.936	14.974	76.370	15.331	78.097	4.656	23.192	56.069	27.266	48.630
6	5.041	26.977	16.573	92.943	19.370	97.467	5.441	28.633	69.463	30.405	43.771
7	5.726	32.703	17.201	110.144	21.968	119.435	6.083	34.716	84.875	35.125	41.384
8	4.299	37.002	13.647	123.791	14.446	133.881	4.556	39.271	96.477	39.250	40.683
9	4.741	41.743	14.618	138.408	15.474	149.355	4.884	44.155	109.441	43.248	39.517
10	4.613	46.356	12.163	150.571	13.262	162.617	5.926	50.081	121.083	46.223	38.175
11	3.642	49.998	10.122	160.693	10.393	173.010	5.312	55.393	131.199	48.758	37.163
12	4.484	54.482	12.619	173.312	11.107	184.116	5.926	61.319	142.403	51.655	36.273
13	4.755	59.238	11.777	185.089	11.792	195.908	6.211	67.530	153.320	54.211	35.358
14	4.670	63.908	9.951	195.040	10.907	206.814	5.954	73.484	163.507	56.543	34.581
15	11.991	75.899	11.520	206.560	9.280	216.094	10.693	84.177	174.644	56.641	32.432
16	11.335	87.234	13.105	219.665	12.191	228.285	11.192	95.369	186.663	56.848	30.455
17	10.964	98.198	11.635	231.300	10.050	238.336	10.907	106.276	198.130	57.518	29.030
18	5.555	103.753	11.107	242.406	7.567	245.903	8.794	115.070	206.983	58.165	28.102
19	5.526	109.279	11.278	253.684	7.981	253.884	8.181	123.251	216.468	58.778	27.153
20	5.869	115.147	10.707	264.391	9.151	263.035	8.010	131.261	226.235	59.836	26.449
21	5.569	120.716	10.350	274.741	9.565	272.600	9.308	140.569	235.977	61.062	25.876
22	4.841	125.558	9.936	284.677	10.350	282.951	7.781	148.350	244.915	61.999	25.315
23	4.684	130.242	9.565	294.243	9.579	292.530	7.453	155.803	253.339	63.188	24.942
24	5.355	135.597	10.664	304.907	11.292	303.822	7.881	163.684	262.767	64.798	24.660
25	4.927	140.523	10.364	315.271	10.336	314.158	7.838	171.522	272.256	66.679	24.491
26	5.284	145.807	11.321	326.592	12.034	326.192	8.637	180.160	282.273	68.384	24.226
27	4.884	150.691	11.078	337.670	9.508	335.700	8.067	188.226	292.056	69.895	23.932
28	4.941	155.632	10.336	348.006	11.335	347.035	8.024	196.250	301.720	71.725	23.772

Table 5.20: Cumulative amount of crystal violet released from ‘one big hole’ group belonging to ‘large tubes’. The amount and cumulative amount values are in microgram units of weight.

Days	Tube1		Tube2		Tube3		Tube4	
	Amt	Cum. Amt.						
0	0.000	0.000	0.000	0.000	0.000	0.000	0.000	0.000
1	7.456	7.456	12.651	12.651	4.516	4.516	16.818	16.818
2	19.159	26.615	14.820	27.471	9.454	13.970	18.217	35.035
3	18.046	44.660	15.305	42.776	9.568	23.538	18.788	53.823
4	19.102	63.762	16.048	58.824	10.110	33.648	19.559	73.382
5	18.731	82.493	15.762	74.586	11.252	44.900	25.010	98.392
6	18.674	101.167	19.559	94.145	12.480	57.380	25.353	123.745
7	19.016	120.183	17.989	112.133	12.194	69.574	23.326	147.071
8	20.072	140.255	15.933	128.067	12.822	82.396	20.900	167.971
9	21.500	161.755	16.190	144.257	12.651	95.047	17.675	185.646
10	20.101	181.855	15.305	159.562	11.480	106.527	18.417	204.063
11	19.644	201.500	15.534	175.096	12.023	118.550	18.702	222.765
12	19.616	221.115	16.304	191.401	12.822	131.372	18.474	241.239
13	18.531	239.646	14.877	206.278	10.910	142.282	21.785	263.024
14	15.848	255.494	15.819	222.097	14.164	156.445	19.901	282.925
15	13.165	268.658	13.050	235.147	11.480	167.926	16.590	299.515
16	16.647	285.305	13.878	249.026	10.481	178.407	21.100	320.615
17	12.194	297.500	13.650	262.676	9.911	188.318	20.814	341.429
18	16.219	313.718	13.479	276.154	9.968	198.285	16.647	358.076
19	18.873	332.592	15.619	291.774	15.819	214.105	20.500	378.577
20	17.817	350.409	14.164	305.937	11.423	225.528	19.758	398.335
21	18.360	368.769	14.763	320.700	10.139	235.667	18.331	416.666
22	14.792	383.560	12.565	333.265	9.111	244.778	18.502	435.168
23	10.567	394.127	12.622	345.888	9.882	254.660	15.248	450.417
24	14.221	408.348	14.107	359.994	9.911	264.571	16.647	467.064
25	12.622	420.971	15.106	375.100	10.367	274.938	16.133	483.197
26	15.220	436.190	14.677	389.777	9.825	284.763	17.475	500.672
27	6.126	442.316	7.838	397.616	4.598	289.362	9.608	510.280
28	8.167	450.482	7.125	404.740	4.884	294.245	7.239	517.519

Standard curve equation: Absorbance (A) = 0.1051 (Conc in µg/ml) -0.0262 was used in the calculations

Table 5.20 continues on next page –

Days	Tube5		Tube6		Tube7		Tube8	
	Amt	Cum. Amt.						
0	0.000	0.000	0.000	0.000	0.000	0.000	0.000	0.000
1	15.248	15.248	25.753	25.753	16.304	16.304	15.762	15.762
2	18.417	33.665	11.309	37.062	12.936	29.241	10.167	25.930
3	18.674	52.339	11.709	48.771	13.165	42.405	10.653	36.582
4	19.559	71.897	12.166	60.936	13.764	56.169	11.052	47.635
5	21.328	93.225	26.238	87.174	17.275	73.444	13.422	61.056
6	29.606	122.832	15.791	102.965	17.560	91.005	11.566	72.622
7	26.580	149.412	25.867	128.832	17.560	108.565	11.366	83.989
8	24.668	174.080	19.644	148.476	15.220	123.785	10.082	94.070
9	28.778	202.858	23.412	171.888	16.447	140.232	10.424	104.495
10	28.750	231.608	23.184	195.071	16.105	156.337	10.310	114.805
11	24.440	256.048	19.987	215.058	16.276	172.613	10.139	124.944
12	26.409	282.457	23.098	238.156	15.933	188.546	11.281	136.225
13	25.467	307.924	18.931	257.087	16.932	205.479	11.224	147.448
14	26.723	334.647	23.355	280.441	17.532	223.010	12.936	160.384
15	21.642	356.289	19.245	299.686	15.905	238.915	12.565	172.950
16	16.390	372.679	22.013	321.699	15.363	254.278	13.621	186.571
17	23.869	396.548	19.016	340.716	14.563	268.841	13.307	199.878
18	18.188	414.736	16.647	357.363	14.392	283.233	13.907	213.785
19	24.925	439.661	17.589	374.951	14.991	298.225	15.705	229.490
20	16.219	455.880	20.586	395.538	14.563	312.788	15.248	244.738
21	23.840	479.720	17.789	413.326	15.876	328.664	12.365	257.104
22	21.814	501.534	21.128	434.455	13.250	341.914	21.899	279.003
23	15.962	517.496	13.450	447.905	14.506	356.421	18.017	297.020
24	16.447	533.943	19.530	467.435	14.535	370.955	18.931	315.951
25	23.298	557.241	16.704	484.139	13.222	384.177	18.674	334.624
26	22.327	579.568	15.990	500.129	13.650	397.827	13.450	348.074
27	12.134	591.702	8.923	509.052	7.167	404.994	7.153	355.227
28	11.292	602.994	8.352	517.404	7.082	412.076	6.868	362.095

Table 5.20 continues on next page -

Days	Tube9		Tube10		Tube11		Tube12		Average Cum. Amt	SD	%CV
	Amt	Cum. Amt.									
0	0.000	0.000	0.000	0.000	0.000	0.000	0.000	0.000	0.000	0.000	n.a
1	9.853	9.853	18.474	18.474	22.099	22.099	12.708	12.708	14.804	5.468	36.936
2	21.728	31.581	16.390	34.864	15.277	37.376	9.625	22.333	29.595	15.661	52.919
3	21.728	53.309	17.075	51.939	15.962	53.338	10.167	32.500	44.665	17.288	38.706
4	22.441	75.751	17.817	69.756	16.590	69.928	10.567	43.068	60.396	19.172	31.744
5	15.077	90.828	16.190	85.947	16.190	86.118	11.766	54.833	77.750	22.272	28.645
6	22.641	113.469	16.533	102.480	22.042	108.160	12.137	66.971	96.412	25.140	26.076
7	18.160	131.629	20.244	122.723	22.213	130.373	11.623	78.594	115.256	25.942	22.508
8	21.414	153.043	19.644	142.367	18.816	149.189	11.623	90.217	132.826	30.106	22.665
9	22.470	175.513	19.901	162.268	19.073	168.263	12.137	102.354	151.215	34.757	22.985
10	19.730	195.243	16.447	178.716	18.502	186.765	14.164	116.518	168.922	39.239	23.229
11	19.302	214.544	16.133	194.849	20.129	206.894	14.506	131.024	186.157	42.927	23.060
12	18.788	233.332	18.559	213.408	22.127	229.022	14.877	145.901	204.348	46.920	22.961
13	22.613	255.945	17.218	230.626	17.332	246.354	14.906	160.807	221.908	50.995	22.980
14	22.470	278.415	15.619	246.245	22.470	268.824	14.078	174.885	240.318	54.929	22.857
15	19.758	298.173	16.019	262.265	19.673	288.497	13.793	188.677	256.392	57.844	22.561
16	22.042	320.215	14.192	276.457	18.902	307.399	14.021	202.698	272.946	60.630	22.213
17	16.076	336.291	14.135	290.592	15.619	323.018	12.879	215.578	288.449	63.978	22.180
18	15.990	352.282	14.592	305.184	15.534	338.552	11.852	227.429	303.233	66.080	21.792
19	22.441	374.723	13.992	319.176	16.476	355.028	12.879	240.308	320.717	68.869	21.473
20	17.446	392.169	13.136	332.312	14.934	369.962	11.623	251.931	336.294	70.950	21.098
21	12.851	405.020	10.710	343.022	13.935	383.897	12.023	263.954	351.376	74.012	21.064
22	20.044	425.064	9.368	352.390	15.762	399.659	11.880	275.834	367.219	76.860	20.930
23	21.243	446.306	9.254	361.644	19.359	419.018	12.365	288.200	381.592	78.418	20.550
24	20.301	466.607	9.225	370.870	19.302	438.320	11.509	299.709	396.980	80.683	20.324
25	19.045	485.652	11.538	382.407	20.015	458.335	13.507	313.216	412.833	83.423	20.208
26	11.709	497.361	8.369	390.776	18.417	476.752	12.736	325.952	427.320	86.225	20.178
27	6.168	503.529	5.869	396.645	10.250	487.002	7.082	333.034	435.063	87.853	20.193
28	6.240	509.769	6.440	403.085	8.552	495.554	7.125	340.159	442.510	89.047	20.123

Table 5.21: Cumulative amount of crystal violet released from ‘two holes’ group belonging to ‘large tubes’. The amount and cumulative amount values are in microgram units of weight.

Days	Tube1		Tube2		Tube3		Tube4	
	Amt	Cum. Amt.						
0	0.000	0.000	0.000	0.000	0.000	0.000	0.000	0.000
1	21.528	21.528	19.587	19.587	22.099	22.099	20.272	20.272
2	30.548	52.076	25.324	44.912	23.697	45.796	26.295	46.567
3	34.316	86.392	28.864	73.775	21.814	67.610	19.073	65.640
4	36.599	122.991	30.291	104.067	22.499	90.108	20.186	85.827
5	26.067	149.058	29.378	133.444	32.375	122.483	21.585	107.412
6	23.212	172.270	31.290	164.735	30.776	153.260	32.118	139.530
7	19.958	192.228	31.119	195.853	32.575	185.834	24.440	163.970
8	22.527	214.755	26.923	222.776	25.496	211.330	27.637	191.606
9	23.640	238.396	29.663	252.440	29.463	240.794	27.551	219.157
10	21.956	260.352	26.894	279.334	25.239	266.032	26.495	245.652
11	17.446	277.798	27.494	306.828	28.150	294.183	22.755	268.407
12	16.847	294.645	26.095	332.923	27.893	322.076	23.840	292.247
13	17.732	312.377	25.610	358.533	30.405	352.481	26.580	318.828
14	17.989	330.365	26.923	385.456	21.214	373.696	17.475	336.303
15	13.907	344.272	23.269	408.725	17.132	390.828	15.134	351.437
16	15.420	359.692	25.210	433.935	18.417	409.245	22.984	374.421
17	15.277	374.969	23.783	457.718	17.075	426.320	21.871	396.291
18	16.362	391.330	22.813	480.531	18.474	444.794	16.704	412.995
19	16.875	408.206	24.354	504.885	20.044	464.837	22.955	435.951
20	16.304	424.510	27.037	531.922	29.406	494.244	16.048	451.998
21	16.219	440.729	23.840	555.762	25.952	520.196	14.135	466.133
22	14.563	455.292	21.814	577.576	25.153	545.349	13.564	479.697
23	15.591	470.883	24.668	602.244	25.153	570.502	14.306	494.004
24	15.049	485.931	22.470	624.714	17.646	588.148	21.442	515.446
25	14.620	500.552	25.467	650.181	16.590	604.738	14.506	529.952
26	15.420	515.971	22.499	672.679	25.068	629.806	14.535	544.487
27	15.933	531.905	25.210	697.890	26.152	655.958	14.649	559.136
28	14.535	546.440	23.498	721.387	24.982	680.940	14.306	573.442

Standard curve equation: Absorbance (A) = 0.1051 (Conc in µg /ml) -0.0262 was used in the calculations.

Table 5.21 continues on next page -

Days	Tube5		Tube6		Tube7		Tube8	
	Amt	Cum. Amt.						
0	0.000	0.000	0.000	0.000	0.000	0.000	0.000	0.000
1	21.300	21.300	20.072	20.072	16.276	16.276	24.011	24.011
2	28.950	50.249	23.983	44.055	25.068	41.343	21.385	45.397
3	32.375	82.624	28.892	72.948	30.691	72.034	18.959	64.356
4	37.142	119.766	30.634	103.581	32.889	104.923	16.932	81.288
5	31.890	151.656	43.621	147.203	25.895	130.818	22.841	104.129
6	33.460	185.115	33.659	180.862	21.899	152.717	18.759	122.889
7	31.775	216.891	36.542	217.404	23.869	176.586	19.387	142.276
8	31.747	248.637	30.891	248.295	26.894	203.480	21.442	163.718
9	28.950	277.587	37.142	285.437	27.151	230.632	18.816	182.535
10	32.889	310.476	27.665	313.102	25.210	255.842	18.759	201.294
11	28.065	338.540	27.893	340.995	25.467	281.309	20.215	221.509
12	26.181	364.721	35.458	376.453	25.353	306.662	16.618	238.127
13	27.237	391.958	35.543	411.996	22.641	329.304	13.621	251.749
14	28.207	420.166	35.657	447.654	17.732	347.035	19.159	270.908
15	17.361	437.526	25.781	473.435	13.364	360.400	17.132	288.040
16	16.647	454.173	31.490	504.925	13.821	374.221	18.103	306.143
17	23.269	477.442	31.376	536.301	13.707	387.928	17.361	323.503
18	32.004	509.446	13.022	549.323	17.618	405.545	7.912	331.416
19	17.960	527.406	36.828	586.150	20.900	426.445	19.473	350.889
20	24.069	551.475	33.831	619.981	16.533	442.978	14.592	365.480
21	15.990	567.465	30.919	650.900	13.393	456.371	17.560	383.041
22	21.471	588.936	22.927	673.827	17.361	473.732	16.847	399.888
23	23.184	612.120	30.206	704.032	18.017	491.749	17.246	417.134
24	22.955	635.075	30.405	734.438	19.187	510.936	17.418	434.552
25	22.556	657.631	23.983	758.421	13.165	524.101	13.707	448.259
26	16.076	673.707	29.463	787.884	17.560	541.661	17.475	465.734
27	22.955	696.662	31.519	819.402	21.728	563.389	14.649	480.382
28	23.041	719.703	30.691	850.093	13.022	576.411	17.589	497.971

Table 5.21 continues on next page -

Days	Tube9		Tube10		Tube11		Tube12		Average	SD	%CV
	Amt	Cum. Amt.	Amt	Cum. Amt.	Amt	Cum. Amt.	Amt	Cum. Amt.	Cum. Amt		
0	0.000	0.000	0.000	0.000	0.000	0.000	0.000	0.000	0.000	0.000	n.a
1	18.816	18.816	27.494	27.494	15.448	15.448	19.245	19.245	20.512	3.208	15.640
2	23.469	42.285	25.638	53.132	20.586	36.034	21.928	41.172	45.252	6.493	14.350
3	19.958	62.244	29.235	82.367	23.640	59.675	24.953	66.126	71.316	14.086	19.752
4	20.929	83.172	30.776	113.144	24.725	84.400	25.353	91.479	98.729	21.656	21.934
5	16.704	99.876	28.379	141.522	21.357	105.756	24.497	115.975	125.778	29.306	23.300
6	19.073	118.950	30.462	171.985	20.129	125.886	22.527	138.502	152.225	36.698	24.108
7	20.757	139.707	40.710	212.695	20.986	146.872	33.260	171.762	180.173	44.258	24.564
8	21.014	160.721	34.230	246.925	21.756	168.628	26.637	198.400	206.606	52.072	25.204
9	21.186	181.907	32.660	279.585	17.589	186.217	25.952	224.352	233.253	59.824	25.648
10	20.329	202.236	34.687	314.272	16.276	202.493	25.524	249.876	258.413	67.455	26.104
11	16.932	219.168	26.438	340.710	17.132	219.625	26.238	276.114	282.099	74.548	26.426
12	20.786	239.954	30.520	371.229	20.443	240.069	24.411	300.525	306.636	81.379	26.539
13	20.872	260.826	32.432	403.661	16.133	256.202	25.952	326.478	331.199	88.562	26.740
14	10.025	270.851	20.700	424.362	20.786	276.988	18.816	345.294	352.423	95.738	27.166
15	128.000	398.851	18.931	443.292	14.363	291.351	22.413	367.707	379.655	106.226	27.980
16	10.196	409.047	19.530	462.822	13.964	305.315	23.212	390.919	398.738	109.651	27.500
17	8.284	417.330	19.187	482.010	15.163	320.478	23.441	414.360	417.887	115.156	27.557
18	20.729	438.059	16.790	498.799	17.161	337.638	0.748	415.108	434.582	120.865	27.812
19	8.712	446.771	22.441	521.241	15.134	352.773	24.611	439.718	455.439	125.522	27.561
20	10.053	456.824	29.149	550.390	16.190	368.963	18.017	457.735	476.375	131.554	27.616
21	8.169	464.993	29.235	579.625	11.794	380.757	22.185	479.920	495.491	137.628	27.776
22	9.425	474.419	29.121	608.746	14.506	395.264	15.305	495.225	513.996	143.038	27.829
23	9.482	483.901	27.437	636.183	16.961	412.225	15.619	510.845	533.818	148.389	27.798
24	8.198	492.099	28.179	664.362	15.077	427.302	21.671	532.516	553.793	154.080	27.823
25	8.141	500.240	27.637	691.998	17.503	444.805	16.190	548.706	571.632	159.885	27.970
26	7.798	508.038	27.037	719.035	15.220	460.025	15.591	564.297	590.277	165.044	27.960
27	8.655	516.693	20.872	739.907	14.849	474.873	23.155	587.452	610.304	170.406	27.921
28	10.539	527.231	27.722	767.629	14.478	489.351	22.727	610.179	630.065	176.155	27.958

Table 5.22: Drug loading data for ‘one small hole’ group.

<b>Tubes</b>	<b>Amount of drug loaded (mg/cm)</b>
T1	5.23
T2	5.52
T3	5.31
T4	5.40
T5	5.90
T6	5.23
T7	4.71
T8	5.22
T9	5.39
T10	5.11
T11	5.30
T12	5.42
<b>Average</b>	5.31
<b>SD</b>	0.28
<b>%CV</b>	5.20

Table 5.23: Drug loading data for ‘one big hole’ group.

<b>Tubes</b>	<b>Amount of drug loaded (mg/cm)</b>
T1	5.26
T2	5.76
T3	5.32
T4	5.58
T5	5.17
T6	5.24
T7	5.46
T8	5.17
T9	5.00
T10	5.31
T11	5.39
T12	5.72
<b>Average</b>	5.37
<b>SD</b>	0.23
<b>%CV</b>	4.28

Table 5.24: Drug loading data for ‘two holes’ group.

<b>Tubes</b>	<b>Amount of drug loaded (mg/cm)</b>
T1	4.94
T2	4.74
T3	5.05
T4	5.81
T5	5.21
T6	5.25
T7	5.57
T8	4.87
T9	5.45
T10	4.74
T11	5.26
T12	5.21
<b>Average</b>	5.17
<b>SD</b>	0.33
<b>%CV</b>	6.38

Table 5.25: Percentage cumulative drug released for ‘one small hole’ group

Days	Tube1		Tube2		Tube3		Tube4	
	Cum. Amt.	% Cum Rel						
0	0.000	0.000	0.000	0.000	0.000	0.000	0.000	0.000
1	28.932	0.553	6.497	0.118	7.153	0.135	8.994	0.167
2	55.553	1.062	13.393	0.243	15.091	0.284	18.588	0.344
3	73.524	1.406	20.689	0.375	24.714	0.465	30.794	0.570
4	102.742	1.964	31.496	0.571	43.741	0.824	49.921	0.924
5	119.358	2.282	38.149	0.691	56.189	1.058	63.440	1.175
6	134.075	2.564	44.860	0.813	71.007	1.337	77.814	1.441
7	154.316	2.951	53.997	0.978	90.905	1.712	95.729	1.773
8	172.987	3.308	60.822	1.102	104.423	1.967	109.447	2.027
9	190.330	3.639	68.775	1.246	121.596	2.290	125.435	2.323
10	204.776	3.915	77.269	1.400	138.254	2.604	138.325	2.562
11	216.554	4.141	85.593	1.551	152.558	2.873	149.946	2.777
12	230.101	4.400	94.601	1.714	167.846	3.161	162.280	3.005
13	242.963	4.646	105.679	1.914	183.605	3.458	173.429	3.212
14	253.998	4.857	115.230	2.088	199.507	3.757	184.935	3.425
15	264.220	5.052	124.467	2.255	213.868	4.028	196.998	3.648
16	276.254	5.282	138.043	2.501	226.102	4.258	210.474	3.898
17	289.073	5.527	147.851	2.678	241.147	4.541	222.437	4.119
18	294.971	5.640	155.147	2.811	252.225	4.750	234.214	4.337
19	301.253	5.760	166.753	3.021	264.146	4.974	246.891	4.572
20	309.077	5.910	177.645	3.218	275.823	5.194	260.167	4.818
21	317.443	6.070	185.640	3.363	287.129	5.407	272.515	5.047
22	323.655	6.188	195.263	3.537	297.108	5.595	283.079	5.242
23	330.123	6.312	202.287	3.665	308.386	5.808	293.886	5.442
24	339.131	6.484	209.598	3.797	320.492	6.036	305.206	5.652
25	348.382	6.661	216.736	3.926	333.682	6.284	316.384	5.859
26	357.234	6.830	223.947	4.057	345.531	6.507	328.319	6.080
27	365.101	6.981	233.298	4.226	358.536	6.752	339.911	6.295
28	373.867	7.149	240.451	4.356	370.284	6.973	351.973	6.518

Calculations were performed using values from Table 5.19 and the drug loading data in Table 5.22

Table 5.25 continues on next page -

Days	Tube5		Tube6		Tube7		Tube8	
	Cum. Amt.	% Cum Rel						
0	0.000	0.000	0.000	0.000	0.000	0.000	0.000	0.000
1	6.825	0.116	8.509	0.163	1.173	0.025	1.287	0.025
2	16.219	0.275	19.730	0.377	3.802	0.081	3.631	0.070
3	28.039	0.475	32.221	0.616	13.096	0.278	5.675	0.109
4	42.628	0.723	49.864	0.953	32.352	0.687	21.634	0.414
5	54.719	0.927	61.941	1.184	46.156	0.980	33.283	0.638
6	70.207	1.190	77.500	1.482	62.486	1.327	49.584	0.950
7	87.137	1.477	94.002	1.797	82.356	1.749	63.060	1.208
8	99.785	1.691	106.108	2.029	96.788	2.055	73.424	1.407
9	115.045	1.950	119.897	2.292	112.476	2.388	86.072	1.649
10	129.191	2.190	132.188	2.528	125.837	2.672	97.536	1.868
11	143.852	2.438	143.124	2.737	138.300	2.936	105.374	2.019
12	158.655	2.689	154.787	2.960	153.188	3.252	114.154	2.187
13	172.130	2.917	166.108	3.176	166.193	3.529	121.964	2.336
14	184.850	3.133	177.328	3.391	177.500	3.769	129.488	2.481
15	198.354	3.362	187.322	3.582	187.179	3.974	140.595	2.693
16	210.146	3.562	198.657	3.798	197.443	4.192	152.286	2.917
17	221.937	3.762	209.363	4.003	208.350	4.424	163.293	3.128
18	232.273	3.937	218.615	4.180	217.444	4.617	171.774	3.291
19	241.467	4.093	228.280	4.365	228.066	4.842	180.668	3.461
20	253.344	4.294	237.973	4.550	237.774	5.048	189.177	3.624
21	266.349	4.514	247.781	4.738	248.295	5.272	197.943	3.792
22	276.728	4.690	256.247	4.900	259.130	5.502	206.238	3.951
23	284.951	4.830	264.728	5.062	268.424	5.699	214.461	4.108
24	295.130	5.002	273.537	5.230	278.489	5.913	223.613	4.284
25	306.822	5.200	282.460	5.401	289.110	6.138	232.022	4.445
26	319.256	5.411	291.268	5.569	300.402	6.378	242.572	4.647
27	331.076	5.611	299.792	5.732	311.652	6.617	253.022	4.847
28	343.324	5.819	308.515	5.899	322.658	6.850	262.644	5.031

Table 5.25 continues on next page -

Days	Tube 9		Tube10		Tube 11		Tube 12		Average Cum. Amt	SD	%CV
	Cum. Amt.	% Cum Rel									
0	0.000	0.000	0.000	0.000	0.000	0.000	0.000	0.000	0.000	0.000	n.a
1	4.028	0.075	8.894	0.174	1.216	0.023	3.985	0.074	0.137	0.142	103.858
2	8.355	0.155	22.884	0.448	19.958	0.377	8.027	0.148	0.322	0.263	81.663
3	12.482	0.232	39.714	0.777	38.058	0.718	12.597	0.232	0.521	0.347	66.509
4	17.880	0.332	61.396	1.201	62.766	1.184	18.537	0.342	0.843	0.460	54.586
5	21.936	0.407	76.370	1.495	78.097	1.474	23.192	0.428	1.062	0.526	49.576
6	26.977	0.501	92.943	1.819	97.467	1.839	28.633	0.528	1.316	0.589	44.759
7	32.703	0.607	110.144	2.155	119.435	2.253	34.716	0.641	1.608	0.683	42.438
8	37.002	0.686	123.791	2.423	133.881	2.526	39.271	0.725	1.829	0.764	41.792
9	41.743	0.774	138.408	2.709	149.355	2.818	44.155	0.815	2.074	0.843	40.639
10	46.356	0.860	150.571	2.947	162.617	3.068	50.081	0.924	2.295	0.902	39.294
11	49.998	0.928	160.693	3.145	173.010	3.264	55.393	1.022	2.486	0.951	38.251
12	54.482	1.011	173.312	3.392	184.116	3.474	61.319	1.131	2.698	1.009	37.391
13	59.238	1.099	185.089	3.622	195.908	3.696	67.530	1.246	2.904	1.060	36.484
14	63.908	1.186	195.040	3.817	206.814	3.902	73.484	1.356	3.097	1.105	35.680
15	75.899	1.408	206.560	4.042	216.094	4.077	84.177	1.553	3.306	1.108	33.512
16	87.234	1.618	219.665	4.299	228.285	4.307	95.369	1.760	3.533	1.115	31.550
17	98.198	1.822	231.300	4.526	238.336	4.497	106.276	1.961	3.749	1.130	30.149
18	103.753	1.925	242.406	4.744	245.903	4.640	115.070	2.123	3.916	1.144	29.224
19	109.279	2.027	253.684	4.964	253.884	4.790	123.251	2.274	4.095	1.160	28.314
20	115.147	2.136	264.391	5.174	263.035	4.963	131.261	2.422	4.279	1.180	27.575
21	120.716	2.240	274.741	5.377	272.600	5.143	140.569	2.594	4.463	1.204	26.974
22	125.558	2.329	284.677	5.571	282.951	5.339	148.350	2.737	4.632	1.224	26.434
23	130.242	2.416	294.243	5.758	292.530	5.519	155.803	2.875	4.791	1.250	26.086
24	135.597	2.516	304.907	5.967	303.822	5.732	163.684	3.020	4.969	1.283	25.812
25	140.523	2.607	315.271	6.170	314.158	5.928	171.522	3.165	5.149	1.320	25.634
26	145.807	2.705	326.592	6.391	326.192	6.155	180.160	3.324	5.338	1.354	25.367
27	150.691	2.796	337.670	6.608	335.700	6.334	188.226	3.473	5.523	1.385	25.074
28	155.632	2.887	348.006	6.810	347.035	6.548	196.250	3.621	5.705	1.421	24.903

Table 5.26: Percentage cumulative drug released for ‘one big hole’ group

Days	Tube1		Tube2		Tube3		Tube4	
	Cum. Amt.	% Cum Rel						
0	0.000	0.000	0.000	0.000	0.000	0.000	0.000	0.000
1	7.456	0.142	12.651	0.220	4.516	0.085	16.818	0.301
2	26.615	0.506	27.471	0.477	13.970	0.263	35.035	0.628
3	44.660	0.849	42.776	0.743	23.538	0.442	53.823	0.965
4	63.762	1.212	58.824	1.021	33.648	0.632	73.382	1.315
5	82.493	1.568	74.586	1.295	44.900	0.844	98.392	1.763
6	101.167	1.923	94.145	1.634	57.380	1.079	123.745	2.218
7	120.183	2.285	112.133	1.947	69.574	1.308	147.071	2.636
8	140.255	2.666	128.067	2.223	82.396	1.549	167.971	3.010
9	161.755	3.075	144.257	2.504	95.047	1.787	185.646	3.327
10	181.855	3.457	159.562	2.770	106.527	2.002	204.063	3.657
11	201.500	3.831	175.096	3.040	118.550	2.228	222.765	3.992
12	221.115	4.204	191.401	3.323	131.372	2.469	241.239	4.323
13	239.646	4.556	206.278	3.581	142.282	2.674	263.024	4.714
14	255.494	4.857	222.097	3.856	156.445	2.941	282.925	5.070
15	268.658	5.108	235.147	4.082	167.926	3.156	299.515	5.368
16	285.305	5.424	249.026	4.323	178.407	3.354	320.615	5.746
17	297.500	5.656	262.676	4.560	188.318	3.540	341.429	6.119
18	313.718	5.964	276.154	4.794	198.285	3.727	358.076	6.417
19	332.592	6.323	291.774	5.066	214.105	4.025	378.577	6.785
20	350.409	6.662	305.937	5.311	225.528	4.239	398.335	7.139
21	368.769	7.011	320.700	5.568	235.667	4.430	416.666	7.467
22	383.560	7.292	333.265	5.786	244.778	4.601	435.168	7.799
23	394.127	7.493	345.888	6.005	254.660	4.787	450.417	8.072
24	408.348	7.763	359.994	6.250	264.571	4.973	467.064	8.370
25	420.971	8.003	375.100	6.512	274.938	5.168	483.197	8.659
26	436.190	8.293	389.777	6.767	284.763	5.353	500.672	8.973
27	442.316	8.409	397.616	6.903	289.362	5.439	510.280	9.145
28	450.482	8.564	404.740	7.027	294.245	5.531	517.519	9.275

Calculations were performed using values from Table 5.20 and the drug loading data in Table 5.23

Table 5.26 continues on next page -

Days	Tube5		Tube6		Tube7		Tube8	
	Cum. Amt.	% Cum Rel						
0	0.000	0.000	0.000	0.000	0.000	0.000	0.000	0.000
1	15.248	0.295	25.753	0.491	16.304	0.299	15.762	0.305
2	33.665	0.651	37.062	0.707	29.241	0.536	25.930	0.502
3	52.339	1.012	48.771	0.931	42.405	0.777	36.582	0.708
4	71.897	1.391	60.936	1.163	56.169	1.029	47.635	0.921
5	93.225	1.803	87.174	1.664	73.444	1.345	61.056	1.181
6	122.832	2.376	102.965	1.965	91.005	1.667	72.622	1.405
7	149.412	2.890	128.832	2.459	108.565	1.988	83.989	1.625
8	174.080	3.367	148.476	2.834	123.785	2.267	94.070	1.820
9	202.858	3.924	171.888	3.280	140.232	2.568	104.495	2.021
10	231.608	4.480	195.071	3.723	156.337	2.863	114.805	2.221
11	256.048	4.953	215.058	4.104	172.613	3.161	124.944	2.417
12	282.457	5.463	238.156	4.545	188.546	3.453	136.225	2.635
13	307.924	5.956	257.087	4.906	205.479	3.763	147.448	2.852
14	334.647	6.473	280.441	5.352	223.010	4.084	160.384	3.102
15	356.289	6.891	299.686	5.719	238.915	4.376	172.950	3.345
16	372.679	7.208	321.699	6.139	254.278	4.657	186.571	3.609
17	396.548	7.670	340.716	6.502	268.841	4.924	199.878	3.866
18	414.736	8.022	357.363	6.820	283.233	5.187	213.785	4.135
19	439.661	8.504	374.951	7.156	298.225	5.462	229.490	4.439
20	455.880	8.818	395.538	7.548	312.788	5.729	244.738	4.734
21	479.720	9.279	413.326	7.888	328.664	6.019	257.104	4.973
22	501.534	9.701	434.455	8.291	341.914	6.262	279.003	5.397
23	517.496	10.010	447.905	8.548	356.421	6.528	297.020	5.745
24	533.943	10.328	467.435	8.921	370.955	6.794	315.951	6.111
25	557.241	10.778	484.139	9.239	384.177	7.036	334.624	6.472
26	579.568	11.210	500.129	9.544	397.827	7.286	348.074	6.733
27	591.702	11.445	509.052	9.715	404.994	7.417	355.227	6.871
28	602.994	11.663	517.404	9.874	412.076	7.547	362.095	7.004

Table 5.26 continues on next page -

Days	Tube 9		Tube10		Tube 11		Tube 12		Average	SD	%CV
	Cum. Amt.	% Cum Rel	Cum. Amt								
0	0.000	0.000	0.000	0.000	0.000	0.000	0.000	0.000	0.000	0.000	n.a
1	9.853	0.183	18.474	0.348	22.099	0.410	12.708	0.222	0.275	0.113	41.194
2	31.581	0.586	34.864	0.657	37.376	0.693	22.333	0.390	0.550	0.132	24.048
3	53.309	0.989	51.939	0.978	53.338	0.990	32.500	0.568	0.829	0.186	22.378
4	75.751	1.405	69.756	1.314	69.928	1.297	43.068	0.753	1.121	0.253	22.532
5	90.828	1.685	85.947	1.619	86.118	1.598	54.833	0.959	1.444	0.317	21.942
6	113.469	2.105	102.480	1.930	108.160	2.007	66.971	1.171	1.790	0.407	22.711
7	131.629	2.442	122.723	2.311	130.373	2.419	78.594	1.374	2.140	0.499	23.295
8	153.043	2.839	142.367	2.681	149.189	2.768	90.217	1.577	2.467	0.581	23.536
9	175.513	3.256	162.268	3.056	168.263	3.122	102.354	1.789	2.809	0.675	24.045
10	195.243	3.622	178.716	3.366	186.765	3.465	116.518	2.037	3.139	0.766	24.419
11	214.544	3.980	194.849	3.669	206.894	3.838	131.024	2.291	3.459	0.840	24.283
12	233.332	4.329	213.408	4.019	229.022	4.249	145.901	2.551	3.797	0.921	24.248
13	255.945	4.749	230.626	4.343	246.354	4.571	160.807	2.811	4.123	1.000	24.261
14	278.415	5.165	246.245	4.637	268.824	4.987	174.885	3.057	4.465	1.079	24.167
15	298.173	5.532	262.265	4.939	288.497	5.352	188.677	3.299	4.764	1.138	23.889
16	320.215	5.941	276.457	5.206	307.399	5.703	202.698	3.544	5.071	1.191	23.495
17	336.291	6.239	290.592	5.473	323.018	5.993	215.578	3.769	5.359	1.258	23.466
18	352.282	6.536	305.184	5.747	338.552	6.281	227.429	3.976	5.634	1.301	23.088
19	374.723	6.952	319.176	6.011	355.028	6.587	240.308	4.201	5.959	1.358	22.794
20	392.169	7.276	332.312	6.258	369.962	6.864	251.931	4.404	6.249	1.400	22.410
21	405.020	7.514	343.022	6.460	383.897	7.122	263.954	4.615	6.529	1.462	22.399
22	425.064	7.886	352.390	6.636	399.659	7.415	275.834	4.822	6.824	1.522	22.307
23	446.306	8.280	361.644	6.811	419.018	7.774	288.200	5.038	7.091	1.554	21.911
24	466.607	8.657	370.870	6.984	438.320	8.132	299.709	5.240	7.377	1.600	21.684
25	485.652	9.010	382.407	7.202	458.335	8.503	313.216	5.476	7.672	1.656	21.589
26	497.361	9.227	390.776	7.359	476.752	8.845	325.952	5.698	7.941	1.712	21.564
27	503.529	9.342	396.645	7.470	487.002	9.035	333.034	5.822	8.084	1.744	21.577
28	509.769	9.458	403.085	7.591	495.554	9.194	340.159	5.947	8.223	1.770	21.523

Table 5.27: Percentage cumulative drug released for ‘two holes’ group

Days	Tube1		Tube2		Tube3		Tube4	
	Cum. Amt.	% Cum Rel						
0	0.000	0.000	0.000	0.000	0.000	0.000	0.000	0.000
1	21.528	0.291	19.587	0.275	22.099	0.292	20.272	0.232
2	52.076	0.703	44.912	0.632	45.796	0.605	46.567	0.534
3	86.392	1.166	73.775	1.038	67.610	0.893	65.640	0.753
4	122.991	1.660	104.067	1.464	90.108	1.190	85.827	0.984
5	149.058	2.012	133.444	1.877	122.483	1.618	107.412	1.232
6	172.270	2.325	164.735	2.317	153.260	2.025	139.530	1.600
7	192.228	2.594	195.853	2.755	185.834	2.455	163.970	1.880
8	214.755	2.898	222.776	3.133	211.330	2.792	191.606	2.197
9	238.396	3.217	252.440	3.550	240.794	3.181	219.157	2.513
10	260.352	3.514	279.334	3.929	266.032	3.514	245.652	2.817
11	277.798	3.749	306.828	4.315	294.183	3.886	268.407	3.078
12	294.645	3.976	332.923	4.682	322.076	4.255	292.247	3.351
13	312.377	4.216	358.533	5.043	352.481	4.656	318.828	3.656
14	330.365	4.458	385.456	5.421	373.696	4.937	336.303	3.857
15	344.272	4.646	408.725	5.749	390.828	5.163	351.437	4.030
16	359.692	4.854	433.935	6.103	409.245	5.406	374.421	4.294
17	374.969	5.060	457.718	6.438	426.320	5.632	396.291	4.545
18	391.330	5.281	480.531	6.759	444.794	5.876	412.995	4.736
19	408.206	5.509	504.885	7.101	464.837	6.141	435.951	4.999
20	424.510	5.729	531.922	7.481	494.244	6.529	451.998	5.183
21	440.729	5.948	555.762	7.817	520.196	6.872	466.133	5.346
22	455.292	6.144	577.576	8.123	545.349	7.204	479.697	5.501
23	470.883	6.355	602.244	8.470	570.502	7.536	494.004	5.665
24	485.931	6.558	624.714	8.786	588.148	7.769	515.446	5.911
25	500.552	6.755	650.181	9.145	604.738	7.989	529.952	6.077
26	515.971	6.963	672.679	9.461	629.806	8.320	544.487	6.244
27	531.905	7.178	697.890	9.816	655.958	8.665	559.136	6.412
28	546.440	7.374	721.387	10.146	680.940	8.995	573.442	6.576

Calculations were performed using values from Table 5.21 and the drug loading data in Table 5.24

Table 5.27 continues on next page -

Days	Tube5		Tube6		Tube7		Tube8	
	Cum. Amt.	% Cum Rel						
0	0.000	0.000	0.000	0.000	0.000	0.000	0.000	0.000
1	21.300	0.273	20.072	0.255	16.276	0.195	24.011	0.329
2	50.249	0.643	44.055	0.560	41.343	0.495	45.397	0.622
3	82.624	1.058	72.948	0.927	72.034	0.863	64.356	0.882
4	119.766	1.533	103.581	1.316	104.923	1.257	81.288	1.114
5	151.656	1.942	147.203	1.870	130.818	1.567	104.129	1.426
6	185.115	2.370	180.862	2.298	152.717	1.829	122.889	1.683
7	216.891	2.777	217.404	2.762	176.586	2.115	142.276	1.949
8	248.637	3.184	248.295	3.155	203.480	2.437	163.718	2.243
9	277.587	3.554	285.437	3.627	230.632	2.762	182.535	2.500
10	310.476	3.975	313.102	3.978	255.842	3.064	201.294	2.757
11	338.540	4.335	340.995	4.333	281.309	3.369	221.509	3.034
12	364.721	4.670	376.453	4.783	306.662	3.673	238.127	3.262
13	391.958	5.019	411.996	5.235	329.304	3.944	251.749	3.449
14	420.166	5.380	447.654	5.688	347.035	4.156	270.908	3.711
15	437.526	5.602	473.435	6.016	360.400	4.316	288.040	3.946
16	454.173	5.815	504.925	6.416	374.221	4.482	306.143	4.194
17	477.442	6.113	536.301	6.814	387.928	4.646	323.503	4.432
18	509.446	6.523	549.323	6.980	405.545	4.857	331.416	4.540
19	527.406	6.753	586.150	7.448	426.445	5.107	350.889	4.807
20	551.475	7.061	619.981	7.878	442.978	5.305	365.480	5.007
21	567.465	7.266	650.900	8.271	456.371	5.466	383.041	5.247
22	588.936	7.541	673.827	8.562	473.732	5.673	399.888	5.478
23	612.120	7.838	704.032	8.946	491.749	5.889	417.134	5.714
24	635.075	8.132	734.438	9.332	510.936	6.119	434.552	5.953
25	657.631	8.420	758.421	9.637	524.101	6.277	448.259	6.141
26	673.707	8.626	787.884	10.011	541.661	6.487	465.734	6.380
27	696.662	8.920	819.402	10.412	563.389	6.747	480.382	6.581
28	719.703	9.215	850.093	10.802	576.411	6.903	497.971	6.822

Table 5.27 continues on next page -

Days	Tube 9		Tube10		Tube 11		Tube 12		Average Cum. Amt	SD	%CV
	Cum. Amt.	% Cum Rel									
0	0.000	0.000	0.000	0.000	0.000	0.000	0.000	0.000	0.000	0.000	n.a
1	18.816	0.230	27.494	0.387	15.448	0.196	19.245	0.246	0.267	0.055	20.487
2	42.285	0.517	53.132	0.747	36.034	0.457	41.172	0.526	0.587	0.087	14.835
3	62.244	0.761	82.367	1.158	59.675	0.756	66.126	0.846	0.925	0.148	16.003
4	83.172	1.017	113.144	1.591	84.400	1.070	91.479	1.170	1.280	0.232	18.085
5	99.876	1.221	141.522	1.990	105.756	1.340	115.975	1.483	1.632	0.297	18.186
6	118.950	1.454	171.985	2.419	125.886	1.596	138.502	1.771	1.974	0.357	18.094
7	139.707	1.708	212.695	2.991	146.872	1.861	171.762	2.196	2.337	0.438	18.729
8	160.721	1.965	246.925	3.473	168.628	2.137	198.400	2.537	2.679	0.494	18.434
9	181.907	2.224	279.585	3.932	186.217	2.360	224.352	2.869	3.024	0.565	18.698
10	202.236	2.472	314.272	4.420	202.493	2.566	249.876	3.195	3.350	0.636	18.974
11	219.168	2.679	340.710	4.792	219.625	2.784	276.114	3.531	3.657	0.690	18.871
12	239.954	2.933	371.229	5.221	240.069	3.043	300.525	3.843	3.974	0.752	18.933
13	260.826	3.189	403.661	5.677	256.202	3.247	326.478	4.175	4.292	0.831	19.364
14	270.851	3.311	424.362	5.969	276.988	3.511	345.294	4.416	4.568	0.899	19.672
15	398.851	4.876	443.292	6.235	291.351	3.693	367.707	4.702	4.914	0.846	17.218
16	409.047	5.001	462.822	6.509	305.315	3.870	390.919	4.999	5.162	0.891	17.260
17	417.330	5.102	482.010	6.779	320.478	4.062	414.360	5.299	5.410	0.943	17.433
18	438.059	5.355	498.799	7.015	337.638	4.279	415.108	5.308	5.626	0.981	17.435
19	446.771	5.462	521.241	7.331	352.773	4.471	439.718	5.623	5.896	1.034	17.545
20	456.824	5.585	550.390	7.741	368.963	4.676	457.735	5.853	6.169	1.127	18.268
21	464.993	5.685	579.625	8.152	380.757	4.826	479.920	6.137	6.419	1.211	18.860
22	474.419	5.800	608.746	8.562	395.264	5.010	495.225	6.333	6.661	1.279	19.204
23	483.901	5.916	636.183	8.948	412.225	5.225	510.845	6.533	6.919	1.358	19.625
24	492.099	6.016	664.362	9.344	427.302	5.416	532.516	6.810	7.179	1.426	19.870
25	500.240	6.115	691.998	9.733	444.805	5.638	548.706	7.017	7.412	1.501	20.255
26	508.038	6.211	719.035	10.113	460.025	5.830	564.297	7.216	7.655	1.576	20.582
27	516.693	6.317	739.907	10.407	474.873	8.960	587.452	7.512	8.160	1.557	19.077
28	527.231	6.445	767.629	10.796	489.351	9.233	610.179	7.803	8.426	1.639	19.453

Table 5.28: Absorbance readings (A) for ‘200 micron’ group belonging to ‘large tubes without holes’

Tube No.	Days							Average	SD	%CV
	1	2	3	4	5	6	7			
1	0.040	0.029	0.023	0.010	0.016	0.060	0.014	0.027	0.018	64.118
2	0.080	0.024	0.015	0.011	0.010	0.057	0.015	0.030	0.027	90.179
3	0.072	0.027	0.023	0.009	0.020	0.062	0.028	0.034	0.023	67.639
4	0.051	0.032	0.028	0.023	0.013	0.060	0.024	0.033	0.017	50.404
<b>Average</b>	0.061	0.028	0.022	0.013	0.015	0.060	0.020			
<b>SD</b>	0.018	0.003	0.005	0.007	0.004	0.002	0.007			
<b>%CV</b>	30.393	12.023	24.168	49.442	28.963	3.450	33.825			

Table 5.29: Absorbance readings (A) for ‘400 micron’ group belonging to ‘large tubes without holes’

Tube No.	Days							Average	SD	%CV
	1	2	3	4	5	6	7			
1	0.095	0.076	0.045	0.047	0.022	0.081	0.046	0.059	0.026	43.576
2	0.162	0.085	0.052	0.051	0.044	0.095	0.056	0.078	0.042	53.574
3	0.305	0.072	0.076	0.065	0.081	0.131	0.129	0.123	0.085	69.116
4	0.110	0.076	0.049	0.049	0.035	0.087	0.041	0.064	0.028	43.402
<b>Average</b>	0.168	0.077	0.056	0.053	0.046	0.099	0.068			
<b>SD</b>	0.096	0.006	0.014	0.008	0.025	0.022	0.041			
<b>%CV</b>	56.988	7.120	25.161	15.406	55.673	22.754	60.503			

Table 5.30: Absorbance readings (A) for ‘600 micron’ group belonging to ‘large tubes without holes’

Tube No.	Days							Average	SD	%CV
	1	2	3	4	5	6	7			
1	0.350	0.146	0.105	0.069	0.055	0.177	0.075	0.140	0.103	73.545
2	0.602	0.280	0.204	0.239	0.097	0.095	0.111	0.233	0.179	76.850
3	0.342	0.326	0.106	0.075	0.170	0.215	0.240	0.211	0.102	48.447
4	0.624	0.210	0.169	0.141	0.133	0.142	0.110	0.218	0.182	83.144
<b>Average</b>	0.480	0.241	0.146	0.131	0.114	0.157	0.134			
<b>SD</b>	0.006	0.127	0.001	0.004	0.081	0.027	0.117			
<b>%CV</b>	1.180	52.923	0.484	3.239	71.488	17.087	87.069			

Table 5.31: Cumulative amount of crystal violet released from '200 microns group. The amount and cumulative amount values are in microgram units of weight.

Days	Tube1		Tube2		Tube3		Tube4		Average Cum. Amt	SD	%CV
	Amt	Cum. Amt.									
0	0.000	0.000	0.000	0.000	0.000	0.000	0.000	0.000	0.000	0.000	n.a
1	2.778	2.778	5.387	5.387	4.865	4.865	3.496	3.496	4.132	1.204	29.146
2	2.061	4.839	1.735	7.122	1.930	6.796	2.257	5.752	6.127	1.039	16.950
3	1.670	6.509	1.148	8.270	1.670	8.465	1.996	7.748	7.748	0.880	11.356
4	0.822	7.330	0.887	9.157	0.757	9.222	1.670	9.417	8.782	0.974	11.088
5	1.213	8.543	0.822	9.978	1.474	10.696	1.017	10.435	9.913	0.960	9.684
6	4.083	12.626	3.887	13.865	4.213	14.909	4.083	14.517	13.979	1.000	7.150
7	1.083	13.709	1.148	15.013	1.996	16.904	1.735	16.252	15.470	1.412	9.127

Standard curve equation: Absorbance (A) = 0.046 (Conc in µg /ml) -0.0026 was used in the calculations

Table 5.32: Cumulative amount of crystal violet released from '400 microns' group. The amount and cumulative amount values are in microgram units of weight.

Days	Tube1		Tube2		Tube3		Tube4		Average Cum. Amt	SD	%CV
	Amt	Cum. Amt.	Amt	Cum. Amt.	Amt	Cum. Amt.	Amt	Cum. Amt.			
0	0.000	0.000	0.000	0.000	0.000	0.000	0.000	0.000	0.000	0.000	0
1	6.365	6.365	10.735	10.735	20.061	20.061	7.343	7.343	11.126	6.244	56.119
2	5.126	11.491	5.713	16.448	4.865	24.926	5.126	12.470	16.334	6.116	37.445
3	3.104	14.596	3.561	20.009	5.126	30.052	3.365	15.835	20.123	7.013	34.850
4	3.235	17.830	3.496	23.504	4.409	34.461	3.365	19.200	23.749	7.539	31.746
5	1.604	19.435	3.039	26.543	5.452	39.913	2.452	21.652	26.886	9.179	34.139
6	5.452	24.887	6.365	32.909	8.713	48.626	5.843	27.496	33.479	10.636	31.769
7	3.170	28.057	3.822	36.730	8.583	57.209	2.843	30.339	38.084	13.268	34.839

Standard curve equation: Absorbance (A) = 0.046 (Conc in  $\mu\text{g/ml}$ ) - 0.0026 was used in the calculations

Table 5.33: Cumulative amount of crystal violet released from ‘600 microns’ group. The amount and cumulative amount values are in microgram units of weight.

Days	Tube1		Tube2		Tube3		Tube4		Average Cum. Amt	SD	%CV
	Amt	Cum. Amt.									
0	0.000	0.000	0.000	0.000	0.000	0.000	0.000	0.000	0.000	0.000	0
1	22.996	22.996	39.430	39.430	22.474	22.474	40.865	40.865	31.441	10.073	32.037
2	9.691	32.687	18.430	57.861	21.430	43.904	13.865	54.730	47.296	11.428	24.163
3	7.017	39.704	13.474	71.335	7.083	50.987	11.191	65.922	56.987	14.380	25.234
4	4.670	44.374	15.757	87.091	5.061	56.048	9.365	75.287	65.700	19.126	29.112
5	3.757	48.130	6.496	93.587	11.257	67.304	8.843	84.130	73.288	19.986	27.270
6	11.713	59.843	6.365	99.952	14.191	81.496	9.430	93.561	83.713	17.658	21.093
7	5.061	64.904	7.409	107.361	15.822	97.317	7.343	100.904	92.622	18.940	20.449

Standard curve equation: Absorbance (A) = 0.046 (Conc in  $\mu\text{g/ml}$ ) - 0.0026 was used in the calculations

Table 5.34: Drug loading data for 200, 400, and 600 microns group

Hole Size (microns)	Avg. Amount of Drug Loaded (mg)	SD	%CV
200	0.373	0.022	5.877
400	1.410	0.018	1.273
600	2.530	0.113	4.486

Table 5.35: Percentage cumulative drug released for ‘200 microns’ group

Days	Tube1		Tube2		Tube3		Tube4		Average % Cum.	SD	%CV
	Cum. Amt.	%Cum									
0	0.000	0.000	0.000	0.000	0.000	0.000	0.000	0.000	0.000	0.000	0
1	2.778	0.745	5.387	1.444	4.865	1.304	3.496	0.937	1.108	0.323	29.146
2	4.839	1.297	7.122	1.909	6.796	1.822	5.752	1.542	1.643	0.278	16.950
3	6.509	1.745	8.270	2.217	8.465	2.269	7.748	2.077	2.077	0.236	11.356
4	7.330	1.965	9.157	2.455	9.222	2.472	9.417	2.525	2.354	0.261	11.088
5	8.543	2.290	9.978	2.675	10.696	2.867	10.435	2.798	2.658	0.257	9.684
6	12.626	3.385	13.865	3.717	14.909	3.997	14.517	3.892	3.748	0.268	7.150
7	13.709	3.675	15.013	4.025	16.904	4.532	16.252	4.357	4.147	0.379	9.127

Calculations were performed using values from Table 5.31 and the drug loading data in Table 5.34

Table 5.36: Percentage cumulative drug released for '400 microns' group

Days	Tube1		Tube2		Tube3		Tube4		Average % Cum.	SD	%CV
	Cum. Amt.	%Cum									
0	0.000	0.000	0.000	0.000	0.000	0.000	0.000	0.000	0.000	0.000	0
1	6.365	0.452	10.735	0.762	20.061	1.424	7.343	0.521	0.790	0.443	56.119
2	11.491	0.816	16.448	1.167	24.926	1.769	12.470	0.885	1.159	0.434	37.445
3	14.596	1.036	20.009	1.420	30.052	2.133	15.835	1.124	1.428	0.498	34.850
4	17.830	1.265	23.504	1.668	34.461	2.446	19.200	1.363	1.686	0.535	31.746
5	19.435	1.379	26.543	1.884	39.913	2.833	21.652	1.537	1.908	0.651	34.139
6	24.887	1.766	32.909	2.336	48.626	3.451	27.496	1.951	2.376	0.755	31.769
7	28.057	1.991	36.730	2.607	57.209	4.060	30.339	2.153	2.703	0.942	34.839

Calculations were performed using values from Table 5.32 and the drug loading data in Table 5.34

Table 5.37: Percentage cumulative drug released for ‘600 microns’ group

Days	Tube1		Tube2		Tube3		Tube4		Average % Cum.	SD	%CV
	Cum. Amt.	%Cum									
0	0.000	0.000	0.000	0.000	0.000	0.000	0.000	0.000	0.000	0.000	0
1	22.996	0.909	39.430	1.559	22.474	0.889	40.865	1.616	1.243	0.398	32.037
2	32.687	1.292	57.861	2.288	43.904	1.736	54.730	2.164	1.870	0.452	24.163
3	39.704	1.570	71.335	2.821	50.987	2.016	65.922	2.607	2.253	0.569	25.234
4	44.374	1.755	87.091	3.444	56.048	2.216	75.287	2.977	2.598	0.756	29.112
5	48.130	1.903	93.587	3.701	67.304	2.661	84.130	3.327	2.898	0.790	27.270
6	59.843	2.366	99.952	3.952	81.496	3.222	93.561	3.700	3.310	0.698	21.093
7	64.904	2.566	107.361	4.245	97.317	3.848	100.904	3.990	3.662	0.749	20.449

Calculations were performed using values from Table 5.33 and the drug loading data in Table 5.34

Table 6.1: The table illustrates the absorbance readings (A) used for the construction of standard curve. Intraday and interday precision was calculated by analyzing standard solutions at predetermined intervals.

Conc (µg/ml)	Day 1	Day 2	Day 3	Average Absorbance (A)	SD	% CV
0.00	0.000 0.000 0.000	0.000 0.000 0.000	0.000 0.000 0.000	0.000	0.000	n/a
1.00	0.025 0.039 0.027	0.022 0.043 0.025	0.021 0.036 0.023	0.029	0.008	28.328
2.00	0.062 0.063 0.063	0.050 0.059 0.056	0.046 0.056 0.051	0.056	0.006	10.987
3.00	0.101 0.099 0.100	0.089 0.089 0.091	0.083 0.086 0.083	0.091	0.007	7.892
5.00	0.159 0.152 0.176	0.145 0.131 0.128	0.136 0.125 0.122	0.142	0.018	12.750
6.00	0.181 0.184 0.196	0.163 0.178 0.195	0.152 0.171 0.183	0.178	0.014	8.048
8.00	0.255 0.254 0.262	0.235 0.234 0.248	0.231 0.227 0.239	0.243	0.012	5.089
10.00	0.319 0.307 0.320	0.274 0.279 0.280	0.258 0.264 0.257	0.284	0.025	8.796

Table 6.2: Absorbance readings for drug release study in phosphate buffered saline

Tubes	Days							Average	SD	%CV
	1	2	3	4	5	6	7			
1	0.701	0.904	0.795	0.908	0.905	0.744	1.014	0.853	0.110	12.90
2	0.964	0.681	0.672	1.112	1.114	0.730	0.729	0.857	0.200	23.34
3	0.917	1.041	1.031	1.009	1.026	1.117	1.090	1.033	0.064	6.18
4	0.771	0.791	0.817	1.091	1.184	1.232	0.939	0.975	0.194	19.86
5	0.852	0.892	0.948	1.015	0.969	1.033	1.042	0.964	0.072	7.51
6	0.432	0.422	0.445	0.484	0.506	0.412	0.623	0.475	0.074	15.49
<b>Average</b>	0.773	0.789	0.785	0.937	0.951	0.878	0.906			
<b>SD</b>	0.192	0.216	0.208	0.233	0.240	0.304	0.188			
<b>%CV</b>	24.88	27.42	26.52	24.89	25.2	34.68	20.74			

Table 6.3: Absorbance readings for drug release study in vitreous humor from the rabbit's eye

Tubes	Days							Average	SD	%CV
	1	2	3	4	5	6	7			
<b>1</b>	0.268	0.252	0.183	0.171	0.186	0.172	0.181	0.202	0.040	20.00
<b>2</b>	0.176	0.220	0.139	0.159	0.113	0.181	0.127	0.159	0.037	22.97
<b>3</b>	0.157	0.245	0.111	0.115	0.112	0.128	0.175	0.149	0.049	32.84
<b>4</b>	0.276	0.151	0.281	0.150	0.162	0.119	0.214	0.193	0.065	33.48
<b>5</b>	0.198	0.251	0.092	0.098	0.168	0.123	0.171	0.157	0.057	36.43
<b>6</b>	0.257	0.189	0.111	0.094	0.128	0.090	0.187	0.151	0.062	41.11
<b>Average</b>	0.222	0.218	0.153	0.131	0.145	0.136	0.176			
<b>SD</b>	0.051	0.041	0.070	0.033	0.031	0.035	0.028			
<b>%CV</b>	23.12	18.70	46.01	25.19	21.62	25.47	16.12			

Table 6.4: Cumulative amount of crystal violet released in phosphate buffered saline. The amount and cumulative amount values are in microgram units of weight.

Days	Tube1		Tube2		Tube3		Tube4		Tube5		Tube6		Average Cum. Amt	SD	%CV
	Amt	Cum. Amt.	Amt	Cum. Amt.	Amt	Cum. Amt.	Amt	Cum. Amt.	Amt	Cum. Amt.	Amt	Cum. Amt.			
0	0.000	0.000	0.000	0.000	0.000	0.000	0.000	0.000	0.000	0.000	0.000	0.000	0.000	0.000	n/a
1	6.919	6.919	9.422	9.422	8.974	8.974	7.585	7.585	8.356	8.356	4.360	4.360	7.603	1.830	24.069
2	8.851	15.770	6.729	16.150	10.154	19.128	7.775	15.361	8.736	17.092	4.265	8.624	15.354	3.560	23.185
3	7.814	23.583	6.643	22.794	10.059	29.187	8.023	23.383	9.269	26.362	4.483	13.108	23.069	5.440	23.579
4	8.889	32.472	10.830	33.623	9.850	39.037	10.630	34.013	9.907	36.268	4.854	17.962	32.229	7.368	22.860
5	8.860	41.332	10.849	44.472	10.011	49.049	11.515	45.528	9.469	45.737	5.064	23.026	41.524	9.395	22.625
6	7.328	48.660	7.195	51.667	10.877	59.926	11.971	57.500	10.078	55.815	4.169	27.195	50.127	11.943	23.825
7	9.897	58.558	7.186	58.853	10.620	70.546	9.184	66.683	10.164	65.979	6.177	33.372	58.998	13.402	22.716

Standard curve equation: Absorbance (A) = 0.1051 (Conc in micrograms/ml) - 0.0262 was used in the calculations

Table 6.5: Cumulative amount of crystal violet released in vitreous humor. The amount and cumulative amount values are in microgram units of weight.

Days	Tube1		Tube2		Tube3		Tube4		Tube5		Tube6		Average Cum. Amt	SD	%CV
	Amt	Cum. Amt.													
0	0.000	0.000	0.000	0.000	0.000	0.000	0.000	0.000	0.000	0.000	0.000	0.000	0.000	0.000	
1	9.227	9.227	6.065	6.065	5.412	5.412	9.502	9.502	6.821	6.821	8.849	8.849	7.646	1.764	23.070
2	8.677	17.904	7.577	13.643	8.436	13.849	5.206	14.708	8.643	15.464	6.512	15.361	15.155	1.542	10.174
3	6.306	24.210	4.794	18.436	3.832	17.680	9.674	24.381	3.179	18.643	3.832	19.192	20.424	3.038	14.877
4	5.893	30.103	5.481	23.918	3.969	21.649	5.172	29.553	3.385	22.027	3.247	22.440	24.948	3.861	15.477
5	6.409	36.512	3.900	27.818	3.866	25.515	5.584	35.137	5.790	27.818	4.416	26.856	29.943	4.654	15.543
6	5.928	42.440	6.237	34.055	4.416	29.931	4.107	39.244	4.244	32.062	3.110	29.966	34.616	5.158	14.901
7	6.237	48.677	4.381	38.436	6.031	35.962	7.371	46.615	5.893	37.955	6.443	36.409	40.676	5.516	13.561

Standard curve equation: Absorbance (A) = 0.0291 (Concentration in micrograms/ml) + 0.0005 was used in the calculations.

*Appendix II – Dose Response Study Data (Tables and Calculations for Chapter 8)*

Table 8.3: Luminescence values (in relative luminescence units) from 20 micron group polyimide tubes

	<b>Day 5</b>	<b>Day 10</b>	<b>Day 15</b>	<b>Day 20</b>	<b>Day 25</b>	<b>Day 30</b>	<b>Average</b>	<b>SD</b>	<b>%CV</b>
<b>Tube 1</b>	6796.86	2990.64	6229.40	4784.02	6206.29	6363.78	5561.83	1431.46	25.74
<b>Tube 2</b>	4651.46	4165.15	6029.58	3461.79	4603.34	6421.32	4888.77	1126.75	23.05
<b>Tube 3</b>	4163.75	4476.08	6485.36	5448.35	7544.59	6502.17	5770.05	1308.03	22.67
<b>Tube 4</b>	5091.87	2634.64	8308.88	2711.06	6147.05	4880.17	4962.28	2150.02	43.33
<b>Tube 5</b>	8536.77	5015.53	5018.73	6482.26	9972.57	6269.23	6882.52	1989.00	28.90
<b>Tube 6</b>	6173.07	4394.65	5056.45	7589.42	7711.51	6746.23	6278.56	1344.93	21.42
<b>Average</b>	5902.30	3946.12	6188.07	5079.48	7030.89	6197.15			
<b>SD</b>	1616.04	928.07	1205.07	1828.51	1829.47	665.16			
<b>%CV</b>	27.38	23.52	19.47	36.00	26.02	10.73			

Table 8.4: Calculation of cumulative luminescence values from values in Table 8.3

Days	Tube 1		Tube 2		Tube 3		Tube 4	
	Lum. (RLU)	Cum. Lum.(RLU)	Lum. (RLU)	Cum. Lum.(RLU)	Lum. (RLU)	Cum. Lum.(RLU)	Lum. (RLU)	Cum. Lum. (RLU)
0	0.00	0.00	0.00	0.00	0.00	0.00	0.00	0.00
5	6796.86	6796.86	4651.46	4651.46	4163.75	4163.75	5091.87	5091.87
10	2990.64	9787.50	4165.15	8816.61	4476.08	8639.83	2634.64	7726.51
15	6229.40	16016.90	6029.58	14846.19	6485.36	15125.19	8308.88	16035.39
20	4784.02	20800.92	3461.79	18307.98	5448.35	20573.54	2711.06	18746.45
25	6206.29	27007.21	4603.34	22911.32	7544.59	28118.13	6147.05	24893.50
30	6363.78	33370.99	6421.32	29332.64	6502.17	34620.30	4880.17	29773.67

Table continues -

Tube 5		Tube 6		Average	SD	%CV
Lum. (RLU)	Cum. Lum.(RLU)	Lum. (RLU)	Cum. Lum. (RLU)	Cum. Lum. (RLU)		
0.00	0.00	0.00	0.00	0.00	0.00	0.00
8536.77	8536.77	6173.07	6173.07	5848.14	1800.69	30.79
5015.53	13552.30	4394.65	10567.72	9704.55	2271.94	23.41
5018.73	18571.03	5056.45	15624.17	16118.94	1469.49	9.12
6482.26	25053.29	7589.42	23213.59	20696.44	2669.99	12.90
9972.57	35025.86	7711.51	30925.10	27591.20	4611.72	16.71
6269.23	41295.09	6746.23	37671.33	33678.54	4825.15	14.33

Table 8.5: Luminescence values (in relative luminescence units) from 30 micron group polyimide tubes

	<b>Day 5</b>	<b>Day 10</b>	<b>Day 15</b>	<b>Day 20</b>	<b>Day 25</b>	<b>Day 30</b>	<b>Average</b>	<b>SD</b>	<b>%CV</b>
<b>Tube 1</b>	7694.00	7349.25	5925.02	4475.68	3652.75	5608.04	5784.12	1574.98	27.23
<b>Tube 2</b>	7048.03	6089.62	5352.40	4247.58	6811.27	4028.70	5596.27	1277.73	22.83
<b>Tube 3</b>	7452.42	7966.81	11327.50	4755.91	5419.04	6836.19	7292.98	2320.08	31.81
<b>Tube 4</b>	4078.01	5542.11	8063.28	6757.74	8984.15	3754.59	6196.65	2118.96	34.20
<b>Tube 5</b>	6404.61	6076.61	5823.16	3899.54	7904.46	4753.81	5810.37	1383.98	23.82
<b>Tube 6</b>	7650.17	4636.55	4488.89	6968.08	2786.28	6353.68	5480.61	1824.13	33.28
<b>Tube 7</b>	5597.74	8233.12	12591.20	4263.79	5094.97	3439.38	6536.70	3383.92	51.77
<b>Average</b>	6560.71	6556.30	7653.06	5052.62	5807.56	4967.77			
<b>SD</b>	1330.37	1328.66	3154.22	1264.73	2233.28	1326.47			
<b>%CV</b>	20.28	20.27	41.22	25.03	38.45	26.70			

Table 8.6: Calculation of cumulative luminescence values from values in Table 8.5

Days	Tube 1		Tube 2		Tube 3		Tube 4		Tube 5	
	Lum. (RLU)	Cum. Lum. (RLU)								
0	0.00	0.00	0.00	0.00	0.00	0.00	0.00	0.00	0.00	0.00
5	7694.00	7694.00	7048.03	7048.03	7452.42	7452.42	4078.01	4078.01	6404.61	6404.61
10	7349.25	15043.25	6089.62	13137.65	7966.81	15419.23	5542.11	9620.12	6076.61	12481.22
15	5925.02	20968.27	5352.40	18490.05	11327.50	26746.73	8063.28	17683.40	5823.16	18304.38
20	4475.68	25443.95	4247.58	22737.63	4755.91	31502.64	6757.74	24441.14	3899.54	22203.92
25	3652.75	29096.70	6811.27	29548.90	5419.04	36921.68	8984.15	33425.29	7904.46	30108.38
30	5608.04	34704.74	4028.70	33577.60	6836.19	43757.87	3754.59	37179.88	4753.81	34862.19

Table continues -

Tube 6		Tube 7		Average	SD	%CV
Lum. (RLU)	Cum. Lum. (RLU)	Lum. (RLU)	Cum. Lum. (RLU)	Cum. Lum. (RLU)		
0.00	0.00	0.00	0.00	0.00	0.00	0.00
7650.17	7650.17	5597.74	5597.74	6535.41	1457.90	22.31
4636.55	12286.72	8233.12	13830.86	13140.29	2325.98	17.70
4488.89	16775.61	12591.20	26422.06	20438.57	3742.19	18.31
6968.08	23743.69	4263.79	30685.85	25265.86	3720.78	14.73
2786.28	26529.97	5094.97	35780.82	31820.19	3320.69	10.44
6353.68	32883.65	3439.38	39220.20	36816.46	4095.24	11.12

Table 8.7: Absorbance values of the drug release samples belonging to the 20 micron group as obtained using ELISA.

Samples	Wells	Absorbance Values	Conc (ng/ml)	Mean Conc (ng/ml)	SD	CV%
<b>Tube 1 Day 5</b>	C2	0.246	0.676	0.672	0.006	0.865
	D2	0.249	0.668			
<b>Tube 1 Day 10</b>	E2	0.298	0.555	0.554	0.001	0.248
	F2	0.299	0.553			
<b>Tube 1 Day 15</b>	G2	0.397	0.407	0.415	0.011	2.625
	H2	0.384	0.423			
<b>Tube 1 Day 20</b>	A3	0.271	0.613	0.607	0.008	1.328
	B3	0.276	0.601			
<b>Tube 1 Day 25</b>	C3	0.404	0.399	0.412	0.017	4.217
	D3	0.383	0.424			
<b>Tube 1 Day 30</b>	E3	0.404	0.399	0.410	0.016	3.809
	F3	0.385	0.421			
<b>Tube 2 Day 5</b>	G3	0.319	0.517	0.497	0.028	5.700
	H3	0.344	0.477			
<b>Tube 2 Day 10</b>	A4	0.318	0.519	0.550	0.045	8.101
	B4	0.285	0.582			
<b>Tube 2 Day 15</b>	C4	0.329	0.500	0.488	0.017	3.381
	D4	0.344	0.477			
<b>Tube 2 Day 20</b>	E4	0.302	0.547	0.552	0.007	1.234
	F4	0.297	0.557			
<b>Tube 2 Day 25</b>	G4	0.320	0.515	0.497	0.026	5.244
	H4	0.343	0.478			
<b>Tube 2 Day 30</b>	A5	0.348	0.471	0.481	0.014	2.898
	B5	0.335	0.491			
<b>Tube 3 Day 5</b>	C5	0.258	0.644	0.648	0.005	0.840
	D5	0.255	0.652			

<b>Tube 3</b>	E5	0.312	0.529			
<b>Day 10</b>	F5	0.295	0.561	0.545	0.023	4.152
<b>Tube 3</b>	G5	0.260	0.639			
<b>Day 15</b>	H5	0.253	0.657	0.648	0.013	1.960
<b>Tube 3</b>	A6	0.302	0.547			
<b>Day 20</b>	B6	0.275	0.603	0.575	0.040	6.866
<b>Tube 3</b>	C6	0.309	0.534			
<b>Day 25</b>	D6	0.294	0.563	0.549	0.020	3.683
<b>Tube 3</b>	E6	0.382	0.425			
<b>Day 30</b>	F6	0.328	0.502	0.463	0.054	11.682
<b>Tube 4</b>	G6	0.261	0.636			
<b>Day 5</b>	H6	0.273	0.608	0.622	0.020	3.250
<b>Tube 4</b>	A7	0.269	0.617			
<b>Day 10</b>	B7	0.261	0.636	0.627	0.014	2.180
<b>Tube 4</b>	C7	0.236	0.705			
<b>Day 15</b>	D7	0.246	0.676	0.690	0.020	2.949
<b>Tube 4</b>	E7	0.278	0.597			
<b>Day 20</b>	F7	0.281	0.590	0.593	0.005	0.783
<b>Tube 4</b>	G7	0.311	0.531			
<b>Day 25</b>	H7	0.335	0.491	0.511	0.029	5.582
<b>Tube 4</b>	A8	0.285	0.582			
<b>Day 30</b>	B8	0.305	0.542	0.562	0.028	4.996
<b>Tube 5</b>	C8	0.207	0.803			
<b>Day 5</b>	D8	0.244	0.681	0.742	0.086	11.541
<b>Tube 5</b>	E8	0.253	0.657			
<b>Day 10</b>	F8	0.259	0.641	0.649	0.011	1.682
<b>Tube 5</b>	G8	0.278	0.597			
<b>Day 15</b>	H8	0.293	0.565	0.581	0.022	3.847
<b>Tube 5</b>	A9	0.271	0.613			
<b>Day 20</b>	B9	0.271	0.613	0.613	0.000	0.000

<b>Tube 5 Day 25</b>	C9	0.306	0.540	0.551	0.015	2.708
	D9	0.295	0.561			
<b>Tube 5 Day 30</b>	E9	0.350	0.468	0.469	0.002	0.439
	F9	0.348	0.471			
<b>Tube 6 Day 5</b>	G9	1.379	0.046	0.042	0.005	11.322
	H9	1.431	0.039			
<b>Tube 6 Day 10</b>	A10	0.266	0.624	0.613	0.016	2.676
	B10	0.276	0.601			
<b>Tube 6 Day 15</b>	C10	0.262	0.634	0.626	0.012	1.905
	D10	0.269	0.617			
<b>Tube 6 Day 20</b>	E10	0.282	0.588	0.566	0.031	5.526
	F10	0.304	0.544			
<b>Tube 6 Day 25</b>	G10	0.326	0.505	0.500	0.007	1.376
	H10	0.332	0.495			
<b>Tube 6 Day 30</b>	A11	0.325	0.507	0.530	0.033	6.213
	B11	0.299	0.553			

The three parameter logistic equation was used to calculate the concentration values (ng/ml). The mean concentration values were used in Table 8.8.

Table 8.8: Concentration (ng/ml) of drug release samples belonging to 20 micron group obtained using ELISA.

<b>Days</b>	<b>T1</b>	<b>T2</b>	<b>T3</b>	<b>T4</b>	<b>T5</b>	<b>T6</b>
<b>0</b>	0.00	0.00	0.00	0.00	0.00	0.00
<b>5</b>	0.672	0.497	0.648	0.622	0.742	0.042*
<b>10</b>	0.554	0.550	0.545	0.627	0.649	0.613
<b>15</b>	0.415	0.488	0.648	0.690	0.581	0.626
<b>20</b>	0.607	0.552	0.575	0.593	0.613	0.566
<b>25</b>	0.412	0.497	0.549	0.511	0.551	0.500
<b>30</b>	0.410	0.481	0.463	0.562	0.469	0.530

Table 8.9: Original concentrations (ng/ml) for 20 micron group

<b>Days</b>	<b>T1</b>	<b>T2</b>	<b>T3</b>	<b>T4</b>	<b>T5</b>	<b>T6</b>	<b>Average</b>	<b>SD</b>	<b>%CV</b>
<b>0</b>	0.00	0.00	0.00	0.00	0.00	0.00	0.00	0.00	0.00
<b>5</b>	671.74	496.77	647.88	622.20	741.98	0.00	530.09	271.82	51.28
<b>10</b>	554.20	550.02	545.06	626.83	649.22	612.70	589.67	45.34	7.69
<b>15</b>	415.01	488.43	647.97	690.24	580.85	625.60	574.68	104.20	18.13
<b>20</b>	606.80	552.30	575.42	593.37	612.50	565.82	584.37	23.78	4.07
<b>25</b>	411.66	496.66	548.76	510.69	550.52	500.15	503.07	50.60	10.06
<b>30</b>	410.44	480.68	463.45	561.68	469.38	529.95	485.93	53.26	10.96

Original concentrations are obtained by multiplying values in Table 8.8 with 1000 (Dilution is 1000 times).

\* An unexpected low concentration was observed indicating error.

Table 8.12: Absorbance values of the drug release samples belonging to the 30 micron group as obtained using ELISA.

<b>Samples</b>	<b>Wells</b>	<b>Abs. Values</b>	<b>Conc (ng/ml)</b>	<b>Mean Conc (ng/ml)</b>	<b>SD</b>	<b>CV%</b>
<b>Tube 1 Day 5</b>	C2	0.342	0.491	0.482	0.013	2.63
	D2	0.352	0.473			
<b>Tube 2 Day 5</b>	E2	0.370	0.443	0.449	0.008	1.78
	F2	0.363	0.454			
<b>Tube 3 Day 5</b>	G2	0.385	0.420	0.395	0.036	9.07
	H2	0.423	0.370			
<b>Tube 4 Day 5</b>	A3	0.408	0.389	0.415	0.037	9.03
	B3	0.371	0.442			
<b>Tube 5 Day 5</b>	C3	0.353	0.471	0.476	0.006	1.31
	D3	0.348	0.480			
<b>Tube 6 Day 5</b>	E3	0.330	0.514	0.486	0.040	8.17
	F3	0.361	0.458			
<b>Tube 7 Day 5</b>	G3	0.267	0.667	0.643	0.034	5.27
	H3	0.284	0.619			
<b>Tube 1 Day 10</b>	A4	0.406	0.391	0.437	0.065	14.95
	B4	0.346	0.484			
<b>Tube 2 Day 10</b>	C4	0.288	0.609	0.617	0.011	1.81
	D4	0.282	0.625			
<b>Tube 3 Day 10</b>	E4	0.289	0.606	0.615	0.013	2.11
	F4	0.282	0.625			
<b>Tube 4 Day 10</b>	G4	0.485	0.304	0.280	0.033	11.81
	H4	0.541	0.257			
<b>Tube 5 Day 10</b>	A5	0.417	0.377	0.441	0.090	20.39
	B5	0.335	0.504			
<b>Tube 6 Day 10</b>	C5	0.298	0.584	0.598	0.020	3.26
	D5	0.287	0.611			

<b>Tube 7 Day 10</b>	E5	0.357	0.464	0.448	0.024	5.32
	F5	0.378	0.431			
<b>Tube 1 Day 15</b>	G5	0.395	0.406	0.375	0.044	11.66
	H5	0.445	0.344			
<b>Tube 2 Day 15</b>	A6	0.397	0.403	0.437	0.048	10.99
	B6	0.353	0.471			
<b>Tube 3 Day 15</b>	C6	0.225	0.816	0.834	0.025	2.95
	D6	0.217	0.851			
<b>Tube 4 Day 15</b>	E6	0.417	0.377	0.368	0.013	3.48
	F6	0.432	0.359			
<b>Tube 5 Day 15</b>	G6	0.273	0.650	0.596	0.076	12.68
	H6	0.316	0.543			
<b>Tube 6 Day 15</b>	A7	0.436	0.354	0.397	0.061	15.25
	B7	0.372	0.440			
<b>Tube 7 Day 15</b>	C7	0.382	0.425	0.443	0.026	5.79
	D7	0.359	0.461			
<b>Tube 1 Day 20</b>	E7	0.326	0.522	0.523	0.001	0.27
	F7	0.325	0.524			
<b>Tube 2 Day 20</b>	G7	0.340	0.495	0.446	0.068	15.34
	H7	0.401	0.398			
<b>Tube 3 Day 20</b>	A8	0.350	0.477	0.501	0.035	6.97
	B8	0.324	0.526			
<b>Tube 4 Day 20</b>	C8	0.299	0.581	0.557	0.035	6.26
	D8	0.321	0.532			
<b>Tube 5 Day 20</b>	E8	0.305	0.567	0.544	0.034	6.17
	F8	0.327	0.520			
<b>Tube 6 Day 20</b>	G8	0.406	0.391	0.376	0.021	5.62
	H8	0.430	0.361			
<b>Tube 7 Day 20</b>	A9	0.352	0.473	0.521	0.068	13.10
	B9	0.304	0.570			

<b>Tube 1 Day 25</b>	C9	0.270	0.658	0.654	0.006	0.94
	D9	0.273	0.650			
<b>Tube 2 Day 25</b>	E9	0.282	0.625	0.617	0.011	1.81
	F9	0.288	0.609			
<b>Tube 3 Day 25</b>	G9	0.302	0.574	0.539	0.050	9.20
	H9	0.335	0.504			
<b>Tube 4 Day 25</b>	A10	0.339	0.497	0.519	0.031	6.01
	B10	0.317	0.541			
<b>Tube 5 Day 25</b>	C10	0.327	0.520	0.531	0.016	3.05
	D10	0.316	0.543			
<b>Tube 6 Day 25</b>	E10	0.344	0.487	0.492	0.007	1.33
	F10	0.339	0.497			
<b>Tube 7 Day 25</b>	G10	0.342	0.491	0.478	0.019	3.93
	H10	0.357	0.464			
<b>Tube 1 Day 30</b>	A11	0.350	0.477	0.505	0.041	8.08
	B11	0.320	0.534			
<b>Tube 2 Day 30</b>	C11	0.287	0.611	0.567	0.063	11.17
	D11	0.326	0.522			
<b>Tube 3 Day 30</b>	E11	0.360	0.459	0.473	0.020	4.17
	F11	0.344	0.487			
<b>Tube 4 Day 30</b>	G11	0.340	0.495	0.486	0.013	2.64
	H11	0.350	0.477			
<b>Tube 5 Day 30</b>	A12	0.334	0.506	0.496	0.015	2.94
	B12	0.345	0.485			
<b>Tube 6 Day 30</b>	C12	0.360	0.459	0.473	0.020	4.17
	D12	0.344	0.487			
<b>Tube 7 Day 30</b>	E12	0.324	0.526	0.543	0.024	4.49
	F12	0.308	0.560			

The three parameter logistic equation was used to calculate the concentration values (ng/ml). The mean concentration values were used in Table 8.13

Table 8.13: Concentration (ng/ml) of drug release samples belonging to 30 micron group obtained using ELISA.

<b>Days</b>	<b>T1</b>	<b>T2</b>	<b>T3</b>	<b>T4</b>	<b>T5</b>	<b>T6</b>	<b>T7</b>
<b>0</b>	0.00	0.00	0.00	0.00	0.00	0.00	0.00
<b>5</b>	0.482	0.449	0.395	0.415	0.476	0.486	0.643
<b>10</b>	0.437	0.617	0.615	0.280	0.441	0.598	0.448
<b>15</b>	0.375	0.437	0.834	0.368	0.596	0.397	0.443
<b>20</b>	0.523	0.446	0.501	0.557	0.544	0.376	0.521
<b>25</b>	0.654	0.617	0.539	0.519	0.531	0.492	0.478
<b>30</b>	0.505	0.567	0.473	0.486	0.496	0.473	0.543

Table 8.14: Original concentrations (ng/ml) for 30 micron group

<b>Days</b>	<b>T1</b>	<b>T2</b>	<b>T3</b>	<b>T4</b>	<b>T5</b>	<b>T6</b>	<b>T7</b>	<b>Average</b>	<b>SD</b>	<b>%CV</b>
<b>0</b>	0.00	0.00	0.00	0.00	0.00	0.00	0.00	0.00	0.00	0.00
<b>5</b>	481.96	448.76	395.00	415.06	475.66	485.77	643.25	477.92	80.72	16.89
<b>10</b>	437.41	616.70	615.42	280.33	440.58	597.59	447.58	490.80	125.38	25.55
<b>15</b>	375.14	437.28	833.58	368.00	596.19	397.15	442.89	492.89	168.80	34.25
<b>20</b>	522.87	446.24	501.22	556.77	543.55	376.24	521.29	495.45	63.46	12.81
<b>25</b>	653.99	616.70	539.18	518.55	531.29	491.89	477.67	547.04	64.89	11.86
<b>30</b>	505.37	566.62	473.31	485.57	495.74	473.31	543.17	506.16	35.86	7.09

Original concentrations are calculated by multiplying values of Table 8.13 with 1000 (Dilution is 1000 times).

Table 8.15: Amount of ethinyl estradiol released for 30 micron group

Days	T1	T2	T3	T4	T5	T6	T7	Average	SD	%CV
0	0.00	0.00	0.00	0.00	0.00	0.00	0.00	0.00	0.00	0.00
5	144.59	134.63	118.50	124.52	142.70	145.73	192.98	143.38	24.22	16.89
10	131.22	185.01	184.62	84.10	132.17	179.28	134.27	147.24	37.61	25.55
15	112.54	131.18	250.07	110.40	178.86	119.15	132.87	147.87	50.64	34.25
20	156.86	133.87	150.37	167.03	163.07	112.87	156.39	148.64	19.04	12.81
25	196.20	185.01	161.75	155.57	159.39	147.57	143.30	164.11	19.47	11.86
30	151.61	169.99	141.99	145.67	148.72	141.99	162.95	151.85	10.76	7.09

Amounts are calculated by multiplying concentrations in Table 8.10 with volume of 0.3 ml.

Table 8.16: Cumulative amount of ethinyl estradiol released (ng) from 30 micron group over 30 days.

Days	T1		T2		T3		T4		T5		T6		T7		Average	SD	%CV
	Amt (ng)	Cum. Amt. (ng)															
0	0.00	0.00	0.00	0.00	0.00	0.00	0.00	0.00	0.00	0.00	0.00	0.00	0.00	0.00	0.00	0.00	0.00
5	144.59	144.59	134.63	134.63	118.50	118.50	124.52	124.52	142.70	142.70	145.73	145.73	192.98	192.98	143.38	24.22	16.89
10	131.22	275.81	185.01	319.64	184.62	303.12	84.10	208.61	132.17	274.87	179.28	325.01	134.27	327.25	290.62	42.26	14.54
15	112.54	388.35	131.18	450.82	250.07	553.20	110.40	319.02	178.86	453.73	119.15	444.16	132.87	460.12	438.48	71.68	16.35
20	156.86	545.22	133.87	584.70	150.37	703.56	167.03	486.05	163.07	616.79	112.87	557.03	156.39	616.50	587.12	68.54	11.67
25	196.20	741.41	185.01	769.71	161.75	865.32	155.57	641.61	159.39	776.18	147.57	704.59	143.30	759.80	751.23	68.73	9.15
30	151.61	893.02	169.99	939.69	141.99	1007.31	145.67	787.28	148.72	924.90	141.99	846.59	162.95	922.76	903.08	70.44	7.80

## References

1. Hollander, P.A., *Evolution of a pulmonary insulin delivery system (Exubera) for patients with diabetes*. MedGenMed, 2007. **9**(1): p. 45.
2. Morimoto, K., et al., *Effects of proteolytic enzyme inhibitors on the nasal absorption of vasopressin and an analogue*. Pharm Res, 1991. **8**(9): p. 1175-9.
3. Dokka, S., et al., *Dermal delivery of topically applied oligonucleotides via follicular transport in mouse skin*. J Invest Dermatol, 2005. **124**(5): p. 971-5.
4. Brown, M.B., et al., *Dermal and transdermal drug delivery systems: current and future prospects*. Drug Deliv, 2006. **13**(3): p. 175-87.
5. Ritch, R., et al., *An improved technique of eye drop self-administration for patients with limited vision*. Am J Ophthalmol, 2003. **135**(4): p. 530-3.
6. Denis, P., et al., *Intraocular pressure control with latanoprost/timolol and travoprost/timolol fixed combinations: a retrospective, multicentre, cross-sectional study*. Clin Drug Investig, 2008. **28**(12): p. 767-76.
7. Uva, M.G., et al., *The effect of timolol-dorzolamide and timolol-pilocarpine combinations on ocular blood flow in patients with glaucoma*. Am J Ophthalmol, 2006. **141**(6): p. 1158-60.

8. Ma, E.L., et al., *In vitro and in vivo evaluation of a novel oral insulin formulation*. Acta Pharmacol Sin, 2006. **27**(10): p. 1382-8.
9. Romeo, V.D., et al., *Effects of physicochemical properties and other factors on systemic nasal drug delivery*. Adv Drug Deliv Rev, 1998. **29**(1-2): p. 89-116.
10. Folkman, J. and D.M. Long, *The Use Of Silicone Rubber As A Carrier For Prolonged Drug Therapy*. J Surg Res, 1964. **4**: p. 139-42.
11. Folkman, J., D.M. Long, Jr., and R. Rosenbaum, *Silicone rubber: a new diffusion property useful for general anesthesia*. Science, 1966. **154**(745): p. 148-9.
12. Langer, R., *Drug delivery and targeting*. Nature, 1998. **392**(6679 Suppl): p. 5-10.
13. Macoull, K.L. and D. Pavan-Langston, *Pilocarpine ocusert system for sustained control of ocular hypertension*. Arch Ophthalmol, 1975. **93**(8): p. 587-90.
14. Hoffman, A.S., *The origins and evolution of "controlled" drug delivery systems*. J Control Release, 2008. **132**(3): p. 153-63.
15. Flach, A., *The pilocarpine Ocusert Delivery System*. Trans Pac Coast Otoophthalmol Soc Annu Meet, 1974. **55**: p. 179-208.
16. Lee, P., Y. Shen, and M. Eberle, *The long-acting Ocusert-pilocarpine system in the management of glaucoma*. Invest Ophthalmol, 1975. **14**(1): p. 43-6.
17. Drance, S.M., D.W. Mitchell, and M. Schulzer, *The duration of action of pilocarpine Ocusert on intraocular pressure in man*. Can J Ophthalmol, 1975. **10**(4): p. 450-2.

18. Drance, S.M., D.W. Mitchell, and M. Schulzer, *The effects of ocusert pilocarpine on anterior chamber depth, visual acuity and intraocular pressure in man*. Can J Ophthalmol, 1977. **12**(1): p. 24-8.
19. Worthen, D.M., T.J. Zimmerman, and C.A. Wind, *An evaluation of the pilocarpine Ocusert*. Invest Ophthalmol, 1974. **13**(4): p. 296-9.
20. Pharriss, B.B., et al., *Progestasert: a uterine therapeutic system for long-term contraception: I. Philosophy and clinical efficacy*. Fertil Steril, 1974. **25**(11): p. 915-21.
21. Badawi, H.M. and F.A. Soliman, *The influence of oestrogen and progesterone on pituitary function*. Experientia, 1957. **13**(10): p. 412-4.
22. Lipschutz, A., R. Iglesias, and et al., *Progesterone and desoxycorticosterone in the steroid control of the gonadotrophic function of the hypophysis; exemplified by the behavior of the intrasplenic ovarian graft in the guinea pig*. Endocrinology, 1948. **42**(3): p. 201-9.
23. Rapport, R.L. and I. Rothchild, *The thermogenic effect of progesterone and its relation to thyroid function*. Endocrinology, 1952. **50**(5): p. 580-3.
24. Belova, M.G., *Effect Of Estrogens And Progesterone On The Follicle-Stimulating Function Of The Pituitary*. Klin Lech Zlokach Novoobraz, 1963. **92**: p. 271-4.
25. Dejongh, S.E. and O.L. Wolthuis, *Factors Determining Cessation Of Corpus Luteum Function; The Possible Role Of Oestradiol And Progesterone*. Acta Endocrinol (Copenh), 1964. **45**: p. SUPPL90:125-32.

26. ALZA, *The Alza T IPCS 52, a longer acting progesterone IUD: safety and efficacy compared to the TCU220C and multiload 250 in two randomized multicentre trials. The World Health Organization's special programme of research, development and research training in human reproduction. Task Force on intrauterine devices for fertility regulation. Clin Reprod Fertil, 1983. 2(2): p. 113-28.*
27. Lopez, G.Z., Perez V, E., Velazquez, J. G., Ramos, R. A., *Determination of progesterone and the beta subunit of chorionic gonadotropin in women with intrauterine devices. Ginecol Obstet Mex, 1979. 46(278): p. 391-401.*
28. Murad, F., *Intrauterine devices containing progesterone. Drug Therapy, 1977. 7(5): p. 119-21.*
29. Parmer, J., *Long-term suppression of hypermenorrhea by progesterone intrauterine contraceptive devices. Am J Obstet Gynecol, 1984. 149(5): p. 578-9.*
30. WyomingHealthCouncil,  
*[http://www.wyhc.org/birth\\_control\\_options/Progestasert-IUD.php](http://www.wyhc.org/birth_control_options/Progestasert-IUD.php) Accessed January 15 2009.*
31. HealthSquare, *<http://www.healthsquare.com/fgwh/wh1ch20.htm> Accessed January 15 2009.*
32. PopulationCouncil, *<http://www.popcouncil.org/biomed/norplantfaq.html> Accessed January 15 2009.*

33. Segal, S.J., *The development of NORPLANT implants*. Stud Fam Plann, 1983. **14**(6-7): p. 159-63.
34. Sivin, I., et al., *Norplant: reversible implant contraception*. Stud Fam Plann, 1980. **11**(7-8): p. 227-35.
35. Sivin, I., et al., *Three-year experience with NORPLANT subdermal contraception*. Fertil Steril, 1983. **39**(6): p. 799-808.
36. Diaz, S., et al., *A five-year clinical trial of levonorgestrel silastic implants (Norplant™)*. Contraception, 1982. **25**(5): p. 447-56.
37. Holma, P., *Long-term experience with Norplant contraceptive implants in Finland*. Contraception, 1985. **31**(3): p. 231-41.
38. Sivin, I., et al., *The NORPLANT contraceptive method: a report on three years of use*. Stud Fam Plann, 1982. **13**(8-9): p. 258-61.
39. Vukelic, J. and Z. Belopavlovic, *Norplant--a subdermal contraceptive implant*. Med Pregl, 1986. **39**(9-10): p. 469-71.
40. HealthSquare, <http://www.healthsquare.com/fgwh/wh1c2102.jpg> Accessed January 15 2009.
41. Bhatt, P.P., [http://www.drugdeliveryreport.com/articles/ddcr\\_w2004\\_article3.pdf](http://www.drugdeliveryreport.com/articles/ddcr_w2004_article3.pdf) Accessed January 15 2009.
42. Gasperino, J.L., *Procardia XL bezoar*. Arch Intern Med, 1992. **152**(4): p. 880-1.

43. Pfizer, [http://media.pfizer.com/files/products/uspi\\_procardia\\_xl.pdf](http://media.pfizer.com/files/products/uspi_procardia_xl.pdf) Accessed January 15 2009.
44. Pfizer, [http://www.pfizer.com/files/products/uspi\\_glucotrol\\_xl.pdf](http://www.pfizer.com/files/products/uspi_glucotrol_xl.pdf) Accessed January 15 2009.
45. Durect, [http://www.durect.com/pdf/duros\\_fact\\_sheet2001.pdf](http://www.durect.com/pdf/duros_fact_sheet2001.pdf) Accessed January 15 2009.
46. Cukierski, M.J., P.A. Johnson, and J.C. Beck, *Chronic (60-week) toxicity study of DUROS leuprolide implants in dogs*. *Int J Toxicol*, 2001. **20**(6): p. 369-81.
47. pSivida,  
[http://www.psivida.com/news/download/ASX/pSivida%20ASX%20Release\\_CDS%20Acquisition.pdf](http://www.psivida.com/news/download/ASX/pSivida%20ASX%20Release_CDS%20Acquisition.pdf) Accessed January 15 2009.
48. Lim, L.L., J.R. Smith, and J.T. Rosenbaum, *Retisert (Bausch & Lomb/Control Delivery Systems)*. *Curr Opin Investig Drugs*, 2005. **6**(11): p. 1159-67.
49. Cadman, J., *Ganciclovir implants: one year later*. *GMHC Treat Issues*, 1997. **11**(4/5): p. 3-6.
50. FDA, *Chiron Vision files FDA application to market intraocular implant for CMV retinitis*. *Food and Drug Administration*. *J Int Assoc Physicians AIDS Care*, 1995. **1**(6): p. 37.
51. Jaffe, G.J., et al., *Fluocinolone acetonide implant (Retisert) for noninfectious posterior uveitis: thirty-four-week results of a multicenter randomized clinical study*. *Ophthalmology*, 2006. **113**(6): p. 1020-7.

52. Bausch&Lomb, *Fluocinolone acetonide ophthalmic--Bausch & Lomb: fluocinolone acetonide Envision TD implant*. *Drugs R D*, 2005. **6**(2): p. 116-9.
53. Hsu, J., *Drug delivery methods for posterior segment disease*. *Curr Opin Ophthalmol*, 2007. **18**(3): p. 235-9.
54. Ufret-Vincenty, R.L., et al., *Cytomegalovirus retinitis after fluocinolone acetonide (Retisert) implant*. *Am J Ophthalmol*, 2007. **143**(2): p. 334-5.
55. Vitrasert-Package-Insert,  
[http://www.bausch.com/en\\_US/package\\_insert/surgical/vitrasert\\_pkg\\_insert.pdf](http://www.bausch.com/en_US/package_insert/surgical/vitrasert_pkg_insert.pdf)  
*Accessed January 15 2009.*
56. Bausch&Lomb, [http://www.retisert.com/professional\\_home.html](http://www.retisert.com/professional_home.html) *Accessed 15 January 2009.*
57. Kane, F.E., et al., *Iluvien: a new sustained delivery technology for posterior eye disease*. *Expert Opin Drug Deliv*, 2008. **5**(9): p. 1039-46.
58. pSivida, <http://www.psivida.com/default.asp> *Accessed January 15 2009.*
59. AlimeraSciences,  
<http://www.alimerasciences.com/Products/IluvienOverview/tabid/82/Default.aspx>  
*Accessed January 15 2009.*
60. Del Amo, E.M. and A. Urtti, *Current and future ophthalmic drug delivery systems. A shift to the posterior segment*. *Drug Discov Today*, 2008. **13**(3-4): p. 135-43.

61. Rehan, N., A. Inayatullah, and I. Chaudhary, *Norplant: reasons for discontinuation and side-effects*. Eur J Contracept Reprod Health Care, 2000. **5**(2): p. 113-8.
62. PhysicsFactbook, <http://hypertextbook.com/facts/1999/BrianLey.shtml> Accessed January 15 2009.
63. Panyam, J. and V. Labhasetwar, *Biodegradable nanoparticles for drug and gene delivery to cells and tissue*. Adv Drug Deliv Rev, 2003. **55**(3): p. 329-47.
64. Sung, J.C., B.L. Pulliam, and D.A. Edwards, *Nanoparticles for drug delivery to the lungs*. Trends Biotechnol, 2007. **25**(12): p. 563-70.
65. Yang, W., J.I. Peters, and R.O. Williams, 3rd, *Inhaled nanoparticles--a current review*. Int J Pharm, 2008. **356**(1-2): p. 239-47.
66. Yang, W., N.P. Wiederhold, and R.O. Williams, 3rd, *Drug delivery strategies for improved azole antifungal action*. Expert Opin Drug Deliv, 2008. **5**(11): p. 1199-216.
67. Green, M.R., et al., *Abraxane, a novel Cremophor-free, albumin-bound particle form of paclitaxel for the treatment of advanced non-small-cell lung cancer*. Ann Oncol, 2006. **17**(8): p. 1263-8.
68. Micha, J.P., et al., *Abraxane in the treatment of ovarian cancer: the absence of hypersensitivity reactions*. Gynecol Oncol, 2006. **100**(2): p. 437-8.

69. Gao, Y., et al., *A multifunctional nano device as non-viral vector for gene delivery: in vitro characteristics and transfection*. J Control Release, 2007. **118**(3): p. 381-8.
70. Kogure, K., *Development of a novel artificial gene delivery system multifunctional envelope-type nano device for gene therapy*. Yakugaku Zasshi, 2007. **127**(10): p. 1685-91.
71. Kogure, K., et al., *Multifunctional envelope-type nano device (MEND) as a non-viral gene delivery system*. Adv Drug Deliv Rev, 2007.
72. Langer, R., *Implantable controlled release systems*. Pharmacol Ther, 1983. **21**(1): p. 35-51.
73. Lou, M. and E. Jonckheere, *Magnetically levitated nano-robots: an application to visualization of nerve cells injuries*. Stud Health Technol Inform, 2007. **125**: p. 310-2.
74. NanotechWeb, <http://nanotechweb.org/cws/article/lab/32077> Accessed January 15 2009.
75. Kam, N.W., et al., *Carbon nanotubes as multifunctional biological transporters and near-infrared agents for selective cancer cell destruction*. Proc Natl Acad Sci U S A, 2005. **102**(33): p. 11600-5.
76. Martin, F., et al., *Tailoring width of microfabricated nanochannels to solute size can be used to control diffusion kinetics*. J Control Release, 2005. **102**(1): p. 123-33.

77. Liang, K.Z., et al., *Biomolecules/gold nanowires-doped sol-gel film for label-free electrochemical immunoassay of testosterone*. J Biochem Biophys Methods, 2008. **70**(6): p. 1156-62.
78. Jain, K.K., *Nanodiagnostics: application of nanotechnology in molecular diagnostics*. Expert Rev Mol Diagn, 2003. **3**(2): p. 153-61.
79. Dost, P., M. Wiemann, and W.J. ten Cate, *Biomaterial studies in cultures of human stapedial bone-like cells*. Hno, 2005. **53**(6): p. 545-7.
80. Reuling, N., B. Pohl-Reuling, and M. Keil, *Biocompatibility of precious metal dental alloys*. Zwr, 1991. **100**(3): p. 146, 148, 150 passim.
81. Stensaas, S.S. and L.J. Stensaas, *Histopathological evaluation of materials implanted in the cerebral cortex*. Acta Neuropathol, 1978. **41**(2): p. 145-55.
82. Blackwood, D.J. and B.P. Pereira, *No corrosion of 304 stainless steel implant after 40 years of service*. J Mater Sci Mater Med, 2004. **15**(7): p. 755-8.
83. Kraft, C.N., et al., *Impact of a nickel-reduced stainless steel implant on striated muscle microcirculation: a comparative in vivo study*. J Biomed Mater Res, 2001. **57**(3): p. 404-12.
84. Reclaru, L., et al., *Corrosion behavior of a welded stainless-steel orthopedic implant*. Biomaterials, 2001. **22**(3): p. 269-79.
85. Skinner, H.B., et al., *Evaluation of a commercial, porous stainless steel as a prosthetic implant material*. Biomater Med Devices Artif Organs, 1979. **7**(1): p. 141-6.

86. Crumbliss, A.L., et al., *Colloidal gold as a biocompatible immobilization matrix suitable for the fabrication of enzyme electrodes by electrodeposition*. Biotechnol Bioeng, 1992. **40**(4): p. 483-90.
87. Wirz, J., *Are the new alloys biocompatible? High gold content is another trump*. Dent Labor (Munch), 1986. **34**(7): p. 1113-6.
88. Park, M., and C. Harrison, et al, *Block Copolymer Lithography: Periodic Arrays of  $\sim 10^{11}$  Holes in 1 Square Centimete*. Science, 1997. **276**. no. (5317): p. 1401 - 1404.
89. Quake, S.R. and A. Scherer, *From micro- to nanofabrication with soft materials*. Science, 2000. **290**(5496): p. 1536-40.
90. Henzla, J., T. Bredowb et al., *Irreversible isomerization of the azobenzene derivate Methyl Orange on Au(111)*. Chemical Physics Letters, 2007. **435**(4-6): p. 278-282.
91. Eaglstein, W.H., et al., *A liquid adhesive bandage for the treatment of minor cuts and abrasions*. Dermatol Surg, 2002. **28**(3): p. 263-7.
92. Eskandari, M.M., et al., *Cyanoacrylate adhesive provides efficient local drug delivery*. Clin Orthop Relat Res, 2006. **451**: p. 242-50.
93. Huang, C.Y. and Y.D. Lee, *Core-shell type of nanoparticles composed of poly[(n-butyl cyanoacrylate)-co-(2-octyl cyanoacrylate)] copolymers for drug delivery application: synthesis, characterization and in vitro degradation*. Int J Pharm, 2006. **325**(1-2): p. 132-9.

94. Vauthier, C., et al., *Drug delivery to resistant tumors: the potential of poly(alkyl cyanoacrylate) nanoparticles*. J Control Release, 2003. **93**(2): p. 151-60.
95. Rastogi, A., et al., *Characterization of Nanoporous Surfaces as Templates for Drug Delivery Devices*. Aaps J, 2009.
96. Price, R.R. and M. Patchan, *Entrapment and release characteristics of 2-methoxynaphthalene from cylindrical microstructures formed from phospholipids*. J Microencapsul, 1993. **10**(2): p. 215-22.
97. Nebeker, J.R., et al., *Hypersensitivity cases associated with drug-eluting coronary stents: a review of available cases from the Research on Adverse Drug Events and Reports (RADAR) project*. J Am Coll Cardiol, 2006. **47**(1): p. 175-81.
98. Pielka, S., et al., *Investigation of local reaction of muscular tissue after injection of polyvinylpyrrolidone preparation*. Polim Med, 2004. **34**(4): p. 9-15.
99. BostonScientific, C., <http://www.fda.gov/cdrh/mda/docs/p030025.html> Accessed January 15 2009.
100. Cordis, <http://www.fda.gov/cdrh/mda/docs/p020026.html> Accessed January 15 2009, in CYPHER™ Sirolimus-eluting Coronary Stent - P020026, FDA.
101. Holmes, D.R., Jr., et al., *Results of Prevention of REStenosis with Tranilast and its Outcomes (PRESTO) trial*. Circulation, 2002. **106**(10): p. 1243-50.
102. Kastrati, A., et al., *Sirolimus-eluting stent or paclitaxel-eluting stent vs balloon angioplasty for prevention of recurrences in patients with coronary in-stent restenosis: a randomized controlled trial*. Jama, 2005. **293**(2): p. 165-71.

103. Moses, J.W., et al., *Sirolimus-eluting stents versus standard stents in patients with stenosis in a native coronary artery*. N Engl J Med, 2003. **349**(14): p. 1315-23.
104. Park, S.J., et al., *A paclitaxel-eluting stent for the prevention of coronary restenosis*. N Engl J Med, 2003. **348**(16): p. 1537-45.
105. Regar, E., et al., *Angiographic findings of the multicenter Randomized Study With the Sirolimus-Eluting Bx Velocity Balloon-Expandable Stent (RAVEL): sirolimus-eluting stents inhibit restenosis irrespective of the vessel size*. Circulation, 2002. **106**(15): p. 1949-56.
106. Baffour, R., et al., *Enhanced angiogenesis and growth of collaterals by in vivo administration of recombinant basic fibroblast growth factor in a rabbit model of acute lower limb ischemia: dose-response effect of basic fibroblast growth factor*. J Vasc Surg, 1992. **16**(2): p. 181-91.
107. Geerts, A.M. and I. Colle, *Angiogenesis in portal hypertension: involvement in increased splanchnic blood flow and collaterals?* Acta Clin Belg, 2007. **62**(5): p. 271-5.
108. Virmani, R., et al., *Mechanism of late in-stent restenosis after implantation of a paclitaxel derivate-eluting polymer stent system in humans*. Circulation, 2002. **106**(21): p. 2649-51.
109. Aziz, S., J.L. Morris, and R.A. Perry, *Late stent thrombosis associated with coronary aneurysm formation after sirolimus-eluting stent implantation*. J Invasive Cardiol, 2007. **19**(4): p. E96-8.

110. Camenzind, E., *Treatment of in-stent restenosis--back to the future?* N Engl J Med, 2006. **355**(20): p. 2149-51.
111. Camenzind, E., P.G. Steg, and W. Wijns, *Stent thrombosis late after implantation of first-generation drug-eluting stents: a cause for concern.* Circulation, 2007. **115**(11): p. 1440-55; discussion 1455.
112. Pfisterer, M.E., *The BASKET-LATE-Study. Basel stent cost-effectiveness trial--late thrombotic events trial.* Herz, 2006. **31**(3): p. 259.
113. Rastogi, A. and S. Stavchansky, *Drug eluting stents and beyond.* Curr Pharm Des, 2008. **14**(21): p. 2111-20.
114. Li, J.J., et al., *Is inflammation a contributor for coronary stent restenosis?* Med Hypotheses, 2007. **68**(5): p. 945-51.
115. Golino, P., et al., *Inhibition of leucocyte and platelet adhesion reduces neointimal hyperplasia after arterial injury.* Thromb Haemost, 1997. **77**(4): p. 783-8.
116. Sainani, G.S. and V.G. Maru, *The endothelial leukocyte adhesion molecule. Role in coronary artery disease.* Acta Cardiol, 2005. **60**(5): p. 501-7.
117. Wang, X., et al., *Enhanced leucocyte adhesion to interleukin-1 beta stimulated vascular smooth muscle cells is mainly through intercellular adhesion molecule-1.* Cardiovasc Res, 1994. **28**(12): p. 1808-14.
118. Virmani, R., Gold, Herman, Finn, Alope, Joner, Mike, and Kolodgie, Frank, *The Vascular Pathology of Drug Eluting Drug Eluting Stents Stents:Delayed Healing*

- and Late Delayed Healing and Late Thrombotic Thrombotic Risk*. FDA Circulatory System Devices Panel, 2006.
119. Bennett, M.R. and M. O'Sullivan, *Mechanisms of angioplasty and stent restenosis: implications for design of rational therapy*. Pharmacol Ther, 2001. **91**(2): p. 149-66.
  120. McLean, D.R. and N.L. Eiger, *Stent design: implications for restenosis*. Rev Cardiovasc Med, 2002. **3 Suppl 5**: p. S16-22.
  121. Rogers, C.D., *Drug-eluting stents: clinical perspectives on drug and design differences*. Rev Cardiovasc Med, 2005. **6 Suppl 1**: p. S3-12.
  122. Cordis, C., <http://www.fda.gov/cdrh/PDF2/p020026c.pdf>, in *Instructions for Use: CYPHER™ Sirolimus-eluting Coronary Stent on RAPTOR™ Over-the-Wire Delivery System*, FDA.
  123. BostonScientific, C., <http://www.fda.gov/cdrh/pdf3/P030025b.pdf> Accessed January 15 2009. Summary of Safety and Effectiveness Data: TAXUS Express Coronary Stent System.
  124. Kereiakes, D.J., et al., *Usefulness of a cobalt chromium coronary stent alloy*. Am J Cardiol, 2003. **92**(4): p. 463-6.
  125. Mirkovic, N., *Mechanical properties of metal-ceramic systems from nickel-chromium and cobalt-chromium alloys*. Vojnosanit Pregl, 2007. **64**(4): p. 241-5.

126. Poncin, P., C. Millet, J. Chevy, J.L. Proft. *Comparing and optimizing Co-Cr Tubing for Stent Applications*. in *Materials Processes for Medical Devices Conference*. 2004.
127. Ghosh, M.K., K. L. Mittal, *Polyimides*. 1996: CRC Press. 891.
128. Metz, S., et al., *Flexible polyimide probes with microelectrodes and embedded microfluidic channels for simultaneous drug delivery and multi-channel monitoring of bioelectric activity*. *Biosens Bioelectron*, 2004. **19**(10): p. 1309-18.
129. Sun, Y., et al., *Assessment of the biocompatibility of photosensitive polyimide for implantable medical device use*. *J Biomed Mater Res A*, 2008.
130. Mian, A., et al., *Performance of laser bonded glass/polyimide microjoints in cerebrospinal fluid*. *J Mater Sci Mater Med*, 2007. **18**(3): p. 417-27.
131. Rodriguez, M. and N. Barroso, *An improved method for carotid artery infusion without vessel occlusion*. *Physiol Behav*, 1992. **52**(6): p. 1211-3.
132. Richardson, R.R., Jr., J.A. Miller, and W.M. Reichert, *Polyimides as biomaterials: preliminary biocompatibility testing*. *Biomaterials*, 1993. **14**(8): p. 627-35.
133. Scheerlinck, T., et al., *Mechanical implications of interfacial defects between femoral hip implants and cement: a finite element analysis of interfacial gaps and interfacial porosity*. *Proc Inst Mech Eng [H]*, 2008. **222**(7): p. 1037-47.

134. Okimoto, K., et al., *Design and evaluation of an osmotic pump tablet (OPT) for prednisolone, a poorly water soluble drug, using (SBE)7 $\alpha$ -beta-CD*. Pharm Res, 1998. **15**(10): p. 1562-8.
135. Rao, V.M., J.L. Haslam, and V.J. Stella, *Controlled and complete release of a model poorly water-soluble drug, prednisolone, from hydroxypropyl methylcellulose matrix tablets using (SBE)7 $\alpha$ -beta-cyclodextrin as a solubilizing agent*. J Pharm Sci, 2001. **90**(7): p. 807-16.
136. Tepe, G., H.P., Wendel, S., Khorchidi, J., Schmehl, J., Wiskirchen, B., Pusich, C., Claussen, and S.H., Duda, *Thrombogenicity of Various Endovascular Stent Types: An In Vitro Evaluation*. Journal of Vascular & Interventional Radiology, 2002. **13**(10): p. 1029-1035.
137. Astrand, M., T.I. Selinder, M.E. Sjostrand, *Deposition of Ti<sub>1-x</sub>Al<sub>x</sub>N using bipolar pulsed dual magnetron sputtering*. Surface & Coatings Technology, 2005. **200**(1-4): p. 625-629.
138. Cheng, Y., W. Cai, H.T. Li, Y.F. Zheng, L.C. Zhao, *Surface characteristics and corrosion resistance properties of TiNi shape memory alloy coated with Ta*. 2004. **186**(3): p. 346-352.
139. Wilson, B., <http://cnx.org/content/m11369/latest/> Accessed January 15 2009.
140. Guidant, <http://www.guidant.com/products/stents.shtml> Accessed January 15 2009.

141. Everard, M.L., S.G. Devadason, and P.N. Le Souef, *Flow early in the inspiratory manoeuvre affects the aerosol particle size distribution from a Turbuhaler*. *Respir Med*, 1997. **91**(10): p. 624-8.
142. O'Neil, A.J., R.D. Jee, and A.C. Moffat, *Measurement of the percentage volume particle size distribution of powdered microcrystalline cellulose using reflectance near-infrared spectroscopy*. *Analyst*, 2003. **128**(11): p. 1326-30.
143. Li, C. and H. Jiang, *Measurement of particle-size distribution and concentration in heterogeneous turbid media with multispectral diffuse optical tomography*. *Appl Opt*, 2005. **44**(10): p. 1838-44.
144. Espi-Metals, [http://www.espi-metals.com/tech/Tech-%20Haynes%2025%20\(L605\)%20-%20Alloy%20Composition.htm](http://www.espi-metals.com/tech/Tech-%20Haynes%2025%20(L605)%20-%20Alloy%20Composition.htm) Accessed January 15 2009.
145. Poletti, G., et al., *A comparative study between AFM and SEM imaging on human scalp hair*. *J Microsc*, 2003. **211**(Pt 3): p. 249-55.
146. Shukla, A.J. and J.C. Price, *Effect of drug loading and molecular weight of cellulose acetate propionate on the release characteristics of theophylline microspheres*. *Pharm Res*, 1991. **8**(11): p. 1396-400.
147. Tsong, T.Y. and K. Kinoshita, Jr., *Use of voltage pulses for the pore opening and drug loading, and the subsequent resealing of red blood cells*. *Bibl Haematol*, 1985(51): p. 108-14.

148. Kim, S.W., Y.H. Bae, and T. Okano, *Hydrogels: swelling, drug loading, and release*. Pharm Res, 1992. **9**(3): p. 283-90.
149. Sousa, R.G., et al., *Dependence of copolymer composition, swelling history, and drug concentration on the loading of diltiazem hydrochloride (DIL.HCl) into poly[(N-isopropylacrylamide)-co-(methacrylic acid)] hydrogels and its release behaviour from hydrogel slabs*. J Control Release, 2005. **102**(3): p. 595-606.
150. Kim, C.J. and P.I. Lee, *Effect of loading on swelling-controlled drug release from hydrophobic polyelectrolyte gel beads*. Pharm Res, 1992. **9**(10): p. 1268-74.
151. Mazzini, R.H., *Considerations on corticoid therapy in dermatology. Our experience with an ointment with a base of prednisolone and hexachlorophene*. Sem Med, 1960. **117**: p. 845-50.
152. Weismann-Netter, R., et al., *Tests of a new corticoid in intra-articular injections; prednisolone butyl-acetate*. Sem Med Prof Med Soc, 1957. **33**(39): p. 1513-4.
153. Holloway, S.A., D.J. Meyer, and C. Mannella, *Prednisolone and danazol for treatment of immune-mediated anemia, thrombocytopenia, and ineffective erythroid regeneration in a dog*. J Am Vet Med Assoc, 1990. **197**(8): p. 1045-8.
154. Kelly, G.E., A. Scheibner, and A.G. Sheil, *Effects of therapy with azathioprine and prednisolone and ultraviolet irradiation on mouse skin immune function and immune cell markers*. Immunol Cell Biol, 1987. **65 (Pt 2)**: p. 153-61.
155. Vernon-Roberts, B. and J.D. Jessop, *Effects of gold and prednisolone on inflammation and phagocytosis in the rat*. Ann Rheum Dis, 1972. **31**(6): p. 536-7.

156. Zarem, H.A. and R. Soderberg, *Tissue reaction to ischemia in the rabbit ear chamber: effects of prednisolone on inflammation and microvascular flow*. *Plast Reconstr Surg*, 1982. **70**(6): p. 667-76.
157. Merck-Index, *The Merck Index*. Fourteenth ed. 2006, WhiteHouse station, New Jersey: Merck & Co., Inc.
158. Wikipedia, <http://en.wikipedia.org/wiki/Prednisolone> Accessed January 15 2009.
159. Lauritsen, K., et al., *Effects of topical 5-aminosalicylic acid and prednisolone on prostaglandin E2 and leukotriene B4 levels determined by equilibrium in vivo dialysis of rectum in relapsing ulcerative colitis*. *Gastroenterology*, 1986. **91**(4): p. 837-44.
160. Smith, S.F., et al., *Lipocortin-1 distribution in bronchoalveolar lavage from healthy human lung: effect of prednisolone*. *J Appl Physiol*, 1995. **79**(1): p. 121-8.
161. Kobza Black, A., M.W. Greaves, and C.N. Hensby, *The effect of systemic prednisolone on arachidonic acid, and prostaglandin E2 and F2 alpha levels in human cutaneous inflammation*. *Br J Clin Pharmacol*, 1982. **14**(3): p. 391-4.
162. Jessop, J.D., B. Vernon-Roberts, and J. Harris, *Effects of gold salts and prednisolone on inflammatory cells. I. Phagocytic activity of macrophages and polymorphs in inflammatory exudates studied by a "skin-window" technique in rheumatoid and control patients*. *Ann Rheum Dis*, 1973. **32**(4): p. 294-300.

163. Oku, H., et al., *Antifibrotic action of pirfenidone and prednisolone: different effects on pulmonary cytokines and growth factors in bleomycin-induced murine pulmonary fibrosis*. Eur J Pharmacol, 2008. **590**(1-3): p. 400-8.
164. Wallwork, B., et al., *Clarithromycin and prednisolone inhibit cytokine production in chronic rhinosinusitis*. Laryngoscope, 2002. **112**(10): p. 1827-30.
165. Chang, M.S., J.G. Xiao, and G.C. Chiou, *Prevention of ocular inflammation by matrine, prednisolone, and cyclooxygenase and lipoxygenase inhibitors*. Zhongguo Yao Li Xue Bao, 1991. **12**(2): p. 121-5.
166. Chiou, G.C., Q.S. Yao, and R.S. Varma, *Inhibition of ocular inflammation by chalcone derivatives and prednisolone*. J Ocul Pharmacol, 1992. **8**(3): p. 213-23.
167. Olejnik, O. and C.A. Weisbecker, *Ocular bioavailability of topical prednisolone preparations*. Clin Ther, 1990. **12**(1): p. 2-11.
168. Ramsell, T.G., W. Trillwood, and G. Draper, *Effects of prednisolone eye drops. A trial of the effects of prednisolone phosphate eye drops on the intra-ocular pressure of normal volunteers*. Br J Ophthalmol, 1967. **51**(6): p. 398-402.
169. Diestelhorst, M., et al., *Effect of dexamethasone 0.1% and prednisolone acetate 1.0% eye drops on the blood-aqueous barrier after cataract surgery: a controlled randomized fluorophotometric study*. Graefes Arch Clin Exp Ophthalmol, 1992. **230**(5): p. 451-3.
170. Struck, H.G. and A. Bariszlovich, *Comparison of 0.1% dexamethasone phosphate eye gel (Dexagel) and 1% prednisolone acetate eye suspension in the treatment of*

- post-operative inflammation after cataract surgery.* Graefes Arch Clin Exp Ophthalmol, 2001. **239**(10): p. 737-42.
171. Voisard, R., et al., *The effect of propranolol, lisinopril, prednisolone, colchicine, etoposide and vincristine on proliferation of re-stenosing human plaque cells in vitro: cell culture as a prescreening system for prevention of restenosis.* Vasa Suppl, 1992. **35**: p. 128-9.
172. Joner, M., et al., *Site-specific targeting of nanoparticle prednisolone reduces in-stent restenosis in a rabbit model of established atheroma.* Arterioscler Thromb Vasc Biol, 2008. **28**(11): p. 1960-6.
173. Goldzieher, J.W., *The history of steroidal contraceptive development: the estrogens.* Perspect Biol Med, 1993. **36**(3): p. 363-8.
174. Lehfeldt, H., *Choice of ethinyl estradiol as a postcoital pill.* Am J Obstet Gynecol, 1973. **116**(6): p. 892-3.
175. Wikipedia, [http://en.wikipedia.org/wiki/Ethinyl\\_estradiol](http://en.wikipedia.org/wiki/Ethinyl_estradiol) Accessed January 15 2009.
176. Dabrosin, C., et al., *Estradiol promotes growth and angiogenesis in polyoma middle T transgenic mouse mammary tumor explants.* Breast Cancer Res Treat, 2003. **78**(1): p. 1-6.
177. Suh, D.Y., *Understanding angiogenesis and its clinical applications.* Ann Clin Lab Sci, 2000. **30**(3): p. 227-38.

178. Chen, Y., et al., *Increased expression of angiogenin in gastric carcinoma in correlation with tumor angiogenesis and proliferation*. World J Gastroenterol, 2006. **12**(32): p. 5135-9.
179. Ahn, A., et al., *Therapeutic angiogenesis: a new treatment approach for ischemic heart disease--Part II*. Cardiol Rev, 2008. **16**(5): p. 219-29.
180. Cho, K.R., et al., *Therapeutic angiogenesis using naked DNA expressing two isoforms of the hepatocyte growth factor in a porcine acute myocardial infarction model*. Eur J Cardiothorac Surg, 2008. **34**(4): p. 857-63.
181. Ishikane, S., et al., *Allogeneic injection of fetal membrane-derived mesenchymal stem cells induces therapeutic angiogenesis in a rat model of hind limb ischemia*. Stem Cells, 2008. **26**(10): p. 2625-33.
182. Motukuru, V., et al., *Therapeutic angiogenesis in Buerger's disease (thromboangiitis obliterans) patients with critical limb ischemia by autologous transplantation of bone marrow mononuclear cells*. J Vasc Surg, 2008. **48**(6 Suppl): p. 53S-60S; discussion 60S.
183. Chandrasekar, B., S. Nattel, and J.F. Tanguay, *Coronary artery endothelial protection after local delivery of 17beta-estradiol during balloon angioplasty in a porcine model: a potential new pharmacologic approach to improve endothelial function*. J Am Coll Cardiol, 2001. **38**(5): p. 1570-6.
184. Clarke, W.H. and I.G. Maddocks, *Crystal Violet For Selective Staining Of Mitoses In Follicle Bulbs Of Sheep Skin*. Stain Technol, 1963. **38**: p. 252-4.

185. Dutt, M.K., *Staining of depolymerised DNA in mammalian tissues with methyl violet 6B and crystal violet*. Folia Histochem Cytochem (Krakow), 1980. **18**(1): p. 79-83.
186. Oregon-Medical-Laser-Centre,  
[http://omlc.ogi.edu/spectra/PhotochemCAD/html/crystalviolet\(H2O\).html](http://omlc.ogi.edu/spectra/PhotochemCAD/html/crystalviolet(H2O).html)  
Accessed January 15 2009.
187. Wikipedia, [http://en.wikipedia.org/wiki/Gentian\\_violet](http://en.wikipedia.org/wiki/Gentian_violet) Accessed January 15 2009.
188. FDA, [www.fda.gov/cder/Offices/ONDQA/presentations/miller\\_poly.pdf](http://www.fda.gov/cder/Offices/ONDQA/presentations/miller_poly.pdf) Accessed January 15 2009.
189. Suitchmezian, V., I. Jess, J. Sehner, L. Seyfarth, J. Senker, C. Nather, *Structural, Thermodynamic, and Kinetic Aspects of the Polymorphism and Pseudopolymorphism of Prednisolone (11,17 $\alpha$ ,21-Trihydroxy-1,4-pregnadien-3,20-dion)*. Crystal, Growth & Design, 2008. **8**(1): p. 98–107.
190. Guguta, C., I. Eeuwijk, J. M. M. Smits, R. de Gelder, *Structural Diversity of Ethinyl Estradiol Solvates*. Crystal Growth & Design, 2008. **8**(3): p. 823-831.
191. Smith, G., U.D. Wermuth, and J.M. White, *Pseudopolymorphism in brucine: brucine-water (1/2), the third crystal hydrate of brucine*. Acta Crystallogr C, 2007. **63**(Pt 8): p. o489-92.

192. Weissbuch, I., et al., *Solvent effect on crystal polymorphism: why addition of methanol or ethanol to aqueous solutions induces the precipitation of the least stable beta form of glycine*. *Angew Chem Int Ed Engl*, 2005. **44**(21): p. 3226-9.
193. Mattamal, G.J., *US FDA perspective on the regulations of medical-grade polymers: cyanoacrylate polymer medical device tissue adhesives*. *Expert Rev Med Devices*, 2008. **5**(1): p. 41-9.
194. Chao, H.H. and D.F. Torchiana, *BioGlue: albumin/glutaraldehyde sealant in cardiac surgery*. *J Card Surg*, 2003. **18**(6): p. 500-3.
195. Hidas, G., et al., *Sutureless nephron-sparing surgery: use of albumin glutaraldehyde tissue adhesive (BioGlue)*. *Urology*, 2006. **67**(4): p. 697-700; discussion 700.
196. Passage, J., et al., *Bioglue: a review of the use of this new surgical adhesive in thoracic surgery*. *ANZ J Surg*, 2005. **75**(5): p. 315-8.
197. Raanani, E., et al., *'BioGlue' for the repair of aortic insufficiency in acute aortic dissection*. *J Heart Valve Dis*, 2004. **13**(5): p. 734-7.
198. Yuen, T. and A.H. Kaye, *Persistence of Bioglue in spinal dural repair*. *J Clin Neurosci*, 2005. **12**(1): p. 100-1.
199. Swarbrick, J. and J.C. Boylan, *Encyclopedia of pharmaceutical technology*. 2 ed. Vol. 1. 2002, New York: Informa Health Care.
200. Robinson, J.R. and V.H.L. Lee, *Controlled Drug Delivery. Fundamentals and Applications*. 2nd ed. 1987, New York: Marcel Dekker.

201. Zhou, Y. and X.Y. Wu, *Modeling and analysis of dispersed-drug release into a finite medium from sphere ensembles with a boundary layer*. J Control Release, 2003. **90**(1): p. 23-36.
202. Huang, X. and C.S. Brazel, *On the importance and mechanisms of burst release in matrix-controlled drug delivery systems*. J Control Release, 2001. **73**(2-3): p. 121-36.
203. Ratner, B.D., et al., *Biomaterial Science: An Introduction to Materials in Medicine*. 2nd ed. 2004, London: Elsevier Academic Press.
204. Bragulat, M.R., et al., *Dyes as fungal inhibitors: effect on colony diameter*. Appl Environ Microbiol, 1991. **57**(9): p. 2777-80.
205. Safarik, I. and M. Safarikova, *Detection of low concentrations of malachite green and crystal violet in water*. Water Res, 2002. **36**(1): p. 196-200.
206. Safarikova, M. and I. Safarik, *Magnetic solid-phase extraction of target analytes from large volumes of urine*. European Cells and Materials, 2002. **3**(Suppl 2): p. 192-195.
207. Geddes, L.A. and R. Roeder, *Criteria for the selection of materials for implanted electrodes*. Ann Biomed Eng, 2003. **31**(7): p. 879-90.
208. Kawakami, H., T. Kanamori, and S. Kubota, *Development of a fluorinated polyimide hollow fiber for medical devices*. J Artif Organs, 2003. **6**(2): p. 124-9.
209. Niwa, M., et al., *Gas transfer and blood compatibility of asymmetric polyimide hollow fiber*. J Biomater Sci Polym Ed, 2001. **12**(5): p. 533-42.

210. Varian-Inc., <http://www.varianinc.com/cgi-bin/nav?products/dissolution/testers/varian400ds&cid=KNHMOHJMFL>  
*Accessed April 25 2009.*
211. FDA, <http://www.fda.gov/CDER/GUIDANCE/4252fnl.htm> *Accessed January 15 2009.*
212. Edman, P., *Biopharmaceutics of ocular drug delivery*, ed. M.A. Hollinger. 1992, New York, NY: Informa Health Care.
213. Loftsson, T., et al., *Topical drug delivery to the posterior segment of the eye: anatomical and physiological considerations*. *Pharmazie*, 2008. **63**(3): p. 171-9.
214. Indevus-Pharmaceuticals, <http://www.vantasimplant.com/md/dosing.php> *Accessed January 15 2009.*
215. Reddy, D.V. and V.E. Kinsey, *Composition of the vitreous humor in relation to that of plasma and aqueous humors*. *Arch Ophthalmol*, 1960. **63**: p. 715-20.
216. Boubriak, O.A., et al., *The effect of hydration and matrix composition on solute diffusion in rabbit sclera*. *Exp Eye Res*, 2000. **71**(5): p. 503-14.
217. Vogler, E.A., *Water and the acute biological response to surfaces*. *J Biomater Sci Polym Ed*, 1999. **10**(10): p. 1015-45.
218. Acharya, C., A. Dutta, and S.C. Kundu, *Surface Treatment of Pure and PEG-4000 Blended Fibroin Films and their Characterizations as Matrices for in vitro Fibroblast Culture*. *J Biomater Appl*, 2008.

219. Liu, L., et al., *Reduced foreign body reaction to implanted biomaterials by surface treatment with oriented osteopontin*. J Biomater Sci Polym Ed, 2008. **19**(6): p. 821-35.
220. Pellenc, D., et al., *Removal of surface by-products from sintered hydroxyapatite: effect of a chelation treatment on fibronectin adsorption and cell adhesion*. J Biomed Mater Res B Appl Biomater, 2006. **76**(1): p. 136-42.
221. Tajima, S., et al., *Differential regulation of endothelial cell adhesion, spreading, and cytoskeleton on low-density polyethylene by nanotopography and surface chemistry modification induced by argon plasma treatment*. J Biomed Mater Res A, 2008. **84**(3): p. 828-36.
222. Wan, Y., et al., *Characterization of surface property of poly(lactide-co-glycolide) after oxygen plasma treatment*. Biomaterials, 2004. **25**(19): p. 4777-83.
223. Hao, L., et al., *Enhanced human osteoblast cell adhesion and proliferation on 316 LS stainless steel by means of CO<sub>2</sub> laser surface treatment*. J Biomed Mater Res B Appl Biomater, 2005. **73**(1): p. 148-56.
224. Kanno, M., et al., *Biocompatibility of fluorinated polyimide*. J Biomed Mater Res, 2002. **60**(1): p. 53-60.
225. Nagaoka, S., K. Ashiba, and H. Kawakami, *Biomedical properties of nanofabricated fluorinated polyimide surface*. Artif Organs, 2002. **26**(8): p. 670-5.

226. Tesfamariam, B., *Platelet function in intravascular device implant-induced intimal injury*. Cardiovasc Revasc Med, 2008. **9**(2): p. 78-87.
227. Brogini, N., et al., *Peri-implant inflammation defined by the implant-abutment interface*. J Dent Res, 2006. **85**(5): p. 473-8.
228. Ren, W., et al., *Implant wear induces inflammation, but not osteoclastic bone resorption, in RANK(-/-) mice*. J Orthop Res, 2006. **24**(8): p. 1575-86.
229. Thakker, M.M., J. Zhang, and B.S. Sires, *Chronic inflammation from polycarbonate motility peg inhibits osteogenesis in a human hydroxyapatite orbital implant*. Ophthal Plast Reconstr Surg, 2005. **21**(5): p. 399-401.
230. Bainton, D.F., et al., *Rapid fragmentation and reorganization of Golgi membranes during frustrated phagocytosis of immobile immune complexes by macrophages*. Am J Pathol, 1989. **134**(1): p. 15-26.
231. Freedman, J.E. and J. Loscalzo, *Platelet-monocyte aggregates: bridging thrombosis and inflammation*. Circulation, 2002. **105**(18): p. 2130-2.
232. Seizer, P., M. Gawaz, and A.E. May, *Platelet-monocyte interactions--a dangerous liaison linking thrombosis, inflammation and atherosclerosis*. Curr Med Chem, 2008. **15**(20): p. 1976-80.
233. Brewer, G.J., *Tetrathiomolybdate anticopper therapy for Wilson's disease inhibits angiogenesis, fibrosis and inflammation*. J Cell Mol Med, 2003. **7**(1): p. 11-20.

234. Jiang, N. and D.S. Pisetsky, *The effect of inflammation on the generation of plasma DNA from dead and dying cells in the peritoneum*. J Leukoc Biol, 2005. **77**(3): p. 296-302.
235. Keane, M.P., et al., *Inflammation and angiogenesis in fibrotic lung disease*. Semin Respir Crit Care Med, 2006. **27**(6): p. 589-99.
236. Sangiorgi, G., et al., *Pregnancy-associated plasma protein-a is markedly expressed by monocyte-macrophage cells in vulnerable and ruptured carotid atherosclerotic plaques: a link between inflammation and cerebrovascular events*. J Am Coll Cardiol, 2006. **47**(11): p. 2201-11.
237. Watanabe, T. and J. Fan, *Atherosclerosis and inflammation mononuclear cell recruitment and adhesion molecules with reference to the implication of ICAM-1/LFA-1 pathway in atherogenesis*. Int J Cardiol, 1998. **66 Suppl 1**: p. S45-53; discussion S55.
238. Ding, A.H., C.F. Nathan, and D.J. Stuehr, *Release of reactive nitrogen intermediates and reactive oxygen intermediates from mouse peritoneal macrophages. Comparison of activating cytokines and evidence for independent production*. J Immunol, 1988. **141**(7): p. 2407-12.
239. Simoni, J., et al., *Cytokines and PAF release from human monocytes and macrophages: effect of hemoglobin and contaminants*. Artif Cells Blood Substit Immobil Biotechnol, 1994. **22**(3): p. 525-34.

240. Tucci, M.A., et al., *Release of inflammatory cytokines by macrophages and synovial cells challenged with tumor necrosis factor*. Biomed Sci Instrum, 2002. **38**: p. 89-94.
241. Armstrong, E.J., D.A. Morrow, and M.S. Sabatine, *Inflammatory biomarkers in acute coronary syndromes: part I: introduction and cytokines*. Circulation, 2006. **113**(6): p. e72-5.
242. Mack, C.L., *Serum cytokines as biomarkers of disease and clues to pathogenesis*. Hepatology, 2007. **46**(1): p. 6-8.
243. Hori, M., et al., *MCP-1 targeting inhibits muscularis macrophage recruitment and intestinal smooth muscle dysfunction in colonic inflammation*. Am J Physiol Cell Physiol, 2008. **294**(2): p. C391-401.
244. Kanno, K., et al., *Angiotensin II participates in hepatic inflammation and fibrosis through MCP-1 expression*. Dig Dis Sci, 2005. **50**(5): p. 942-8.
245. Ramos, C.D., et al., *MIP-1alpha[CCL3] acting on the CCR1 receptor mediates neutrophil migration in immune inflammation via sequential release of TNF-alpha and LTB4*. J Leukoc Biol, 2005. **78**(1): p. 167-77.
246. Rampart, M., et al., *Different pro-inflammatory profiles of interleukin 1 (IL 1) and tumor necrosis factor (TNF) in an in vivo model of inflammation*. Agents Actions, 1989. **26**(1-2): p. 186-8.
247. Shahan, T.A., et al., *Concentration- and time-dependent upregulation and release of the cytokines MIP-2, KC, TNF, and MIP-1alpha in rat alveolar macrophages*

- by fungal spores implicated in airway inflammation. Am J Respir Cell Mol Biol*, 1998. **18**(3): p. 435-40.
248. Zhao, B., et al., *Effect of interleukin-1beta and tumor necrosis factor-alpha on gene expression in human endothelial cells. Am J Physiol Cell Physiol*, 2003. **284**(6): p. C1577-83.
249. Haines-Butterick, L.A., et al., *In vitro assessment of the pro-inflammatory potential of beta-hairpin peptide hydrogels. Biomaterials*, 2008. **29**(31): p. 4164-9.
250. Bhatia, S.K., et al., *Interactions of polysaccharide-based tissue adhesives with clinically relevant fibroblast and macrophage cell lines. Biotechnol Lett*, 2007. **29**(11): p. 1645-9.
251. Yim, E.S., et al., *Biocompatibility of poly(ethylene glycol)/poly(acrylic acid) interpenetrating polymer network hydrogel particles in RAW 264.7 macrophage and MG-63 osteoblast cell lines. J Biomed Mater Res A*, 2008.
252. Yoon, H.J., et al., *Chitosan oligosaccharide (COS) inhibits LPS-induced inflammatory effects in RAW 264.7 macrophage cells. Biochem Biophys Res Commun*, 2007. **358**(3): p. 954-9.
253. de Kok, J.B., et al., *Normalization of gene expression measurements in tumor tissues: comparison of 13 endogenous control genes. Lab Invest*, 2005. **85**(1): p. 154-9.
254. FDA, <http://www.fda.gov/cdrh/g951.html> Accessed January 15 2009.

255. Muller, U., *In vitro biocompatibility testing of biomaterials and medical devices*. Med Device Technol, 2008. **19**(2): p. 30, 32-4.
256. van Loon, J. and P. Mars, *Biocompatibility: the latest developments*. Med Device Technol, 1997. **8**(10): p. 20-4.
257. Lemasters, J.J. and C.R. Hackenbrock, *Continuous measurement of adenosine triphosphate with firefly luciferase luminescence*. Methods Enzymol, 1979. **56**: p. 530-44.
258. ExPASy-Proteomics-Server, <http://www.expasy.org/cgi-bin/nicezyme.pl?1.13.12.7> Accessed January 15 2009.
259. Branchini, B.R., et al., *The role of active site residue arginine 218 in firefly luciferase bioluminescence*. Biochemistry, 2001. **40**(8): p. 2410-8.
260. Marques, S.M. and J.C. Esteves da Silva, *Firefly bioluminescence: a mechanistic approach of luciferase catalyzed reactions*. IUBMB Life, 2009. **61**(1): p. 6-17.
261. Gomi, K. and N. Kajiyama, *Oxyluciferin, a luminescence product of firefly luciferase, is enzymatically regenerated into luciferin*. J Biol Chem, 2001. **276**(39): p. 36508-13.
262. Thorpe, G.H., et al., *Enhancement of the horseradish peroxidase-catalyzed chemiluminescent oxidation of cyclic diacyl hydrazides by 6-hydroxybenzothiazoles*. Anal Biochem, 1985. **145**(1): p. 96-100.

263. Williams, T.M., et al., *Advantages of firefly luciferase as a reporter gene: application to the interleukin-2 gene promoter*. *Anal Biochem*, 1989. **176**(1): p. 28-32.
264. Mayer-Kuckuk, P., et al., *Role of reporter gene imaging in molecular and cellular biology*. *Biol Chem*, 2004. **385**(5): p. 353-61.
265. Schwartz, O., et al., *A microtransfection method using the luciferase-encoding reporter gene for the assay of human immunodeficiency virus LTR promoter activity*. *Gene*, 1990. **88**(2): p. 197-205.
266. Wilson, V.S., K. Bobseine, and L.E. Gray, Jr., *Development and characterization of a cell line that stably expresses an estrogen-responsive luciferase reporter for the detection of estrogen receptor agonist and antagonists*. *Toxicol Sci*, 2004. **81**(1): p. 69-77.
267. Legler, J., et al., *Development of a stably transfected estrogen receptor-mediated luciferase reporter gene assay in the human T47D breast cancer cell line*. *Toxicol Sci*, 1999. **48**(1): p. 55-66.
268. AbraxisKits, <http://www.abraxiskits.com/moreinfo/PN590051USER.pdf> Accessed on Jun 05 2009.
269. DeSilva, B., et al., *Recommendations for the bioanalytical method validation of ligand-binding assays to support pharmacokinetic assessments of macromolecules*. *Pharm Res*, 2003. **20**(11): p. 1885-900.

270. Little, J.A., *Comparison of curve fitting models for ligand binding assays*. Chromatographia Supplement, 2004. **59**: p. S177.
271. Choi, D.H., et al., *Validation of a method for predicting the precision, limit of detection and range of quantitation in competitive ELISA*. Anal Sci, 2007. **23**(2): p. 215-8.
272. Hayashi, Y., et al., *Detection limit estimated from slope of calibration curve: an application to competitive ELISA*. Anal Sci, 2005. **21**(2): p. 167-9.
273. Suli, J., et al., *Correction of measurement errors in the ELISA test*. Bratisl Lek Listy, 2000. **101**(10): p. 565-8.
274. Angioi-Duprez, K., *Retinopathy, a major cause of blindness in the adult diabetic*. Soins, 2006(703 Suppl 1): p. 1S12-5.
275. Foster, R.A., *Age-related macular degeneration: a leading cause of blindness*. Med J Aust, 1997. **166**(6): p. 331.
276. Kingman, S., *Glaucoma is second leading cause of blindness globally*. Bull World Health Organ, 2004. **82**(11): p. 887-8.
277. Engerman, R.L. and T.S. Kern, *Hyperglycemia as a cause of diabetic retinopathy*. Metabolism, 1986. **35**(4 Suppl 1): p. 20-3.
278. Logan, P., P. Eustace, and R. Robinson, *Hypertensive retinopathy: a cause of decreased visual acuity in children*. J Pediatr Ophthalmol Strabismus, 1992. **29**(5): p. 287-9.

279. Haik, G.M., Jr., W.L. Terrell, 3rd, and G.M. Haik, Sr., *Diabetic retinopathy: a leading cause of new blindness*. South Med J, 1989. **82**(5): p. 575-9.
280. National-Institute-of-Health, <http://www.nei.nih.gov/glaucoma/> Accessed January 15 2009.
281. Bedell, A.J., *Senile macular degeneration: a common cause of defective sight in the elderly*. J Am Geriatr Soc, 1954. **2**(3): p. 193-7.
282. Haik, G.M., Jr., W.L. Terrell, 3rd, and G.M. Haik, Sr., *Macular degeneration: the major cause of severe vision loss in persons fifty-five years or older*. J Miss State Med Assoc, 1989. **30**(7): p. 207-10.
283. National-Institute-of-Health, [http://www.nei.nih.gov/health/maculardegen/armd\\_facts.asp](http://www.nei.nih.gov/health/maculardegen/armd_facts.asp) Accessed January 15 2009.
284. National-Institute-of-Health, <http://www.nlm.nih.gov/medlineplus/ency/article/000665.htm> Accessed January 15 2009.
285. Forster, R.K., et al., *Further observations on the diagnosis cause, and treatment of endophthalmitis*. Am J Ophthalmol, 1976. **81**(1): p. 52-6.
286. Myles, M.E., D.M. Neumann, and J.M. Hill, *Recent progress in ocular drug delivery for posterior segment disease: emphasis on transscleral iontophoresis*. Adv Drug Deliv Rev, 2005. **57**(14): p. 2063-79.

287. National-Institute-of-Health,  
*<http://www.nei.nih.gov/health/eyediagram/images/NEA09.gif> Accessed on  
October 31 2009.*
288. Camenzind, E., P.G. Steg, and W. Wijns, *Stent thrombosis late after implantation  
of first-generation drug-eluting stents: a cause for concern.* *Circulation*, 2007.  
**115**(11): p. 1440-55.
289. Szygula, J., B. Puzio, and L. Polonski, *Restenosis after percutaneous coronary  
angioplasty--cause, prevention strategies.* *Wiad Lek*, 1998. **51**(1-2): p. 76-81.
290. Jakabcin, J., et al., *The lack of endothelization after drug-eluting stent  
implantation as a cause of fatal late stent thrombosis.* *J Thromb Thrombolysis*,  
2008. **26**(2): p. 154-8.
291. Kopell, B.H., et al., *Subfascial implantation of intrathecal baclofen pumps in  
children: technical note.* *Neurosurgery*, 2001. **49**(3): p. 753-6; discussion 756-7.
292. Byrd, L.M., et al., *Chronic pain and obstetric management of a patient with  
tuberous sclerosis.* *Pain Med*, 2007. **8**(2): p. 199-203.
293. Coombs, D.W., *Management of chronic pain by epidural and intrathecal opioids:  
newer drugs and delivery systems.* *Int Anesthesiol Clin*, 1986. **24**(2): p. 59-74.
294. Anderson, K.O., et al., *Pain behavior of rheumatoid arthritis patients enrolled in  
experimental drug trials.* *Arthritis Care Res*, 1994. **7**(2): p. 64-8.
295. Smith, H.S., et al., *Intrathecal drug delivery.* *Pain Physician*, 2008. **11**(2 Suppl):  
p. S89-S104.

296. Decosterd, I., et al., *Spinal opioids: mechanisms of action and chronic pain management*. Rev Med Suisse, 2006. **2**(71): p. 1636-8, 1640.
297. Milne, B., et al., *Analgesia and tolerance to intrathecal morphine and norepinephrine infusion via implanted mini-osmotic pumps in the rat*. Pain, 1985. **22**(2): p. 165-72.
298. Bramanti, P., et al., *Quality of life of patients with telemetric pumps for intrathecal baclofen infusion: data and limitations of assessment scales*. Funct Neurol, 2004. **19**(4): p. 227-31.
299. Portenoy, R.K. and S.R. Savage, *Clinical realities and economic considerations: special therapeutic issues in intrathecal therapy--tolerance and addiction*. J Pain Symptom Manage, 1997. **14**(3 Suppl): p. S27-35.
300. Smith, T.J., C. Swainey, and P.J. Coyne, *Pain management, including intrathecal pumps*. Curr Oncol Rep, 2004. **6**(4): p. 291-6.
301. National-Cancer-Institute, <http://cancer.net.nci.nih.gov/cancertopics/chemo-side-effects> Accessed January 15 2009.
302. Westphal, M., et al., *Gliadel wafer in initial surgery for malignant glioma: long-term follow-up of a multicenter controlled trial*. Acta Neurochir (Wien), 2006. **148**(3): p. 269-75; discussion 275.
303. Perry, J., et al., *Gliadel wafers in the treatment of malignant glioma: a systematic review*. Curr Oncol, 2007. **14**(5): p. 189-94.

304. Tsutsumi, K., et al., *Tumor growth inhibition by synthetic and expressed siRNA targeting focal adhesion kinase*. *Int J Oncol*, 2008. **33**(1): p. 215-24.
305. Chen, Y. and L. Huang, *Tumor-targeted delivery of siRNA by non-viral vector: safe and effective cancer therapy*. *Expert Opin Drug Deliv*, 2008. **5**(12): p. 1301-11.
306. Savitt, J.M., V.L. Dawson, and T.M. Dawson, *Diagnosis and treatment of Parkinson disease: molecules to medicine*. *J Clin Invest*, 2006. **116**(7): p. 1744-54.
307. Mars, H., *Levodopa, carbidopa, and pyridoxine in Parkinson disease. Metabolic interactions*. *Arch Neurol*, 1974. **30**(6): p. 444-7.
308. Teychenne, P.F., et al., *Interactions of levodopa with inhibitors of monoamine oxidase and L-aromatic amino acid decarboxylase*. *Clin Pharmacol Ther*, 1975. **18**(3): p. 273-7.
309. Bounds, J.A. and G.M. Hunt, *Neurology-Epitomes of Progress: Carbidopa-Levodopa Combination in Treatment of Parkinson Disease*. *West J Med*, 1977. **127**(2): p. 135-136.

## VITA

Ashish Rastogi, the son of Mr. Sudhir Rastogi and Mrs. Veena Rastogi, was born in New Delhi, India. After completing his high school education at Father Agnel School, New Delhi, India, he joined M.S. Ramaiah College of Pharmacy, Bangalore, Karnataka, India which is affiliated to Rajiv Gandhi University of Health Sciences. Afterwards, he worked as a Sales and Marketing Executive in M/s. V.M.A. Enterprises, New Delhi, India. In January 2003, he joined the Pharmaceutics program at The University of Texas at Austin. During his graduate career, Ashish has presented at a number of regional and national scientific meetings and published in various peer reviewed journals. During the course of his graduate program, he was awarded Schering-Plough Research Institute Graduate Fellowship in Pharmacy (2005), Max and Mary Anne Burlage Scholarship in Pharmacy (2005), and Academic Competitive Scholarship Award (2008) apart from various intra-college professional development travel scholarships (2004-2008). His various professional associations include: Chair – American Association of Pharmaceutical Scientist's (AAPS), University of Texas at Austin Student Chapter (2007-2009); Member - Outstanding Graduate Teaching Awards Committee (2007 – 2009); President – Pharmacy Graduate Student Association, College of Pharmacy, The University of Texas at Austin (2005 – 2007); Treasurer –AAPS University of Texas at

Austin Student Chapter (2005 – 2007); Member - Administrative Subcommittee – Student Representative, College of Pharmacy, The University of Texas at Austin (2004 – 2005); Member – Rho Chi Pharmacy Honor Society (2003 – present). He also held position of Teaching Assistant in College of Pharmacy and School of Biological Sciences from 2003-2007. Ashish was married to Tanvi Rastogi in 2007.

Permanent Address: 8555 Laurens lane,

Apt 702

San Antonio, TX 78218

This dissertation was typed by the author.